Design and Analysis of a Novel 3-D Elliptical Hyperboloid Static Solar Concentrator for Process Heat Applications

A THESIS

Submitted by

Imhamed M. Saleh Ali

Submitted for the degree of Doctor of Philosophy

Institute of Mechanical, Process and Energy Engineering

School of Engineering and Physical Sciences

Heriot-Watt University

Edinburgh, United Kingdom

August 2013

ABSTRACT

In the present thesis, performance characterisation of a novel non-imaging concentrator, a 3-D elliptical hyperboloid concentrator (EHC) for process heat applications (medium temperature) is investigated. In this investigation, optical and thermal characterisations are extensively carried out for the novel 3-D static concentrator. In the optical study, a 2-D ray tracing simulation was carried out in MATLAB® to predict the optical efficiency of the EHC. The 3-D ray tracing was also carried out in Optis™ software to obtain the optical efficiency. Detailed flux distributions on the receiver are also analysed.

Ray tracing and flux distributions were investigated for different solar incidence angle by varying the system parameters such as concentrator height, receiver diameters and concentration ratio. A parametric analysis of four different system configurations, (I) Elliptical Hyperboloid Concentrator (EHC), (ii) Circular Hyperboloid Concentrator (CHC), (iii) Elliptical Parabolic Concentrator (ECPC) and (IV) Circular Parabolic Concentrator (CCPC) were performed. Based on the parametric analysis it was found that the EHC gives better optical performance compared to other configurations. It was found that the EHC gives better optical performance than others. It was also found that for a wide range of acceptance angles (±30) the optimised concentration ratio of 20× resulted in an optimised optical efficiency of 28%.

For thermal performance, separate indoor and outdoor characterisations were conducted to predict the receiver stagnation and fluid temperatures. In the indoor test, the performances of three different hyperboloid solar concentrators (EHC1, EHC2 and CHC) were investigated. The outdoor performance test was also carried out for a scaled-up version of the developed prototype of the 3-D static elliptical hyperboloid concentrator system (EHC) of 20× concentration ratio. The tests were carried out at Chennai, INDIA to obtain the maximum stagnation temperature and daily performance of the EHC system. It was observed that a maximum temperature of 150°C is obtained as the stagnation temperature. In the daily performance test, the maximum fluid temperature of 90°C was observed. Thus, the developed 3-D static elliptical hyperboloid concentrator system can be effectively used for medium temperature applications.

DEDICATION

Dedicated

To

My Mother

and

My lovely wife

and

My children

ACKNOWLEDGEMENT

I would like to express my deep gratitude to Professor Tapas Mallick my research supervisor, for his patient guidance, enthusiastic encouragement and useful critiques of this research work. I am greatly indebted to my PhD supervisor Tapas Mallick for making this PhD possible. I cannot find the words to express my gratitude for your continuous guidance, encouragement and help during my PhD. Your support and supervision has been invaluable to me.

I would also like to thank Dr. K. S. Reddy, for his advice and assistance during experimental work in IITM Chennai and he was keeping my progress on schedule. I am thankful to the Indian Institute of Technology IITM Chennai for providing the financial support and research facilities during my outdoor experimental work. I would also like to take the opportunity to thank to Dr. Tadhg O'Donovan: your suggestions and guidance have been invaluable. Your expertise and knowledge has always been helpful for me to rectify my mistakes and to learn new things. I am thankful to the School of Engineering and Physical Sciences, Heriot-Watt University for providing the financial support and research facilities during my PhD. I specially thank to my colleagues Dr. Nazmi Sellami, Dr. N. Sendhil Kumar, and Nabin Sharma for their support and great inspiration. And also, I am grateful to all the staff of EPS and specially Aftab, Rebecca, George and Cameron. I cannot forget all technicians Richards, Kenny and Chris in the mechanical engineering workshop for their help in making my experimental hardware. I would like to thank all of the technicians in the mechanical engineering workshop for their help in making my experimental hardware and for their assistance, providing support and help as and when needed setting up the solar energy testing facilities. I would like to express my gratitude to my mother for her support over the long years of study and also my brothers and sister for everything and to my wife for putting up with me throughout the whole process and for her understanding and love. She was always there for me, keeping me focussed and maintaining my perspective on life when things got tough, Thanks to my four children (Moftah, Sajda, Mayar and Sand) for their patience during the busy times of my PhD. My grateful thanks are also extended to all my friends during my PhD study. Finally and above all, greatest thanks and deepest gratitude to almighty Allah, for without him this journey would not be possible.

ACADEMIC REGISTRY
Research Thesis Submission

Name*:*	Imhamed M. Saleh		
School/PGI:	EPS		
Version: *(i.e. First, Resubmission, Final)*	Final	Degree Sought (Award **and** Subject area)	PhD

Declaration

In accordance with the appropriate regulations I hereby submit my thesis and I declare that:

1) The thesis embodies the results of my own work and has been composed by myself
2) Where appropriate, I have made acknowledgement of the work of others and have made reference to work carried out in collaboration with other persons
3) The thesis is the correct version of the thesis for submission and is the same version as any electronic versions submitted*.
4) my thesis for the award referred to, deposited in the Heriot-Watt University Library, should be made available for loan or photocopying and be available via the Institutional Repository, subject to such conditions as the Librarian may require
5) I understand that as a student of the University I am required to abide by the Regulations of the University and to conform to its discipline.

* *Please note that it is the responsibility of the candidate to ensure that the correct version of the thesis is submitted.*

Signature of Candidate*:*		Date:	

Submission

Submitted By (name in capitals):	IMHAMED M. SALEH ALI
Signature of Individual Submitting:	
Date Submitted:	

For Completion in the Student Service Centre (SSC)

Received in the SSC by (name in capitals):			
Method of Submission (Handed in to SSC; posted through internal/external mail):			
E-thesis Submitted (**mandatory for final theses**)			
Signature:		Date:	

TABLE OF CONTENTS

ABSTRACT i
DEDICATION ii
ACKNOWLEDGEMENT iii
TABLE OF CONTENTS v
LIST OF TABLES x
LIST OF FIGURES xi
GLOSSARY xvii
LIST OF PUBLICATIONS .....
CHAPTER 1: INTRODUCTION 1
1.1 Background of Solar Concentrating Thermal Technologies 1
1.2 Concentrating Collector Configurations 2
1.3 Importance of Tracking in Concentrating Collectors 3
1.4 Merits and Demerits of Concentrating Collectors 4
1.4.1 Merits 4
1.4.2 Demerits 5
1.5 Concentration Ratio (*CR*) 5
1.5.1 Geometric Concentration Ratio (CR_g) 5
1.5.2 Optical Concentration Ratio (CR_{Opt}) 6
1.6 State of the Art - Solar Thermal Technology 7
1.6.1 Different Types of Solar Concentrating Collectors 7
1.6.2 Low-Temperature Concentrating Collector 7
1.6.2.1 Compound Parabolic Concentrator (CPC) 7
1.6.2.2 Trumpet Concentrator 9
1.6.3 Medium-Temperature Concentrating Collector 9
1.6.3.1 Parabolic Trough System 9
1.6.3.2 Compact Linear Fresnel Reflectors 11
1.6.4 High-Temperature Concentrating Collector 11
1.6.4.1 Parabolic Dish Systems 12
1.6.4.2 Power / Solar tower systems 13
1.7 Applications of solar thermal collectors 15
1.7.1 Water heating 15

1.7.2 Water desalination 16
1.7.3 Cooking system 17
1.7.4 Drying 17
1.7.5 Process Heat 18
1.8 Review of Solar Concentrators and Receivers 19
1.8.1 Solar Dish Concentrators 19
1.8.2 Solar Trough Concentrators 26
1.8.3 Ray Tracing of Solar Concentrators 27
1.8.4 Receiver and Heat Losses 28
1.9 Motivation for Present Work 29
1.10 Approach 30
1.11 Objective of the Present Work 31
1.12 Organization of the Thesis 31
1.13 Closure 33
CHAPTER 2: DESIGN AND OPTICAL RAY TRACING PROCEDURES FOR STATIC 2-D AND 3-D EHC 34
2.1 Introduction 34
2.1.1 Edge-Ray Method 34
2.1.2 Tailored Edge-Ray Approach 36
2.1.3 Flow-Line Method 36
2.2 Design and Method of Optimisation 37
2.3 Design of a 2-D Hyperboloid Concentrator 37
2.3.1 Theoretical Model of 2-D HC 37
2.3.2 Optical Modelling of the 2-D HC Using Ray Tracing Modelling 39
2.4 Optical Modelling of a 3-D HC Using Ray Tracing Modelling 41
2.4.1 New 3-D Elliptical Hyperboloid Non-Imaging Solar Concentrator 42
2.4.2 Design and Conceptualization of 3-D EHC 44
2.4.3 Material of Elliptical Hyperboloid Concentrator 46
2.5 Ray Tracing Procedure in OptisWorks 47
2.5.1 Modelling the Geometry 47
2.5.2 Surface Definition of Solar Concentrator 47
2.5.3 Modelling of the Source 48
2.5.4 Illuminance Detector 49
2.5.5 Simulation of ray tracing 49
2.5.6 Theoretical Performance Analysis of 3-D HC 50

2.6 Optimisation of the EHC 52
2.7 Closure 53
CHAPTER 3: OPTICAL PERFORMANCE OF A STATIC 2-D AND 3-D EHC 54
3.1 Introduction 54
3.2 Optical Analysis of 2-D Hyperboloid Concentrator 55
3.2.1 2-D Hyperboloid Concentrator 55
3.2.2 Ray tracing Technique for Hyperboloid Concentrator 56
3.2.3 Optical Efficiency of 2-D Hyperboloid Concentrator (2-D HC) 58
3.2.4 Effect of Concentration Ratio on the Optical Efficiency 61
3.2.5 Effect of Variation of Receiver diameter on Optical Efficiency 62
3.3 Optical Analysis of 3-D Hyperboloid Concentrator 65
3.3.1 3-D Hyperboloid Concentrator 65
3.3.2 Effect of Receiver diameter and Concentrator Height on Effective Concentration Ratio 65
3.3.3 Effect of Receiver Aspect Ratios on Optical Efficiency 66
3.3.4 Effect of Concentrator Height on Effective Concentration Ratio and Optical Efficiency 68
3.3.5 Effect of Concentration Ratio on the Optical Efficiency Using Optimum Concentrator Height and Optimum Aspect Ratio 72
3.3.6 Incidence Angle Modifier (IAM) 73
3.4 Effect of Truncation of EHC on the optical performance 74
3.5 Energy Flux Distribution at the Receiver of EHC 76
3.6 Closure 79
CHAPTER 4: COMPARISON OF OPTICAL PERFORMANCE FOR DIFFERENT GEOMETRIC CONFIGURATIONS 81
4.1 Introduction 81
4.2 Different Geometric Configurations 81
4.3 Ray Tracing and Optical Efficiency of Different Geometries 83
4.4 Flux Distribution of Different Geometric Configurations 86
4.5 Energy Absorbed by Receiver 88
4.5.1 Average Energy Absorbed by Receiver of Parabolic and Hyperboloid Concentrator 88
4.5.2 Daily Average Energy Absorbed By Receiver of Parabolic and Hyperboloid Concentrator 90
4.6 Effect of Truncation 91
4.7 Closure 92

CHAPTER 5: FABRICATION AND INDOOR TESTING OF STATIC 3-D EHC 93
5.1 Design and Fabrication of the Static 3-D EHC 93
5.1.1 Optical Analysis of Static 3-D EHC1 94
5.1.2 Fabrication of first Elliptical Hyperboloid Concentrator (EHC1) 95
5.1.3 Measurement of Concentration Ratio of EHC1 99
5.1.4 Inlet and Outlet Temperature of the Receiver 100
5.1.5 Fabrication of Elliptical Hyperboloid Concentrator EHC2 101
5.2 Receivers 103
5.3 Solar Simulator for Indoor Characterisation 105
5.3.1 Design of a Solar Simulator for Characterisation of Solar Systems 105
5.3.2 Fabrication of Solar simulator 106
5.3.3 Manufacturing of the reflectors 107
5.4 Indoor Experimental Testing of Hyperboloid Concentrator 108
5.5 Closure 117
CHAPTER 6: Outdoor Experimental Investigation of 3-D EHC 118
6.1 Introduction 118
6.2 Optical study of EHC 119
6.2.1 Ray tracing of EHC at different incidence angles 119
6.2.2 Effect of the variation of the solar azimuth angle 120
6.2.3 Flux distribution on the receiver area for different azimuth angle 121
6.3 Outdoor Experimental Characterisation of EHC 125
6.3.1 Materials and Equipment that will be used to perform the Experiment 126
6.3.2 Apparatus Required. 126
6.4 Assembling the Components and Conducting the Experiment 126
6.4.1 Components: Hyperboloid Concentrator 126
6.5 Receiver Elliptical Shape 127
6.6 Parameters Measurement 129
6.7 Storage system for EHC 130
6.8 Piping line for circulating the water using CPVC Pipe 133
6.9 Experimental testing of a 3-D EHC 135
6.10 Results and Discussion 136
6.10.1 Solar Radiation on the Receiver 136
6.10.2 Stagnation Testing 137
6.10.3 Thermal Performance Testing 139
6.10.4 Thermal images on the receiver area 140

6.11 Closure 142
CHAPTER 7: Overall Conclusions and Future work 143
7.1 Overall Conclusion 143
7.2 Suggestion for Future Work 146
7.2.1 Suggestion 1: 146
7.2.2 Suggestion 2: 146
7.2.3 Suggestion 3: 148
REFERENCES 149
Appendix A 161
Appendix B 170

LIST OF TABLES

Table 1.1: Comparison of low, medium and high concentrating solar technologies 14
Table 3.1: Variation of Optical Efficiency and Acceptance Angle for Different Concentration Ratio of Hyperboloid Concentrator Height of 0.4 m 61
Table 3.2: Variation of Optical Efficiency of EHC for Different Solar Incidence Angles and Different Concentrator Heights 72
Table 3.3: Optical Efficiency of EHC for Different Solar Incidence Angles and Different Concentration Ratio 73
Table 4.1: Optical Efficiency and Acceptance Angle for Different Solar Concentrator 91
Table 4.2: Average Energy Flux under Normal Incidence Angle for Different Solar Concentrator 91
Table 4.3: Effect of Truncation on Optical Efficiency and Acceptance Angle 92
Table 5.1: Specifications of EHC1 95
Table 5.2: Specifications of CHC 103
Table 5.3: Specifications of EHC2 103
Table 5.4: Properties of the OSRAM HMI 1200 W/SEL lamp [164] 106
Table 6.1: 2-D Dimension of the Receiver Dimension 129
Table 6.2: Installation Conditions of Solar Collectors. 130
Table 6.3: Specifications of Hyperboloid Collector Design. 130
Table 6.4: Dimensions of the Cold Water Storage Tank. 131
Table 6.5: Dimensions of the Outlet Storage Tank (Hot Water Tank) 132
Table 6.6: Dimension of the CPVC Pipe 134

LIST OF FIGURES

Figure 1.1: Possible Concentrating Collector Configurations: (a) Tubular Absorbers with Diffuse Back Reflector; (b) Tubular Absorbers with Specular Cusp Reflectors; (c) Plane Receiver with Plane Reflectors; (d) Parabolic Concentrator; (e) Fresnel Reflector; (f) Array of Heliostats with Central Receiver [1] 3
Figure 1.2: Schematic Diagram of Sun Concentration Geometry [1] 6
Figure 1.3: Basic design of compound parabolic concentrator [15] 9
Figure 1.4: Parabolic trough systems [19] 10
Figure 1.5: Parabolic dish Stirling engine systems [31] 12
Figure 1.6: Solar central receiver plants in Barstow, California [35] 14
Figure 1.7: Solar water heating system[54] 16
Figure 1.8: Solar Bowl in Auroville, India, to produce steam for cooking [43]. 17
Figure 1.9: Photograph of NRG solar dryer [58] 18
Figure 1.10: Paraboloidal Dish Solar Concentrator Developed by Australian National University [71, 72] 21
Figure 1.11: One-sheet 3-D hyperbolic asymmetric concentrators [92] 24
Figure 1.12: Methodology of thesis 32
Figure 2.1: Edge-Ray Principle and CPC [140] 35
Figure 2.2: Schematic of 2-D Hyperboloid Concentrator 39
Figure 2.3: Flow Chart of the MATLAB Simulation Code for Ray Tracing of 2-D HC40
Figure 2.4: Development of 3-D Elliptical Hyperboloid a) Isometric, b) Front View, c) Top View, d) Position of Hyperboloid Branches and e) Four Symmetric Section 44
Figure 2.5: Geometric Parameters of Elliptical Hyperboloid Concentrator 46
Figure 2.6: Geometry of EHC in Optisworks 47
Figure 2.7: Source of Solar Radiation with the 3-D EHC 48
Figure 2.8: (a) Aperture of the Concentrator Detector; (b) Receiver Detector for Incoming and Absorbing Solar Radiation Measurement 49
Figure 2.9: Simulated Ray Tracing and Flux Distribution with Incoming Solar Radiation from Source and EHC 50
Figure 2.10: Flow Chart of Optical Simulation 52
Figure 3.1: 2-D Hyperboloid Curvatures for Different Concentration Ratio 55
Figure 3.2: 2-D Hyperboloid Curvature for Different Concentrator Heights (0.4 m, 0.8 m, 1 m) 56

Figure 3.3: Ray Tracing Diagrams for Concentrator Heights of 0.2 m (top five) and 0.4 m (Bottom Five) for Different Incidence Angles (a) 0°, (b) 15°, (c) 30°, (d) 45° and (e) 60° 57
Figure 3.4: Ray Tracing Diagrams for Concentrator Heights of 1 m for Different Incidence Angles (a) 0°, (b) 15,° (c) 30° and (d) 45° 58
Figure 3.5: Variation of Optical Efficiency with Solar Incident Angle for 2-D Hyperboloid Concentrator for Different Concentration Ratios (5×, 10×, 15×. 20× and 25×) and Different Concentrator Heights 61
Figure 3.6: Variation of Optical Efficiency for Different Geometrical Concentration Ratio and Incidence Angles at Concentrator Height 0.4 m 62
Figure 3.7: Ray Tracing Diagram for Concentration Ratio of 20× Based on Different Receiver Diameters ((a) is 0.05m, (b) is 0.01 and (c) is 0.1 m) and Incidence Angles (0^o, 15^o, 30^o and 45^o) 64
Figure 3.8: Effect of Optical Efficiency on the Receiver Diameter for Different Solar Incidence Angles 64
Figure 3.9: Variation of Effective Concentration Ratio with (H/a) & (H/b) Ratio for Different Incidence Angles 66
Figure 3.10: Variation of the Optical Efficiency for Different Solar Incidence Angles and Different Major and Minor Axis Diameter for A Fixed Concentrator Height and Concentration Ratio 68
Figure 3.11: Variation of the Optical Efficiency for Different Concentrator Heights and Receiver Major and Minor Axis Diameter for Different Incidence Angles 70
Figure 3.12: Variation of Effective Concentration Ratio, When the Source Is Moving Along the Receiver Major Axis Diameter for Different Concentrator Heights (0.1 m to 1 m) and Solar Incidence Angles at Aspect Ratio of 5 and *CR* of 20× 71
Figure 3.13: Variation of Optical Efficiency for Different Concentration Ratio and Incidence Angles at Concentrator Height 0.4 m and Aspect Ratio of 5 73
Figure 3.14: Transversal IAM as Function of the Transversal Angle for Major and Minor Axis at H = 0.4 m & *CR* = 20× 74
Figure 3.15: Variation of Optical Efficiency with Solar Incidence Angles for Different Truncation Heights along (a) Receiver Major Axis, (b) Receiver Minor Axis. 75
Figure 3.16: Variation Of Effective Concentration Ratio with Solar Incidence Angles for Different Truncation Heights Along (a) Receiver Major Axis, (b) Receiver Minor Axis 76

Figure 3.17: Variation of Flux Distribution for Different Geometry Aspect Ratios (a), Along the Receiver Major Axis Diameter (b) and (c) Minor Axis Diameter 78
Figure 3.18: Effect Of Variation of Aspect Ratio of an EHC on (a) 3-D Flux Distribution, (b) Flux Distribution in One Plane (c) Ray Tracing 79
Figure 4.1: Profiles of the Various Geometries (i) Parabolic Geometry Profile (ii) Hyperboloid Geometry Profile 82
Figure 4.2: Different Orientations of the Incidence Angle 83
Figure 4.3: Ray Tracing of Parabolic and Hyperboloid Geometry Profile 84
Figure 4.4: Optical Efficiency of Parabolic Concentrator for Elliptic and Circular Cross Section 85
Figure 4.5: Optical Efficiency of Hyperboloid Concentrator for Elliptic and Circular Cross Section 85
Figure 4.6: Flux Distribution of Parabolic Profile Concentrator for Circular and Elliptic Cross Section 86
Figure 4.7: Flux Distribution of Hyperboloid Profile Concentrator for Circular and Elliptic Cross Section 87
Figure 4.8: Average Energy Absorbed by Receiver of Parabolic and Hyperboloid Concentrator 89
Figure 4.9: Daily Average Energy Absorbed by Receiver of Parabolic and Hyperboloid Concentrator 90
Figure 5.1: Flux Distribution of the Receiver Area for EHC1 when the Concentrator Height of 0.860 m for (a) 3-D Flux Distribution (b) Flux Distribution in One Plane. ... 95
Figure 5.2: Variation of Optical Efficiency with Solar Incidence Angles (In Degrees) For EHC1 95
Figure 5.3: Fabrication Process of the Elliptical Hyperboloid Concentrator (EHC1) 97
Figure 5.4: Assembly of the Elliptical Hyperboloid Concentrator (EHC1) 98
Figure 5.5: Schematic of the Indoor Open Cycle of the EHC1 99
Figure 5.6: Variation of Solar Radiation Intensity at Receiver and Aperture with Time for EHC1 100
Figure 5.7: Variation of Inlet and Outlet Temperature of the Receiver for EHC1 101
Figure 5.8: Prototype of Circular (CHC) and Elliptical Hyperboloid Concentrator (EHC2) 102
Figure 5.9: Aluminium Grooved Flat Receiver 104
Figure 5.10: Copper Coil Tube Receiver 104

Figure 5.11: Comparison of the spectrum of HMI 1200 lamp and AM1.5G sun spectrum 106
Figure 5.12: Dimensions of the Base Plate and Positioning of the Lamps. 107
Figure 5.13: Cross Sectional View of Parabolic Reflector for Each Source Lamp 107
Figure 5.14: Photograph of the In-House Built Solar Simulator at Heriot-Watt University 108
Figure 5.15: Schematic of the Solar Collector CHC with Desalination System 110
Figure 5.16: Schematic of the Solar Collector EHC with Desalination System 110
Figure 5.17 : Experimental Setup for EHC2 for Open Cycle 111
Figure 5.18: Experimental Setup for EHC2 for Water Distillation 112
Figure 5.19: Experimental Setup for CHC for Water Distillation 113
Figure 5.20: Variation of Stagnation Temperature with Time for EHC2 114
Figure 5.21: Photographs of Thermal Imaging Temperature of Flat Grooved Aluminium and Copper Coil Receiver Where (a) Avage Temperature on Groove Receiver Area for EHC2, (b) Temperature Different Along Major Axis (C) Temperature Different Along Major Axis and Minor Axis (d) Temperature Different Along Vertical on Coil Receiver for CHC (e) Temperature Different Along Major Axis and Minor Axis on Coil Receiver for CHC 116
Figure 5.22: Variation of Inlet and Outlet Temperatures with Time for CHC 117
Figure 6.1: Ray Tracing of EHC for Different Incidence Angles (0°, 15°, 30°, 45° and 60°) 119
Figure 6.2: EHC with Variation of Major Axis Aperture 120
Figure 6.3: Variation Of Optical Efficiency with Azimuth and Incident Angles 121
Figure 6.4: Flux Distributions on Plane Angle is 0° and Incidence Variation for 0°-45° 122
Figure 6.5: Flux Distributions on Plane Angle is 15° and Incidence Variation for 0°-45° 122
Figure 6.6: Flux Distributions on Plane Angle is 30° and Incidence Variation for 0°-30° 122
Figure 6.7: Flux Distributions on Plane Angle is 45° and Incidence Variation for 0°-30° 123
Figure 6.8: Flux Distributions on Plane Angle is 75° and Incidence Variation for 0° -15° 123
Figure 6.9: Flux Distributions on Plane Angle is 90° and Incidence Variation for 0° -15° 123

Figure 6.10: Flux Distributions on Centre Line of a) Major Axis and b) Minor Axis for Different Plan (ψ=15°) and Different Incident Angle 123
Figure 6.11: Flux Distributions on Centre Line of a) Major Axis and b) Minor Axis for Different Plan (ψ=30°) and Different Incident Angle 124
Figure 6.12: Flux Distributions on Centre Line of a) Major Axis and b) Minor Axis for Different Plan (ψ=45°) and Different Incident Angle 124
Figure 6.13: Flux Distributions on Centre Line of a) Major Axis and b) Minor Axis for Different Plan (ψ=45°) and Different Incident Angle 124
Figure 6.14: Flux Distributions on Centre Line of a) Major Axis and b) Minor Axis for Different Plan (ψ=75°) and Different Incident Angle 125
Figure 6.15: Flux Distributions on Centre Line of a) Major Axis and b) Minor Axis for Different Plan (ψ=90°) and Different Incident Angle 125
Figure 6.16: Fabrication of The 3-D Elliptical Hyperboloid 127
Figure 6.17: Receivers with High Absorptive Without and With Coating 128
Figure 6.18: Measured Reflective Coefficient for Coated and Uncoated Receiver 129
Figure 6.19: Photograph of the Inlet Storage Tank (Cold Water Storage) for the System 131
Figure 6.20: Photograph of the Motor and Pump Used in the Experimental Setup 132
Figure 6.21: Photograph of the Storage Tank for Hot Water (Outlet Tank) 132
Figure 6.22: Stand for the Circulating Pipe 133
Figure 6.23: Dimension Definitions of the CPVC Pipe 134
Figure 6.24: Photograph of the Experimental EHC Apparatus located at IITM Chennai 135
Figure 6.25: Schematic of the Experimental EHC at IITM Chennai 135
Figure 6.26: Comparison of Experimental and Numerical Receiver Performance Optical Ray Tracing ((a)-(c)) Thermal Imaging ((d)-(f)) of Receiver Aperture for Different Incident Angles (a, d) 0°(b, e) 15° (c, f) 30° 137
Figure 6.27: Stagnation Temperature of Receiver 138
Figure 6.28: Image Thermal Shown the Stagnation Average Temperature and Solar Radiation of the Receiver for 1st Feb. 2013. 138
Figure 6.29: Inlet and Outlet Temperature of Fluid for Flow Rate of 0.5 kg/min on ... 140
Figure 6.30: Inlet and Outlet Temperature of Fluid for Flow Rate of 1kg/min on 3rd February 2013 140
Figure 6.31: Photograph of the Usage of Thermal Imaging Camera 141
Figure 6.32: Experimental Thermal Imaging of Receiver Surface Area ((a)–(e)) 141

Figure 6.33: Experimental Thermal Imaging of Concentrator Surface 142
Figure 7.1: Geoemtry of Square Hyperboloid Concentrator..... 147
Figure 7.2: Variation of Optical Efficieny with Solar Incidence Angle 147
Figure 7.3: Varaiation of Absorbed Energy with Solar Incidence Angle..... 148
Figure 7.4: Flux Distribution of the Square Hyperboloid Concentrator..... 148

GLOSSARY

Nomenclatures

a	Length of receiver semi-major axis (m)
A	Length of aperture semi-major axis (m)
A_p	Area of aperture (m^2)
A_r	Area of receiver (m^2)
b	Length of receiver semi-minor axis (m)
B	Length of aperture semi-minor axis (m)
CR	Concentration ratio
CRg	Geometric concentration ratio
CR_{Opt}	Optical concentration ratio
C_{eff}	Effective concentration ratio
f_1	Focus number 1
f_2	Focus number 2
H	Height of the concentrator (m)
I_i	Intensity of a single ray (W/m^2)
I_o	Total intensity at the aperture (W/m^2)
J	Number of reflections
M	Maximum number of reflections
N	Number of rays
n	Normal to the surface
r_{inc}	Incident ray vector
r_{reft}	Reflected ray vector
y_1	Coordinates of the endpoints of the major axis
y_2	Coordinates of the endpoints of the minor axis

Greek symbols

Θ	Solar incidence angle (degrees)
Φ	Solar acceptance angle (degrees)
η_{opl}	Optical efficiency of the concentrator
P	Internal reflectivity from hyperboloid sides
Ψ	Solar azimuth angle (degrees)
Ω	Angles between different planes and the major axis (degrees)
Φ	Flux (W/m^2)

Abbreviations

2-D	Two Dimensional
3-D	Three Dimensional
CPC	Compound Parabolic Concentrator
CCPC	Circular Parabolic Concentrator
ECPC	Elliptical Parabolic Concentrator
CLFR	Compact Linear Fresnel Reflector
ANU	Australian National University
HPC	Hyper Parabolic Concentrator
EHC	Elliptical Hyperboloid Concentrator
EHC1	Elliptical Hyperboloid Concentrator (HWU)
EHC2	Elliptical Hyperboloid Concentrator (China)
CHC	Circular Hyperboloid Concentrator (China)
PTC	Parabolic Trough Collector
HTF	Heat transfer fluid
DSG	Direct steam generation
ABC	Australian Broadcasting Corporation
IITM	Indian Institute of Technology Chennai
HWU	Heriot Watt University

LIST OF PUBLICATIONS

Journal Articles:

- **Imhamed M. Saleh Ali**, Tadhg S. O'Donovan, K.S. Reddy, Tapas K. Mallick, An optical analysis of a static 3-D solar concentrator, Solar Energy 88 (2013) 57–70
- **Imhamed M. Saleh Ali**, T. Srihari Vikram, Tadhg S. O'Donovan, K.S. Reddy, Tapas K. Mallick, Design and Experimental Analysis of a Static 3-D Elliptical Hyperboloid Concentrator for Process Heat Applications. Solar Energy under review.

Conference Proceedings:

- **Imhamed M. Saleh Ali**, Peter Kew, Tadhg S. O'Donovan, K.S. Reddy, Tapas K. Mallick, Optical performance evaluation of a 2-D and 3-D novel hyperboloid solar concentrator, in: World Renewable Energy Congress, Abu Dhabi 2010

- **Imhamed M. Saleh Ali**, Tadhg S. O'Donovan, K.S. Reddy, Tapas K. Mallick (2011),Optical study of a 3-D elliptical hyperboloid concentrator, 30th ISES Biennial Solar World Congress 2011 Germany, SWC 2011, Volume 4, pages 2672-2678.

- **Imhamed M. Saleh Ali**, Tadhg S. O'Donovan, K.S. Reddy, Tapas K.Mallick, Comparison of Optical Performance of 3-D Solar Concentrator for Circular and Elliptical Absorber, World Renewable Energy Forum, WREF 2012, Including World Renewable Energy Congress XII and Colorado Renewable Energy Society (CRES) Annual Conference, Volume 1, pages 181-188.

CHAPTER 1: INTRODUCTION

1.1 Background of Solar Concentrating Thermal Technologies

Because of the energy crisis, the need to use alternative renewable energy sources such as solar and wind energy has gained lots of momentum in many developing countries. The research and development activities in solar energy include investigations into the feasibility of concentrating solar power and concentrating photovoltaic, as an alternative to existing conventional fossil fuels. There are three main reasons for using a solar concentrator:

1. To increase the delivery temperature in order to achieve a thermodynamic match between temperature level and task. The task may be to operate thermionic, thermodynamic, or other higher temperature devices.
2. To improve thermal efficiency by reducing the heat loss area relative to the receiver area. There would also be a reduction in transient effects, since the thermal mass is usually much smaller than that for a flat plate collector.
3. To reduce cost of production by replacing an expensive receiver by a low cost reflecting or refracting area.

Concentrating solar power converts solar radiation to thermal energy and then to electricity and concentrating photovoltaic directly converts solar radiation to electricity. Concentrating solar power is an effective way for the production of non-domestic hot water [1] improved steam cycles [2], electricity production [3], cooking and photovoltaic electricital applications [4, 5]. These days, the hot water production for process heat applications requires very high temperatures from 100°C to 200°C, which can be easily produced through solar concentrators. By decreasing the concentrating area from which heat losses occur, energy flux and temperatures can be increased. This area reduction is ensured by interposing an optical device between the radiation source and the energy absorbing surface or receiver. Technically, it is known as concentration ratios (i.e. the ratio of collector aperture area to absorber or receiver area, representing the factors of the radiation flux increase on the energy-absorbing surface). Normally, it can vary over several orders of magnitude and depends upon the imaging and non-imaging solar systems. Imaging concentrators are preferred for achieving high concentration ratio. For low and medium concentration ratio, the non-imaging concentrators are generally used.

Imaging or non-imaging concentrators are in the form of reflectors or refractors, which may be continuous or segmented. Receivers in turn can be convex, flat, or concave and can be either covered or uncovered. Many tracking modes are possible. For imaging concentrators, tracking modes are required to track the sun continuously throughout the day. In non-imaging concentrators, a prescribed illumination pattern of radiation is produced on the receiver or flat surface, where heat is transferred to other fluid or object. In this type of concentrator, tracking systems are normally not used. Many designs of imaging and non-imaging concentrators were proposed for this purpose. The design of imaging or non-imaging concentrators and associated receivers is the main challenge in solar system design. This is because increasing the concentration ratio is equivalent to increasing temperatures at which energy can be delivered and thus increasing optical system requirements for precision in optical quality and their positioning. At the highest range of concentration (with correspondingly highest precision of optics), study of concentrating collectors materials properties are important.

1.2 Concentrating Collector Configurations

Radiation flux on receivers may be increased by many concentrators of various types. They can be reflectors or refractors, cylindrical to focus on a "line" or circular to focus on a "point". Receivers can be flat, concave, or convex. Figure 1.1 shows examples of six concentrator configurations. The first two (figure 1.1(a), (b)) are evacuated tubes arrays with cylindrical absorbers spaced apart, and back reflectors to direct radiation onto the area between the tubes to the absorbers. The first configuration uses a flat diffuse back reflector (figure 1.1 (a)), while the second uses a one-cusp-shaped specular reflector (figure1.1 (b)). The configuration shown in figure1.1 (c) has a plane receiver with plane reflectors at the edges to reflect additional radiation onto the receiver. The concentration ratios of this configuration type are low, with maximum value of less than 4. Some of the diffuse components of radiation incident on the reflectors would be absorbed at the receiver. These collectors can be viewed as flat-plates with augmented radiation. Figure 1.1 (d) shows a parabolic shaped reflector, which could have a cylindrical surface (with a tubular receiver) or a surface of revolution (with a spherical or hemispherical receiver). Cylindrical collectors of this type have been studied in some detail and are being applied [6]. The continuous parabolic reflector can be replaced by a Fresnel reflector, a set of flat reflectors on a moving array as shown in figure 1.1 (e), or by its refracting equivalent. The facets of the reflector can also be individually mounted and adjusted in position as shown in figure 1.1 (f). Large arrays of heliostats of this

type, with receivers mounted on a tower, are the basis of designs of "central receiver" collectors. For the concentrators shown on figure 1.1 (c)-(f), single-sided flat receivers may be used (if the receiver is not "inside" of the reflector). Cylindrical, hemispherical, or other convex shapes and cavity receivers may also be possible.

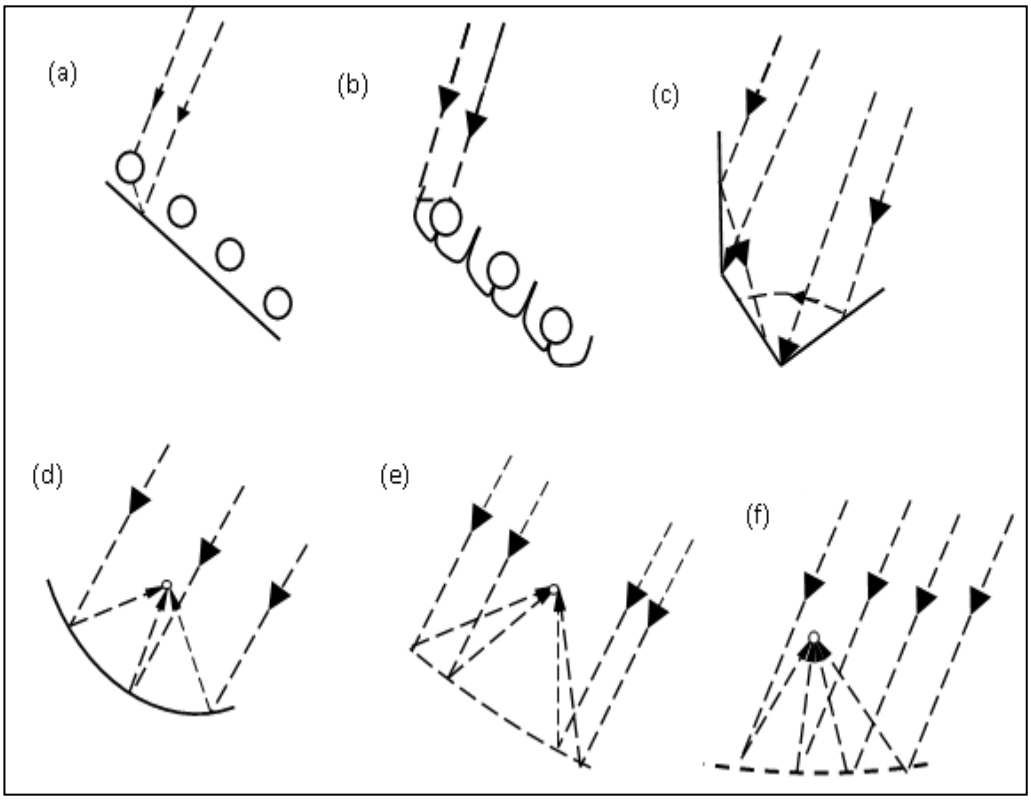

Figure 1.1: Possible Concentrating Collector Configurations: (a) Tubular Absorbers with Diffuse Back Reflector; (b) Tubular Absorbers with Specular Cusp Reflectors; (c) Plane Receiver with Plane Reflectors; (d) Parabolic Concentrator; (e) Fresnel Reflector; (f) Array of Heliostats with Central Receiver [1]

1.3 Importance of Tracking in Concentrating Collectors

In general, concentrators with receivers much smaller than the aperture (the plane opening of the concentrator through which the solar radiation passes) are effective only on beam (direct) radiation. Therefore it becomes evident that the incidence angle of the beam radiation on the concentrator is important and thus sun tracking will be needed for these collectors. A number of orienting mechanisms have been designed in order to move focusing collectors in such a way that the incident beam radiation gets continually reflected to the receiver. The motions needed to accomplish the sun tracking vary according to the design of the optical system, and a particular resultant motion may be performed by more than one system of component motions. Linear (e.g. cylindrical) optical systems constantly focus beam radiation onto the receiver while the sun is in the

central plane of the concentrator (the plane, including the reflector's focal axis and the vertex line). These collectors may be rotated about a single rotation axis, which can be north-south, east-west, or inclined and parallel to the Earth's axis (in which case the rate of rotation is 15°/h). Reflectors that geometrically represent surfaces of revolution (e.g. in circular concentrators) optically are oriented in such a way that their axis is in line with the sun and it thus must be able to move about two axes. These axes may be horizontal and vertical, or one axis of motion might be inclined so that it is parallel to the earth's axis of rotation (a polar axis) and another one perpendicular to it. Orientation systems shall provide adjustments, which are continuous or nearly continuous, whereas movement of the collector has to compensate for the changing position of the sun.

For some linear low concentration collectors it is possible to intermittently adjust their position, with weekly, monthly, or seasonal changes possible for some designs. Continuous orientation systems may be based on manual or mechanized operation. Manual orientation systems depend on the observations performed by operators and their skills at making the necessary corrections. If concentration ratios are not too high and if labour costs are not prohibitive, then this may be adequate for some purposes. Mechanised orientating systems can be sun-seeking or programmed ones, whereas the sun-seeking ones employ detectors in order to determine system misalignment.

1.4 Merits and Demerits of Concentrating Collectors

1.4.1 Merits

As compared with the flat-plate collector the advantages of concentrating collectors over flat-plate collectors are listed below [3]:

1. A higher thermodynamic efficiency can be reached in a concentrating collector as compared with flat-plate collector. The working fluid in a concentrating collector system can produce higher temperatures that compared to the flat-plate system.
2. In a concentrating collector system it is possible to achieve a thermodynamic match between temperature level and task. In a concentrating collector system the heat loss relative to the receiver is a small due to an increase in the thermal efficiency
3. The cost per unit area of a concentrating collector system is about 10% less than that of a flat-plate collector because the reflecting surfaces require less material

4. The concentrating collector is economically viable because of the relatively small area of receiver per unit of collected solar energy. Selective treatment and vacuum insulation can also reduce the amount of heat loss.

1.4.2 Demerits

However, due to high solar energy flux at the receiver, key concerns of the concentrating systems are:

1. Depending on the concentration ratio, concentrating collector systems collect small amount of diffuse solar radiation.
2. The concentrating collector system requires some form of tracking system so that the collector will be able to follow the position of the sun.
3. The solar reflecting surfaces may require periodic cleaning and refurbishing because they may lose their reflectance with time if not well maintained.

1.5 Concentration Ratio (*CR*)

Concentration ratio is defined as the amount of solar flux received by the absorber compared to the incident flux. It is the factor by which radiation flux is increased on the absorber to the aperture of the solar collector system. It is important to increase the radiation flux by optical focusing if there is a need to generate high temperature. This can be obtained by using a series of devices that cover the range of *CR* from about 2 up to an order of 1000. The angle of acceptance of a focusing collector decreases with increasing concentration ratio. Therefore most concentrating collectors must track the sun with a degree of precision that increases with concentration ratio. There are two definitions of concentration ratio:

1. Geometric concentration ratio
2. Optical concentration ratio

1.5.1 Geometric Concentration Ratio (CR_g)

Geometric concentration ratio is the extent to which the aperture area of the receiver is reduced to that of the concentrator (as shown in figure 1.2) and it can be expressed as;

$$CR = \frac{A_a}{A_r}; \qquad \text{For flat plate } CR_g = 1 \text{ and for concentrators } CR_g > 1 \qquad (1.1)$$

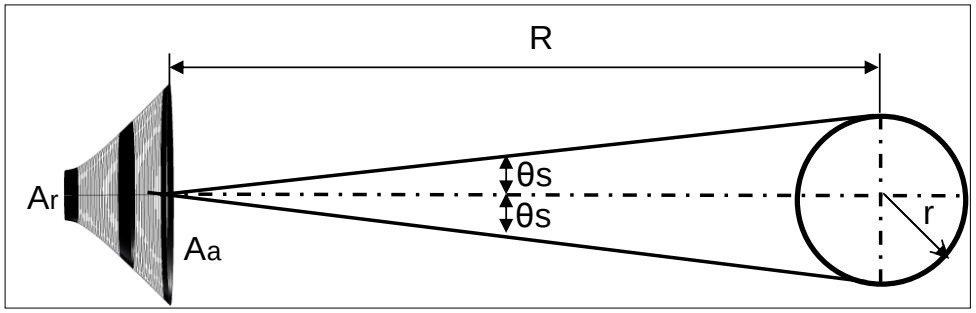

Figure 1.2: Schematic Diagram of Sun Concentration Geometry [1]

A fundamental trade-off exists however, between increasing the geometric concentration ratio and reducing the cost of the collector because collectors with high concentration ratios must be manufactured precisely. If the concentrator is perfect, the radiation from the sun on the aperture (and thus also on the receiver) is the fraction of the radiation emitted by the sun which is intercepted by the aperture. The maximum concentration ratio for 2-D and 3-D concentrators based on the half acceptance, θs, can be obtained as:

$$CR_{2D} = \frac{1}{\sin \theta s} \qquad \text{(2-D)} \qquad (1.2)$$

$$CR_{3D} = \frac{1}{\sin^2 \theta s} \qquad \text{(3-D)} \qquad (1.3)$$

θs = 0.27°, the maximum possible concentration ratio for circular concentrators 3-D is 45,000, and for linear concentrators 2-D the maximum concentration ratio is 212[1].

1.5.2 Optical Concentration Ratio (CR_{Opt})

An optical concentration ratio is defined as the ratio of average energy flux on the receiver to the aperture of concentrator. The energy flux on the absorber surface is not generally homogeneous; the average of the thermal radiation on the receiver is considered. In another approach local flux concentration ratios on the receiver can be defined, which state the ratio of the flux at any point of the absorber to that at the aperture. Optical concentration ratio is termed as 'suns'. If the flux on the receiver is 10 times the flux on aperture, the concentration ratio is termed as 10 suns.

$$CR_{opt} = \frac{I_{Flux.receiver}}{I_{flux\ Incident}} \qquad (1.4)$$

Where $I_{flux,\ receiver}$ is the flux on the receiver area.

$I_{flux,incident}$ is the flux on the aperture area.

1.6 State of the Art - Solar Thermal Technology

Solar Thermal Technology is one of the effective ways of harnessing solar energy for thermal energy. Solar thermal collectors are classified as low-, medium-, or high-temperature collectors. Low-temperature collectors are flat plates generally used to heat the water or fluid for swimming pool purpose. Medium-temperature collectors are also usually flat plates but are used for heating water or air for residential and commercial use. High temperature collectors are used to concentrate sunlight using reflector and lenses and are generally used for electric power production. The important applications of solar thermal technology are: HVAC, (Heating Ventilation and air condition), solar air heat, solar chimney, solar air conditioning; solar drying; solar cooking; solar distillation; solar water heating systems; solar steam generation systems. Among all the applications, solar steam generation systems offer efficient and viable paths for the large scale use of electrical energy. Mainly concentrating collectors are used in the steam generation system.

1.6.1 Different Types of Solar Concentrating Collectors

Concentrating collectors absorb direct solar radiation over a large area and focus it onto a small absorbing area. As a result of solar radiation being focused on a small absorbing area, the intensity of solar energy is magnified. However, the design of concentrating collector requires mechanical equipment that constantly places the collectors towards the position of the sun and keeps the absorber at the point of focus. Typical concentration ratios are in the range of 100 to 10,000. Based on the concentration ratio, the low, medium and high surface temperature is achieved at the focal receiver. Depending on the temperature value, the collectors are classified as low-temperature, medium-temperature or high-temperature collectors. A detailed description is discussed below.

1.6.2 Low-Temperature Concentrating Collector

Low-temperature collectors assume the form of flat plate collectors that operate at a ‘stagnation temperature’ of approximately 80°C. They are used for collecting solar radiation to heat air and water for domestic and industrial applications including space heating, desalination, solar cooking and crop drying.

1.6.2.1 Compound Parabolic Concentrator (CPC)

This type of thermal collector uses a CPC to focus solar radiation on an absorber. A CPC consists of two different parabolic reflectors that are capable of reflecting both

direct and diffuse solar radiation and focus it onto the absorber. A CPC reflector shape can be designed in different ways according to the shape of the absorber. Compound parabolic concentrator designs makes use of the fact that when the rim of a parabola is tilted towards the sun, the rays will not be concentrated at a point but are reflected below the focus. This design is called a non-imaging concentrator since the rays are no longer concentrated at a single point. A receiver is placed in the region below the focal zone that will trap sun rays coming from any angle between the focal lines of the two parabola segments. Receivers can be made of flat plates at the base of the intersection of the two parabolas, or a cylindrical tube that passes through the region below the focus. The basic design of a CPC is shown in figure 1.3. There are two basic designs of CPC collectors: the symmetric and the asymmetric. These designs usually use two types of absorbers: a fin type with a pipe or a tubular absorber [7-11].

Buttinger et al. [12] developed a new flat stationary (non-tracking) evacuated CPC collector for process heat applications could achieve temperatures in the range of 120-150°C. A prototype tested under atmospheric temperature achieved an efficiency of 50% and has claimed that the system shows great potential for solar process heat supply. Hsieh [13] developed mathematical formulations to study thermal processes in a compound-parabolic concentrator. Four nonlinear, simultaneous equations were derived to predict heat exchange among various components in the system. Test results indicated that, because of the high thermal resistance between the receiver jacket and the envelope, the collector performance is quite stable and is nearly independent of many parameters tested. The efficiency of the collector was shown to be high and shows only a very slight drop at high operating temperatures. Jadhav et al. [14] performed experimental studies on a CPC collector and suggested a design improvement without reducing the concentration ratio. A prototype was developed and tested for its performance and achievable temperatures.

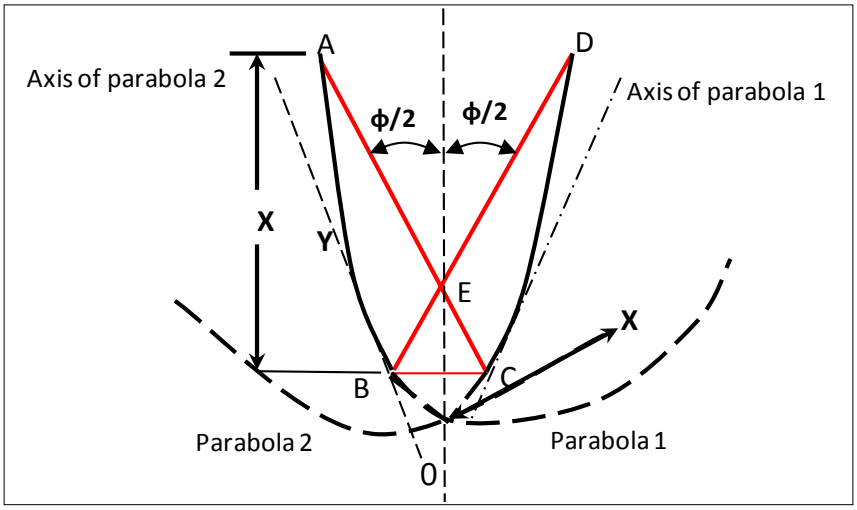

Figure 1.3: Basic design of compound parabolic concentrator [15]

1.6.2.2 Trumpet Concentrator

A trumpet concentrator is one of the ideal non-imaging concentrators discovered by O'Gallagher [16]. The trumpet is composed of a hyperboloid of revolution with an asymptotic angle that must be at least as large as the rim angle to intercept all the radiation from the primary. In practice, the trumpet is truncated by widening its asymptotes several degrees above the rim angle. Shading of the trumpet can also be minimised by truncating the reflector at the height at which the flux reflected by the primary is equal to that of the sunlight striking the back surface. It has a number of advantages over CPCs: short focal ratio geometries; the trumpet's effective aperture is in the same plane as the physical exit aperture; it has relatively low reflection losses [16] and no skew-ray loss at all.

1.6.3 Medium-Temperature Concentrating Collector

In medium-temperature collectors, normally evacuated type flat plate collectors are employed for producing hot water for residential and commercial use in the temperature range of 100°C to 400°C [17]. The efficient conversion of solar radiation to heat at these medium temperatures range requires the use of concentrating or evacuated solar collector's types. The well-known medium temperature concentrators are parabolic trough systems, linear Fresnel reflectors and Trumpet Concentrators

1.6.3.1 Parabolic Trough System

Parabolic troughs are "U" shaped concentrators that use linear parabolic mirrors to concentrate sunlight onto a receiver tube that is positioned along its focal line (as shown in figure 1.4). Energy of solar radiation is absorbed by a fluid in pipes located along the

focal line. To reduce heat loss a transparent glass tube is used to envelope the receiver tube [18]. The parabolic trough uses single-axis or dual-axis tracking respectively. The concentration ratio of the parabolic trough system is in the range 30-100 and the temperature at the receiver can be as high as 400°C. The trough concentrator allows the production of cost effective process heat or electricity with energy provided by direct solar radiation. Many troughs placed in parallel rows are called a "collection field". Trough designs can incorporate thermal storage-setting apart from the heat transfer fluid hot phase; this allows electricity generation for several hours into the evening. Optical efficiency of parabolic trough collectors is less than that of flat-plate collectors because the shape of the parabola can never be perfect and also the reflectivity of the mirrors is always less than 100%. This system is currently used in some commercial solar thermal power generation plants.

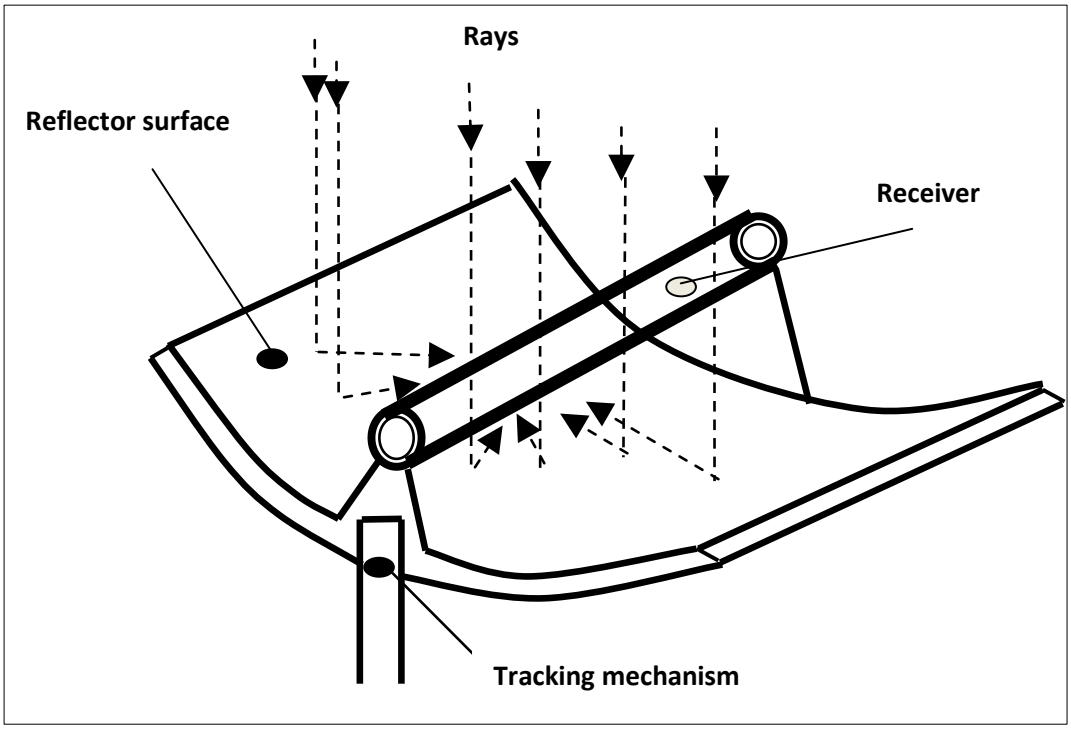

Figure 1.4: Parabolic trough systems [19]

The most recent development in the design of parabolic trough systems is the design and manufacture of Euro trough, a new Parabolic Trough Collector (PTC), in which an advanced lightweight structure is used to achieve cost efficient solar power generation [20, 21]. The best known application of parabolic trough collectors is for power generation and one example is the 354 MWe of the SEGS plants in California [22] . For these systems, troughs of approximately 6 m aperture width have been used to heat thermal oil up to 400°C. The heat generated is used to produce steam in a turbine to

generate electricity. The concentration ratio of these collectors is approximately 26. Smaller parabolic troughs, with concentration ratios between 10 and 15, can operate at temperatures between 100°C and 250°C. The aperture width of these small troughs range from 50 cm to 2.3 m. Parabolic trough collectors are also used in industrial processes to produce heat at a temperature range between 100°C and 130°C. They are also used to generate steam either directly, using direct steam generation mode or indirectly, using an indirect fired steam generator. They are also used for driving absorption chillers, either single or double-stage machines.

1.6.3.2 Compact Linear Fresnel Reflectors

The Compact Linear Fresnel Reflector (CLFR) is a solar concentrator designed for use in large-scale thermal power stations [23]. It consists of a series of long, narrow, shallow-curvature (or even flat) mirrors to focus solar energy onto one or more linear receivers positioned above the mirrors. It produces steam by 'direct steam generation', which is to say that steam is generated directly in pipes rather than through the use of solar heated oil and a heat exchanger. The mirrors are individually motorised to track the sun daily from east to west. Above the mirrors, a linear absorber is located and contains a bank of high-pressure water pipes onto which the solar radiation is focused. The absorber pipes are contained within an inverted trapezoidal cavity with a glass cover and rock wool-insulated steel top and sides; this cavity acts to reduce radiative losses and largely eliminates convective losses [24]. These systems aim to offer lower overall costs by sharing a receiver between several mirrors using the line-focus geometry with one axis for tracking [25]. The varying solar irradiation levels can cause problems in direct steam generation systems. If superheated steam is being generated, then there are (spatial) thermal gradients along the pipe; when irradiation varies, these thermal gradients move along the pipe causing local pipe temperature to vary quite rapidly. This can lead to high stresses and metal fatigue.

1.6.4 High-Temperature Concentrating Collector

High-temperature collectors concentrate sunlight for the purpose of electrical power generation and employ mirrors or lenses. These collectors reflect and concentrate direct insolation by sun-tracking mirrors called collectors or heliostats. Some modern solar radiation concentration systems have maximum concentration factors in the 1500-5000 range and can provide high-temperature solar thermal power up to a few hundred kiloWatts [26, 27]. The concentrated solar radiation is focused upon a solar receiver,

where maximum temperatures can exceed 1500°C depending upon the configuration of the solar concentrating system [28]. Concentrated solar high-temperature heat has the potential to produce hydrogen from water via thermo-chemical means [29]. Among several solar high-temperature collector types; parabolic dish and solar tower systems are popular. Normally, for high temperature production, cavity type receivers are preferred [30].

1.6.4.1 Parabolic Dish Systems

Parabolic dish-engine systems use a collection of mirrors made from stretched membranes or flat glass facets to form a parabolic surface that focuses solar radiations onto a receiver located at the focal point of the dish. The parabolic dish collector has a mirror-like reflector and an absorber at the focal point. Low start-up losses and high optical efficiency make dish-engine systems the most efficient of all solar technologies. The dish system is primarily made up of a collector, a receiver and an engine. The dish-engine system operates by collecting and concentrating the solar energy using the dish shaped mirror-like collectors onto a receiver that absorbs the energy and transfers it to the engine which is attached to the receiver tube. The engine then converts the heat energy to mechanical energy which is used to generate electricity. The view of parabolic dish Stirling engine systems is shown in figure 1.5.

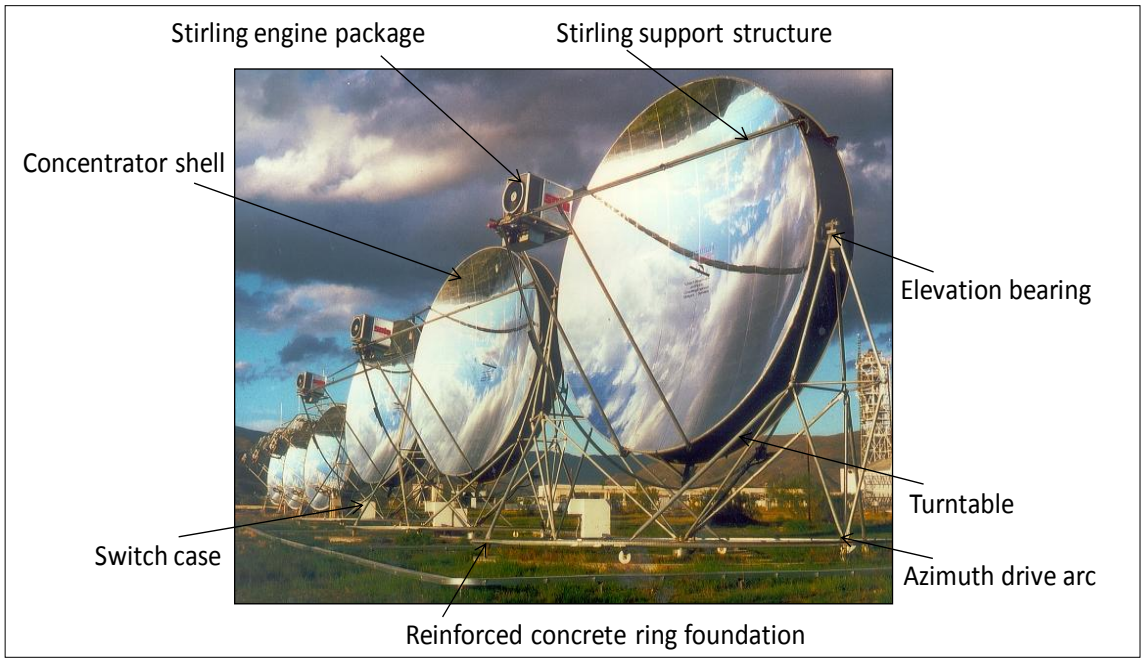

Figure 1.5: Parabolic dish Stirling engine systems [31]

In most high-temperature concentrating collectors, there is a need for continuous tracking of the sun because the collectors can only focus and concentrate the direct solar radiation; it is therefore imperative for the system to always follow the position of the sun. If the orientation of the collector is east-west the concentrator requires approximately ($\pm 30^{o}$ /day motion), while if the orientation is north-south it requires approximately ($\pm 15^{o}$ /day motion) [32]. A parabolic dish system therefore requires a computer to track the position of the sun. The concentration ratio of parabolic dish systems range from 1000 to 1500 and they can generate temperatures of up to 1000^{o}C at the receiver. They can also achieve the highest efficiency for converting solar energy to electricity in the small capacity range. The greater concentration is achievable with dish type concentrators. However, this requires two dimensional tracking, which can be expensive. Stirling and Brayton cycles (turbines) are currently the engines under design consideration for these applications. There are several other prototype dish-engine systems that range in output size from 7 to 25kW that have been deployed in the USA. In 1984, a 29% net efficiency was measured at Rancho Mirage, California, this was generated by a Stirling engine based parabolic dish system and it holds the world record for converting sunlight into electricity. In 2008 Stirling Energy Systems achieved a record 31.25% net efficiency.

1.6.4.2 Power / Solar tower systems

Power tower systems also referred to as the central receiver systems, use a field of large mirrors called heliostats that follow the position of the sun and concentrate its energy onto a receiver mounted on top of a high tower. A computer is used to keep the mirrors aligned so the reflected rays of the sun are always aimed at the receiver. The power tower system usually has concentration ratios of 300-1500 [33], and the maximum temperature of the receiver can be up to 1500°C [34]. The first power tower system, Solar One was built in the mid-1980s in southern California, United States; used water as the heat-transfer fluid to generate steam that powered 10MW steam turbine [34]. In 1992, the aptly named Solar Two was developed in pilot test plants such as 59 MW Solar Two plant in Barstow, California (as shown in figure 1.6). The technology used molten salt as both the heat-transfer fluid and energy storage medium. The molten salt was pumped from a "cold" tank and cycled through the receiver, where it was heated and returned to a hot tank. The hot salt could then be used to generate electricity when needed. The summary of low-, medium- and high-temperature collectors system is given in Table 1.1.

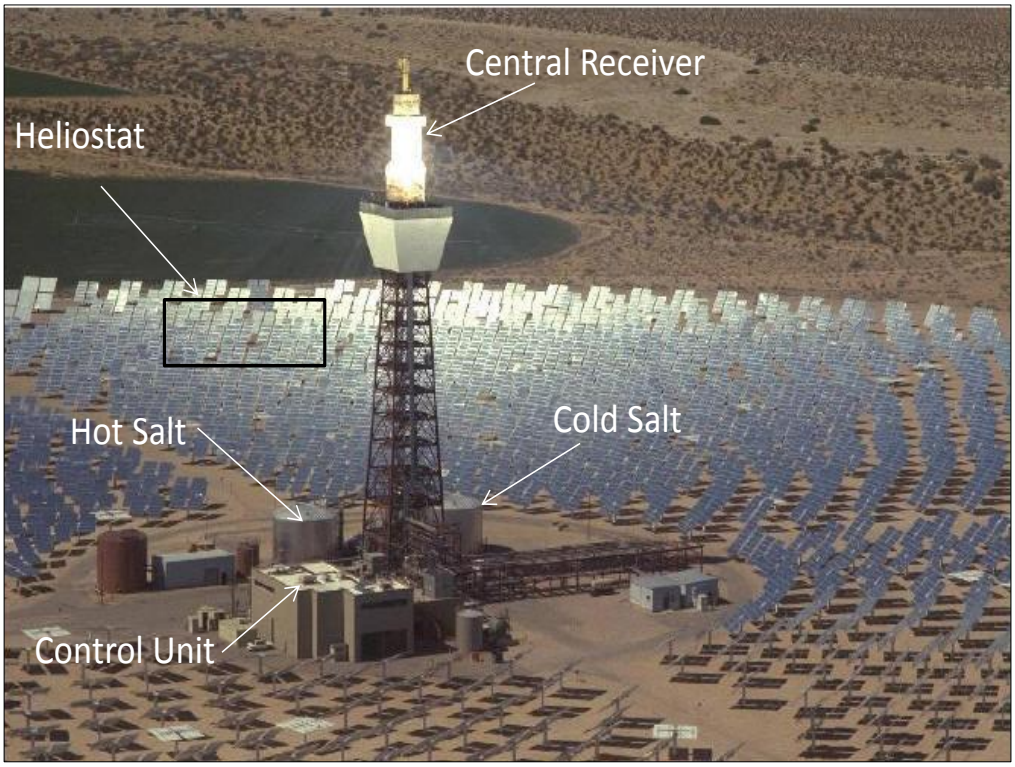

Figure 1.6: Solar central receiver plants in Barstow, California [35]

Table 1.1: Comparison of low, medium and high concentrating solar technologies

Technology	Tracking axes	Concentration Ratio Range	Operating Temperature (K)	Maximum Conversion Efficiency (%)
Flat–plate Evacuated tube	None	1	Up to 75 Up to 200	30-50
Parabolic trough	1	8-80	533-673	56
Compact linear Fresnel reflectors	1	8-80	533-673	56
Parabolic dish	2	800-8000	773-1473	80
Soar power tower	2	600-1000	773-1073	73

The double concentration system is also under investigation. It implements a solution revolving around the concept of the reflective solar tower, with beam-down optics. In addition to a heliostat field, it comprises of a modified central tower, called a 'reflective tower', and a number of secondary ground concentrators fitted with receivers. Thus, in comparison with classical central tower systems, the optical path of the reflective tower is augmented to include a special hyperboloid reflector, reflecting downwards the beams coming from the radiation transmitted by the heliostats located in the field around the tower. This system was proposed by Rabl [36] and further investigated by Winter,

Sizmann et al. [37]. The concentration factor for double-concentration systems could reach the 500-10000 range [38], while the receiver on the ground can achieve temperatures exceeding 1300°C. The idea of a reflective solar tower is based on inverting the path of the solar rays originating from a heliostat field to a solar receiver that can be placed on the ground. This solution consists of reflecting each ray oriented at one of its foci to its second focus and employs two shapes of surfaces: one, the ellipsoid, is concave, and the hyperboloid is convex (with two sheets). The optical performances of these types of reflectors with the hyperboloid surface represent a superior reflector [39]. They are usually very large (generally more than 10 MW), they thus benefit from economies of scale [40].

1.7 Applications of solar thermal collectors

A simple and efficient ways to harness solar energy is the conversion to solar thermal energy for different applications such as water heating [34], water pumping [41], water desalination [42], air conditioning [43], cooking [44, 45], drying [46] and industrial process heat [47, 48]. Each of these applications is discussed in this section.

1.7.1 Water heating

One of the most straightforward ways to use solar energy is in water heating systems. The solar water collectors are unique heat exchangers that convect solar radiation energy to the fluid flowing through tubes [49]. The main component of any solar water heating system is the solar collector, which absorbs the incident solar radiation, transforms it into heat, and transfers this heat to a working fluid such as water, air or oil flowing through the collector. One of the most important applications of the solar thermal energy is the production of hot water [50]. The best way to improve the efficiency of solar water heaters is using solar selective coatings to maximise the solar radiation on the collectors [51, 52]. In solar water heaters, where materials with high thermal conductivity such as copper are used, it is reported that materials with good thermal conductivity used for tubing like copper, aluminium a solar selective coating is always necessary for the best outcome [53]. Efficient SWHS require good spectral selective coatings. A typical solar water heating system is shown in figure 1.7.

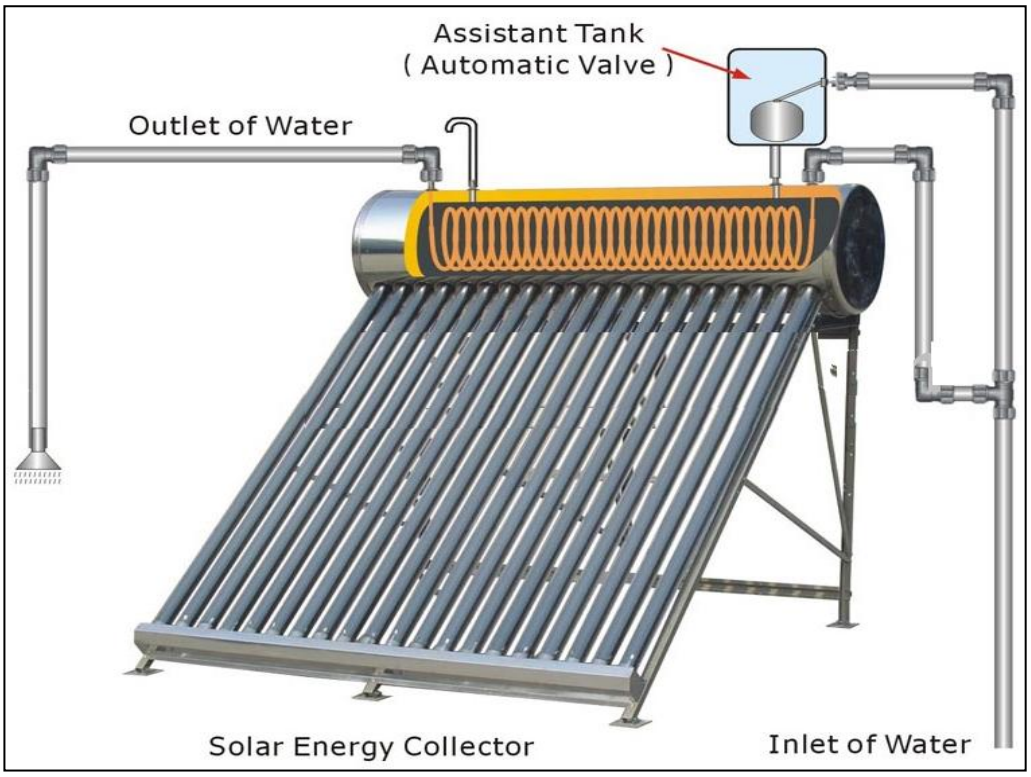

Figure 1.7: Solar water heating system[54]

1.7.2 Water desalination

In the present world, supply of potable water is a major problem and in many places people do not have access to adequate and inexpensive supplies of potable water. Solar energy systems are expected to have an important role in the domain of brackish and seawater desalination. Of special interest are small desalination plants that can be operated with small quantities of energy. Small-scale desalination plants can be based on solar thermal systems, for providing potable water to remote and isolated communities where the potential of solar energy is enormous. By exploiting solar energy, for fresh water production, three main problems can be addressed: potable water scarcity, fossil energy depletion and environmental degradation due to fossil fuel combustion. In addition to that, sea water desalination with the use of solar energy can remove salt and other minerals from the sea water and finally produces pure (potable) water. In 1873 in Chilean mining town of Las Salinas, the first large–scale solar desalination system was constructed and operated for 40 years [55]. It made use of a parabolic trough collector which has a concentration ratio from 10 to 100 and can achieve temperatures from 100°C to 400°C. It usually requires a tracking system to follow the sun for maximising its energy capture [42].

1.7.3 Cooking system

Solar cookers use the sun radiation for pasteurization, cooking and drying and can reach temperatures up to 315°C. They are distinguished in three different types of cookers:

(i) Box Cookers, which are the simplest solar cooker and consists from an insulated container with transparent lid;

(ii) Panel Cookers, which use a reflective panel in order to direct sun radiation into an insulated container and achieve high temperatures, similar to Box Cookers;

(iii) Reflector Cookers, which use plenty of concentrating geometries, such as Dish, Trough and Fresnel Mirrors [56], in order to concentrate the sun radiation on a cooking container. A solar bowl for steam generation for cooking is shown in figure 1.8.

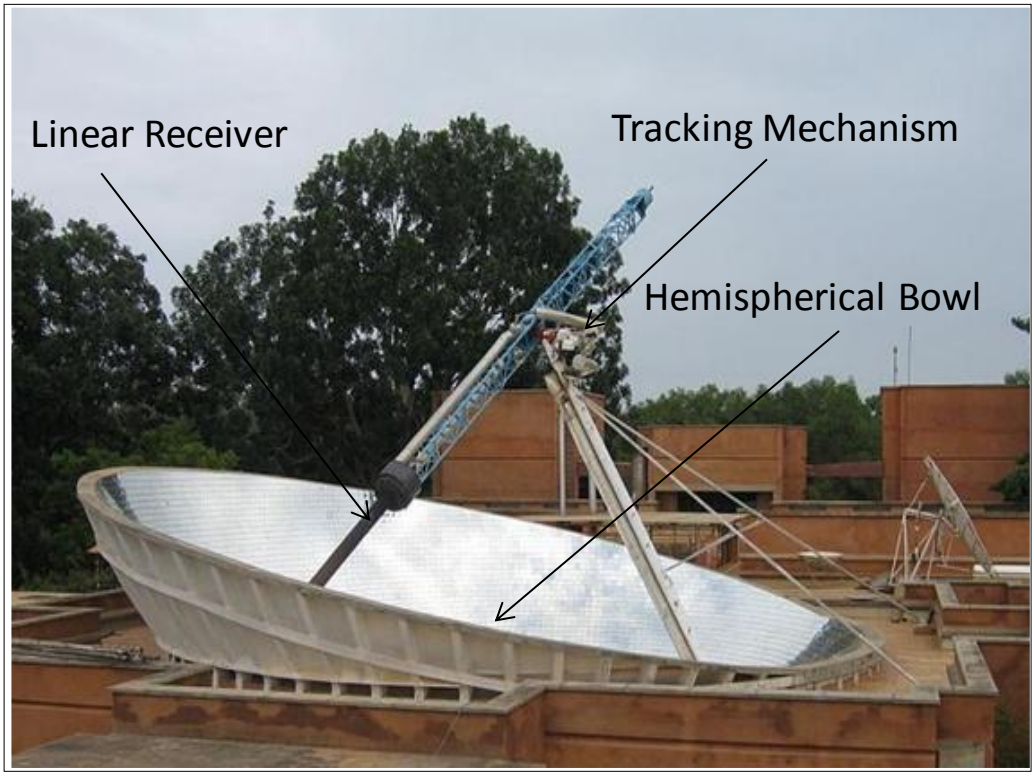

Figure 1.8: Solar Bowl in Auroville, India, to produce steam for cooking [43].

1.7.4 Drying

According to their operating temperature ranges, the drying systems are classiified as high temperature dryers and low temperature dryers [57]. In solar drying, box or tray type equipment is used to collect the sun's radiation to harness the radiative energy for drying applications, which differs from open sun drying. In most developing countries, there has been very little field penetration of solar drying technology [46]. The exposure of the sun results case hardening, which develops hard outer shell and trapped moisture

inside. Solar energy has been used throughout the world to dry products. The solar dryer removes the moisture and ensures good quality products. Solar dryers improve upon the traditional open sun drying [46]. One of the leaders in solar air heating/solar drying systems in India is the NRG. The solar energy dryer produced by the NGN is shown in figure 1.9. They are economic, reliable, removes maximum amount of moisture and retain colour and nutrients much better than any other drying mechanism.

Figure 1.9: Photograph of NRG solar dryer [58]

1.7.5 Process Heat

For process heat applications, medium-temperature solar collectors can be deployed. The main application is of heat production for industrial processes. Many studies [57-60] reveal that industrial sectors have very good favorable conditions for the production of hot water through solar energy. A medium temperature level of process heat application include sterilizing, pasteurizing, drying, hydrolyzing, distillation and evaporation, washing and cleaning, and polymerization. Depending on the range of temperatures, applications may vary from near ambient to low-pressure steam. The energy can be provided either from flat-plate collector systems or concentrating collectors of low concentration ratio. Hot water or low pressure steam at medium temperatures (150°C) can be used either for preheating of water or for steam generation or by direct coupling of the solar system to an individual process working at temperatures lower than the central steam supply. The common applications of solar industrial and agricultural process applications were described and presented by Ekechukwu and Norton [57, 59]. Spate, Hafner et al. [60] presented the decentralised solar process heat applications for community kitchen, bakeries and post-harvest treatment. The system uses a fix-focus parabolic collector, a high temperature FPC and pebble bed oil storage. Benz [61] presented the utilisation of a solar thermal system for

space heating in brewing and dairy industries. The same author [62] presented the utilisation of non-concentrating collectors for the food industry. It is found from the analysis of industrial strategies that, many processes have great potential to implement solar heat resources in various studies [63, 64] at low or medium temperatures.

1.8 Review of Solar Concentrators and Receivers

1.8.1 Solar Dish Concentrators

In recent years, utilisation of solar energy for various process heat applications has drawn major attention across the world. Several types of solar collectors have been employed to achieve medium temperature applications such as heating water for desalination, drying, cooking etc. The most common collector used for these applications are flat plate collectors, evacuated tube collectors and compound parabolic collectors (CPC) with evacuated tubes.

Rabl [65] presented the dependence of concentration ratio, acceptance angle and operating temperature of a solar collector. Grass et al. [66] compared non-tracking and tracking evacuated compound parabolic (CPC) collectors which can achieve working temperatures of between 200-250°C. TRNSYS simulation was carried out to decide the type of collector that is suitable for specific regions. For non-tracking collectors the acceptance angle is limited to lower values. Kumar et al. [67] reported on findings for a truncated pyramid non-tracking system that could be used for domestic cooking and water heating; this study focused on the performance of the system as a water heating system.

The quality of heat produced by a solar collector system is governed by configurations of the concentrator and the receiver. The study of concentrator optics and its flux distribution in the focal region are important parameters in the design of receivers. During the past few decades, numerous investigations have been carried out on design aspects such as the reflective materials for the concentrator, and focal image characteristics of solar parabolic dish systems. The review of literature pertaining to solar concentrators (parabolic dish, parabolic trough, CPC, trumpet, CLFR) is presented here.

Three dish systems with silvered polymer (ECP-300X) as the reflective material were developed in the United States [68]. Acurex and Solar Kinetics, Inc., Dallas, USA,

(SKI) designs employed sheet metal reflective panels which were structurally integrated with the support structure to reduce structural weight and cost. The Lajet (LEC-1700) innovative employed circular stretched membrane reflective facets [69]. The Schlaich Bergermann and Partner (SBP) dish concentrator was the largest and single stretched membrane focused by internal vacuum.

In 1994, Australian National University (ANU) developed a prototype of 400 m^2 aperture area of a solar parabolic dish concentrator [70]. It consists of 54 mirror panels supported on a hexagonal aperture space frame structure. Altitude and azimuth tracking are employed with a horizontal axis near the base of the dish so that it can be parked in a horizontal position relatively close to the ground. A cavity type receiver based on a single helical winding of stainless steel tubing is used. The receiver acts as a "once through" boiler which produces superheated steam at 5 MPa and 773 K. The prototype is connected to a small reciprocating steam engine which is capable of generating 45 kWe and is connected to the local grid. The thermal efficiency from solar to steam is approximately 85%. Recently, due the commercialisation of this technology ANU has re-designed the concept of the Big Dish for mass production. The new design is a 494 m^2 concentrator with 13.4 m focal length and altitude-azimuth tracking. It uses 380 identical spherical 1.17 × 1.17 m mirror panels, which integrate the Glass-on-Metal Laminate mirrors [71]. The 500 m^2 Paraboloidal Dish Solar Concentrator developed by Australian National University system is shown in figure1.10.

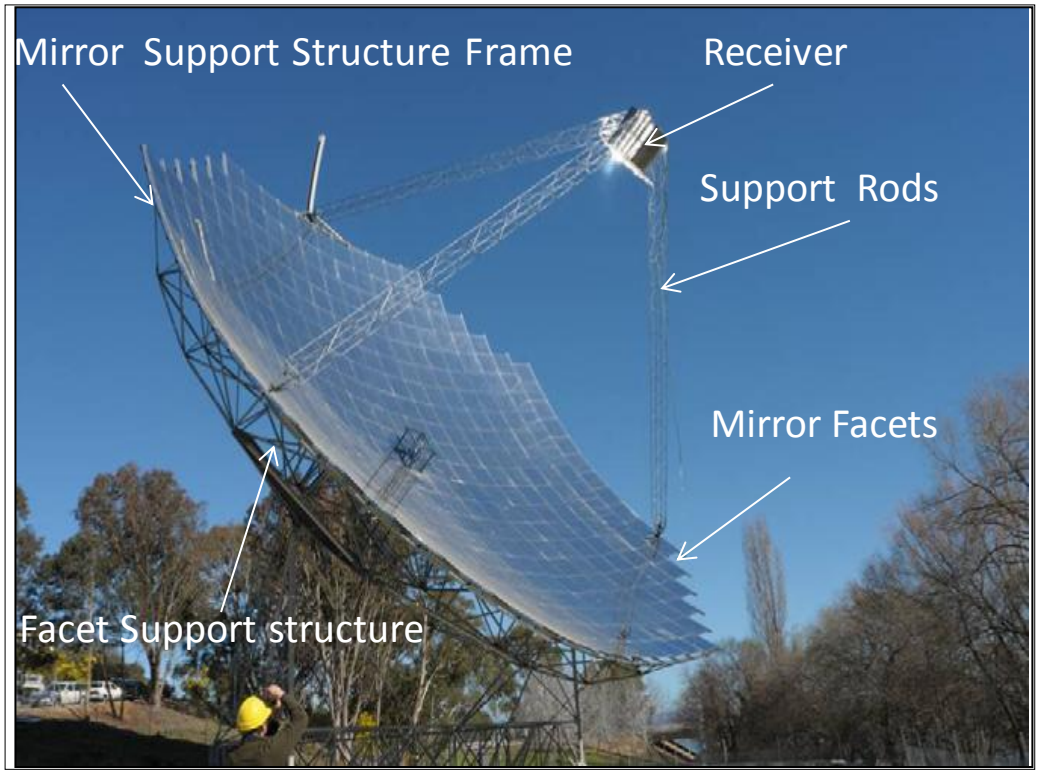

Figure 1.10: Paraboloidal Dish Solar Concentrator Developed by Australian National University [71, 72]

Jaffe [73] briefly described a wide variety of point-focusing concentrators for solar thermal energy use. These point focusing concentrators have different operating parameters such as optical configuration, optical elements materials, structure for support of the optical elements and receiver mount, foundation, drive, and controls. Jaffe [70] presented methods for calculating and optimising the performance of parabolic dish solar collectors and their cost/output ratio. The effects of variables such as concentrator optical surface, specularity, pointing errors, receiver aperture size, absorptance and temperature on optimisation were examined [74]. The performance may be improved by the use of a secondary concentrator, if the errors of the primary concentrator are large. Harris [75] studied the thermal performance of a solar concentrator with different cavity receivers shapes (cylindrical, hetero-conical, conical, spherical and elliptical). Deviations in concentrator rim angle and cavity geometry caused large variation in power profiles inside the cavity receiver. Kaushika [76] presented the characteristics relevant to the design and cost considerations of multifaceted dish collectors. Kaushika [76] suggested some alternatives used for concentrator mirror materials and discussed cost effective optical mirror materials of second surface silver on glass. An elliptic normal distribution was used to estimate the flux distribution at the focal region of the fuzzy focal dish.

Stine and Diver [77] presented the results of a survey on the solar dish technology status, system specification, performance and operation of parabolic dish solar collectors that use Stirling engine to generate electrical power. An overview of status of dish/stirling technology development and the operating experience for each system was also presented. Becker [78] discussed the scope and possibilities for applying concentrating solar energy to a number of industrial processes. Trieb, Langniβ et al. [79] compared different solar electricity technologies by taking into consideration their performance costs and environmental impact. They presented a practical tool that facilitates an estimate of performance and costs of solar power plants under local conditions and reviewed the parabolic dish steam generating systems for high performance and low cost.

Different solar concentrator materials such as low iron glass mirror, pure polished aluminium and polymers coated with silver-aluminum alloy have been tried in the development of low cost parabolic dishs. The mirror made of polymer film material coated with Ag-Al alloy provides the advantage of being light-weight. The index of reflectivity is also very close to that of a glass mirror; it is easy formable and shatter resistant. The resultant concentrator had a rather fuzzy focal image of large cavity aperture would be required. Kaushika [80] presented the design, development and thermal performance characteristics of a low-cost solar parabolic dish of silvered polymer reflectors. The intercept factor at the focal region of the fuzzy focal dish concentrator was evaluated using elliptic normal distribution functions. The thermal optimisation of cavity receiver for low cost solar dish has been presented.

Lovegrove et al. [81] demonstrated a solar driven closed-loop thermo-chemical energy storage system using ammonia in a 20 m^2 dish solar concentrator. They have shown that ammonia dissociation receiver/reactors are well suited for high-quality superheated steam production. Based on catalyst material, a cavity receiver consisting of 20 reactor tubes filled with iron based catalyst material was used in the system. The study attempted to maximise the potential for electrical power production from an ammonia synthesis reactor. Mills [82] presented various solar thermo-electric technologies. Kennedy [83] provided the extensive status of the material for solar reflectors. The development, performance and durability of the solar reflectors were discussed. The glass with silvered polymer and front-surface mirrors has been shown to be an excellent candidate for solar reflectors. Klaus and Palavras and Bakos [84, 85] dealt with the

development and performance characteristics of a low-cost dish solar concentrator and its application in zeolite desorption. Klaib [85] discussed the technical and economic development of different solar thermal power plants such as parabolic trough, central receiver, and dish systems.

Hassib [86] discussed the geometric analysis of a compound conical concentrator with receivers of various geometries. The shape of the receiver determines the profile the reflector. It was also shown that the resulting flux distribution determines the shape of the receiver and its position relative to the reflector. El-Refaie [87] described the conical solar energy concentrator with tubular axial absorber. The effects of apex angle, diameter ratio and truncation ratio on the concentrated power, concentration profile and the reflector-surface area have been investigated.

Mancini [88] presented analytical models to evaluate a performance of the single element stretched-membrane dish. Several configurations for the faceted stretched-membrane dish were discussed. Garcia-Botella [89] presented the profile generation of a hyper parabolic concentrator (HPC) from a field lines of a two–dimensional truncated wedge based on hyperbola and a tilted parabola. Bortz [90] explored the mathematical relationships between methods (generalised functional method, edge ray method, aplanatic method and simultaneous multiple surface methods) of optical design of the non-imaging concentrators.

Garcia-Botella [91] presented concentration ratios and the skew invariant of an elliptical concentrator. The application of an elliptical concentrator as a solar concentrator and illuminator was also discussed. Numerical results of ray tracing of the elliptical concentrator were also presented. It was stated that elliptical concentrators, have two principal acceptance angles in the transversal and longitudinal directions. They can therefore achieve higher concentration ratios compared to translational symmetric concentrators and lower for the rotational types. Garcia-Botella [92] studied a 3-D asymmetric concentrators without rotational and translational symmetry based on photometric field theory and elliptic ray bundles for non-tracking solar applications as shown in figure 1.11.

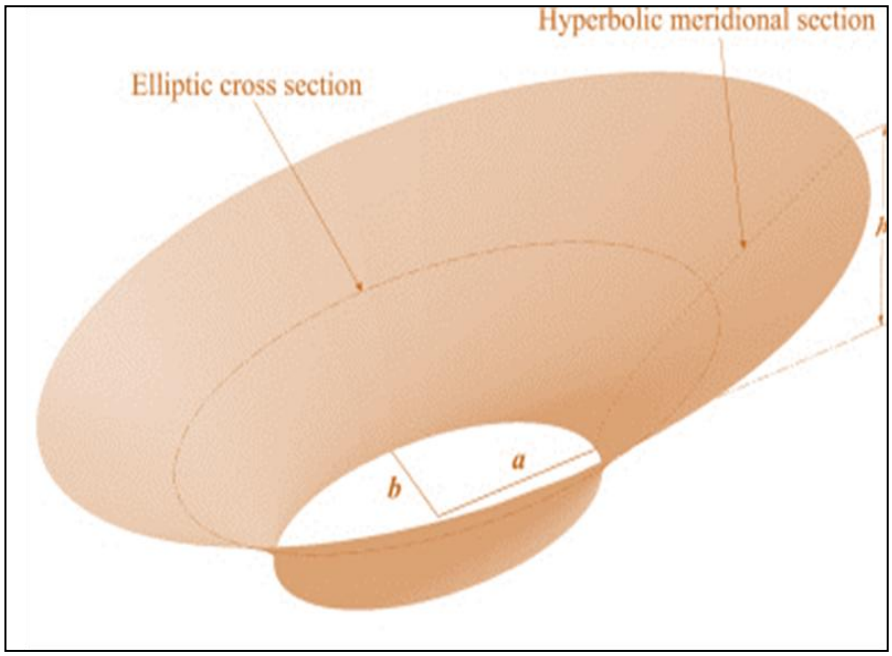

Figure 1.11: One-sheet 3-D hyperbolic asymmetric concentrators [92]

Minano and González [93] presented a new method of designing two non-imaging concentrators - aspheric lens concentrator and lens-mirror combination concentrator. Based on ray tracing, it was found that the lens-mirror combination concentrator has a high transmission value and the optical surfaces were not in contact with the receiver.

Senthilkumar [94] investigated the optical and thermal performance on horizontally segmented 3-D CPC. The steam generation efficiency of the CPC was reported to be 38%. Gutiérrez [95] suggested the Lorentz technique to design three dimensional ideal non-imaging concentrators. Gutierrez [96] used the Lorentz technique to design flow-line concentrators and cone concentrators. Kribus [97] studied the performance (calorimetric and radiometric measurement) of a new concentrator with rectangular cross section and elliptic contour with high eccentricity. It was constructed and tested at the Weizmann Institute.

Garcia et al. [98] reported a study on a 3-D asymmetrical ideal concentrator. The concepts of the flow line of Winston and Welford [99] and the pharosage vector of Moon have been used to develop an ideal 3-D asymmetric concentrator that could be used without the need for tracking, where different acceptance angles and transversal and longitudinal directions are needed. The concentrator presented is suitable for infinite concentrating applications with the help of lenses, but since this design was

fully modelled, a finite source concentrator, may deviate from the ideal character when scaled up and used as an infinite source application.

Garcia et al. [91] presented a new generation of concentrator referred to as elliptical concentrator. Two classes of elliptical concentrator have been defined namely non-homo-focal and homo-focal. This paper also discussed special cases for which elliptical concentrators are applicable; these included both the translational and rotational. It was also remarked that elliptical concentrators have two principal acceptance angles; the transversal and longitudinal directions. Therefore this type of concentrator, can achieve higher concentration ratios in comparison to translational symmetric concentrators and rotational types.

Benitez et al. [100] presented a new method to obtain elliptical ray bundles in a 3-D geometry by reformulating the conditions of a bundle to be considered elliptical and also looked for the shapes and profiles produced by these elliptical bundles with a flow lines design method. The solution of the problem provided may allow the design of a new set of 3-D concentrators that are "ideal". Sellami et al. [101] designed a novel 3-D static concentrator and evaluated the best combination of optical efficiency and acceptance angle. A good agreement between experimental measurements from a manufactured square elliptical hyperboloid and optical simulation results was observed. Ali et al. [102] evaluated the performance of a 3-D elliptical hyperboloid concentrator using ray tracing software and carried out the optimisation study of the profile and geometry to improve the overall performance of concentrator. The optical efficiency was found to be 28% for a concentration ratio of 20×. Arunkumar et al. [103] studied a pyramid solar still which was directly coupled with a non-tracking compound parabolic concentrator for heating saline water. It is observed that the basin water temperature increased within a short time which starting the distillation process and found that the distilled yield rate is more than conventional solar still.

Luminosu [104-106] presented a ray tracing tool for a small sized non-imaging paraboloidal concentrator. O'Gallagher and Winston studied different applications for the flow-line concentrator. They examined it as a second stage concentrator and its application in nearly ideal optical systems. They highlighted the compound parabolic concentrator (CPC) as the first non-imaging system that has been designed by the principles of non-imaging optics and are limited in attaining the theoretical ideal

concentration ratio as 3-D solutions due to skew ray losses. It was states that no 3-D non-imaging concentrators could reach the theoretical limit. Winston and Welford [107] introduced the geometrical vector flux as a concept for illustrating light flow in the geometrical optics model and for initiating new designs of non-imaging concentrators. They showed how the use of the vector flux naturally leads to an entirely new path for the design of the compound parabolic concentrator. They also showed that the two-dimensional form of the compound parabolic concentrator has precisely the maximum theoretical concentration ratio and the three-dimensional form cannot quite achieve this performance. Kritchman optimised the second stage concentrator by incorporating a second-stage trumpet-like reflective element at the focal plane of a paraboloidal dish reflector. Kritchman [108] stated that an optimally adapted trumpet compensates for the optical aberrations or short comings of the dish.

1.8.2 Solar Trough Concentrators

Similar to a solar parabolic dish system, the performance of a solar parabolic trough system depends on the contour of the concentrator and receiver. Among these two, the receiver design influences the overall efficiency of the energy conversion of the solar parabolic trough collector system. The energy absorbed by the receiver has to be transferred to the heat transfer fluid (HTF) essentially by means of convection. Several studies have been reported on the performance and its improvements of line-focus concentrating systems. In 1870 a parabolic trough based solar collector system of aperture area 3.25 m^2 was developed to drive a 373 W heat engine to produce steam directly: this is now called direct steam generation (DSG). In direct steam generation, instability in the receiver occurred due to stratified two-phase flow during the steam generation [109]. It was also found that the instability leads to the bending of the absorber and rupturing of the glass envelope of the receiver due to thermal gradient of the hot two phase flow. To avoid the instability caused by the thermal gradient, bimetallic receivers were suggested. In order to predict the thermal stress, Yapıcı and Baştürk [110, 111] simulated a 2-D conjugate heat analysis with uniform and non-uniform heat flux on the horizontal circular pipe.

Ericsson [112] developed a large parabolic trough collector (3.35 m long and 4.88 m wide) with a manual sun tracking motor to focus the solar radiation on a 15.88 cm receiver boiler tube. Three parabolic trough collector systems with 2.13 m aperture, 3.66 m long with a rim angle of 90^o was constructed at Sandia laboratory. The receiver was

enclosed with a 4 cm diameter glass tube and a 1 cm evacuated annulus. Anodized aluminium by Alzak and backside coated silvered glass surfaces fixed to the support materials [113-115] identified the influencing factors (such as spectral directional reflectivity of the mirror, the reflector -receiver intercept factor, the incident angle modifier, absorptivity-transmissivity product of the receiver tube and cover tube, the end or edge loss factor, a tracking errors and misalignment of receiver) that determine the performance of a parabolic trough concentrator. Odeh, Morrison et al. [116] studied the performance improvement and cost reduction of the parabolic trough collector system with synthetic oil and water as a working fluid. Huang [117] revised the testing procedure of ANSI/ASHRAE 93-1986 for performance analysis of solar collectors. Kalogirou [118] analysed the collector time constant, acceptance angle, collector thermal efficiency and incident angle modifier for parabolic trough collector of different tracking systems.

Zhang, Zhao et al. [119] developed stainless steel–aluminium nitride cermet material as a solar absorbing layer for solar thermal applications with absorptivity of 0.95 and emissivity of 0.05. Brooks [120] conducted a performance test for the parabolic trough collector system with and without an evacuated glass shield receiver. It was found that the efficiency of the trough was 55.2% and 53.8% for both cases of the receiver. Valan Arasu and Sornakumar [121] investigated the performance analysis of a fibre glass reinforced parabolic trough collector system for hot water generation system. A heat loss energy balance of the parabolic trough receiver was analysed by Lüpfert, Riffelmann et al. Liu [122, 123] developed and investigated the performance of a parabolic trough solar collector system using synthetic oil and efficiency was found to be 40% and 60% respectively. Qiu [124] developed the mathematical model and experimentally analysed the thermal performance of the closed cycle parabolic trough collector system. The mathematical results were compared with experimental results. Hamad [125] experimentally investigated the effect of angle of inclination and diameter ratio on heat transfer for a cylindrical annulus pipe.

1.8.3 Ray Tracing of Solar Concentrators

Dominic Groulx [126] conducted a ray tracing analysis on a two-stage parabolic concentrator; fabricated by Lunenburg Industrial Foundry and Engineering (LIFE). In this ray tracing analysis, the effects of the secondary mirror's focal length, misalignment, and distance between secondary mirror and target were studied. It was

stated that a maximum flux of 1.2×10^4 M/W^2 was obtained for the optimum focal length of 157.9''. It was also found that imperfection of ±0.2°, leads to zero concentration efficiency. Antonio [127] presented the optical simulation of solar PV concentrators using two inverse characterisation methods (inverse illumination, and inverse luminescence operating with electroluminescent light). It was stated that the inverse illumination method enhances the simulation process. Shortis [128] described the assessment of the quality of paraboloidal reflecting surfaces as a derivation of the photogram-metrically produced surface coordinates. Ray tracing of the reflecting surfaces to predict the expected flux distribution showed the close correlation with the video graphically measured flux distribution at the focal point of the dish.

Benítez [129] presented a method of obtaining elliptical ray bundles based on a flow-line design method for 3-D non-imaging geometry. It was reformulated that the rays passing through any point of the space form a cone with an elliptic base. He stated the solution of the problem provided may allow the design of a new set of 3-D concentrators that are ideal. Jenkins [130] presented an integral design method based on a variable edge-ray principle to transform non-uniform input and output radiance distributions to maximize the concentration ratio. Using the integral design method, 25% improvement in concentration was predicted over conventional non-imaging secondaries. Wijeysundera [131] presented methods for analysing the behaviour of 3-D concentrator systems and for determining the sensitivity of a reflector designs. The ray-tracing technique has been proposed to study the behaviour of conical, spherical and parabolic reflectors when the angular deviation between the direction of the solar beam and the axis of the reflector is large.

1.8.4 Receiver and Heat Losses

The choice of the receiver type, optical and thermal (convection and radiation) losses from the receiver, and the effect of a glass envelope around the receiver are some of the practical design considerations when designing a concentrating collector [132]. Several researchers studied different shapes of the receivers and its impact on the energy losses. From the work of Harris [75], it was concluded that the deviation in concentrator rim angle and cavity geometry cause large variation in power profiles inside the cavity receiver for different shapes of cavity receivers (cylindrical, hetero conical, conical, spherical and elliptical). A simple model for the convective heat transfer from a solar cavity receiver based on the results of experimental studies from cubical cavities was

presented by Sandia et al. [133]. McDonald [134] proposed a modified correlation for a cylindrical shaped frustum receiver incorporating the aperture size, surface temperature and receiver angle.

Two distinct receivers, the semi cavity and modified cavity, were introduced in a solar dish collector system [76]. The modified cavity receiver was found to be more efficient receiver than the semi cavity [97] conducted experiments on a multistage solar cavity tubular receiver to minimise the heat losses by dividing the aperture into separate stages according to the irradiance distribution levels. An experimental analysis of laminar free convection heat transfer from an isothermal hemispherical cavity was carried out [135]. A simplified analytical solution, numerical calculations and experimental studies of laminar natural convection heat transfer from an isothermal hemispherical cavity was presented.

By considering the different shapes of concentrators and receivers, the combination of the elliptical (receiver) and hyperboloid (concentrator) can increase the thermal efficiency of the system by reducing the heat loss. In the literature review, according to author's knowledge no hyperboloid (concentrator) and elliptical (receiver) is considered. It can also be concluded that from this design, for same concentration ratio, there will be reduction in the dimension of the receiver. This reduction in the dimension is directly proportional to the area and which in turn gives lower heat losses. This optimum shape of a collector system will have an advantage over other forms designs because it can collect rays from any angle of the sun's position. For the same cross sectional area, the proposed design will be economical and cost effective when compared to other conventional system.

1.9 Motivation for Present Work

The present work is carried out based on the unavailability of more information about elliptical hyperboloid concentrator. Also, very few papers were presented on hyperboloid concentrators. Garcia-Botella [89] applied the photometric field theory and elliptic ray bundles method to study 3-D asymmetric and symmetry concentrators. They observed that the hyperbolic concentrator is an ideal 3-D asymmetric concentrator [92]. They also stated that the shape of the concentrator is not disturbed in the flow lines of an elliptical disc, so it can be applied for non-tracking concentrators. Errez studied optimal concentration of light from a source distribution to a receiver. The technique

has been developed to design three-dimensional ideal concentrators. Garcia-Botella [92] obtained a two-dimensional truncated wedge. The wedge was based on the union shape between a hyperbola and a tilted parabola. A hyper parabolic surface was obtained, by revolving the profile. It was found that the focal length of the designed concentrator approaches infinity.

From the detailed literature review, it is clearly evident that elliptical and hyperboloid concentrator for solar application have not been explored in greater detail. Inadequate information of their optical efficiency analysis using ray-tracing technique is also revealed in the literature. On the other hand, the numbers of the current existing technologies design of solar concentrator have low optical efficiency or required solar tracking, which makes the cost per unit output higher and also requires regular maintenance. To minimise the cost of the system by eliminating the tracking device to improve the optical efficiency, the present work has been proposed. The goal of this thesis is to develop an optimal optical efficiency and concentration ratio for a 3-D static solar concentrator. Hence, the present new type of solar concentrator (Elliptical hyperboloid concentrator – EHC) has been considered in this research work to carry out optical, thermal modelling and experimental characteristics of the design. In addition to this, extensive optical analysis has been performed for the optimization 3-D elliptical hyperboloid concentrator system design to be viable. Furthermore, the integration of the solar desalination system has also been investigated for the viability aspects.

1.10 Approach

This research proposed the development of an innovative three-dimensional medium concentrating design, which captured a large part of the diffuse solar radiation in addition to the direct component. The 2-D concentrator is designed to an optical efficiency of 19% based on detailed analysis of the worldwide state of art of concentrating solar energy system; this was improved upon by the 3-D system. A computational model was developed to aid the design of a three dimensional elliptical-hyperboloid concentrator with a concentration ratio of 20×. A prototype system was also constructed and indoor testing characterization was carried out at Heriot-Watt University (HWU) and the final design of the EHC was fabricated and tested out door in Madras, Chennai India (IITM). A three-dimensional solar concentrator was designed to have an optical efficiency of 28%. The EHC system was fabricated and incorporated

into a water desalination system. The numerical data was compared to experimental measurements collected by a prototype system.

1.11 Objective of the Present Work

The objectives of the present work are:

1. To identify an appropriate static solar concentrator for process heat applications.
2. To develop in-house codes and perform the optical characterisation of the 2-D and 3-D Static Elliptical hyperboloid concentrator (EHC) for wide range of acceptance angles.
3. To design and fabricate a three-dimensional hyperboloid reflector base concentrator with elliptical receiver.
4. To manufacture a range of prototype 3-D EHC for indoor characterisation
5. To perform indoor experiment of the 3-D EHC in order to predict the thermal behaviour of the system and to utilise the system for medium temperature applications.
6. To optimise different parameters within concentrator geometry in order to achieve high optical efficiency.
7. To perform outdoor characterisation of the scale-up version of the 3-D EHC for water and process heat use.

1.12 Organization of the Thesis

This thesis has been divided into seven chapters. The review of literature pertaining to the present work is outlined in chapter 1. It also includes the objectives and scope of the work undertaken. The current state-of-the-art in solar thermal concentrator technologies are presented and discussed. A discussion on the explanation for this work and the identification of a gap in the literatures are outlined at the end of this Chapter 1. The designs of 2-D and 3-D elliptical hyperboloid static solar concentrator are extensively discussed in chapter 2. The optical performances of a static 2-D and 3-D EHC and its flux distribution are discussed in chapter 3. A part of the chapter 2 and few sections of the chapter 3 have been published in International Journal of Solar Energy. The other part of the chapter 2 has been published in the World Renewable Energy Congress, Abu Dhabi. The comparisons of the optical performance for different geometrical EHC are presented in chapter 4. The work related to chapter 4 has been published in the two International conferences, ISES Solar World Congress 2011-Germany; WREF 2012 - Denver, USA. The fabrication and indoor experimental behaviour characteristics of the static EHC under different solar insolations are presented in chapter 5. The outdoor unit

was fabricated and tested at the Indian Institute of Technology (IITM), Chennai in India. This chapter will provide a detailed description of the all dimensions and material used for the fabrication of the EHC Based on this, the thermal performance of the medium temperature elliptical-hyperboloid solar collectors has been presented in chapter 6. This chapter will provide a detailed description of the all dimensions and material used for the fabrication of the EHC. The work related to chapter 6 has been communicated to the International Journal of Solar Energy and it is under review. The highlights of the present work, conclusion from the present research work study, and the suggestion for the future work are given in chapter 7. The methodology of the thesis is given in figure 1.12.

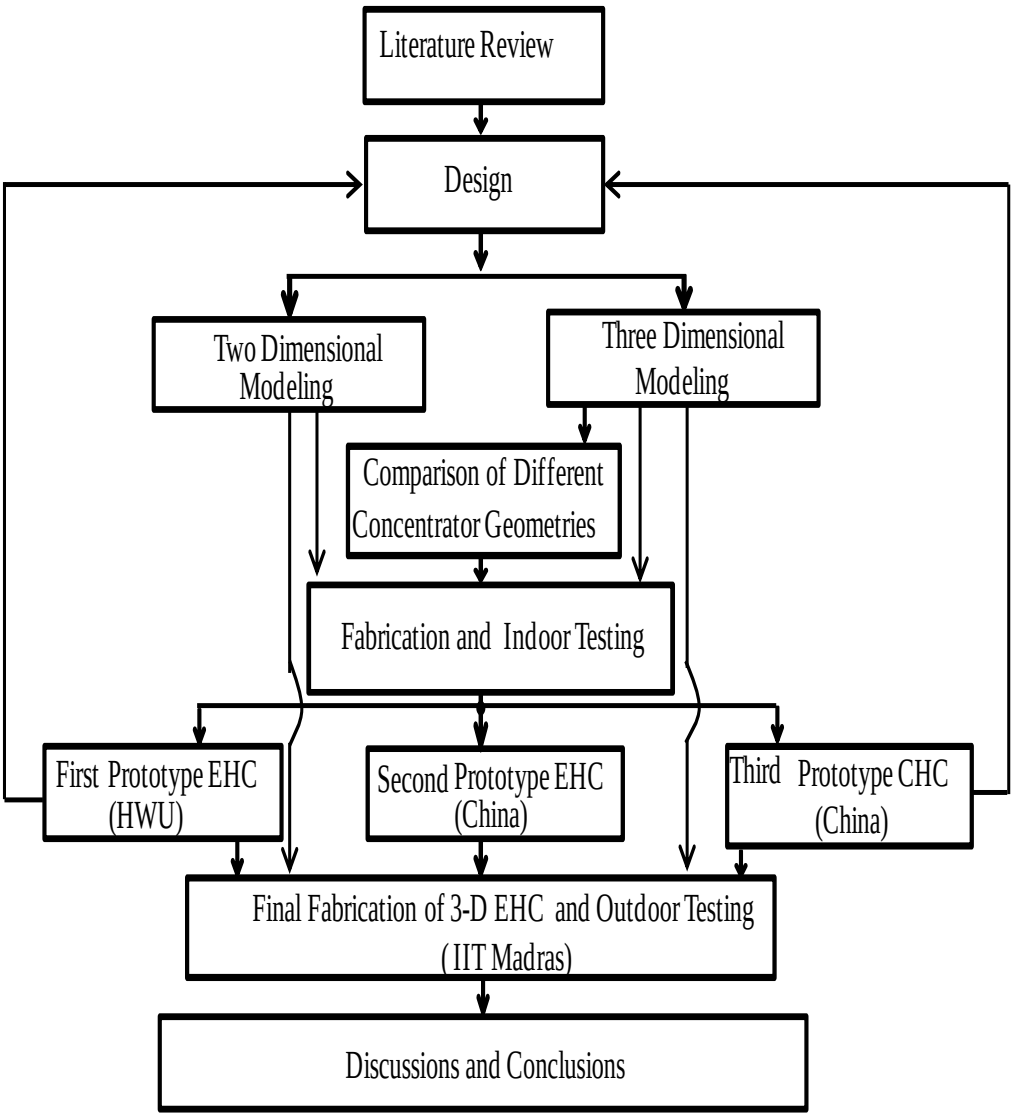

Figure 1.12: Methodology of thesis

1.13 Closure

In this chapter, the background and the motivation of the present research work have been discussed. Broad outlines of the organization of the thesis and the salient features of the individual chapters have also been highlighted. The next chapter deals with the design aspects of 2-D and 3-D elliptical hyperboloid static solar concentrator.

CHAPTER 2: DESIGN AND OPTICAL RAY TRACING PROCEDURES FOR STATIC 2-D AND 3-D EHC

A non-imaging solar concentrator system of reflecting surfaces redirect the solar radiation from source to target (receiver). The present research work is focused on a 3-D elliptical hyperboloid geometric design of solar collectors, though many design concepts and procedures for 2-D and 3-D are discussed in this chapter. Based on the general equation for a solar concentrator, parameters vary slightly to determine the optical efficiency. 2-D MATLAB code is written to obtain the different shapes of the concentrator. Optis software is used to obtain ray tracing, flux distribution and optical efficiency for a 3-D EHC.[102].

2.1 Introduction

A new approach of non-imaging optics was introduced in 1960 by Kritchman [136]. Compared to imaging concentrators, a non-imaging system has a wider acceptance angle. Due to this, the system has the capability of approaching the thermodynamic limit of the concentration ratio and is capable of collecting the solar radiation for eight hours per day [137]. Furthermore, the diffuse radiation is also captured, which is lost in imaging systems. During the past few decades, several designs of non-imaging concentrators have been developed. Compound parabolic concentrators (CPCs) and trumpets (hyperbola) are the most common non-imaging systems. Without a tracking system, the maximum concentration ratio for an imaging concentrator with secondary reflector was found to be 3 or 4 [138]. Winston [137] showed that a concentration ratio of 9.6 could be achieved with a trough-CPC system. They achieved a concentration ratio exceeding the sine law of concentration. A comparison between the characteristics of parabolic and Fresnel concentrator systems and CPCs was presented by Rabl [139]. The continuous development of non-imaging systems has led to the development of optic techniques to analyses the non-imaging systems, which are discussed below.

2.1.1 Edge-Ray Method

The edge-ray optics is one of the simplest methods, which has been extensively used in designing non-imaging systems [140, 141]. Winston, Miñano et al. [142] described the edge-ray method for a non-imaging system. The important aspect of the analysis in solar energy collection is whether the redirected radiation reaches its target or not, rather than the radiation distribution pattern. In the edge ray method, the boundary of the beam is redirected onto the boundaries of the region. Hence, in designing a collector, edge

rays of the source are reflected onto the target. Remaining source rays will also reach the target. The contour of the CPC is a very good example to explain the principle of edge ray method and is shown in figure 2.1. If the acceptance angle of the incoming rays is less than half acceptance angle of the CPC, then the rays are focused onto the opposite edge of the receiver with a single reflection. If the incoming rays are greater than the half acceptance angle of the CPC, then the rays are reflected onto the opposite reflecting surface and then rejected.

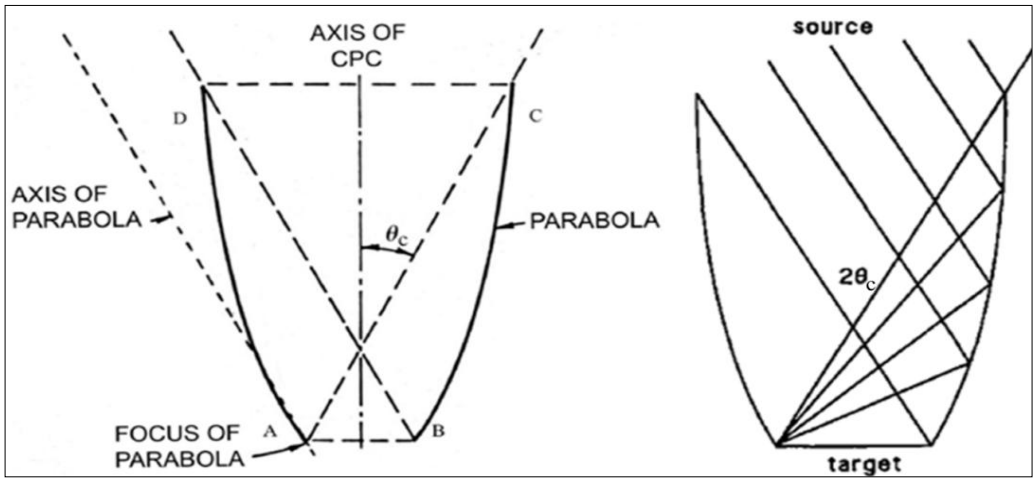

Figure 2.1: Edge-Ray Principle and CPC [140]

The principle of edge ray can be used to design both symmetric and asymmetric type concentrators with non-concave absorbers. Winston and Hinterberger [143] used edge ray principle for designing ideal linear concentrators for various absorbers such as cylindrical tube absorbers and vertical fin absorbers. For reflectors located in the shadow of the absorber, the edge ray method cannot be applied [144]. For several asymmetric geometries of CPCs the edge ray method were used for building-integrated PV concentrators [145]. Adsten, Helgesson et al. [49] presented the asymmetric concentrators for static collections in high-latitude locations. The edge ray method resulted in a differential equation for each side of the reflector to maximise the collection in two dimensions. Winston, Miñano et al. [142] however formulated a technique called a string method, in which a string and rod are used to trace the required contour surface. The main advantage of the edge ray method is its ease of use, but it is limited to only narrow problems under assumptions of specular reflection and homogeneous irradiance. By using the edge ray method, optimal reflector geometry is resulted without reasonable assumptions in practice.

2.1.2 Tailored Edge-Ray Approach

For the tailored edge-ray approach, one of the practical difficulties of the edge ray method, homogeneous irradiation, is eliminated to handle the reflecting surfaces and to achieve the desired radiation pattern. This approach was adopted in the design of the lighting system. Using the tailored edge ray approach, a uniform angular radiation pattern from a given source of light was achieved. In the edge-ray method, only a single set of edge-rays were used to determine the contour of the reflector with a single acceptance angle. For the tailored edge-ray method, an entire family of edge rays was used to determine the reflector geometry with a desired irradiation. The acceptance angle function for reflector shape based on the radiation pattern at the source and on the target was given by Winston and Ries [146]. Ries and Winston [147] applied the method to obtain a constant irradiance to ±43° with constant brightness from a cylindrical source. Later, the method was used for a concentrator design. Gordon and Ries and Gordon [148, 149] applied tailored edge-ray method to design a secondary concentration of 2-D and 3-D parabolic and Fresnel systems. Despite the benefits of the tailored edge ray method, the method is still limited to the practical assumption of perfect optics.

2.1.3 Flow-Line Method

A flow-line method is also a generally used technique in non-imaging optical system analysis. This method is also known as the geometric vector-flux approach. In this method, light propagation is manipulated by means of “phase space” whose dimensions are twice the ordinary space. Similar to fluid dynamics, the phase space consists of both the position and momentum of fluid particles. In optics, the momentum of a light ray is obtained by multiplying its direction with the refractive index of the medium (ray flows). The method of analysing the optics by means of phase space is useful, the quantities related to the physical law of radiation propagation is conserved. The quantity is geometric vector flux, which is similar to the volume conservation in incompressible flow. In this way, the flow lines are mapped in vector phase space for a Lambertian source. Based on the information of the flow lines, the reflector geometry surfaces are deduced, in which geometric vector flux is conserved. Winston and Welford [107, 150] described the overall method of tailored edge ray method in detail with various examples.

2.2 Design and Method of Optimisation

Using the various types of design methods of solar concentrator, Winston, Miñano et al. and Garcia-Botella [89, 142] designed a hyperboloid of revolution. It was stated that, the hyperboloid designs can be optimised to improve the performance by using the elliptical cross section of the concentrator, such as an elliptical hyperboloid solar concentrator. In the elliptical hyperboloid design, there are many parameters, such as major receiver axis, minor receiver axis, concentrator height and concentration ratio that needs to be optimised for higher optical efficiency with a wider acceptance angle. In order to optimise the design of a 3-D elliptical hyperboloid, as a primary reflecting surface, the study of 2-D and 3-D hyperboloid solar concentrator is carried out in the present thesis.

2.3 Design of a 2-D Hyperboloid Concentrator

To study and optimise 2-D hyperboloid concentrators (HC), first a 2-D design of the hyperboloid concentrator was carried out. In designing the 2-D hyperboloid concentrator, a 2-D ray tracing of hyperboloid concentrators (HC) has been carried out using MATLAB software. 2-D ray tracing simulation code was written in MATLAB and code details are presented in Chapter 3. The influencing parameters for optical efficiency such as incidence angle, concentrator height, and receiver diameter and concentration ratio have been investigated in the 2-D ray tracing analysis. An extensive investigation of 2-D ray tracing technique was adopted to calculate the optical efficiency of the hyperboloid concentrator. It is very clear that the optical efficiency is directly proportional to the receiver diameter. As the receiver diameter increases, the optical efficiency also increases and the concentration ratio decreases.

2.3.1 Theoretical Model of 2-D HC

For non-imaging concentrators, an interesting feature is the distribution of energy over the receiver area. In CPCs, the flux on the receiver of the CPC is well distributed for wider incidence angles. The flux distribution on the receiver is homogeneous and it is varying along the whole receiver length. The flux distribution of energy in CPCs is varied with the incidence angle and it is asymmetric in nature. The flux distribution at the receiver of the CPC is given by Luminosu, Zaharie et al [105],

$$I_{rec} = I_O - \sum_{i=1}^{N} \left(\tau_g I_i + \tau_d I_i + j\rho I_i \right) \tag{2.1}$$

Where,

I_o is total energy flux of radiation at aperture, I_i the Energy of the individual ray considered, τ_g the Energy loss factor during transmission through the glass cover, τ_d is Energy loss factor during transmission through concentrator material, ρ is Reflection loss factor for reflector, N is Number of rays considered and j is Number of reflections of individual rays.

In the flux distribution, high intensity occurs at some positions. This is due to concentration of radiation by the sides of the hyperboloid concentrator. In order to evaluate the optical performance for complicated geometries, ray tracing techniques are appropriate to evaluate the performance. Optical analysis by ray tracing have been studied in solar devices by many researchers. A summary of the ray tracing related to solar energy context is also provided by Luminosu, Zaharie et al. and Spencer and Murty [104], [151]. The optical analysis of a novel tubular solar thermal collector (cusp mirror and cylindrical heat pipes) is presented by Ortabasi and Buehl [152]. The optical performance of a CPC were studied by El-Assay Cairo and Clark [153]. Luminosu, Zaharie et al. [106] presented the optical analysis of a CPC solar collector with four different absorber-envelope configurations. The effect of the non-uniform distribution of the absorbed solar radiation on flat receivers combined with symmetric and asymmetric CPC-type reflectors were studied by means of ray tracing [154]. Ray tracing is a promising technique to evaluate the optical performance of solar concentrators. In ray tracing analysis, all the incident rays are assumed to to be parallel and have equal energy. After entering through the aperture of the hyperboloid concentrator, some of the rays directly reach the receiver without any reflection. Some of the rays are reflected back out of the concentrator. Few rays may be undergoing total internal reflection by the hyperboloid surface. The ray may be reflected more than once before reaching the receiver. Some of the rays may exit after a finite number of reflections within the concentrator. In the present research work, a ray tracing technique is used to evaluate the optical performance of a hyperboloid concentrator. All the incident rays are taken as parallel and have an equal amount of energy. The vector form of reflection law in ray tracing technique is given in Eq. (2.2):

$$\vec{r}_{reft} = \vec{r}_{inc} - 2\left(n.\vec{r}_{inc}\right) n \tag{2.2}$$

Where,

r_{reft}. is direction vector of the reflected ray, r_{inc} is incident direction of the incoming ray and and n is normal to the surface.

The ray coming through the aperture of the concentrator can reach the receiver directly or by one or two reflections. Some of the rays may escape after two or three reflections. Rays may be reflected one, two or more times before reaching the receiver [155]. The schematic of the number of ray's incident on the aperture of the HC is shown in figure 2.2.

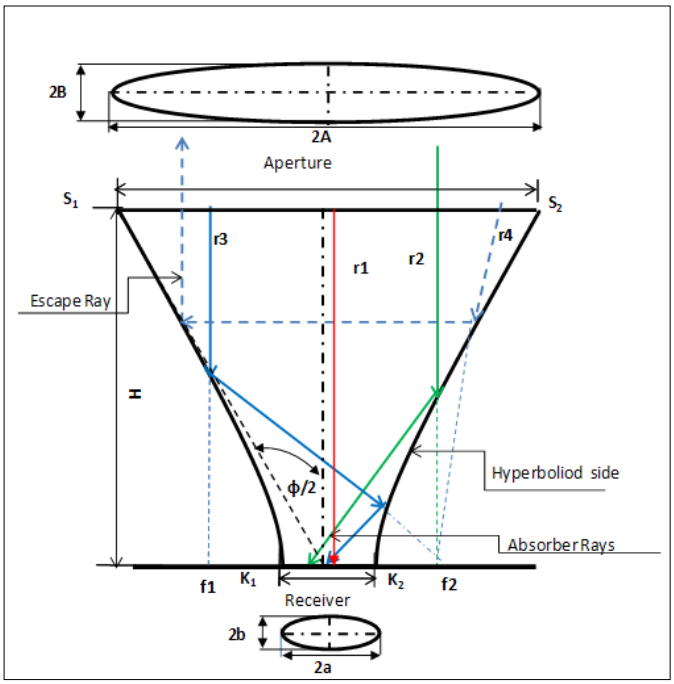

Figure 2.2: Schematic of 2-D Hyperboloid Concentrator

It is also evident that rays coming through S_1 S_2, may be reflected back and forth between the reflectors S_1 K_1 and S_2 K_1 multiple times before reaching the receiver. Some of the possible behaviours of the rays entering the concentrator are: reaches the receiver without any reflection (r_1); reaches the receiver with reflection within the concentrator (r_2); reaches the receiver with two reflections within the concentrator (r_3); escape from the concentrator through the aperture after two or more reflections (r_4).

2.3.2 Optical Modelling of the 2-D HC Using Ray Tracing Modelling

2-D ray tracing simulation code was developed for 2-D hyperboloid concentrator using MATLAB software. The flow chart for the 2-D ray tracing technique is given in figure 2.3.

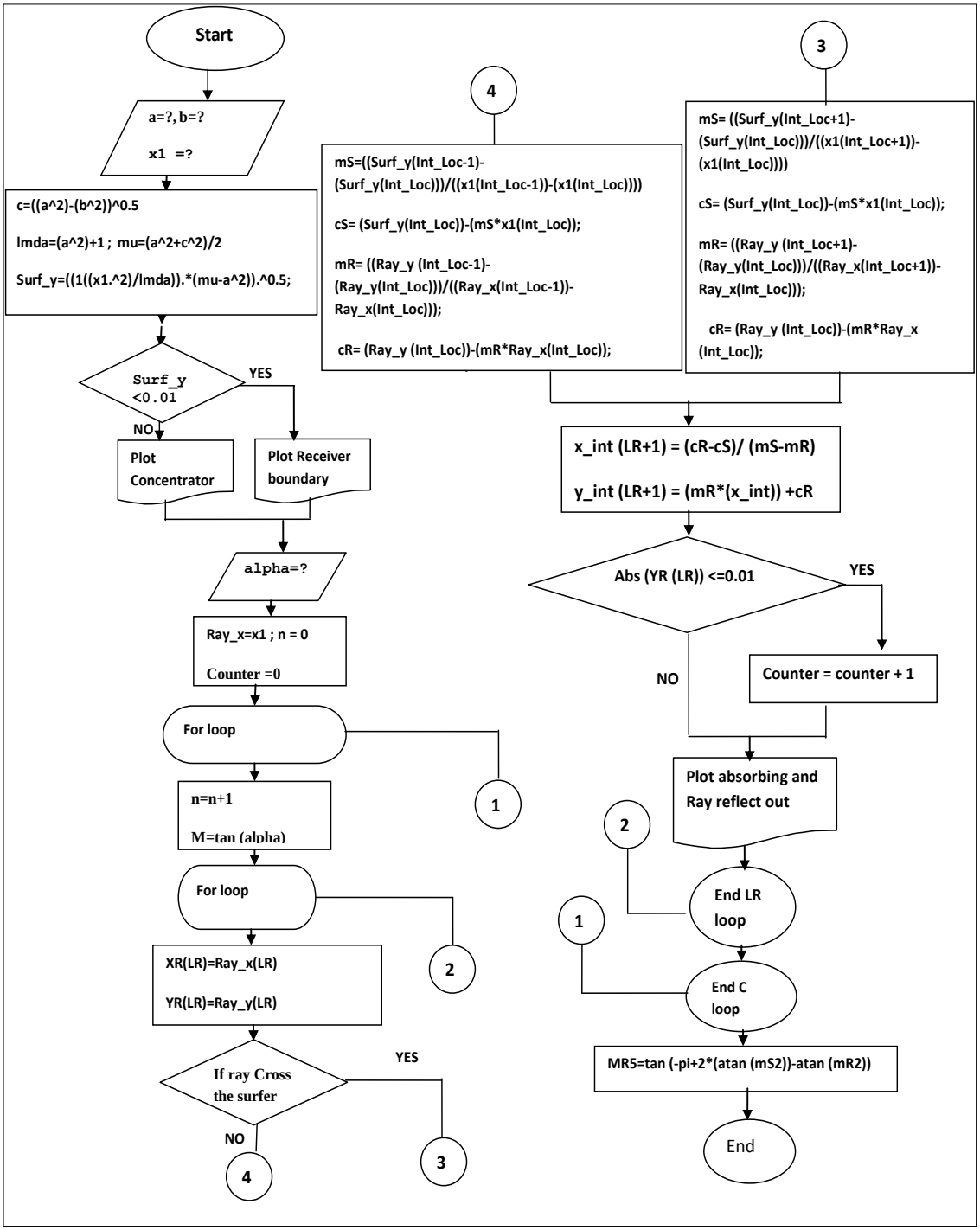

Figure 2.3: Flow Chart of the MATLAB Simulation Code for Ray Tracing of 2-D HC

The effects of incidence angle, concentrator height and receiver diameter on optical efficiency for 2-D HC were investigated. The incident rays are simulated in MATLAB software in an anticlockwise direction to follow the daily path of the sun. The hyperboloid concentrator profile was generated by defining the input vectors for *x* values for the surface and the *y* values of the surface defined by its mathematical equation in 2D

$$\text{Surf}_y = 1 - \left(\left(\frac{x^2}{lmda} \right) \times (mu - a^2) \right)^{0.5} \quad (2.3)$$

Where, $lmda = (a^2 + 1)$ and $mu = a^2 + \frac{C^2}{2}$

Equation of rays is

$$Ray_{\_y} = M\ Ray_{\_x} + \ \text{C} \quad (2.4)$$

Where, C is Intercept of the y axis at defined intervals.

Inputs are assumed which are:

- The length of the major semi axes (a)
- The length of the minor semi axes (b)
- The angles of incidence (θ)
- x = [-500:500] depending in concentration ratio

The value of x is assigned to be equal to the surface x values and the intercept is defined to start at -1000 to 1000 at intervals of 10. The slope of the incident rays and reflected rays are calculated based on the tangent of the incident angle. The angles of incidence are considered in the range of ±90˚. Therefore alpha is taken from -90˚ to +90˚. If the parallel rays intersect on a curved reflecting surface, the rays after reflection will not proceed to the point, instead the rays spread in a wider range of angles. This wider range of angles forms a radiation characteristics pattern. The algorithm used to develop MATLAB code for the 2-D hyperboloid ray tracing is described below. A fully written MATLAB code is given in appendix A. The algorithm is:

- Define hyperboloid geometric profile (equation of the reflector)
- Define incident rays (vector)
- Calculation of the intersection point
- Define the tangent plane and normal vector
- Calculate the reflecting line (vector)
- Programming steps 2-steps 5 in a loop
- Plot the geometric of solar concentrator.

2.4 Optical Modelling of a 3-D HC Using Ray Tracing Modelling

OptisWork is commercially available optical software, which is used in the present research work for theoretical simulation of a 3-D hyperboloid concentrator. In SolidWorks software, the OptisWork application such as architecture and lighting are

incorporated. OptisWork provides an excellent solution for ray tracing of the optical study of the 3-D EHC by considering different physical design characteristic features. It also includes the feature for changing the orientation of the light source and surface properties of the concentrator surface.

In the ray tracing simulation of OptisWork, optimisation of the optical performance of static 3-D EHC are to be investigated. Through OptisWork software, optical efficiency (η_{opt}) and the geometrical concentration ratio (CR_g), concentrator height and the aspect ratio of both the receiver and the aperture of concentrator are to be investigated for 3-D EHC. Besides, optical flux distribution of the 3-D EHC can also be studied and analysed in OptisWork. Different names have been given for optical flux distribution in several literatures. For clarification, Schweiger, Mendes et al. [64] used the term "energy distribution" in their ray tracing study on the CPC. Wei, Lu et al [156] used the term "concentrated spot distribution" for flux distribution in the optical study of beam-down solar concentrator system using the optical software ZEMAX. Chen and Hopkins and Li [72, 157] used the term "flux densities distribution" for the ray tracing optical study of the trough funnel concentrator.

2.4.1 New 3-D Elliptical Hyperboloid Non-Imaging Solar Concentrator

The present thesis proposed a 3-D solar concentrator for process heat applications. The entry aperture of the concentrator has to be designed in such a way that it allows the sunlight onto the receiver for wider acceptance angles. The 3-D circular hyperbolic concentrator with circular exit were designed by Garcia-Botella [89]. Instead of considering, circular concentrator cross section, a trumpet (hyperbolic) concentrator cross section (sides of the concentrator) is discussed extensively in Chapter 4. On the other hand, the design of the 3-D EHC cannot be obtained from the revolution of a 2-D profile. The design of the proposed 3-D solar geometry concentrator is based on three main geometrical parameters, which are discussed below. The first parameter is an elliptical entry aperture that allows the solar radiation to enter into the concentrator. In order to allow the maximum collection of light rays, the length of the elliptical major axis related to the elliptical entry aperture needs to be optimised based on the acceptance angle of the geometry [99, 107]. The second parameter is an elliptical exit, which deviates from the conventional 3-D solar concentrator. The third parameter is a hyperboloid profile, which connects the elliptical entry aperture and elliptical exit.

Based on these three parameters, the configuration of the geometry is named as Elliptical Hyperboloid Concentrator (EHC). The joining of the 'elliptical entry aperture' and 'elliptical exit receiver' by a hyperboloid profile generates a smooth 3-D geometry. The generated geometry is an innovative design, which has not been examined or studied by researchers in the literature as per the author's knowledge. The idea of creating smooth 3-D elliptical hyperboloid concentrator geometry shows a lot of strengths. In the literature review, it was found that the hyperbolic profile in non-imaging concentrators shows improved performance in acceptance angle and energy collection [59-62, 104, 107]. It was also stated that the 3-D solar concentrator based on the hyperboloid revolution has the ability of concentrating all the incoming solar rays [158].

The design features of the elliptical hyperboloid concentrator are given in figure 2.4 (a) and (b). In the parametric equation that describes the 3-D EHC, there is a link between each hyperboloid segments and the angle formed in which a hyperboloid segment is subtended is shown in figure 2.4 (c) and (d). The terminology description of the EHC and the dimension of the EHC are also given in figure 2.4. They are:

- *A*: Major axis of the elliptical entry (Aperture).
- *B*: Minor axis of the elliptical entry (Aperture).
- *a*: Major axis of the elliptical exit (Receiver).
- *b*: Minor axis of the elliptical exit (Receiver).
- *H*: Height of the EHC solar concentrator.
- $\acute{\omega}$: Angles between different planes and the major axis.

The EHC geometry consists of four symmetric sections, which are shown in figure 2.4. The first symmetry section lies in *xz* plane and the second symmetry section is in the *yz* plane. This results in two symmetric sections of EHC geometry. In one section, two different cases are considered. The hyperboloid branch connects the right side of the elliptical exit receiver (dotted line in figure 2.4 (d),) start at $x = a$ for different values of *y* between 0 and *b*. The hyperboloid branch located in planes perpendicular to the *xy* plane makes an angle $\acute{\omega}$ with *xz* plane. The angle $\acute{\omega}$ is varying from 0˚ to 90˚. The hyperboloid branch connects the left side of the elliptical exit aperture (dark black line in figure 2.4 (d),) start at $y = B$ for different values of *x* between 0 and *A*. The hyperboloid branch located in planes perpendicular to the *xy* plane makes an angle $\acute{\omega}$ with *xz* plane and varies from 0˚ to 90˚.

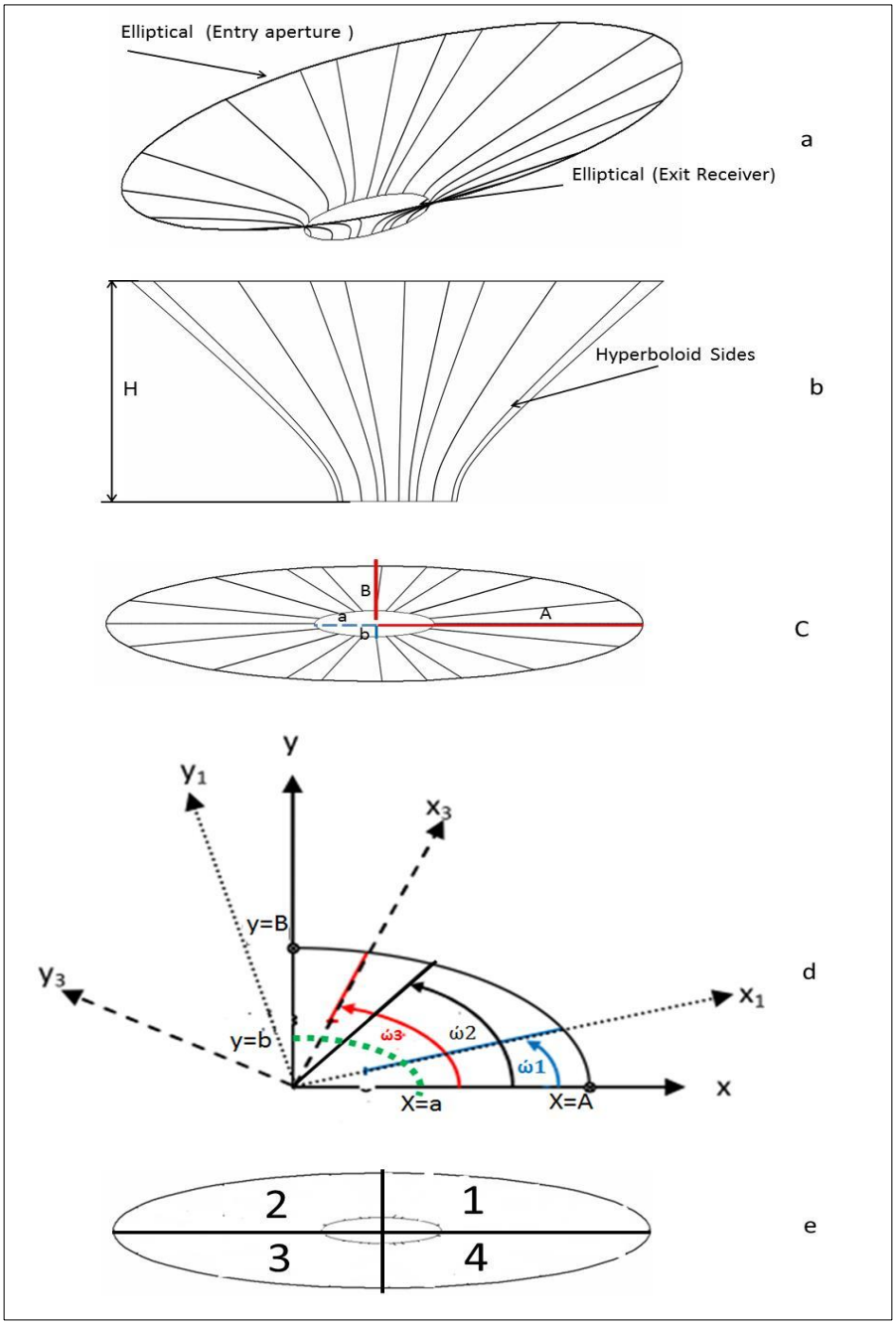

Figure 2.4: Development of 3-D Elliptical Hyperboloid a) Isometric, b) Front View, c) Top View, d) Position of Hyperboloid Branches and e) Four Symmetric Section

2.4.2 Design and Conceptualization of 3-D EHC

The proposed and designed configuration of the EHC is shown in figure 2.5. The EHC will redirect the incoming radiation within a half acceptance angle ($\varphi/2$). The EHC is symmetric along vertical *Y* axis. At any vertical plane, each surface of the EHC is a tilted hyperboloid. As shown in figure 2.5, the geometry of the EHC is defined by two parameters namely, the receiver semi major axis (a) and receiver semi minor axis (b). The equations (2.6 and 2.7) are used to generate the concentrator profile coordinates. Based on the equation developed by Gracia et al. [99], the design of hyperboloid

concentrator is carried out. In order to optimise the 3-D solar concentrator profile, the equation is modified to design different dimensions of concentrator profile such as concentrator height, concentration ratio and aspect ratio of the ellipse. In the present thesis, the optical analysis of 3-D static EHC geometry are carried out to find the optimum concentration and optical efficiency using the ray tracing technique; these are discussed in later sections of the thesis.

If $a = b$, it is a hyperboloid of equal revolution, and is also called a circular hyperboloid.

$$\frac{X^2}{a^2} + \frac{Y^2}{b^2} - \frac{Z^2}{c^2} = 1 \tag{2.5}$$

y_1 is coordinates of the profile connecting the end points of the major axis, A and a as shown in figure 2.5 and is given by

$$y_1 = \sqrt{[\{(x^2/a^2)-1\} \times \{H^2 \times (CR-1)\}]}$$
$$A = \sqrt{CR \times (a)^2} \tag{2.6}$$

y_2 is the coordinates of the profile connecting the end points of the minor axis, B and b as shown in figure 2.5 and is given by:

$$y_2 = \sqrt{[\{(x^2/b^2)-1\} \times \{H^2 \times (CR-1)\}]}$$
$$B = \sqrt{CR \times (b)^2} \tag{2.7}$$

The geometric parameters involved in the design of the concentrator are shown in figure 2.5.

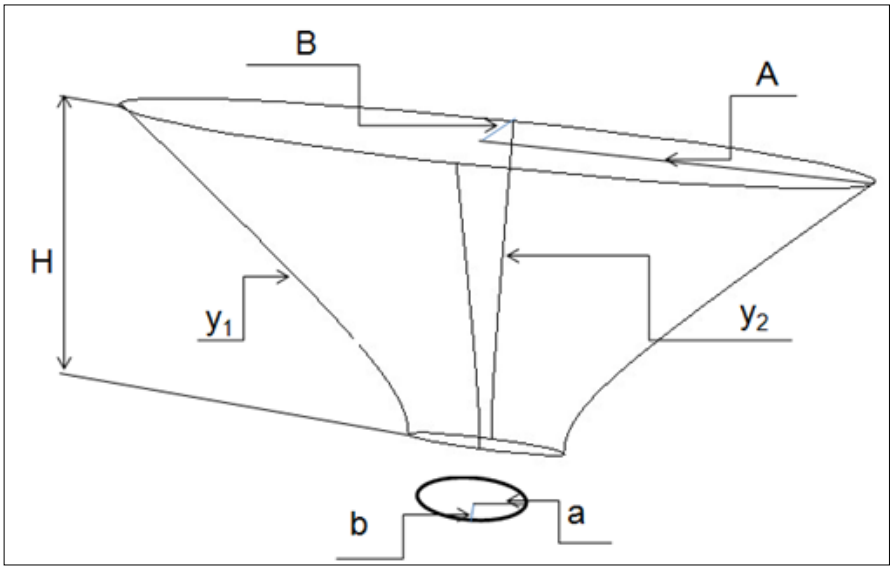

Figure 2.5: Geometric Parameters of Elliptical Hyperboloid Concentrator

The optical efficiency (η_{opt}) is given as [6]:

$$\eta_{opt} = \left[\left(\sum_{i=1}^{N} \left(I_i \rho^J \right) \Big/ I_0 \right) \right] \qquad 0 \le J \ge m \tag{2.8}$$

The geometric relation between the areas of entrance of the concentrator over the exit area, and it is given as:

$$CR_g = A_p \Big/ A_r \tag{2.9}$$

Where

A_p is aperture area of the entrance of the concentrator aperture area

$A_p \quad = \Pi \times A \times B$

A_r is aperture area of the exit of the concentrator aperture (receiver area)

$A_r \quad = \Pi \times a \times b$

The effective concentration ratio is defined as geometric concentration ratio to the optical efficiency. The effective concentration ratio is therefore given as:

$$C_{eff.} = CRg \times \eta_{opt} \tag{2.10}$$

Where

C_{eff} is effective concentration ratio, CR_g is geometric concentration ratio and η_{opt} is optical efficiency

2.4.3 Material of Elliptical Hyperboloid Concentrator

Normally, mirrors are expensive and fragile. Currently, the mirrors are replaced with metalised (silver) plastic films. Compared to mirrors, the films are very cost effective.

Moreover, low-end reflector - Mylar type "mirror films" will last for five years without deterioration of the reflectivity. Reflectors from Sky Trough/NREL, and 3M film are UV stabilised with high reflectivity of 94% or more (Reflectech, 2010) and 3M solar film (3M, 2011). Another film product developed by silver-based ReflecTech® is mirror film and has a specular reflectance is (ρ= 0.94). The films are lightweight with high mechanical strength. In the present thesis, the reflective film of 94% reflectivity is used in the EHC.

2.5 Ray Tracing Procedure in OptisWorks

The procedure for simulating the ray tracing analysis using OptisWorks software is as follows: modelling of the geometry; surface definition of solar concentrator; modelling of the source; illuminance detector and initiating the program with set of rays.

2.5.1 Modelling the Geometry

The new 3-D EHC geometric profile was created using SolidWorks software through the coordinates specified in Microsoft Excel. The coordinates of the geometry were generated from equation 2.6 and 2.7. In order to integrate the OptisWork and solid works software for the ray tracing simulations, the new solar concentrator were created in CAD software; this is shown in figure 2.6.

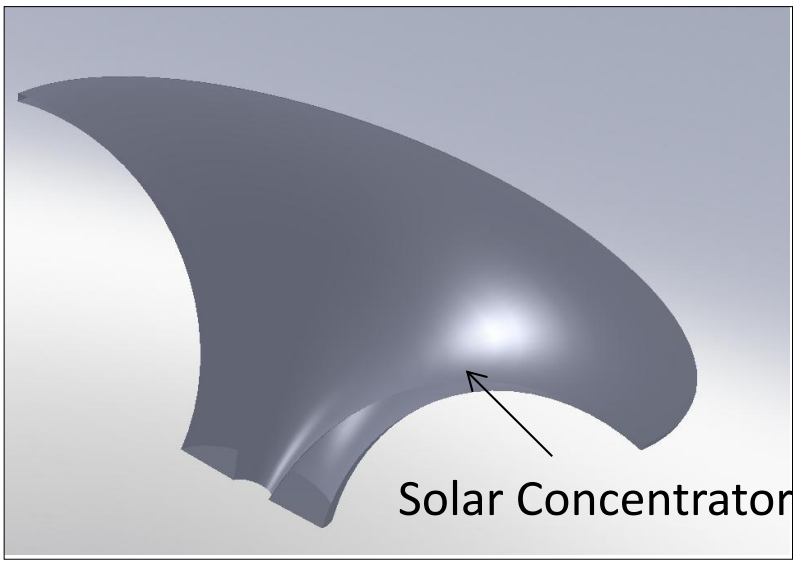

Figure 2.6: Geometry of EHC in Optisworks

2.5.2 Surface Definition of Solar Concentrator

After creating the geometric model of the Solar Concentrator using the SolidWorks software, the properties of the different surfaces in which the solar radiations travel

through were defined. The internal reflecting material was defined as 94% because of high reflectivity of the reflecting material, the intermediate material was defined as Plymetry Metharcrylate (PMMA) and the external material was defined as air because of the external atmosphere.

2.5.3 Modelling of the Source

In OptisWork software, a circle/ellipse was drawn to create the source of solar radiation. The area of the circle or ellipse should be higher than the aperture of the concentrator profile, as shown in figure 2.7. The internal surface of the source was defined as polished aluminium and air is considered as the external material. The source of light was defined to be applied at different incident angles on the elliptical entry aperture of the EHC. And the source is set up to generate 10 Mega rays, each ray having a uniform radiation intensity of 1000 W/m^2. This energy corresponds to 10000 rays per 1 mm^2 resulting in a light resolution and precision in the ray tracing simulation.

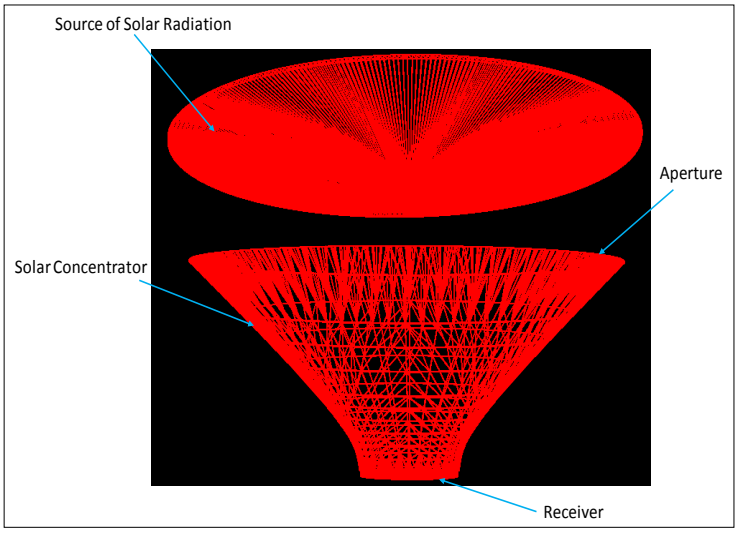

Figure 2.7: Source of Solar Radiation with the 3-D EHC

A xenon arc lamp was used as a light source in the solar simulation that emits a 5800 K blackbody spectrum [159]. The intensity of the light rays generated by the source is considered as lambertian with a limited half angle equal to 0°. That means that all the rays generated by the light source are parallel and perpendicular to the surface of the light source. "A lambertian surface that reflects or emits equal to (isotropic) luminance in all direction" [160], meaning that all of the rays are emitted in one direction, making an angle 0° to the normal of the surface of the light source. This assumption made for the light source helps to investigate the optical performance and behaviour of the EHC

concentrator for different angles of the incident rays. In the simulation, the angle can be varied from ± 90° to model the angular movement of the sun.

2.5.4 Illuminance Detector

The radiation source and the concentrator geometric profile were drawn in the OptisWork software, which is shown in figure 2.8. Two radiation/illuminance detectors were created. They were an aperture detector and a receiver detector. The aperture detector is placed at the entry of the EHC to measure the incoming radiation flux in W/m^2. The receiver detector is placed at the exit of the EHC to measure the total energy absorbed by the receiver of the EHC.

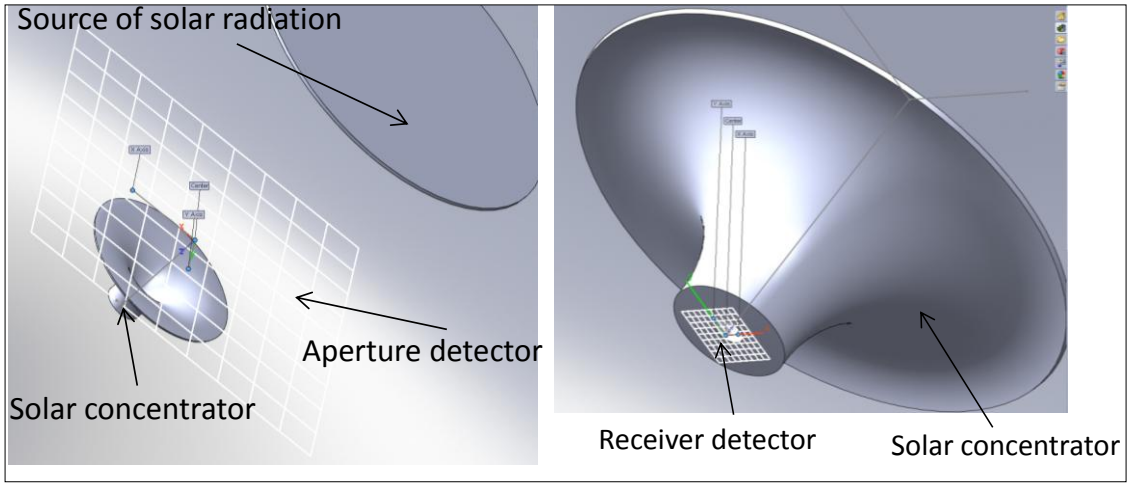

(a) (b)

Figure 2.8: (a) Aperture of the Concentrator Detector; (b) Receiver Detector for Incoming and Absorbing Solar Radiation Measurement

The optical efficiency of the geometric profile is defined as the ratio of the absorbed flux in the receiver to the incoming incident flux. The optical efficiency of the EHC (η_{opt}) is calculated according to Eq. 2.11.

$$\eta_{opt} = \frac{\varphi \text{ Exit(Receiver)}}{\varphi \text{Entry (Aperture)}} \times 100 \qquad (2.11)$$

Where

φ Entry (Aperture) is the flux in W/m^2, measured by the detector at the entry aperture and φ Exit (Receiver) is the flux in W/m^2, measured by the detector at the exit (receiver).

2.5.5 Simulation of ray tracing

After creating the detector at the entry and exit of the concentrator, the geometry can be readily used for simulation. The initial numbers of rays are set in the source. Once the

program is run, the rays pass through the source and enter the concentrator. As it is discussed, some of the rays are directly absorbed at the receiver; some of the rays pass reflected to and from and escape the concentrator. After multiple reflections, some of the rays enter the receiver region. The simulated ray tracing and flux distribution with incoming solar radiation from source and EHC is shown in figure 2.9.

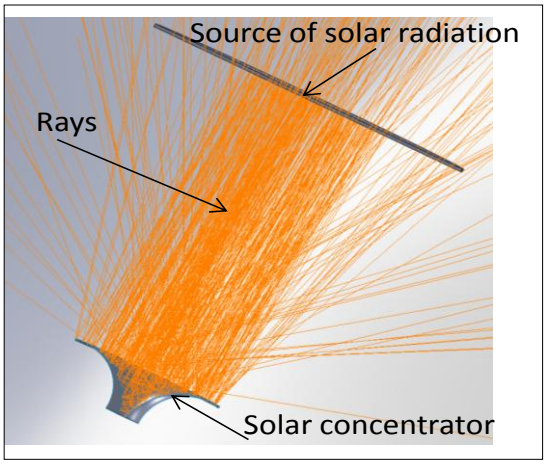

Figure 2.9: Simulated Ray Tracing and Flux Distribution with Incoming Solar Radiation from Source and EHC

2.5.6 Theoretical Performance Analysis of 3-D HC

Modelling and analysis of the 3-D EHC was carried out using the software Optis™ [161, 162]. Different dimensions of receiver major and minor axis with the concentrator height were studied. To improve the performance and consequently to reduce the EHC material, effect of truncation of the 3-D EHC was also analysed. Based on the ray tracing, the Optis™ software was used as the simulation tool to investigate the optical efficiency of the EHC. With the aid of the CAD software packages SolidEdge and SolidWorks, the geometry of EHC was created for different aspect ratios of the receiver, concentrator height and geometrical concentration ratios. The mirror is considered as the internal material used for the analysis of the rays, whose reflectivity is 0.94. The source of the solar radiation was varied to achieve different angles of incident rays at the entry of the aperture of the EHC. The radiation source was positioned to produce 10 Mega rays with an intensity of 1000 W/m^2. SolidWorks was used to illustrate the incident rays to enable a visual check on the degree of reflectivity of the internal concentrating surfaces of the EHC. Depending on the incident angle, the light ray will reflect on the internal surfaces of the EHC. For calculation purposes, the perpendicular incident angle to the aperture of the EHC was taken to be at 0°. Two luminance detectors were placed at the entry of the aperture and the exit of the concentrator of the EHC. The detectors measure the flux and energy of the incoming rays at the aperture

and concentrated rays at receiver of the EHC. The optical simulation stages of the optical model and geometric design are summarized in figure 2.10. The design of the elliptical hyperboloid to achieve optimum configuration is complex in nature. In order to formulate an optimisation problem, the first step is to define a mathematical formula for the hyperboloid shape. The parameters involved in the mathematical equation depend on a set of design parameters that represent the shape of a design, such as concentration ratio, concentrator height and receiver aspect ratio. The minimum aspect ratio corresponds to the ideal design performance. Two important concepts are considered for optimisation; i.e. for maximum power collection, to minimise radiation that enters the aperture of the system and does not arrive at the intended receiver, to achieve some desired irradiance distribution. On the other hand, the goal is to minimise the function, which measures the deviation between expected and resulted radiation pattern. Finally, an optimisation technique is employed to obtain the optimum design configuration. In addition, the value of y_1 (which connects the major axis dimensions of A and a, as shown in figure 2.5) and y_2 (which connects minor axis dimensions of B and b, as shown in figure 2.5) have to be found. Once the value of y_1 and y_2 are obtained, the 3-D elliptical hyperboloid concentrator is drawn using CAD software SolidWorks, for different concentrator heights and cross section of the ellipse.

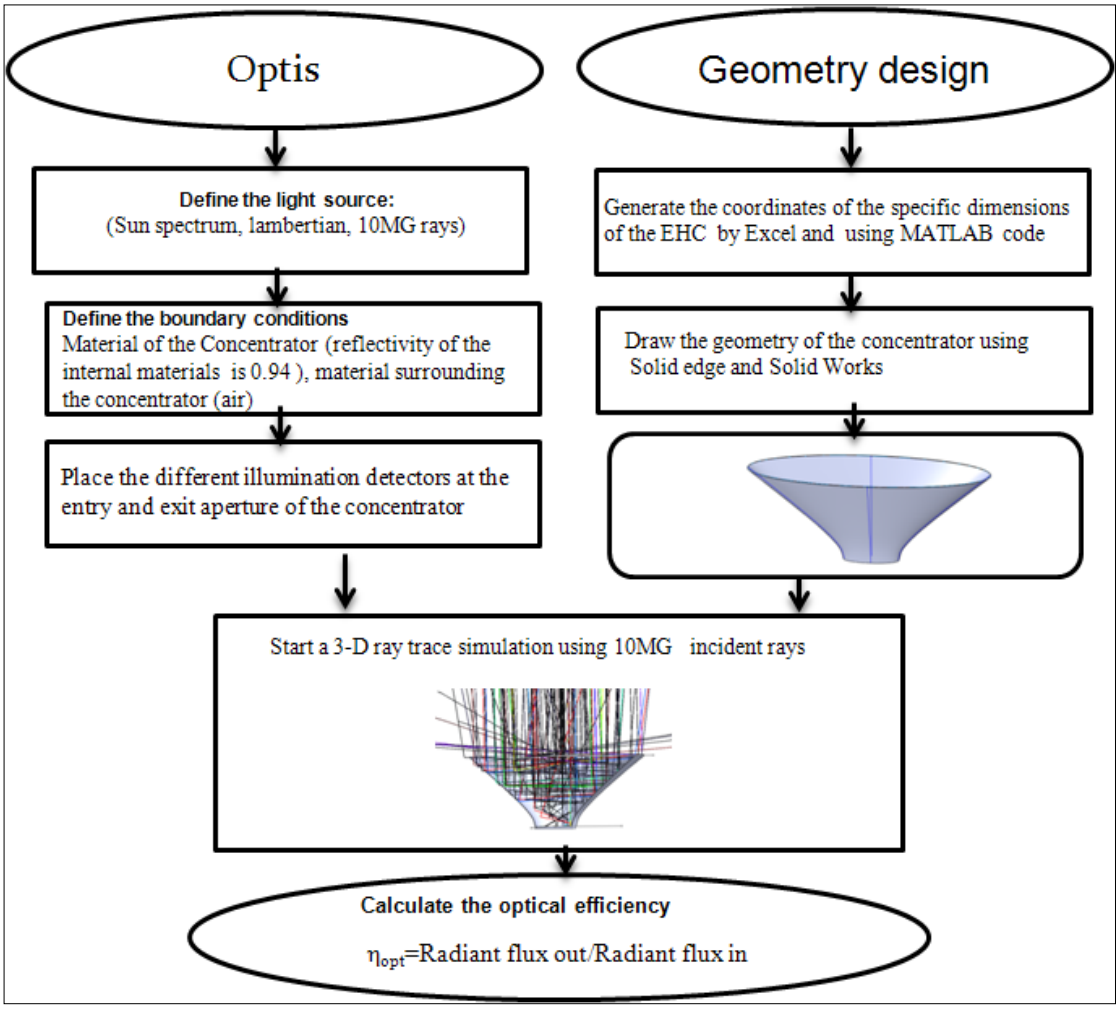

Figure 2.10: Flow Chart of Optical Simulation

2.6 Optimisation of the EHC

In order to optimise, the ray tracing simulation can be carried out for different EHC concentrator with:

- Different geometrical concentration ratios varying from: 5× to 30×
- Different dimensions of the geometry

The objective of the ray tracing simulations is to optimise the dimensions of the EHC concentrator with respect to its optical performance. The optimisation process passes through different stages, starting from obtaining the optimum profile of the entry aperture and exit receiver of the EHC, to obtaining the optimum concentration height and geometrical concentration ratio. The optimisation of the shape of the elliptical aperture and receiver starts from a circle when $a = b$, moving to different aspect ratio of both the aperture and receiver (a/b), where, a is the receiver major axis and b is the receiver minor axis.

2.7 Closure

In this chapter, a 3-D elliptical hyperboloid geometric design of solar collectors was considered. Three different methods of design of solar concentrator were presented. A review of the concepts and techniques used in designing the solar concentrator shape in terms of mathematical equations was also discussed. The modification of the equation of solar concentrators to produce 3-D EHC design was presented. The use of MATLAB code and Optis software to produce ray tracing for the design of the 2-D HC and 3-D EHC respectively was highlighted. The analysis of the fabrication of the 3D-EHC was also presented. By using the ray technique that has extensively explained in this chapter, the optimisation of the different optical characteristics such as optical efficiency, concentration ratio (CR), height of concentrator (HC) and receiver aspect ratio (AR) of the 2-D HC and the 3-D EHC are further investigated in chapter 3.

CHAPTER 3: OPTICAL PERFORMANCE OF A STATIC 2-D AND 3-D EHC

In this chapter the results of 2-D hyperboloid concentrator (2-DHC) and the 3-D static hyperboloid concentrator (3-DEHC) have been reported. The optical efficiency, effective concentration ratio, receiver aspects ratio, concentrator height and concentration ratio have been investigated through ray trace analysis. The optimisation of the concentrator profile and geometry is also carried out. The flux distributions of the receiver were obtained for concentrator profile.

3.1 Introduction

In the past few decades, the use of concentrating technology in the solar thermal applications is increased tremendously. Along with the concentrator system, the tracking system is also used to track the sun continuously from east to west. This would increases the overall cost of the system. To overcome this, a static hyperboloid concentrator is used in the solar thermal application of desalination. In order to study the feasibility analysis, a static 2-D and 3-D hyperboloid concentrator have been considered for ray tracing. First, a detailed 2-D ray tracing simulation code for hyperboloid concentrator has been developed in MATLAB. The optical efficiency have been investigated through ray trace analysis by varying large number of parameters such as incidence angle, concentrator height, receiver diameters and concentration ratio. Later, 3-D optical analysis is performed to investigate the effects of the degree of curvature of the hyperboloid shape on the optical perfomance. The optical efficiency of the 3-D static hyperboloid concentrator has been evaluated using ray tracing optic software. The performance parameters such as effective concentration ratio, and geometric concentration ratio are also evaluated for different aspect ratios of the elliptical profile. The optimisation of the concentrator profile and geometry is also carried out by varying the concentrator height, solar incidence angle and aspect ratio of the ellipse. The flux distribution on the receiver area for different concentrator aspect ratio of the ellipse is also carried out. Thus, the overall performance of the concentrator was obtained based on the optical efficiency, effective concentration ratio and acceptance angle.

3.2 Optical Analysis of 2-D Hyperboloid Concentrator

3.2.1 2-D Hyperboloid Concentrator

The acceptance angle is one of the important parameters for determination of optical efficiency. The angle subtends between the extreme rays of concentrator aperture and optical axis of the receiver is called half acceptance angle (Ø/2). For a fixed concentrator height (0.4 m) and receiver diameter (0.2 m), the 2-D hyperboloid curvature for different concentration ratio (5×, 10×, 15×, 20× and 25×) is obtained. The 2-D hyperboloid curvature for different concentration ratio is shown in figure 3.1. It is clear that the aperture area of the concentrator of 5× is five times higher than that of area of the receiver. As the concentration ratio increases, the half acceptance angle also increases. In order to see the variation of concentrator height on the acceptance angle, the concentrator height is varied for a fixed concentration ratio of 20× and receiver diameter of 0.2 m. The concentrator height is varied from 0.4 m to 1 m (0.4 m, 0.8 m, 1 m). The 2-D hyperboloid concentrators of different height (0.4 m,0.8 m and 1 m) are shown in figure 3.2. It is found that as the concentration ratio increases, the half acceptance angle also increases. In order to compare all the hyperboloid curvatures are superimposed. Ray tracing simulation were carried out to study the effect of change in the different optical parameters on optical efficiency.

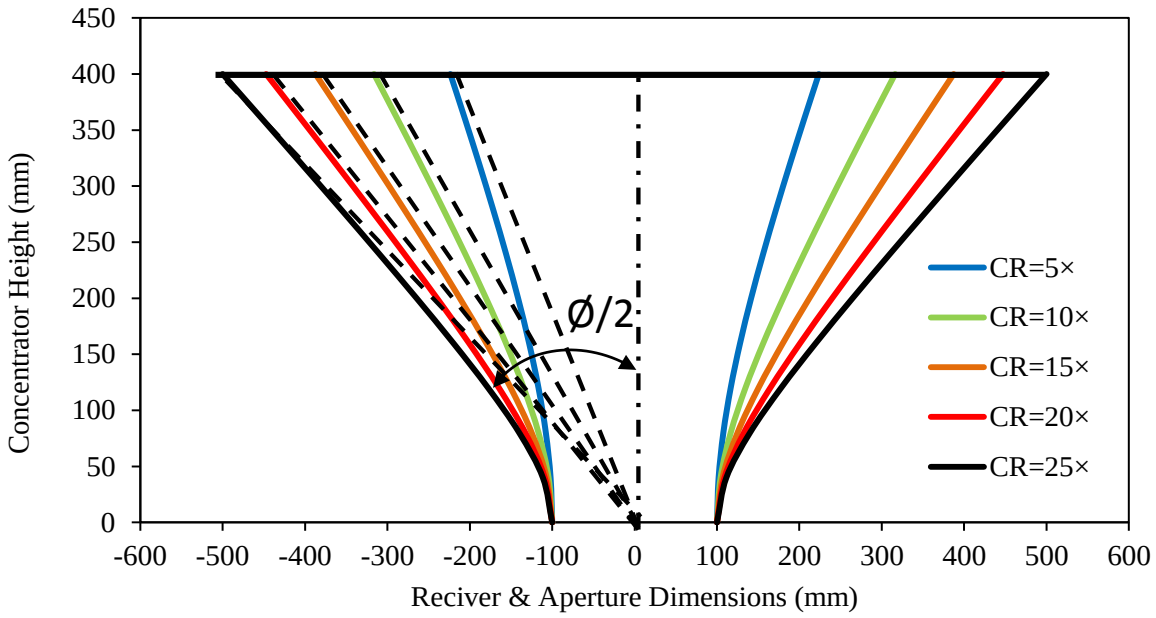

Figure 3.1: 2-D Hyperboloid Curvatures for Different Concentration Ratio

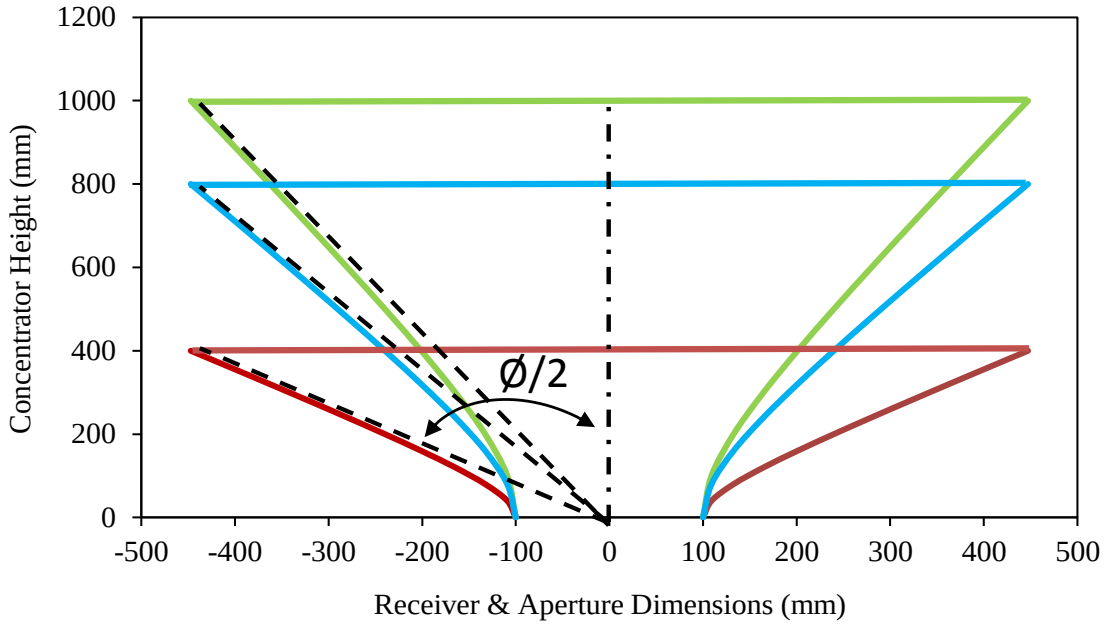

Figure 3.2: 2-D Hyperboloid Curvature for Different Concentrator Heights (0.4 m, 0.8 m, 1 m)

3.2.2 Ray tracing Technique for Hyperboloid Concentrator

In ray trace analysis, the sun rays are modeled to redirect the maximum fraction of incoming radiation onto the receiver diameter. The basic laws of optics (reflection) are used to model the behavior of the rays at the incident surface. In the ray trace analysis, the concentration ratio of 20× and the receiver diameter of 0.1 m are considered (located at the bottom of the concentrator). The incident angle is varied from 0° to 90° in the anticlockwise direction. The sun rays are perpendicular to the collector aperture at 0° (normal sun rays). At a 90° incident angle, the sun rays are horizontal. Ray tracing analysis is carried out for different incidence angle (0°, 15°, 30°, 45° and 60°) and for different concentrator heights (0.2 m, 0.4 m and 1 m). Ray tracing diagrams for concentrator height of 0.4 m and 0.2 m for different incidence angles of 0°, 15°, 30°, 45° and 60° are shown in figure 3.3. The ray tracing for concentrator height of 0.1 m for incidence angles of 0°, 15°, 30° and 45° is shown in figure 3.4.

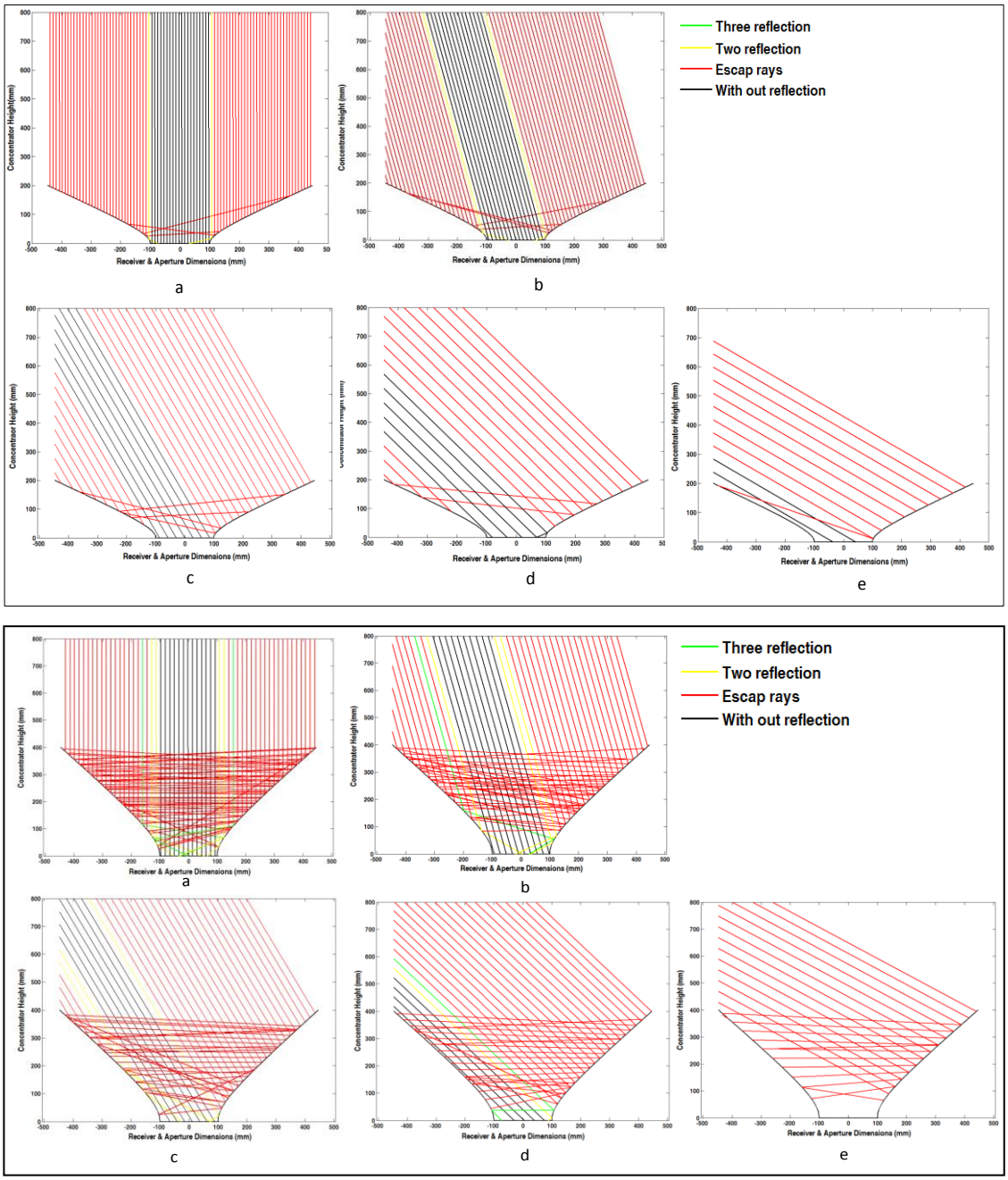

Figure 3.3: Ray Tracing Diagrams for Concentrator Heights of 0.2 m (top five) and 0.4 m (Bottom Five) for Different Incidence Angles (a) 0°, (b) 15°, (c) 30°, (d) 45° and (e) 60°

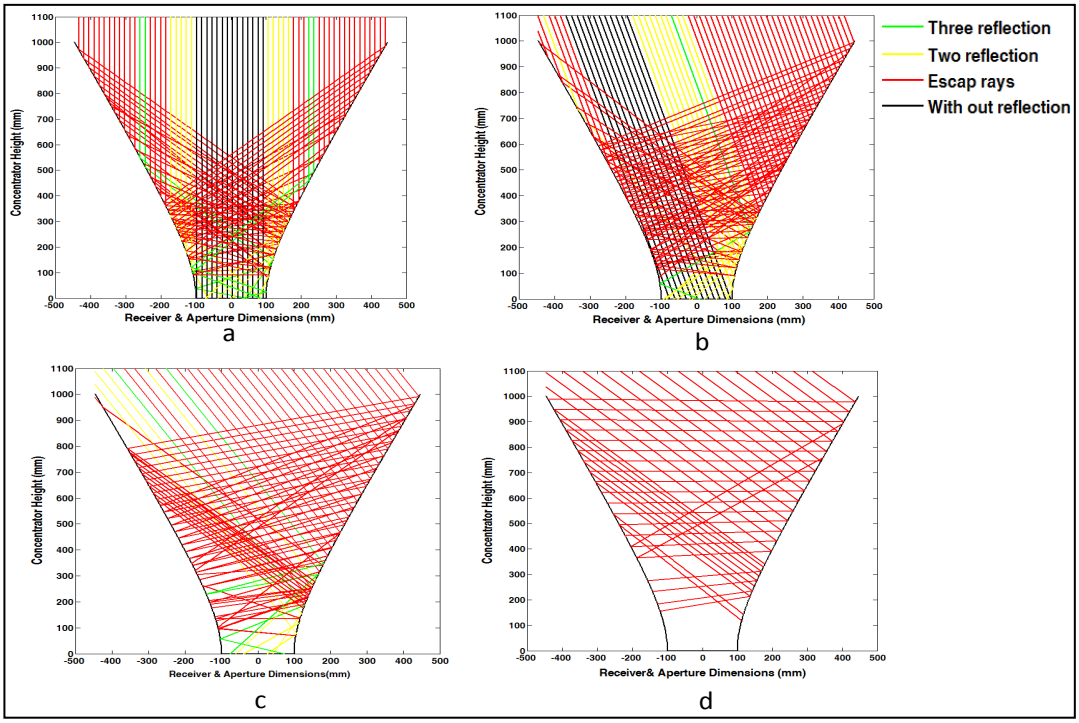

Figure 3.4: Ray Tracing Diagrams for Concentrator Heights of 1 m for Different Incidence Angles (a) 0°, (b) 15,° (c) 30° and (d) 45°

The 2-D optical performance of the hyperboloid concentrator is predicted based on the parameters such as geometrical concentration ratio (CR_g), geometrical concentrator profile and the height of concentrator (H). The optical efficiency is found based on the ratio of the total number of rays absorbed at the receiver to the total number of rays incident at the aperture of concentrator. In order to predict the optimum configuration of the hyperboloid concentrator, simulations were carried out so that the effect of one parameter (concentrator height) on the optical efficieny is varied and the other parameters are fixed as a constant (area of the concentrator aperture, receiver width).

3.2.3 Optical Efficiency of 2-D Hyperboloid Concentrator (2-D HC)

The impact of concentration ratio and concentration height on optical efficiency is investigated for different geometrical concentration ratios and concentrator heights. The concentrator height is varied from 0.1 m to 1.0 m over the angular range of ±90° (sun incidence angle). The geometrical concentration ratio is also varied from 5× to 25×. The variation of optical efficiency for different concentrator heights (0.1 m, 0.2 m, 0.3 m, 0.4 m, 0.5 m, 0.6 m, 0.7 m, 0.8 m, 0.9 m, 1 m) and concentration ratios (5×, 10×, 15×. 20× and 25×) are shown in figure 3.5. It is observed that the increase in the concentrator height increases the optical efficiency. The optical efficiency decreases for increasing the concentration ratio. For a fixed concentrator height of 0.4 m, the effect of

concentration ratio on optical efficiency is given in Table 3.1. It is found, at lower concentration ratio (e.g. 5×), the optical efficiency is found to be 51%. And optical efficiency of 28% is observed for *CR* of 10×. Beyond 10× (15×, 20×, 25×), the variation of optical efficiency is not significant (15%, 14%, 12%) and acceptance angle of ±30° is observed for the *CR* of 15×, 20×, 25×. It is concluded that the hyperboloid concentrator of 20× can be used to harness large amount of energy over a period during the day with average (not high) optical efficiency and has average energy flux distribution throughout the day.

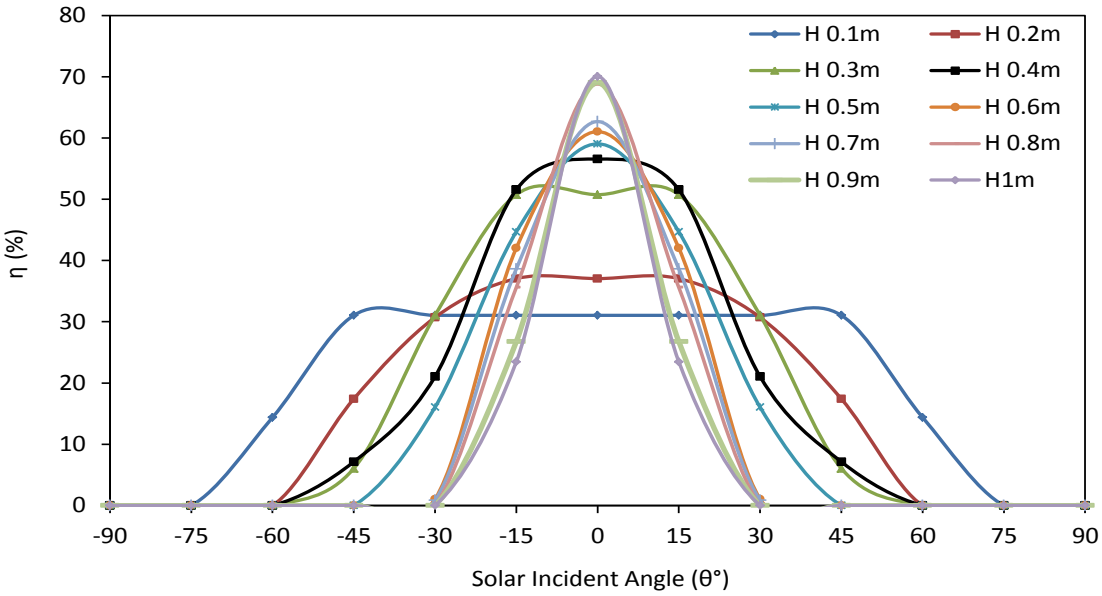

(a) 5×

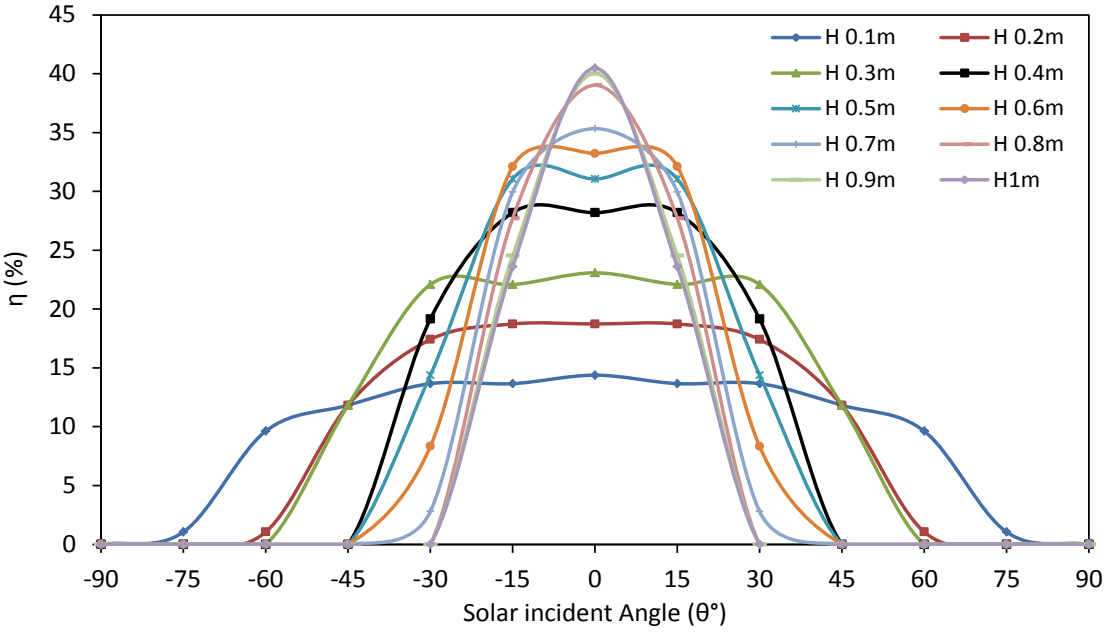

(b) 10×

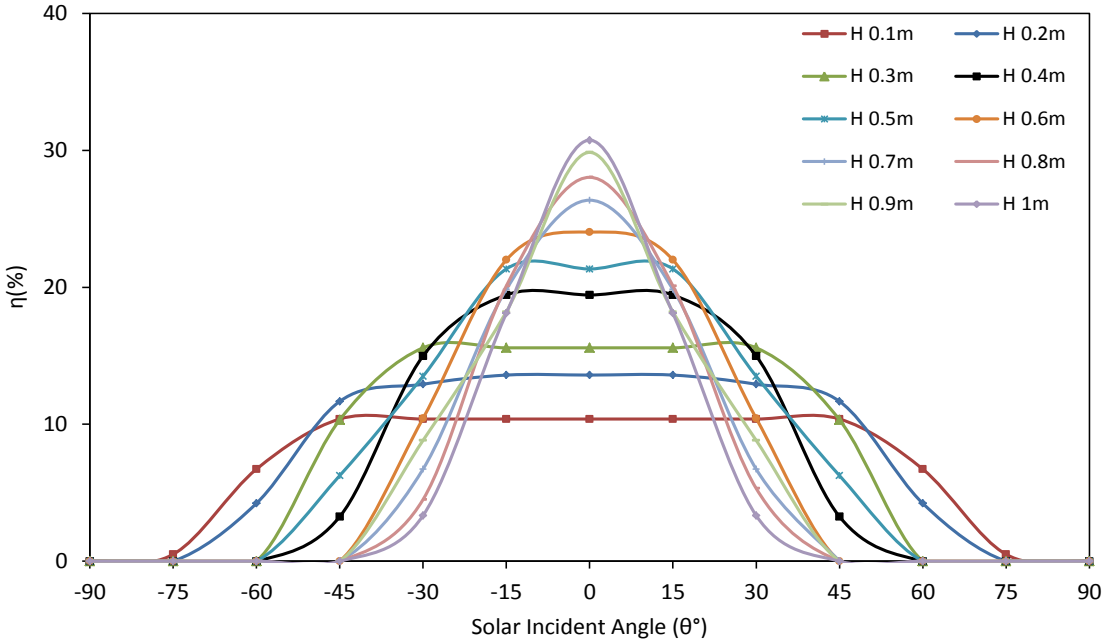
H 0.1m
H 0.2m
H 0.3m
H 0.4m
H 0.5m
H 0.6m
H 0.7m
H 0.8m
H 0.9m
H 1m
η(%)
Solar Incident Angle (θ°)

(c) 15×

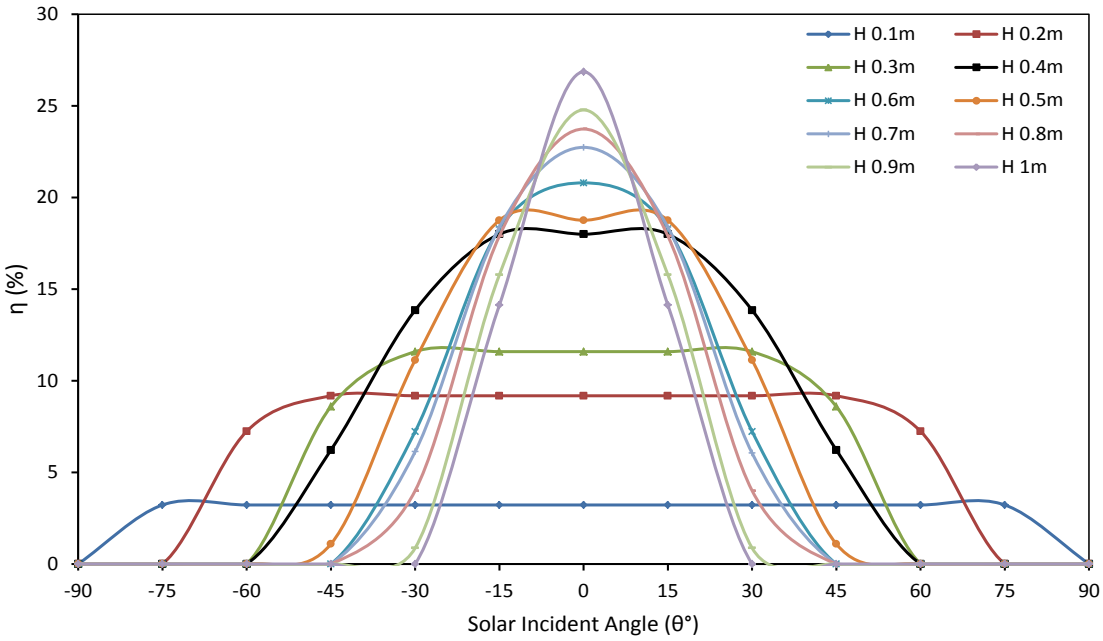
H 0.1m
H 0.2m
H 0.3m
H 0.4m
H 0.6m
H 0.5m
H 0.7m
H 0.8m
H 0.9m
H 1m
η (%)
Solar Incident Angle (θ°)

(d) 20×

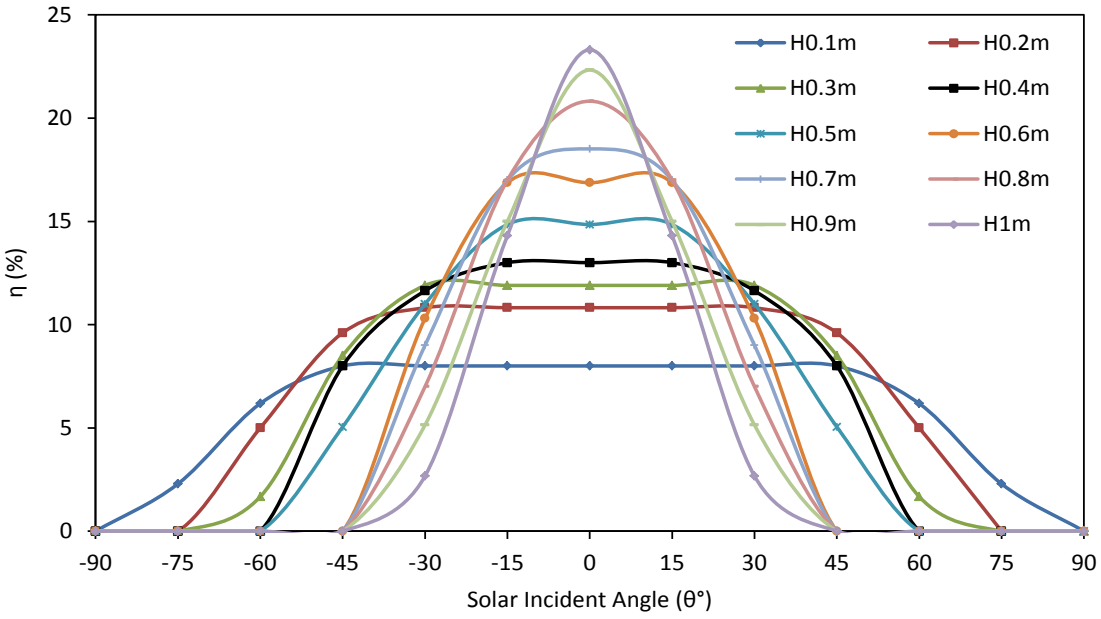

(e) 25×

Figure 3.5: Variation of Optical Efficiency with Solar Incident Angle for 2-D Hyperboloid Concentrator for Different Concentration Ratios (5×, 10×, 15×. 20× and 25×) and Different Concentrator Heights

Table 3.1: Variation of Optical Efficiency and Acceptance Angle for Different Concentration Ratio of Hyperboloid Concentrator Height of 0.4 m

2-D Hyperboloid Concentrator		
Concentration Ratio (*CR*)	Acceptance Angle (°)	Optical Efficiency (%)
5	±15	51
10	±15	28
15	±30	15
20	±30	14
25	±30	12

3.2.4 Effect of Concentration Ratio on the Optical Efficiency

At concentrator height of 0.4 m and major axis is 0.1 m; the effect of concentration ratio on the optical efficiency is investigated. The concentration ratio is varied from 5× to 25×. The optical efficiency is evaluated for different concentration ratios and solar incidence angle and the variation of optical efficiency is shown in figure 3.6. As the geometrical concentration ratio increases, the optical efficiency decreases. For

concentration ratio of 20×, the variation of optical efficiency is found to be 19%, 14% for the corresponding acceptance angle of 0° and 30°.

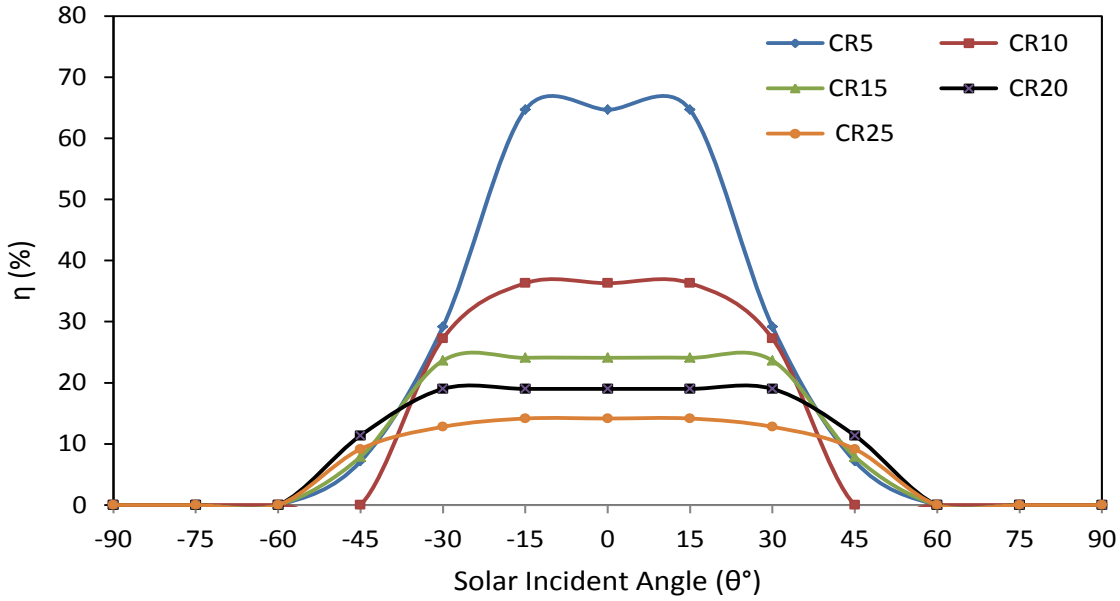

Figure 3.6: Variation of Optical Efficiency for Different Geometrical Concentration Ratio and Incidence Angles at Concentrator Height 0.4 m

3.2.5 Effect of Variation of Receiver diameter on Optical Efficiency

Ray tracing analysis is carried out for 2-D hyperboloid concentrator of 20× and the incidence angles are varied from 0° to 45°. The ray tracing diagram for 2-D hyperboloid concentrator with different receiver diameter for various incidence angles are shown in figure 3.7. Depending on the total number of rays absorbed at the receiver, compared to the total number of rays incident at the aperture of concentrator, optical efficiency is obtained for the various receiver diameters. The optical efficiency is obtained for a fixed concentration ratio of 20× and concentrator height of 0.4 m. The receiver diameter is varied from 0.01 m to 0.1 m. The increase in the receiver diameter, leads to wider acceptance angle and decreases the optical efficiency. The effect of optical efficiency on the receiver diameter for different solar incidence angle is shown in the figure 3.8. It is observed the lower receiver diameter leads to higher optical efficiency and lower acceptance angle. For higher receiver diameter low optical efficiency and high acceptance angle is observed.

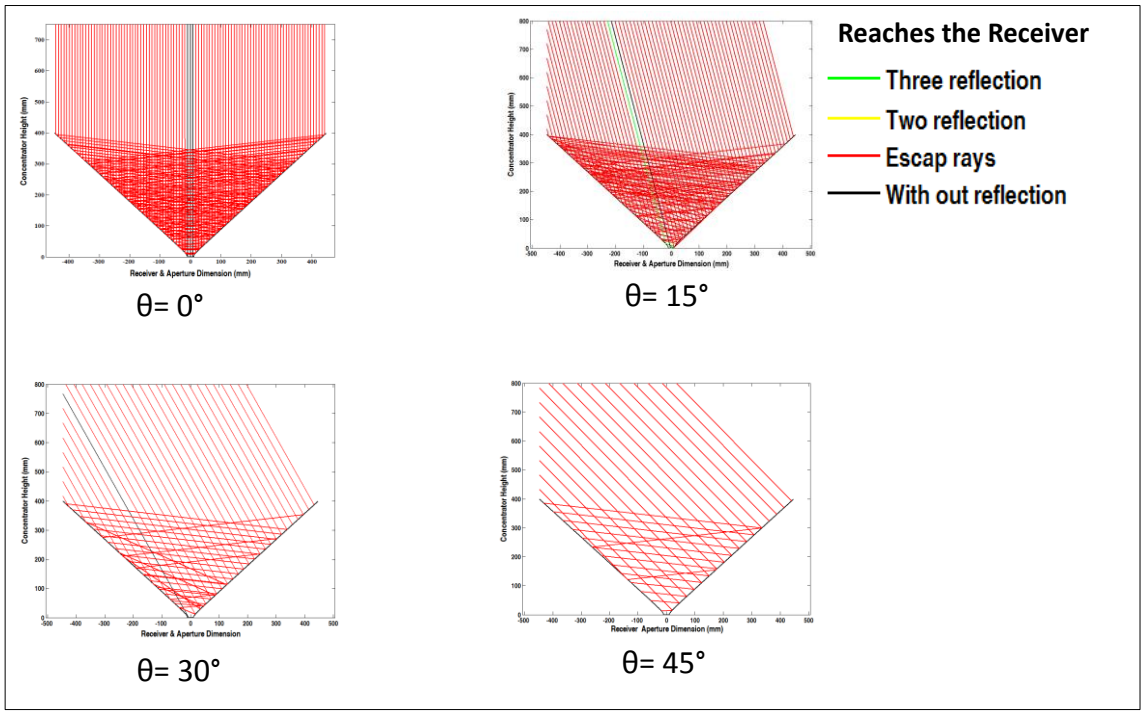

(a) Receiver Diameter of 0.05 m

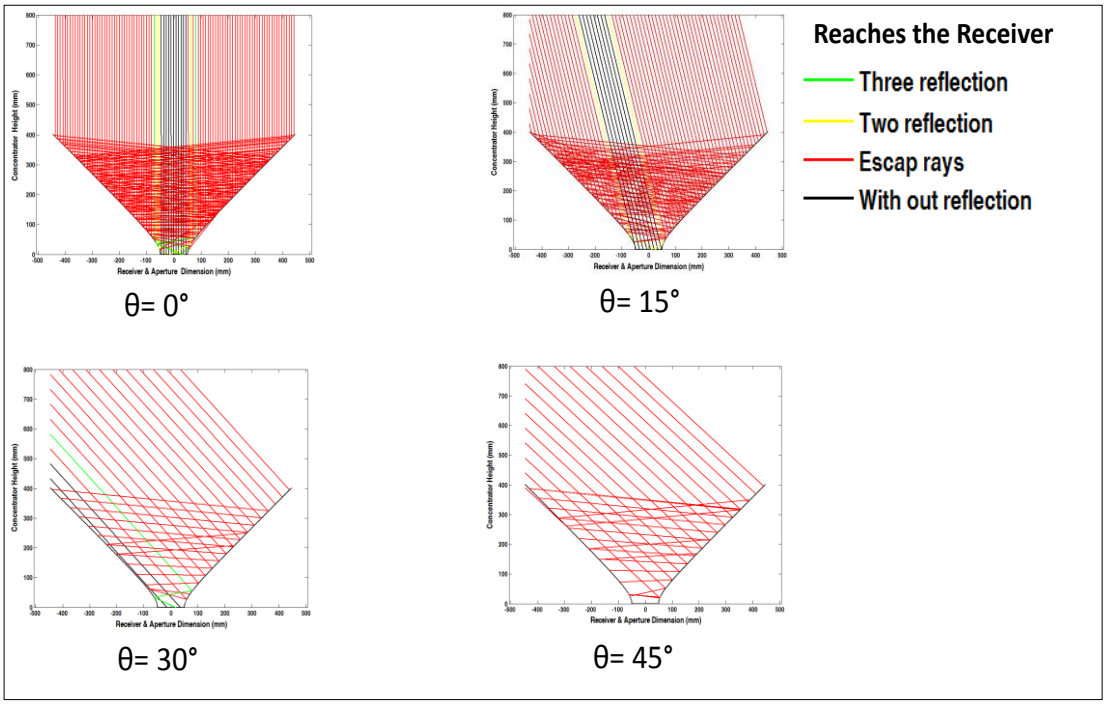

(b) Receiver Diameter of 0.01 m

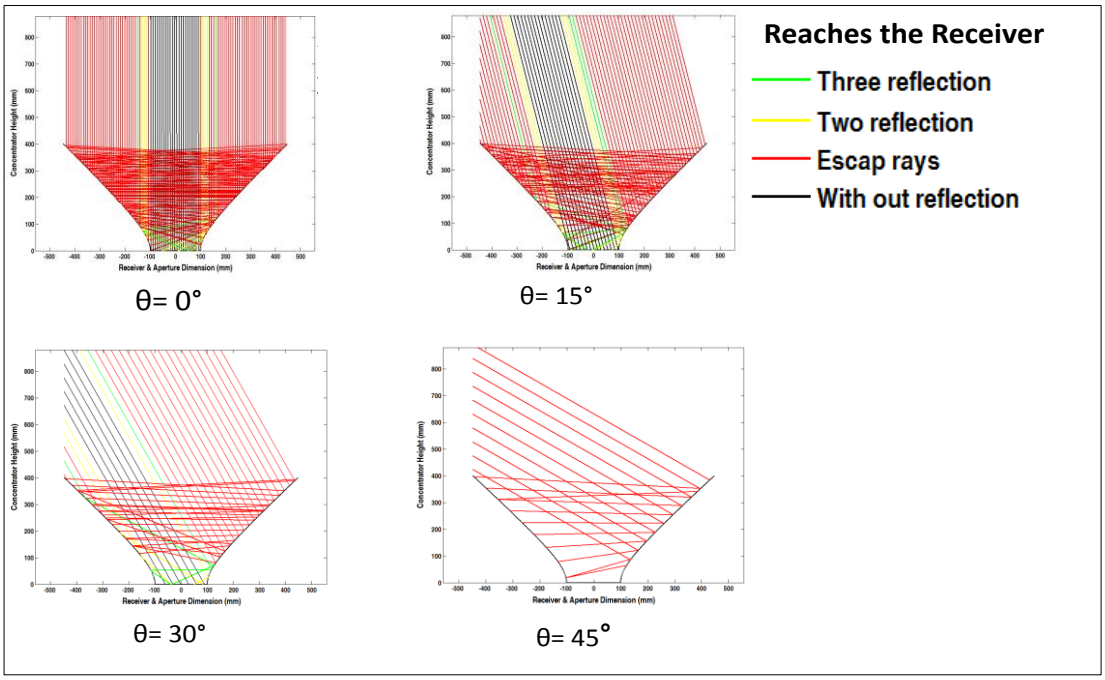

(c) Receiver Diameter of 0.1 m

Figure 3.7: Ray Tracing Diagram for Concentration Ratio of 20× Based on Different Receiver Diameters ((a) is 0.05m, (b) is 0.01 and (c) is 0.1 m) and Incidence Angles (0^o, 15^o, 30^o and 45^o)

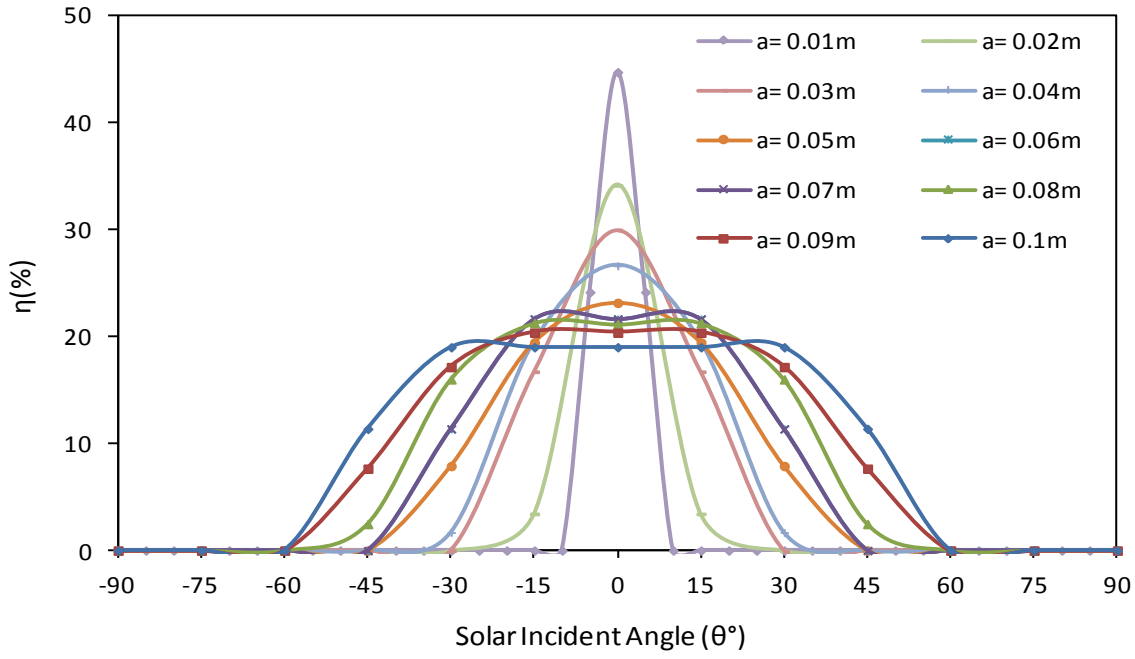

Figure 3.8: Effect of Optical Efficiency on the Receiver Diameter for Different Solar Incidence Angles

3.3 Optical Analysis of 3-D Hyperboloid Concentrator

3.3.1 3-D Hyperboloid Concentrator

In the previous section, 2-D analyses of hyperboloid concentrator have been carried out. In order to see the effect of curvature on the optical efficiency, 3-D investigations are also carried out for the hyperboloid concentrator. To obtain the optimum 3-D elliptical hyperboloid configuration and to predict the optimum optical efficiency and effective concentration ratio, 3-D ray tracing analysis have been carried out using the software Optis^{TM} [161, 162]. The 3-D geometry is created with the aid of the CAD software SolidEdge and SolidWorks. The 3-D EHC geometry is designed for different area ratio of the receiver, concentrator height and geometric concentration ratios. The effect of receiver major and minor axis and the effect of concentrator height on the optical efficiency are studied in the 3-D analyses. The effect of truncation are also carried out to improve the performance and to reduce the material consumption. The reflectivity of the inner material is considered as 0.94. In the SolidWorks, above the top of the 3-D geometry source of solar radiation are created with different angles. The source was positioned to produce 10 mega rays with energy flux value of 1000 W/m^2. OptisWorks has provisions to check the degree of reflectivity on the internal concentrating surfaces of the EHC. The rays perpendicular to the source and aperture opening of the concentrator are considered as 0° incident angle. Depending on the incident angle, the light ray will reflect on the internal surfaces of the EHC and finally reached the receiver area. Two luminance detectors are placed, one at the entry aperture and other at the exit concentrator area (receiver area) to measure the incoming flux at the opening aperture of the concentrator and outgoing flux at the receiver area of the EHC

3.3.2 Effect of Receiver diameter and Concentrator Height on Effective Concentration Ratio

The effect of receiver diameter and concentrator height on the effective concentration ratio is studied. The effect of ratio of concentrator height and receiver major axis and minor axis diameter (H/a & H/b) on the effective concentration ratio is obtained for different incidence angles (0°, 15°, 30°, 45°) are shown in figure 3.9. It is observed, for all the incident angles, the effective concentration ratio increases until the ratio (H/a) reaches 4. Beyond this value, the effective concentration ratio decreases for the incident angles of 30° and 45°. For the incident angles of 10° and 15°, the effective concentration ratio increases as the ratio of (H/a) increases. It can be concluded that the

optimum value is reached at the ratio of (*H*/*a*) 4. Beyond this value, the effect of increasing the effective concentration ratio is not significant. This is due to the incidence angle and the total number of reflection of the internal surface of the hyperboloid mirror on the incoming rays. The ratio (*H*/*a*) increases the degree of curvature of the reflecting surface decreases. For values of (*H*/*a*) less than 4, most of the rays were reflected away from the aperture. For values greater than 4, a number of the rays are reflected inside the profile itself increases before reaching the receiver area. Similar effects are observed for the variation of concentrator height and receiver minor diameter (*H*/*b*). However, there is an abrupt drop in the effective concentration ratio for values greater than 20. For values greater than 25, there is little variation observed on the effective concentration ratio.

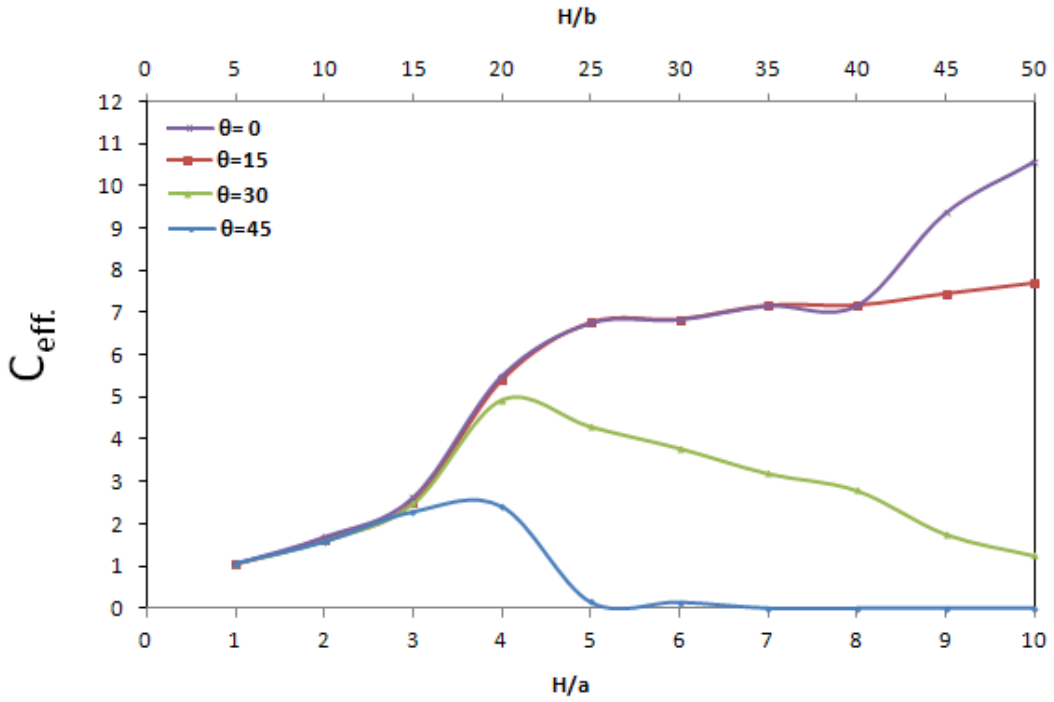

Figure 3.9: Variation of Effective Concentration Ratio with (*H*/*a*) & (*H*/*b*) Ratio for Different Incidence Angles

3.3.3 Effect of Receiver Aspect Ratios on Optical Efficiency

The effect of aspect ratio (ratio of the receiver major axis to the receiver minor axis) on the optical efficiency of the hyperboloid concentrator was carried out to determine the optimum receiver dimensions. This study was carried out for a fixed concentration ratio of 20×. The ratio of *H*/*a* of 4 is considered. By keeping the concentrator height of 0.4 m, the source is varied along the receiver major diameter and the aspect ratio is varied from 1 to 10, to obtain the variation of optical efficiency. Similarly, the source is varied along

the receiver minor diameter and the aspect ratio is varied from 1 to 10, to obtain the variation of optical efficiency. The variation of the optical efficiency for different solar incidence angles and different aspect ratio (*a*/*b*) for constant concentrator height and concentration ratio are shown in figure 3.10 (a), (b). As the aspect ratio increases, the optical efficiency increases till aspect ratio 5. Beyond the aspect ratio 5, there is a drop in the optical efficiency of less than 3-4%. In another study, at aspect ratio 5, the effect of concentrator height on the optical efficiency for different solar incidence angles is also carried out. By keeping the aspect ratio of 5 as constant, the concentrator height and the source is varied along the receiver major axis to obtain the variation of optical efficiency, which is shown in figure 3.11 (a). In a similar study, the concentrator height and the source were varied along the receiver minor axis to determine the resulting variation of optical efficiency, which is shown in figure 3.11 (b). From the results it is clear that as the concentrator height increases, the optical efficiency increases while the acceptance angle decreases irrespective of the receiver major and minor axis diameter.

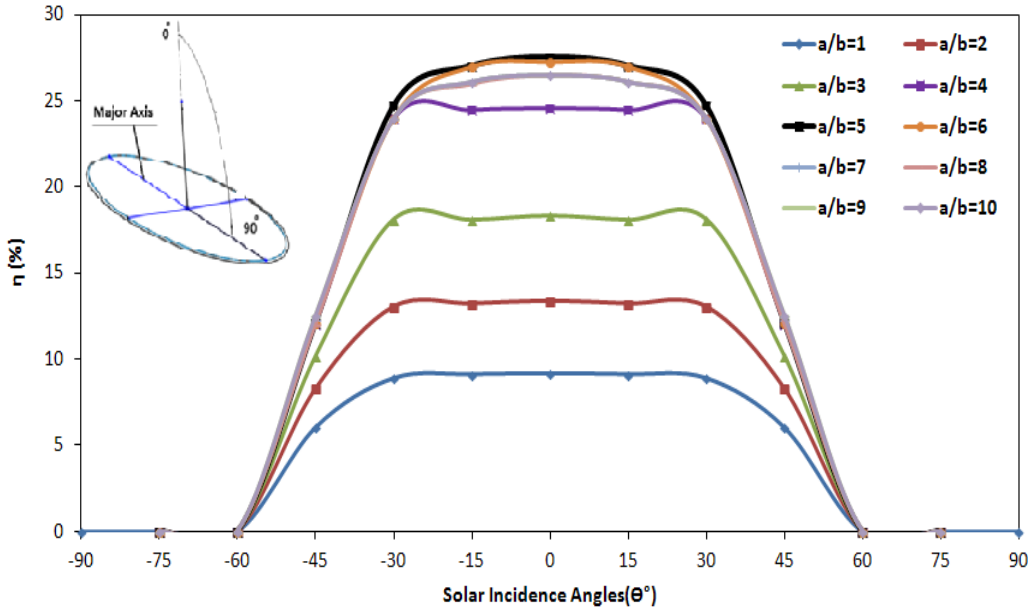

(a) Variation of the Source in Receiver Major Axis Diameter

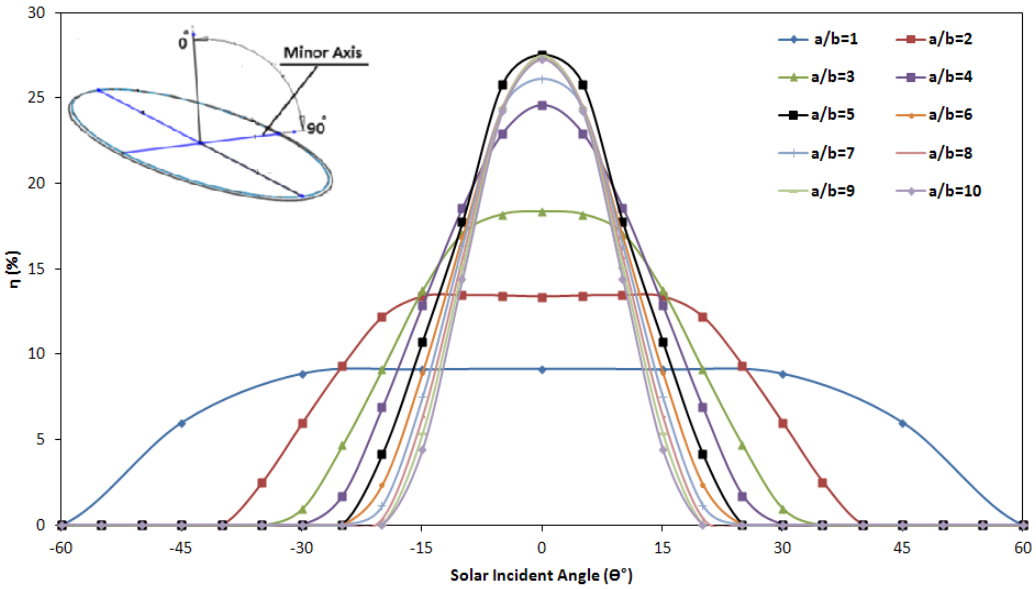

(b) Variation of Source in Receiver Minor Axis Diameter

Figure 3.10: Variation of the Optical Efficiency for Different Solar Incidence Angles and Different Major and Minor Axis Diameter for A Fixed Concentrator Height and Concentration Ratio

3.3.4 Effect of Concentrator Height on Effective Concentration Ratio and Optical Efficiency

In the study of different aspect ratio, it is found that the aspect ratio (*a*/*b*) of 5 gives the maximum optical efficiency. The study of effect of concentrator height on the effective concentration ratio and optical efficiency is carried out for 3-D EHC. The source is moving along the major and minor axis diameter for the aspect ratio of 5 and its effect is

also investigated. The variation of effective concentration ratio, when the source is moving along the receiver major axis diameter for different concentrator heights (0.1 m to 1 m) and solar incidence angles is shown in figure 3.12 (a), Similar effects were also discovered by varying the source along receiver minor axis diameter is shown in figure 3.12 (b). As the concentrator height increases, the effective concentration ratio increases, optical efficiency increases and acceptance angle decrease. At concentrator height of 0.4 m and acceptance angle ±30º, the optical efficiency is 25% and for the acceptance angle ±45º, the optical efficiency is 12%, at concentrator height of 0.5 m and acceptance angle ±30º, the optical efficiency is 22% and for the acceptance angle ±45º, the optical efficiency is 7%. By comparing this, EHC with concentrator height of 0.4 m is an optimum design with an acceptance angle of ±45º; give an efficiency of 12%. The tabular form of variation of optical efficiency for different solar incidence angles and concentrator heights are given in table 3.2.

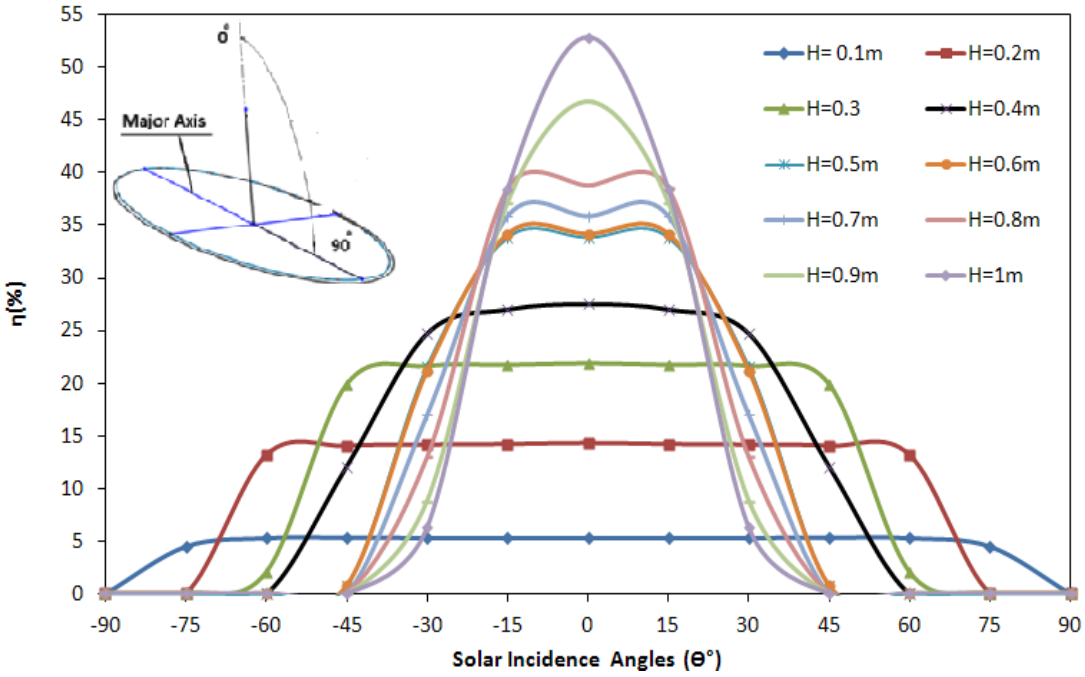

(a) Variation of the Source in Receiver Major Axis Diameter

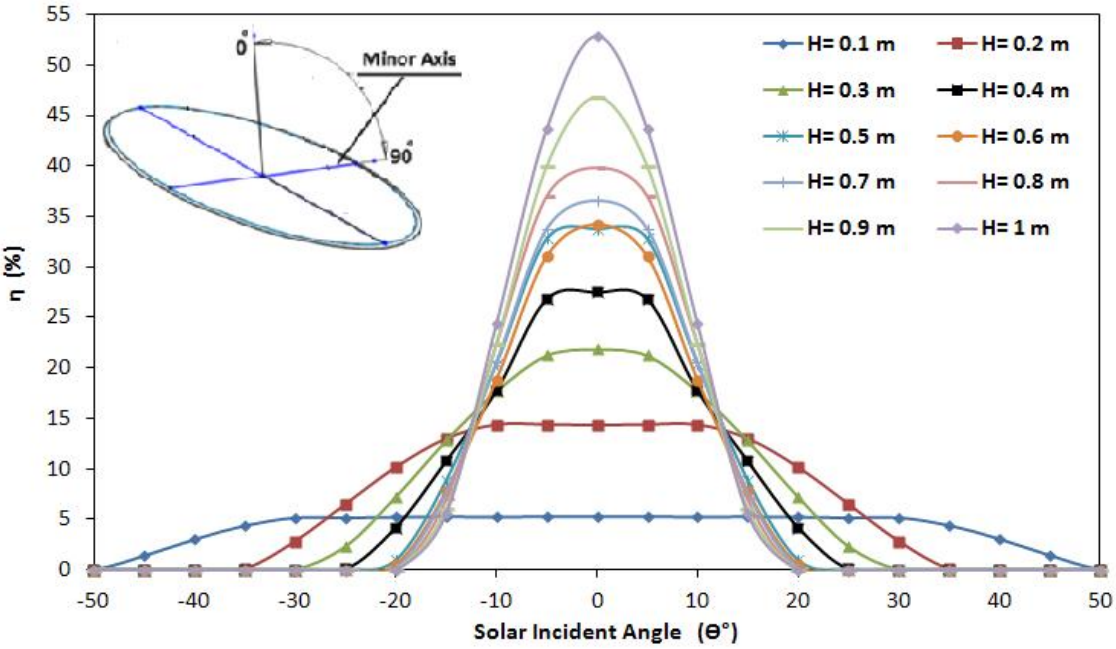

(b) Variation of the Source in Receiver Minor Axis Diameter

Figure 3.11: Variation of the Optical Efficiency for Different Concentrator Heights and Receiver Major and Minor Axis Diameter for Different Incidence Angles

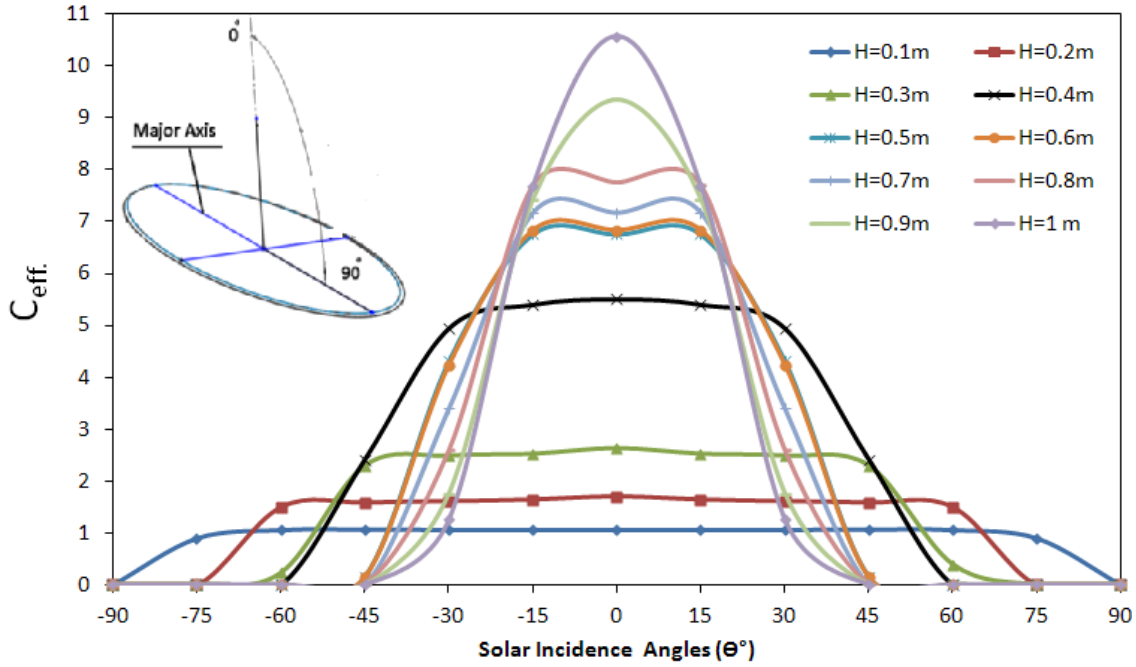

(a) Variation with Receiver Major Axis Diameter

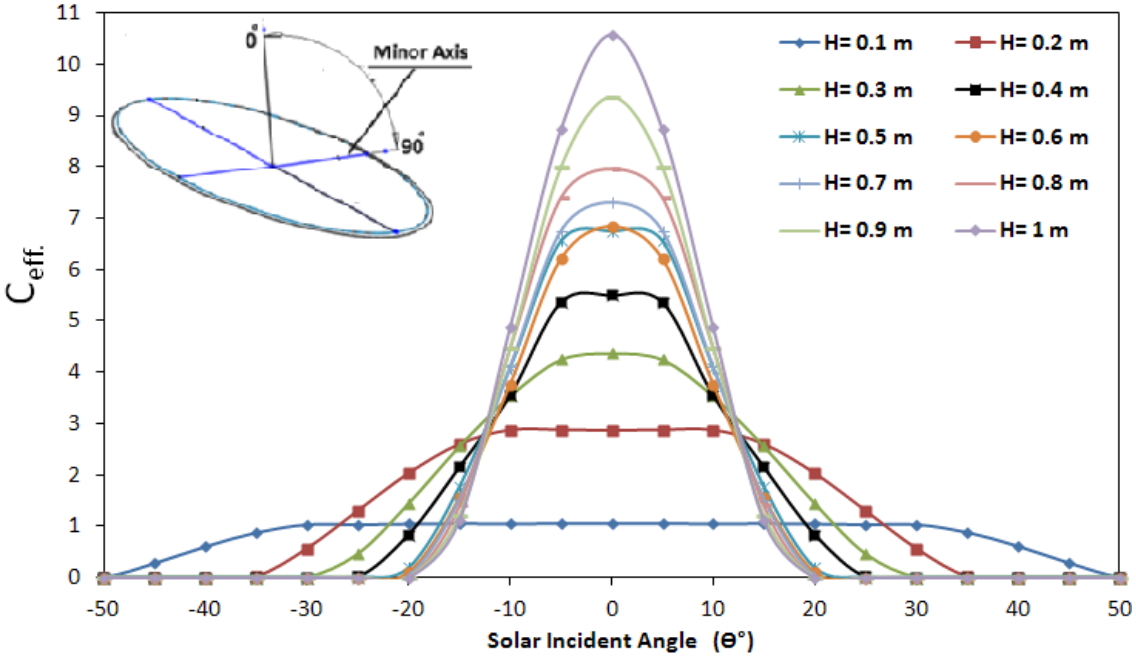

(b) Variation with Receiver Minor Axis Diameter

Figure 3.12: Variation of Effective Concentration Ratio, When the Source Is Moving Along the Receiver Major Axis Diameter for Different Concentrator Heights (0.1 m to 1 m) and Solar Incidence Angles at Aspect Ratio of 5 and *CR* of 20×

Table 3.2: Variation of Optical Efficiency of EHC for Different Solar Incidence Angles and Different Concentrator Heights

H (m)	Optical efficiency of EHC (%)							
	Solar incidence angle along major axis, θ(°)				Solar incidence angle along to minor axis, θ(°)			
	0	15	30	45	0	15	30	45
0.2	14	14	14	14	14	13	3	0
0.4	28	27	25	12	28	11	0	0
0.6	34	34	21	0	34	8	0	0
0.8	39	39	13	0	39	7	0	0
1	53	38	6.2	0	53	6	0	0

3.3.5 Effect of Concentration Ratio on the Optical Efficiency Using Optimum Concentrator Height and Optimum Aspect Ratio

At concentrator height of 0.4 m and aspect ratio of 5, the effect of concentration ratio on the optical efficiency is investigated. The concentration ratio is varied from 5× to 40×. The optical efficiency is evaluated for different concentration ratios and solar incidence angle and the variation of optical efficiency is shown in figure 3.13. As the concentration ratio increases, the optical efficiency decreases. For concentration ratio of 20×, the variation of optical efficiency is found to be 28%, 25%, and 12% for the corresponding acceptance angles of 0°, 30°, and 45°. The variation of optical efficiency for different concentration ratios and different incidence angles at concentrator height of 0.4 m and aspect ratio of 5 is also given table 3.3.

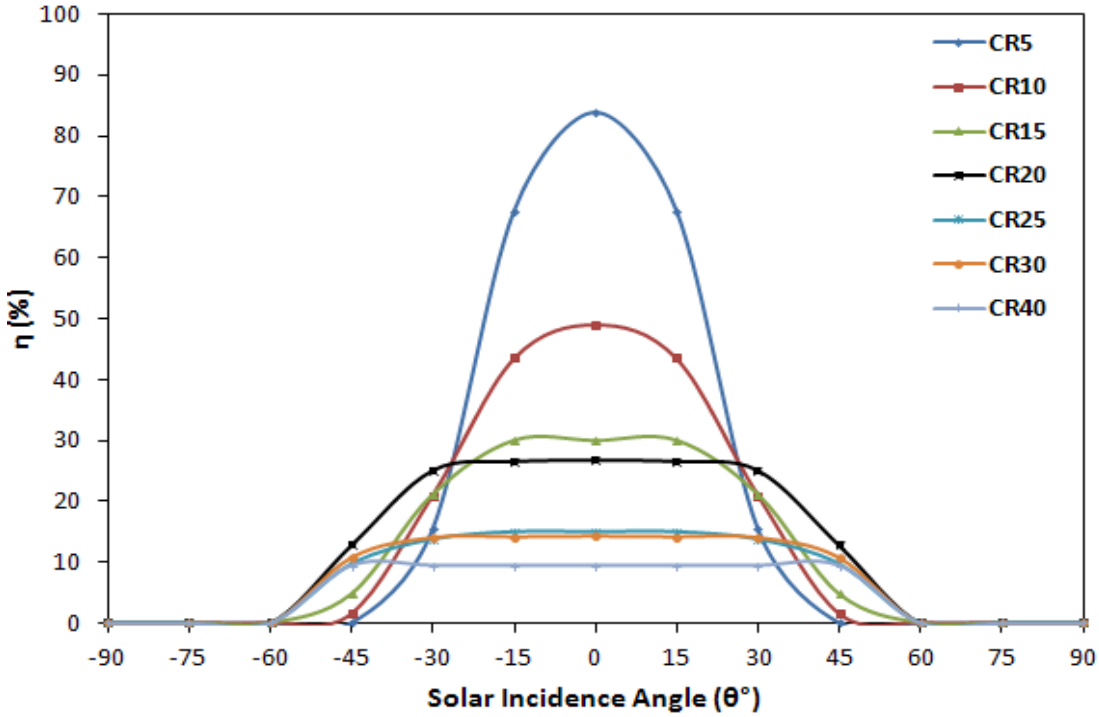

Figure 3.13: Variation of Optical Efficiency for Different Concentration Ratio and Incidence Angles at Concentrator Height 0.4 m and Aspect Ratio of 5

Table 3.3: Optical Efficiency of EHC for Different Solar Incidence Angles and Different Concentration Ratio

	Optical Efficiency (η %) of EHC, a/b=5 & H=0.4 m						
θ	Concentration Ratio						
	5	10	15	20	25	30	40
0	84	49	30	28	15	14	9
15	68	43	30	27	15	14	9
30	15	21	21	25	15	14	9
45	0	1	5	12	14	11	9

3.3.6 Incidence Angle Modifier (IAM)

The incidence angle modifier is given by Eq. (3.1) [163]. The IAM variation along with the elliptical dimensions, at the concentrator height of 0.4m and concentration ratio of 20× is shown in figure 3.14.

$$k(\theta, \quad 0) = \frac{\eta_{opt} \quad (\theta, \quad 0)}{\eta_{opt} \quad (0, \quad 0)} \tag{3.1}$$

Where $\eta_{opt} \quad (\theta, \quad 0)$ is optical efficiency for the normal incidence.

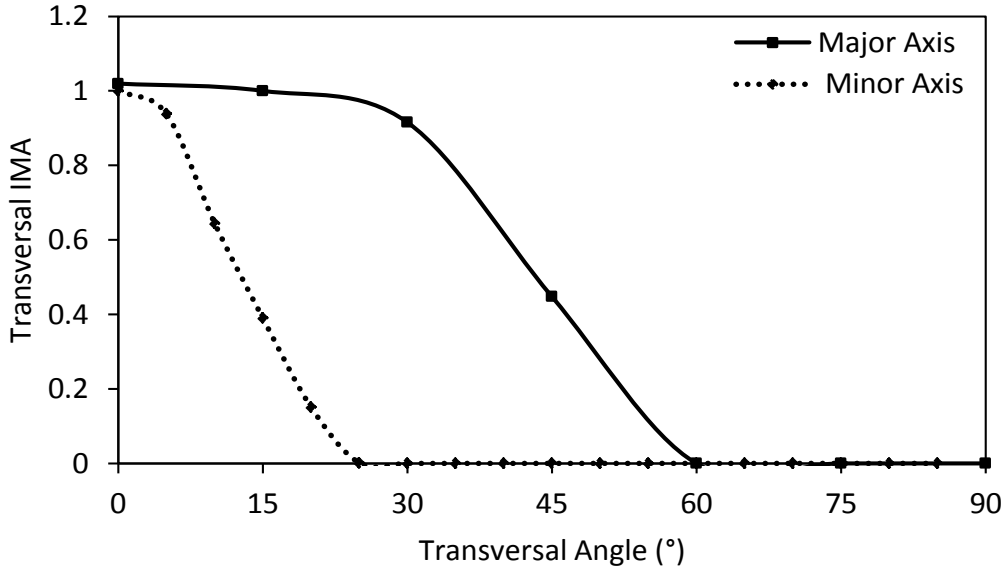

Figure 3.14: Transversal IAM as Function of the Transversal Angle for Major and Minor Axis at H = 0.4 m & *CR* = 20×

3.4 Effect of Truncation of EHC on the optical performance

Truncation of the 3-D EHC is also carried out to predict its effect on optical efficiency and effective concentration ratio. Because, truncation can reduce the concentrator materials with desired output. For the aspect ratio of 5, the variation of the optical efficiency with solar incidence angle when the source is moving along the aperture major axis and minor axis for different percentage of concentrator heights is shown in figure 3.15 (a), (b). As the truncation percentage increases, there is an increase in the optical efficiency and decrease in the concentration ratio. The corresponding decrease in the concentration ratio is also given in the figure 3.15. At 10% truncation of the concentrator height, the maximum optical efficiency of 32% is observed and the corresponding concentration ratio is dropped to 16.4 (initial *CR* = 20×). It is also observed that no rays are absorbed when the acceptance angle goes beyond 60° and 25° for the case of the source moving along the receiver major and minor axis diameter. Again, for the aspect ratio of 5, the variation of the effective concentration ratio with solar incidence angle when the source is moving along the aperture major axis and minor axis for different percentage of concentrator heights is shown in figure 3.16 (a), (b). By decreasing the concentrator height, a drop in effective concentration ratio and geometrical concentration ratio occurs, but there is an increase in the optical efficiency. For 10% truncation of concentrator height, the effective concentration ratio is dropped to 13%, but the optical efficiency is increased to 13%

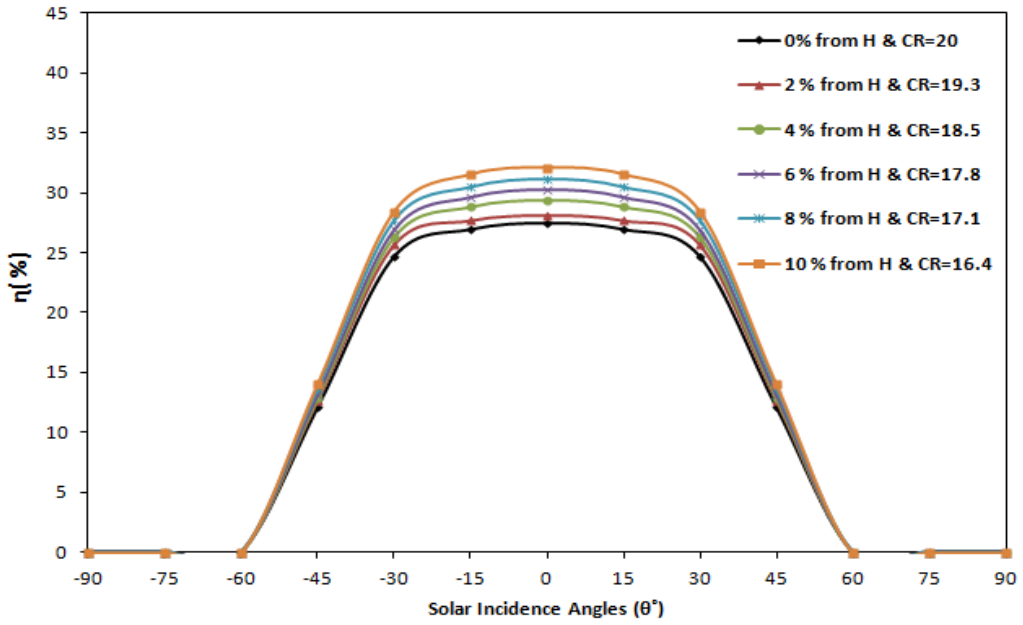

(a) Variation of the Source in Receiver Major Diameter

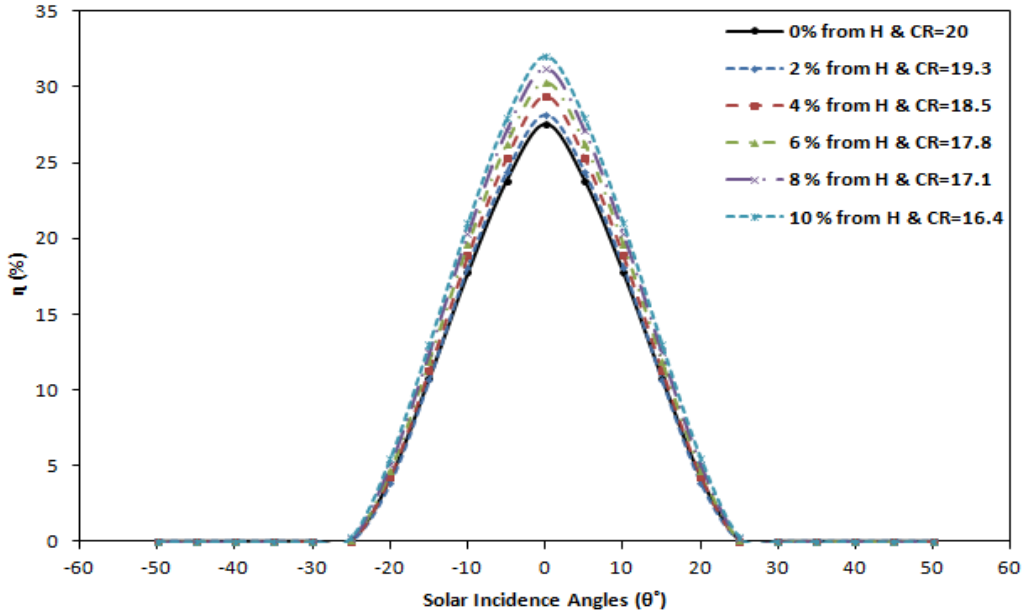

(b) Variation of the Source in Receiver Minor Diameter

Figure 3.15: Variation of Optical Efficiency with Solar Incidence Angles for Different Truncation Heights along (a) Receiver Major Axis, (b) Receiver Minor Axis.

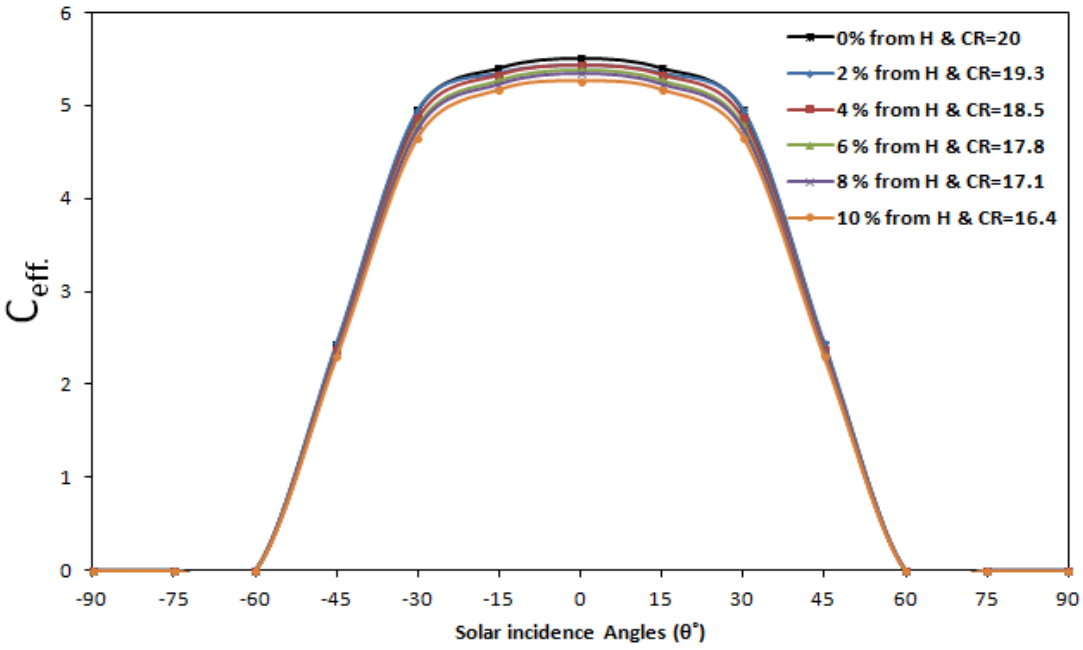

(a) Variation of the Source in Receiver Major Diameter

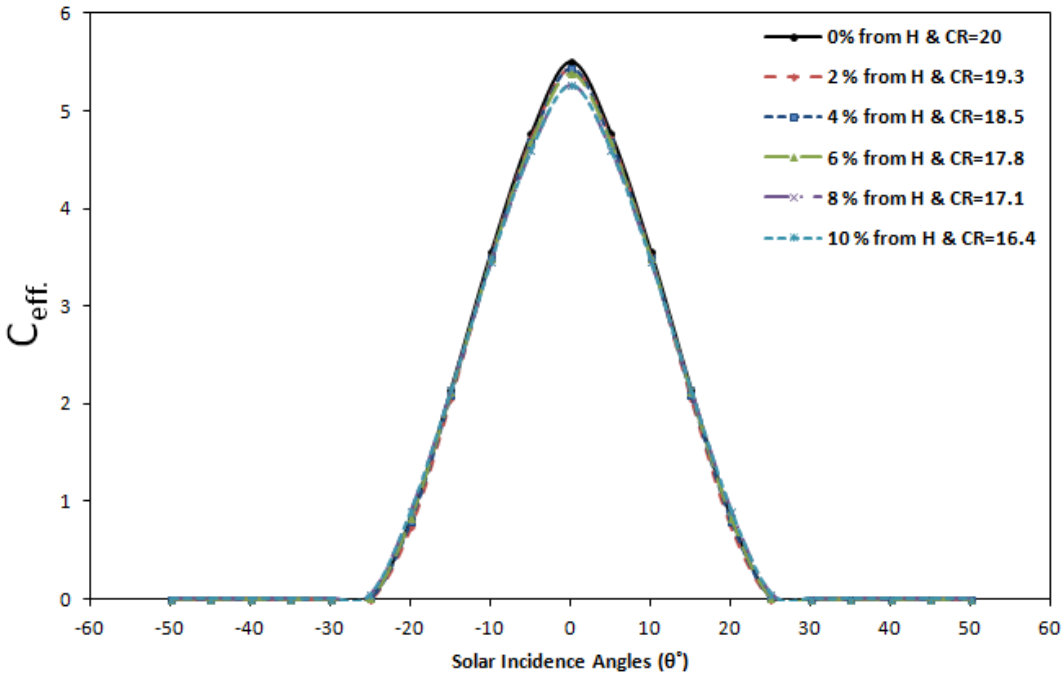

(b) Variation of the Source in Receiver Major Diameter

Figure 3.16: Variation Of Effective Concentration Ratio with Solar Incidence Angles for Different Truncation Heights Along (a) Receiver Major Axis, (b) Receiver Minor Axis

3.5 Energy Flux Distribution at the Receiver of EHC

In the ray tracing analysis, the energy flux distributions along the receiver major and minor axis diameter for three different geometrical aspect ratios (a/b = 1; a/b = 5; a/b=10) were carried out. The value of 1000 W/m^2 is considered as normal flux in the simulation. The variation of the flux distributions along the receiver major and minor

axis diameter at the concentrator height of 0.4 m for three different aspect ratios are shown in figure 3.17. As the aspect ratio varies from 1 to 5, there is a drop in the irradiance (in kW/m^2) at the receiver. Beyond the aspect ratio 5, the increase in the irradiance at the receiver is observed. The 3-D flux distributions and flux distribution in one plane, and the ray tracing for three aspect ratios are also shown in figure 3.18. It is found that the number of rays coming out of the concentrator for the aspect ratio of 1 is less than the others.

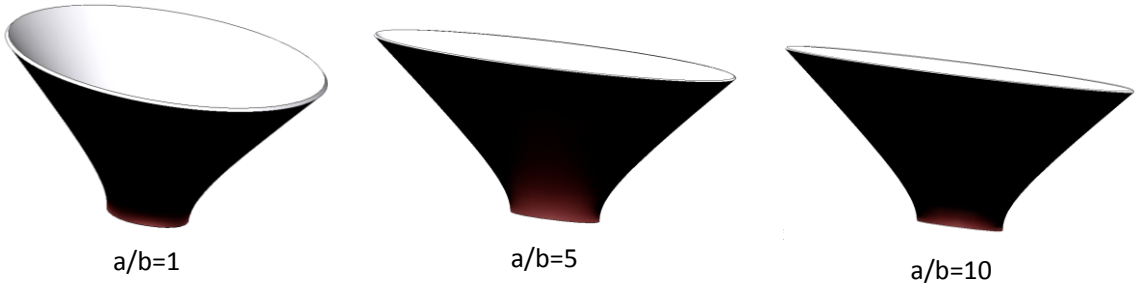

(a)

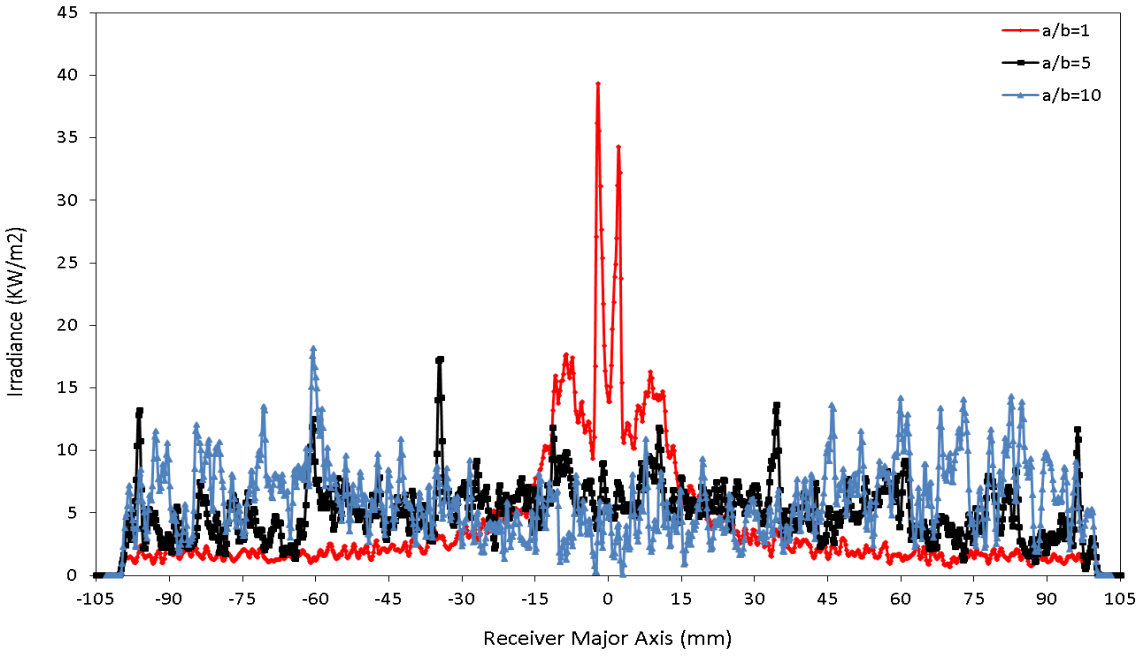

(b)

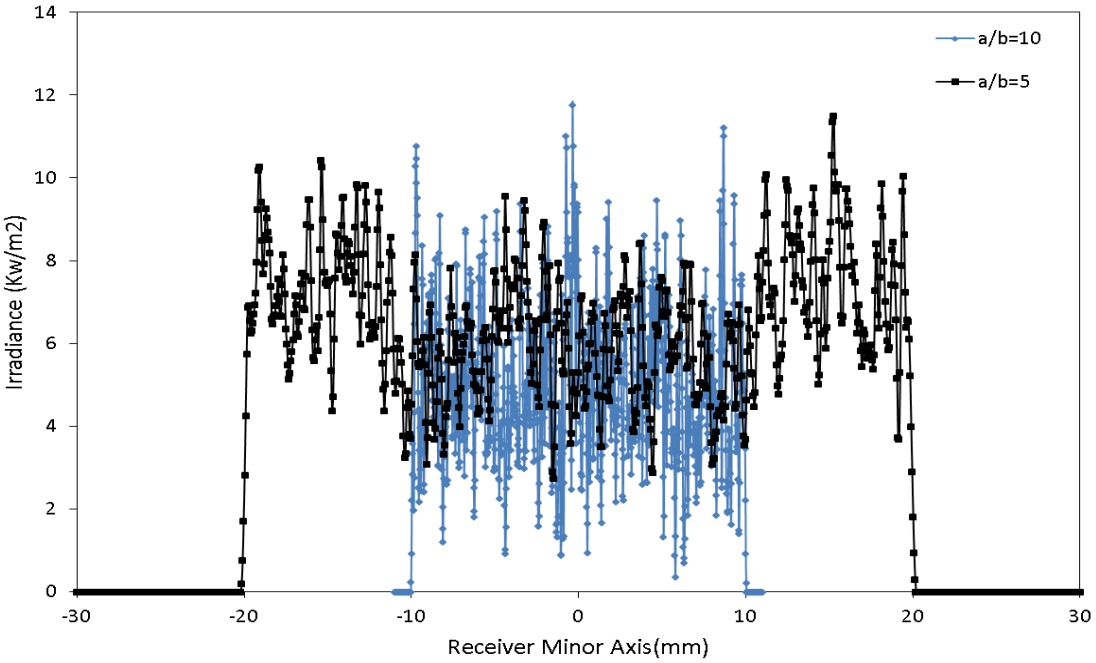

(c)

Figure 3.17: Variation of Flux Distribution for Different Geometry Aspect Ratios (a), Along the Receiver Major Axis Diameter (b) and (c) Minor Axis Diameter

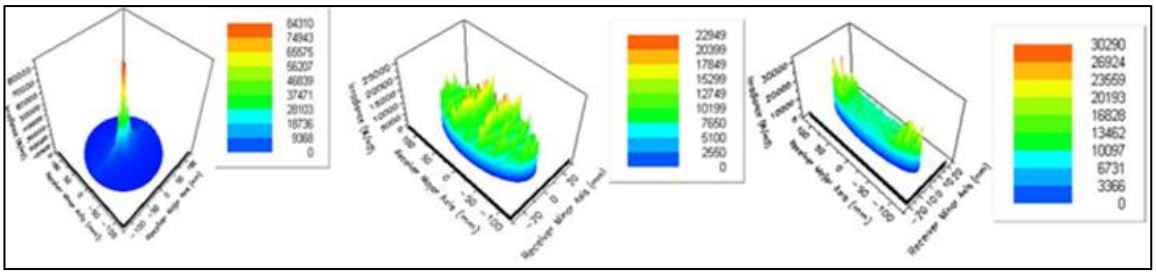

(a) 3-D Flux Distribution

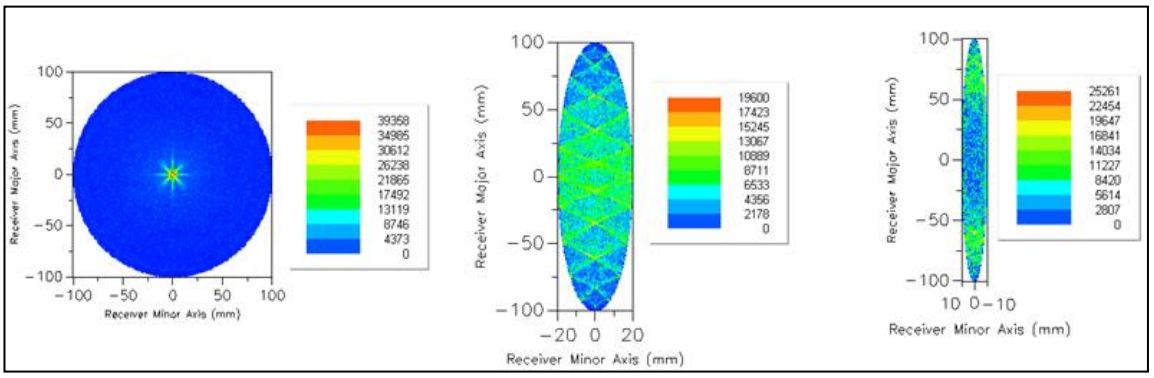

(b) Flux Distribution in One Plane

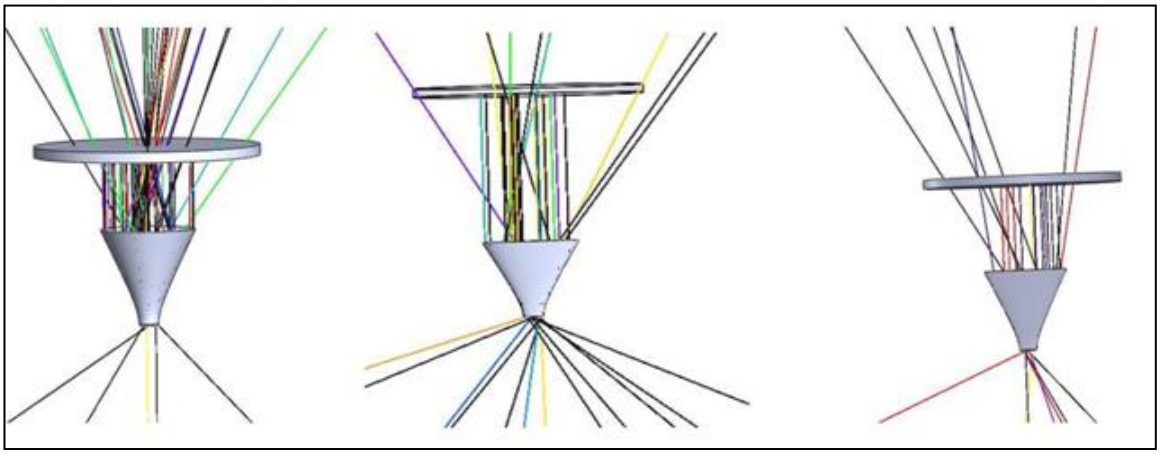

(c) Ray Tracing

Figure 3.18: Effect Of Variation of Aspect Ratio of an EHC on (a) 3-D Flux Distribution, (b) Flux Distribution in One Plane (c) Ray Tracing

3.6 Closure

The 2-D ray tracing simulation code for the elliptical hyperboloid concentrator was developed in MATLAB and parametric studies such as the effect of acceptance angle; concentration ratio, concentrator height, receiver axis diameter and the effect of truncation on the optical efficiency were investigated. The 2-D results reveal that there is a possibility of increasing the optical efficiency of the hyperboloid concentrator. Hence, to bring the curvature effects 3-D elliptical hyperboloid concentrator optical study were also carried out. In the 3-D analysis, the effective concentration ratio

increases and acceptance angle decreases for increasing the concentrator height for different aspect ratios. In the optical study, it was found that the optimum aspect ratio was found to be 5. When compared to circular and elliptical cross section of the receiver, the optical efficiency of the elliptical aspect ratio of 5 is three times higher than the circular profile. For the concentration ratio and concentrator height of 20× and 0.4 m, the optical efficiency was found to be 28% for the acceptance angle of ±30°. The effect of moving the source along the receiver major and minor axis was studied. Finally, the study of effect of truncation was also carried out and it was found that the 10% truncation of concentrator height reduces the concentration ratio to 16.4.

CHAPTER 4: COMPARISON OF OPTICAL PERFORMANCE FOR DIFFERENT GEOMETRIC CONFIGURATIONS

4.1 Introduction

In the previous chapter, optimisation of 3-D static elliptical hyperboloid concentrator (EHC) were presented for wide range of incidence angles and obtained the concentration ratio of 20×. To compare the EHC with other geometries, optical performance study was carried out through ray tracing technique for four different concentrator configurations. The four different configurations were Elliptical parabolic concentrator (ECPC) and Circular parabolic Concentrator (CCPC) Elliptical Hyperboloid Concentrator (EHC); Circular Hyperboloid Concentrator (CHC). Extensive parametric study was carried out to improve the overall performance of the concentrator for fixed parameters such as receiver area of 1 m^2 concentration ratio of 20× and aspect ratio of the ellipse of 5. The solar incidence angles were varied from ±90º. The flux distributions of the receiver were obtained for each concentrator profile. It was observed that the EHC with wider acceptance angle shows better optical efficiency than others.

4.2 Different Geometric Configurations

The four different geometries were considered to study the effect of concentrator geometric profile on optical performance. The different geometries are Elliptical parabolic concentrator (ECPC), Circular parabolic Concentrator (CCPC), Circular hyperboloid concentrator (CHC) and Elliptical hyperboloid concentrator (EHC) respectively. The profile of the geometries is shown in the figure 4.1. The comparison was made between the two different geometric profiles: parabola and hyperbola (both are symmetrical along the vertical axis). In each geometric profile, the aperture and receiver cross sections were circular and elliptic. To study the optical performance of different contours, the height of the concentrator, receiver area and concentration ratio were considered to be the same for all four geometric concentrators. The orientation of the incidence angle considered in this study is shown in figure 4.2. When the source of the radiation starts from the east (sunrise) the angle is considered to be +90˚, when the orientation of the source radiation is perpendicular to the receiver that is at noon, when the sun is at zenith the incident angle is considered to be 0˚. When the source moves to the west the incidence angle is ±90˚.

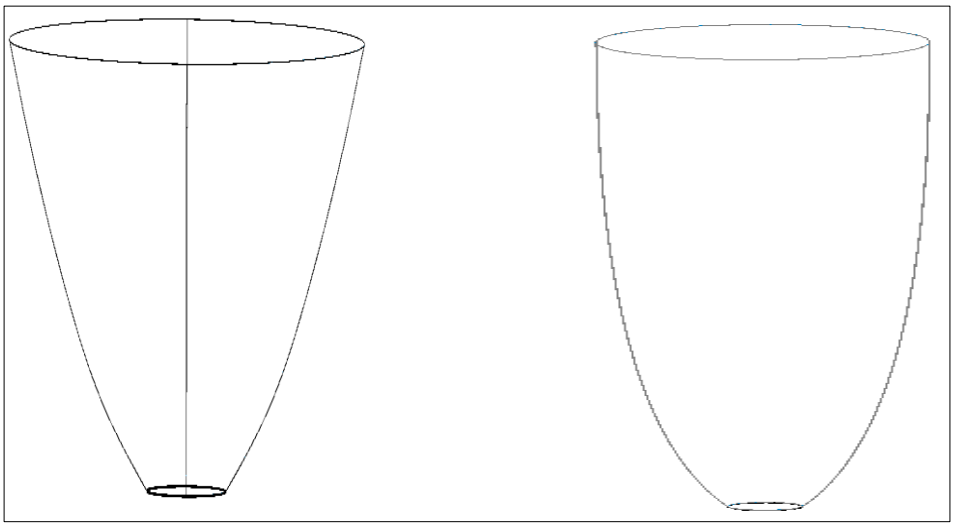

(a) Elliptical (b) Circular

(i) Parabolic Geometry Profile

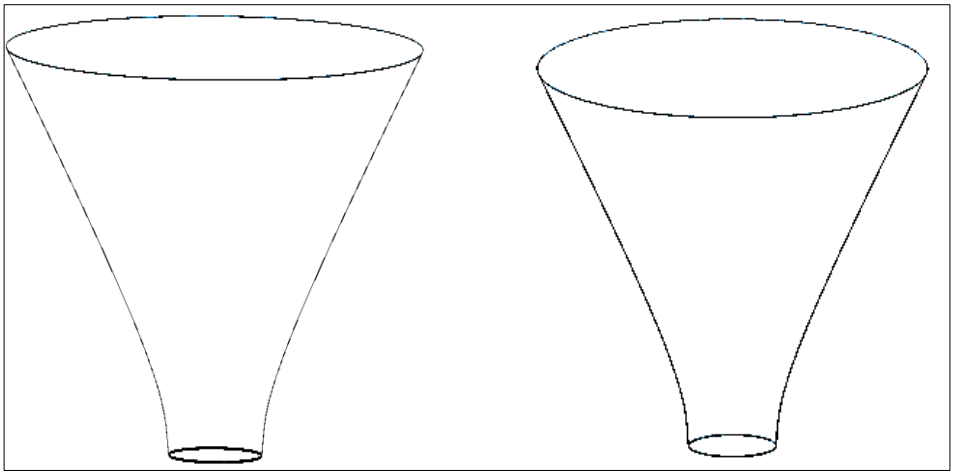

(a) Elliptical (b) Circular

(ii) Hyperboloid Geometry Profile

Figure 4.1: Profiles of the Various Geometries (i) Parabolic Geometry Profile (ii) Hyperboloid Geometry Profile

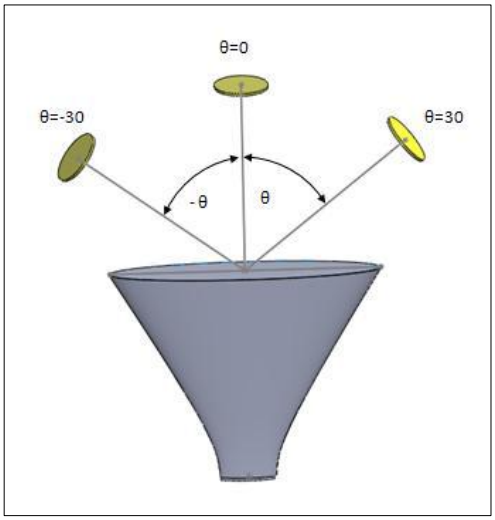

Figure 4.2: Different Orientations of the Incidence Angle

4.3 Ray Tracing and Optical Efficiency of Different Geometries

The ray tracing analyses were carried out for the four geometries. The methodology and concept of ray tracing were given in the Chapter 2. The ray tracing results were obtained for the four static 3-D solar concentrators. The ray tracing of parabolic and hyperboloid geometry profile with elliptic and circular cross section is shown in the figure 4.3. Based on the ray tracing, the optical efficiency was obtained for parabolic and hyperboloid geometry for different angle of incidence. The variation of optical efficiency of parabolic concentrator for elliptic and circular cross section (ECPC, CCPC) for different angle of incidence is shown in figure 4.4. It was observed that the CPC has higher optical efficiency with peak at 92% but with a narrow acceptance angle of ± 15˚, while the ECPC has lower optical efficiency with peak at 33% but with wider acceptance angle of ±30˚ twice that of the ECPC.

Similarly, the variation of optical efficiency of hyperboloid concentrator for elliptic and circular cross section (EHC, CHC) for different angles of incidence is shown in figure 4.5. It was found that the EHC produced higher optical efficiency of 28% for an acceptance angle ±30˚. But the CHC produced lower optical efficiency of 21% for a narrower acceptance angle of ±15˚. It is well understood that the parabolic and hyperbolic concentrator has some advantages. The parabolic concentrators have higher optical efficiencies at lower acceptance angle; such parabolic system can be used along with a tracking device. The hyperboloid concentrators have lower optical efficiency at wider acceptance angles; such device can be used for non-tracking system.

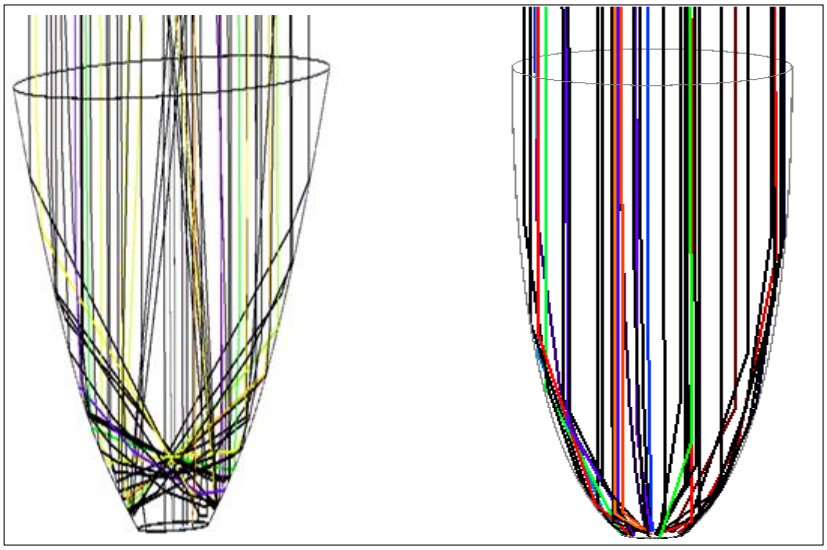

(a) Elliptical (b) Circular

(i) Ray Tracing of Parabolic Geometry Profile at Zero Incidence Angle

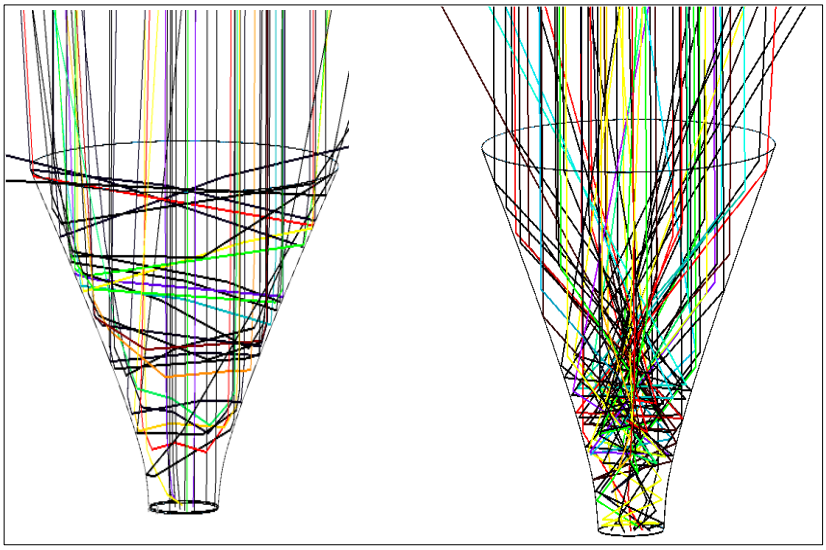

(a) Elliptical (b) Circular

(ii) Ray Tracing of Hyperboloid Geometry Profile at Zero Incidence Angle

Figure 4.3: Ray Tracing of Parabolic and Hyperboloid Geometry Profile

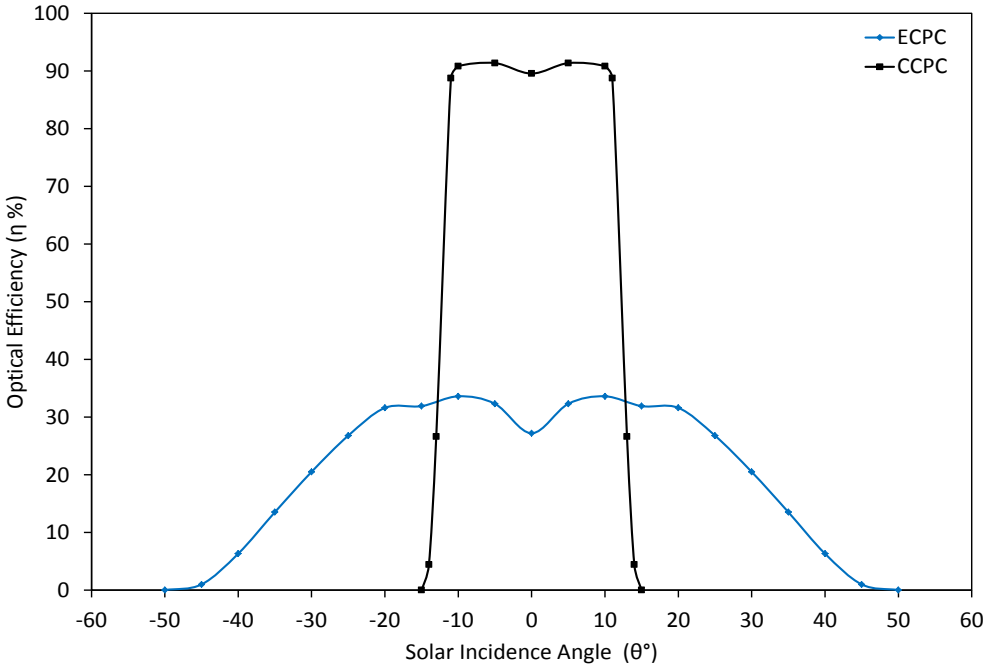

Figure 4.4: Optical Efficiency of Parabolic Concentrator for Elliptic and Circular Cross Section

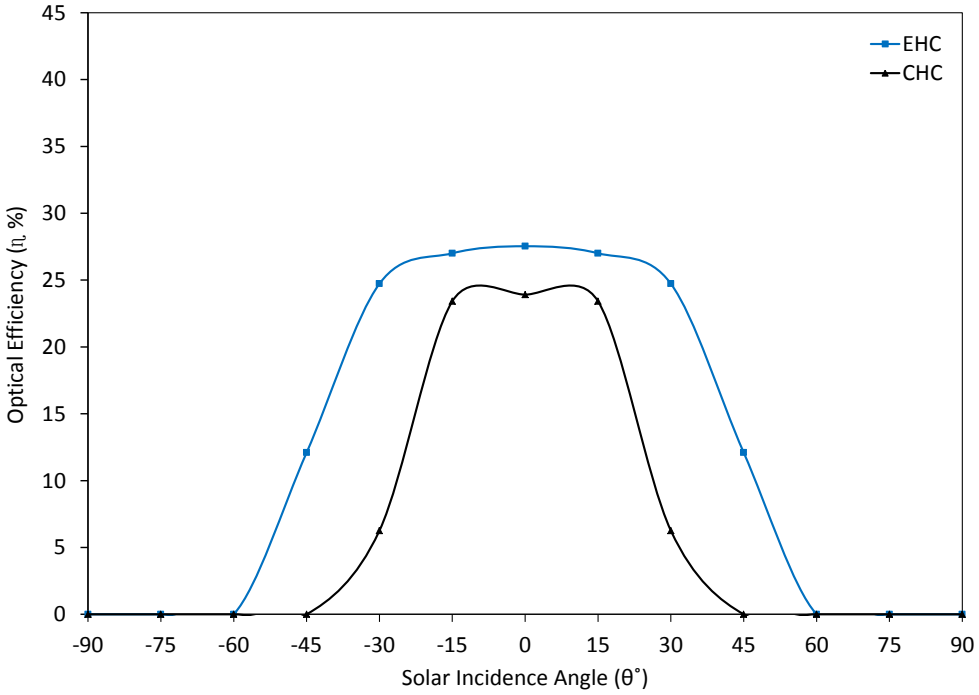

Figure 4.5: Optical Efficiency of Hyperboloid Concentrator for Elliptic and Circular Cross Section

4.4 Flux Distribution of Different Geometric Configurations

The flux distributions on the receiver area for different geometric shape and different cross sections have been studied. The flux distribution of parabolic profile concentrator for circular and elliptic cross section is shown in figure 4.6 (i) and (ii). It was observed that the maximum flux value for CCPC was found to be 603.174 kW/m^2. Similarly, the maximum flux value for ECPC was found to be 77.024 kW/m^2. It is well understood that the very high and peak flux occur only at the focal zone of the two parabolas (eccentricity = 1). The flux value decreases down based on the Gaussian distribution. From figure 4.6 (ii), the peak flux is at the intersection of the major and minor axis and also flux decreases and scattered along the major axis of the elliptical section.

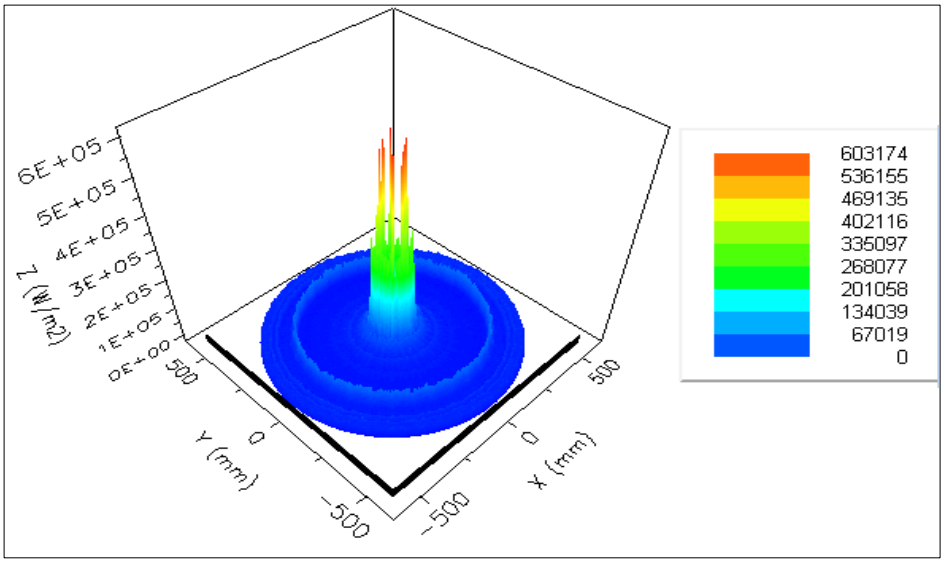

(i) Flux Distribution of Circular Parabolic Concentrator

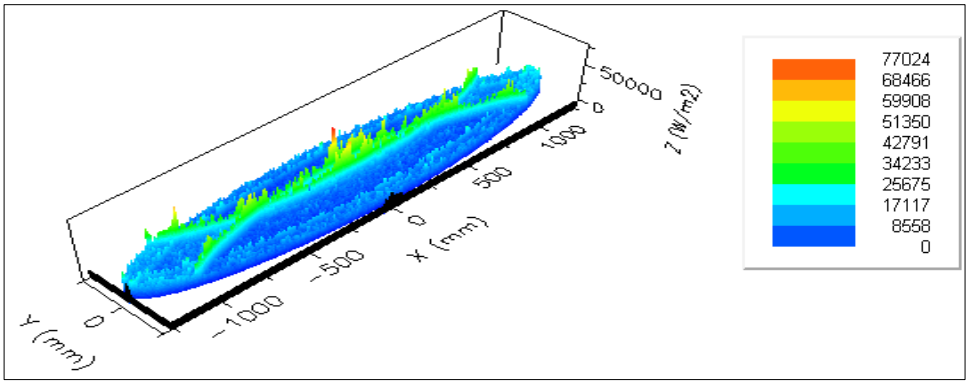

(ii) Flux Distribution of Elliptical Parabolic Concentrator

Figure 4.6: Flux Distribution of Parabolic Profile Concentrator for Circular and Elliptic Cross Section

The flux distribution of hyperboloid profile concentrator for circular and elliptic cross section is also shown in figure 4.7 (i) and (ii). It was observed that the maximum flux

value for CHC was found to be 497.257 kW/m^2. Similarly, the maximum flux value for EHC was found to be 28.617 kW/m^2. From the figure 4.7 (i), it is well understood, the very high and peak flux occur only at the centre of the receiver area. Due to circular and hyperboloid (eccentricity < 1), the width of the flux distribution is very narrow and small compared to the CCPC, whereas in the EHC (from figure 4.7(ii)), the flux distribution is scattered along the elliptic receiver area. And the peak occurs at the intersection of the major and minor axis. In general, the parabolic shape of the concentrator produces very high flux with small distributed area. The elliptic shape of the concentrator produces low flux with large distributed area.

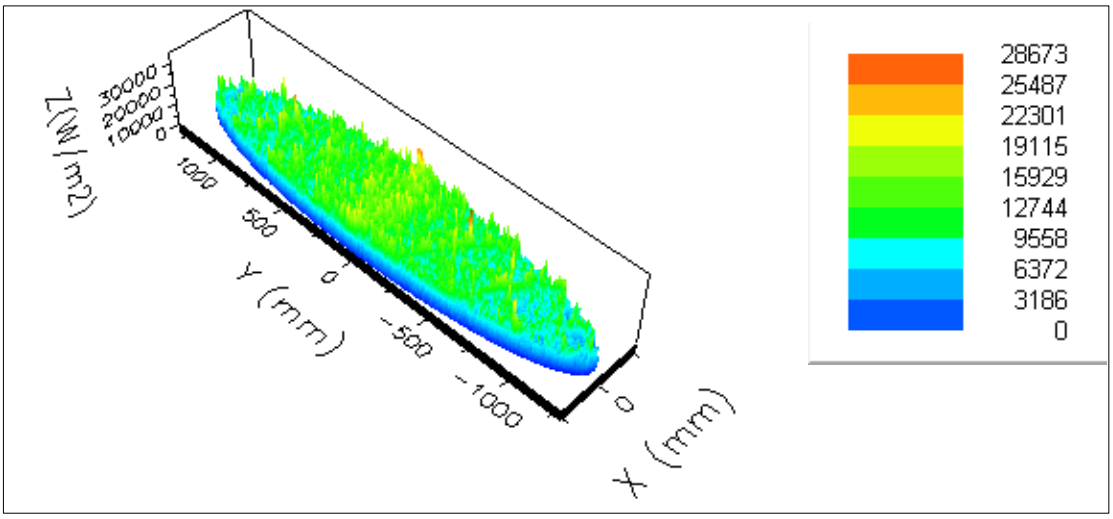

(i) Flux Distribution of Elliptic Hyperboloid Concentrator

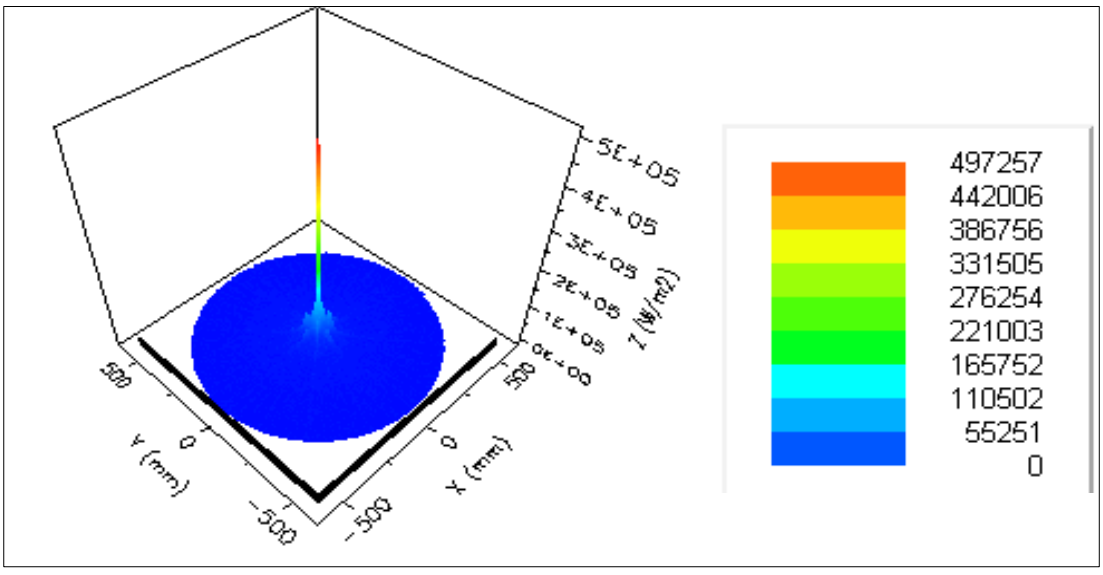

(ii) Flux Distribution of Circular Hyperboloid Concentrator

Figure 4.7: Flux Distribution of Hyperboloid Profile Concentrator for Circular and Elliptic Cross Section

4.5 Energy Absorbed by Receiver

4.5.1 Average Energy Absorbed by Receiver of Parabolic and Hyperboloid Concentrator

The average energy absorbed by the receivers of the parabolic (CCPC, ECPC) and hyperboloid (CHC, EHC) concentrator of circular and elliptic cross section were studied for different incidence angle. It was noted that the CCPC has higher absorbed energy flux than ECPC. The CCPC peak flux of 18,000 W/m^2 occurred at acceptance angle of ±15° and the ECPC peak flux of 6,000 W/m^2 occurred at acceptance angle of ±45°. It is clearly understood, that CCPC peak flux occurred at lower acceptance angle than EPC. Similar study was extended to receiver of hyperboloid concentrator with circular and elliptic cross section. It was found that the EHC has higher absorbed energy with peak flux of 5,500 W/m^2 at the acceptance angle of ±60° . Whereas, CHC has lower absorbed energy flux of 4,500 W/m2 at narrow acceptance angle of ±45°. The variation of average energy absorbed by the receivers of the parabolic (CCPC, ECPC) and hyperboloid (CHC, EHC) concentrators of circular and elliptic cross section for different incidence angle are shown in figure 4.8 (a), (b).

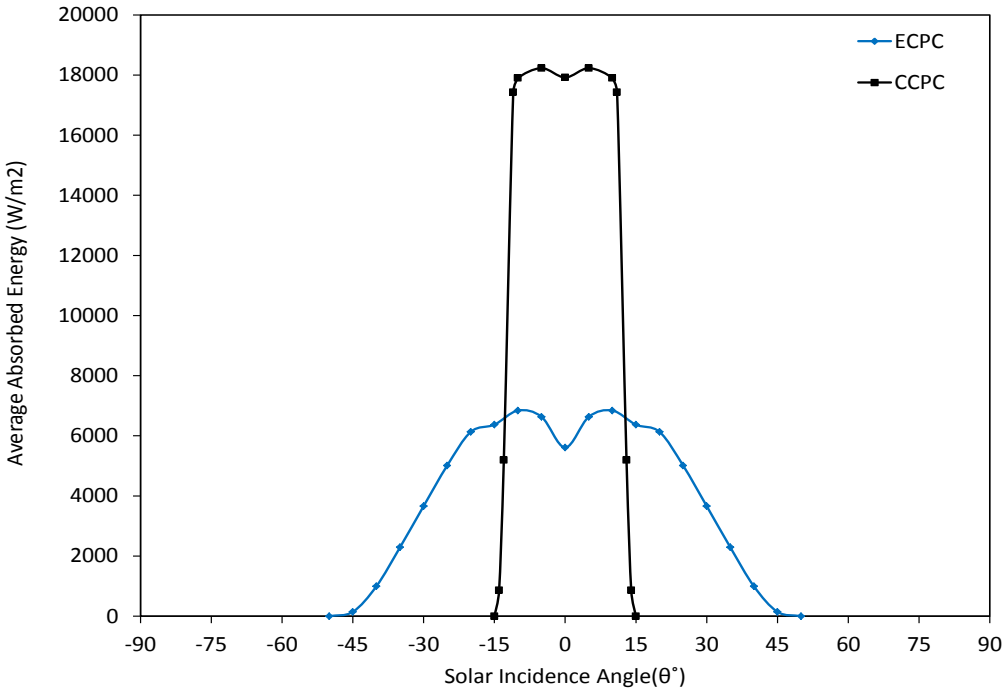

(a) Average Energy Absorbed by Receiver of Parabolic Concentrator

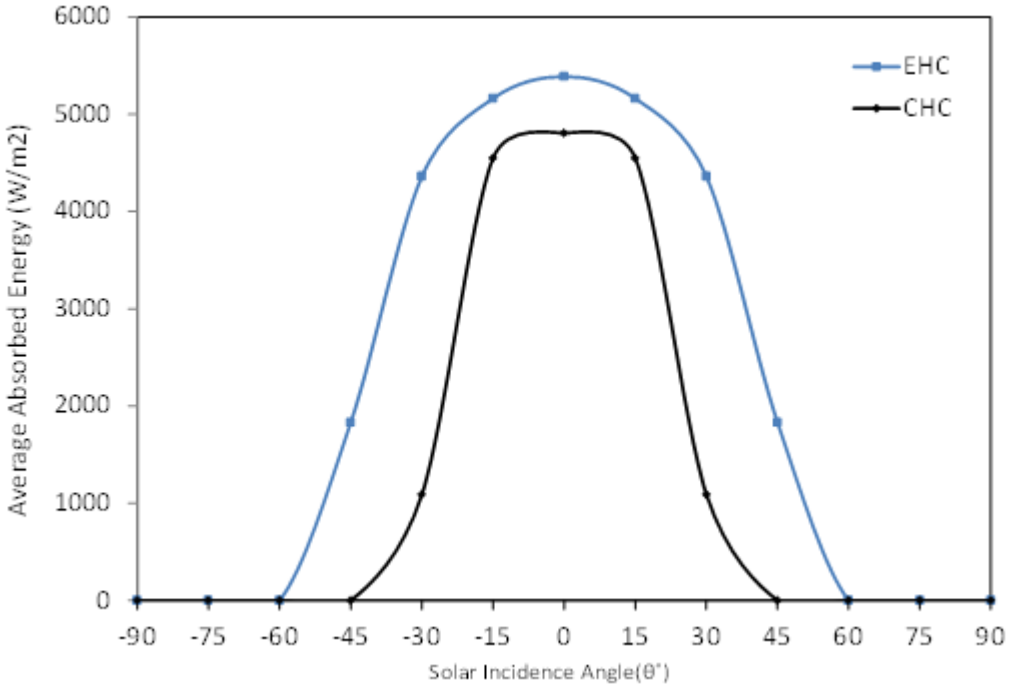

(b) Average Energy Absorbed by Receiver of Hyperboloid Concentrator

Figure 4.8: Average Energy Absorbed by Receiver of Parabolic and Hyperboloid Concentrator

4.5.2 Daily Average Energy Absorbed By Receiver of Parabolic and Hyperboloid Concentrator

Through ray tracing analysis, daily average energy absorbed by the receiver of parabolic and hyperboloid concentrators for circular and elliptic cross section were also carried out. The daily average energy absorbed by receiver of parabolic and hyperboloid concentrators for circular and elliptic cross section are shown in figure 4.9. It was observed that the ECPC absorbed daily average energy of 12.3 kW/m^2 and the CCPC absorbed daily average energy of 20.7 kW/m^2. Similarly, the CHC absorbed daily average energy of 16.1 kW/m^2 and the EHC absorbed the highest daily average energy of 28.8 kW/m^2 it was observed from figure 4.9. In addition to that, the optical efficiency and acceptance angle for different concentrators are given in table 4.1. Under normal incidence angle, the average energy flux for different concentrators is given in table 4.2.

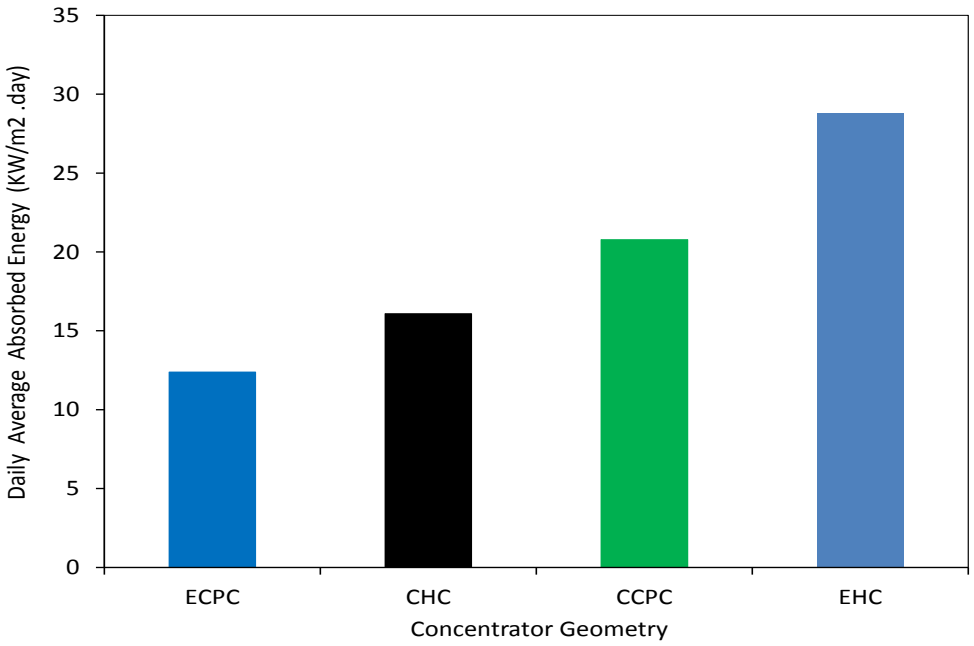

Figure 4.9: Daily Average Energy Absorbed by Receiver of Parabolic and Hyperboloid Concentrator

Table 4.1: Optical Efficiency and Acceptance Angle for Different Solar Concentrator

Cross Section	**Acceptance Angle**	**Optical Efficiency**
Parabolic		
ECPC	±30°	25%
CCPC	±15°	92%
Hyperboloid		
EHC	±45°	25%
CHC	±15°	24%

Table 4.2: Average Energy Flux under Normal Incidence Angle for Different Solar Concentrator

Cross Section	**Flux (at Zenith Angle) (W/m^2)**
Parabolic	
ECPC	5610
CCPC	17920
Hyperboloid	
EHC	5390
CHC	4807

4.6 Effect of Truncation

In order to see the effect of truncation on the optical efficiency, the height of the concentrators (parabolic and hyperboloid) is reduced 10% of its original height. The 10% truncation of the concentrator height reduces the concentration ratio to 18×. The effect of truncation of the parabolic and hyperbolic concentrator height on the optical efficiency and the acceptance angle is given in Table 4.3. It was observed that the optical efficiency and acceptance angle of ECPC and CCPC are obtained as 29%, ±30°and 92%, ±15° respectively. Similarly, the optical efficiency and acceptance angle of EHC and CHC are obtained as 30%, ±45°and 27%, ±15° respectively. In general, it is concluded that the EHC has wide acceptance angle of ±45° and highest diurnal absorbed energy compared to other concentrators (CCPC, ECPC and CHC). With respect to highest efficiency, CCPC has highest optical efficiency, but the highest efficiency obtained in a very narrow acceptance angle. Hence, it is very well clear that

the elliptical hyperboloid concentrator (EHC) is ideal geometric contour for non-tracking system.

Table 4.3: Effect of Truncation on Optical Efficiency and Acceptance Angle

Cross Section	Acceptance Angle	Optical Efficiency	Concentration Ratio
Parabolic			
ECPC	± 30°	29 %	18
CCPC	± 15°	92 %	18
Hyperboloid			
EHC	± 45°	30 %	18
CHC	± 15°	27 %	18

4.7 Closure

In this chapter, optical performance comparison of four different geometric profiles (CCPC, ECPC, CHC and EHC) was extensively studied. The optical study was also extended for the effect of truncation on optical performance. It was noted that the optical efficiency of 92% for CCPC for the acceptance angle of ± 15°, 29% for ECPC for the acceptance angle of ± 30°, 30% for EHC for the acceptance angle of ± 45°,and 28% for CHC for the acceptance angle of ± 15°. In both of these studies, it was concluded that the EHC has an ideal characteristic feature for non-tracking system based on the moderate optical efficiency with ±45° acceptance angle. The next chapter discusses the indoor experimental characterisation of EHC with two different cross sections.

CHAPTER 5: FABRICATION AND INDOOR TESTING OF STATIC 3-D EHC

The design and experimental investigations of three different hyperboloid (elliptical (HWU), elliptical (China) and circular (China)) solar concentrators have been reported in this chapter. These prototypes have been fabricated from two different places; Heriot-Watt University (HWU, UK) and Star prototype in China. The cost of fabrication of the prototype of the EHC produced at the HWU, UK was £1200. After careful and extensive comparison of the production cost of the prototype of the EHC and CHC from different companies in Europe, America and China, a company was most competitive. The cost of the CHC and EHC were £1834 and £1148 respectively. The details of the Chinese company and the cost of both the CHC and EHC are found in the quotation in Appendix B. The design details and optical performance analysis of hyperboloid concentrator have been presented. Indoor tests have been carried out for three prototypes to predict the optical efficiency of the concentrator. In order to estimate the temperature of the surface area of the receiver tubes for process heat application, thermal imaging analysis have also been carried out and also presented in this chapter.

5.1 Design and Fabrication of the Static 3-D EHC

The design and fabrication of three hyperboloid concentrators are discussed. The three hyperboloid concentrators are: EHC1: Elliptical Hyperboloid Concentrator fabricated (HWU); EHC2: Elliptical Hyperboloid Concentrator fabricated (China); CHC: Circular Hyperboloid Concentrator fabricated (China).

1. EHC1: Elliptical Hyperboloid Concentrator (HWU).
   The EHC1 means elliptical hyperboloid concentrator, fabricated at Heriot-Watt University (HWU). The EHC1 system was fabricated according to the specific dimensions; such as height of the concentrator of 0.86 m, concentration ratio of 18×.
2. EHC2: Elliptical Hyperboloid Concentrator (China).
   The EHC2 means elliptical hyperboloid concentrator, fabricated at star prototype, China. The concentration ratio of 20× and concentrator height of 0.4 m were considered and fabricated.
3. CHC: Circular Hyperboloid Concentrator (China).

The CHC means circular hyperboloid concentrator which is also fabricated from China with the same dimensions of EHC2. The entry and exit of the concentrator is circular in shape.

For the fabricated concentrator, the optical analysis of the elliptical hyperboloid concentrator and then the fabrication process of the elliptical hyperboloid concentrator are discussed.

5.1.1 Optical Analysis of Static 3-D EHC1

Based on Optis™ software, a detailed flux distribution of a 3-D EHC1 is carried out for the height of 0.860 m. The distribution of the incoming radiant energy on the receiver area representing in red colour indicates the maximum available flux. The 3-D flux distribution for major and minor axis of the receiver is shown in figure 5.1 (a) and the top view of the flux distribution is also shown in figure 5.1 (b).The optical efficiency of the 3-D EHC1 with the concentration ratio of 18× and concentrator height of 0.86 m is carried out for different solar incidence angles. The variation of the optical efficiency with different solar incidence angles is shown in figure 5.2. It was observed that the maximum efficiency of 87% is obtained for the solar incidence angle of ±15°.

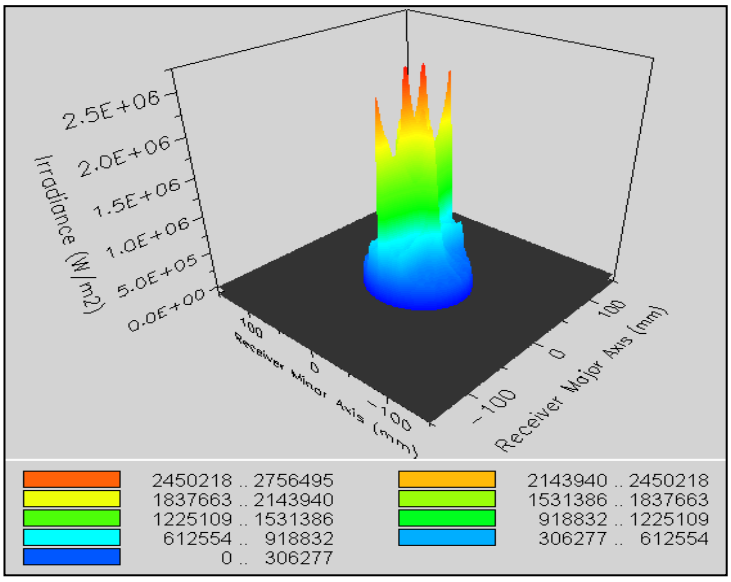

(a) 3-D Flux Distribution

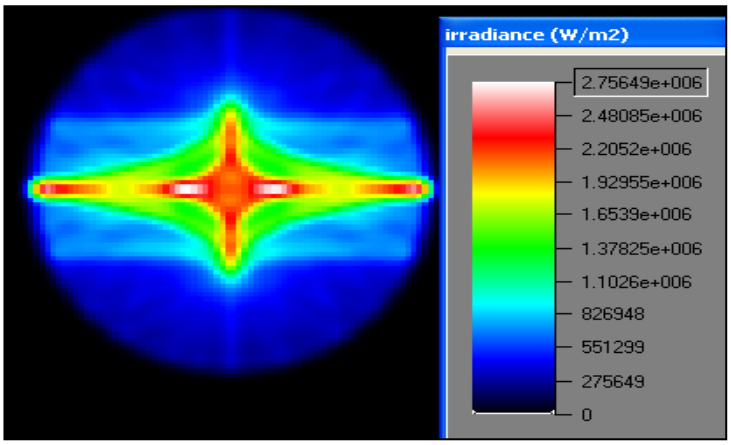

(b) Flux Distribution in One Plane

Figure 5.1: Flux Distribution of the Receiver Area for EHC1 when the Concentrator Height of 0.860 m for (a) 3-D Flux Distribution (b) Flux Distribution in One Plane.

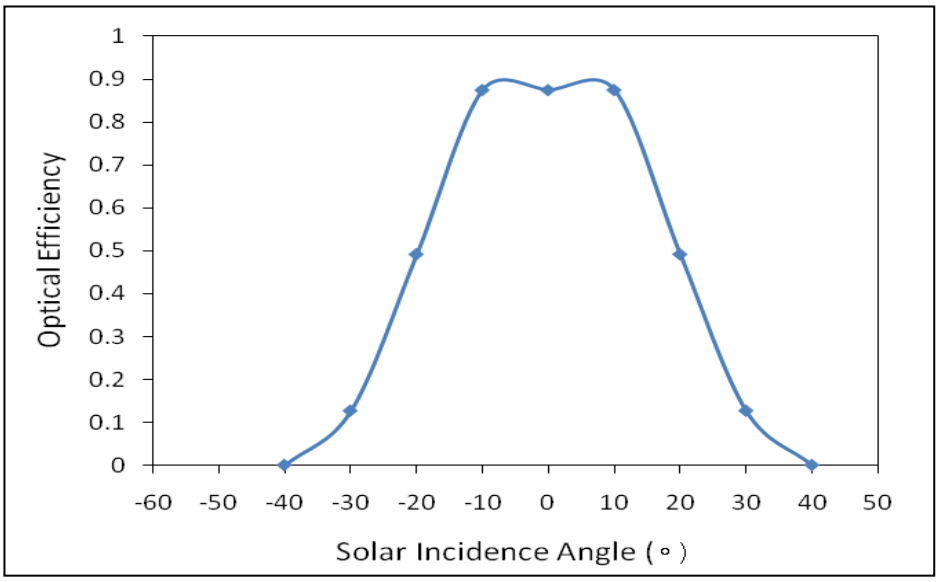

Figure 5.2: Variation of Optical Efficiency with Solar Incidence Angles (In Degrees) For EHC1

5.1.2 Fabrication of first Elliptical Hyperboloid Concentrator (EHC1)

Based on the optical analysis of the 3-D EHC, the fabrication of the EHC1 is carried out at Heriot Watt University (HWU). The specifications of the EHC1 fabricated at HWU are given in table 5.1.

Table 5.1: Specifications of EHC1

Specifications of the EHC	
Height of the concentrator	0.86 m
Aperture major axis of the concentrator	0.259 m
Aperture minor axis of the concentrator	0.223 m
Receiver major axis	0.061 m

Receiver minor axis	0.053m
Acceptance angle	$\pm 15^{o}$
Concentration ratio	18×
Reflectivity of the Aluminium sheet	0.94

The elliptical hyperbolic shapes of wooden strips or segments are made based on the profile obtained from optical analysis. All the wooden strips are aligned to form a 3-D EHC1. The highly polished aluminium sheet of 1 mm is pasted on the inner surfaces of the wooden strips. The reflectivity of the sheet material is 0.95. The wound copper coil tube, receiver is placed at the bottom of the EHC1. The process of fabrication of the EHC1 and assembly of the EHC1 is shown in figure 5.3 (a, b, c, d, and e) and figure 5.4 (a, b, c, d). The schematic of the EHC open cycle is shown in figure 5.5.

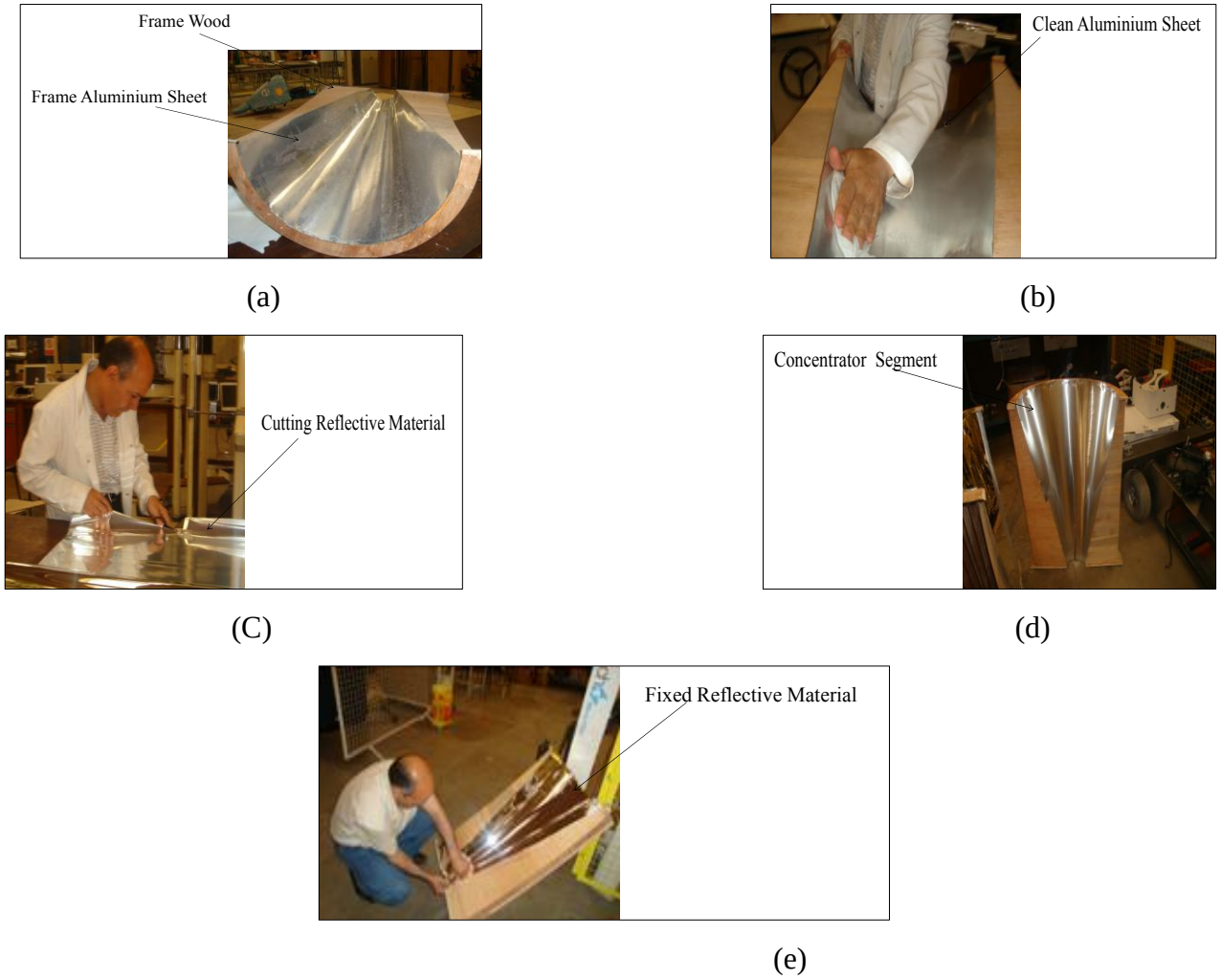

Figure 5.3: Fabrication Process of the Elliptical Hyperboloid Concentrator (EHC1)

(a)

(b)

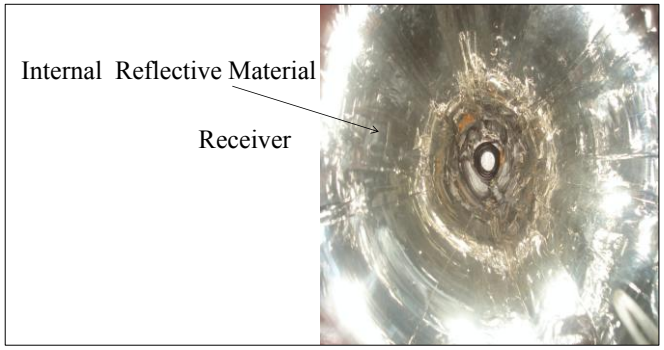

(c)

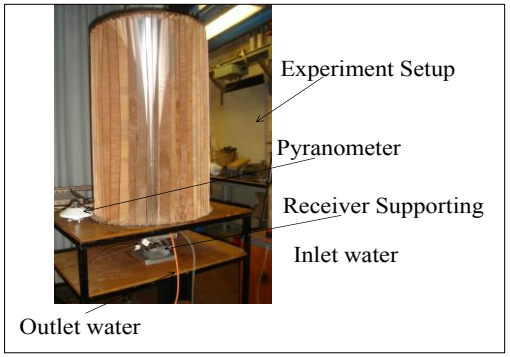

(d)

Figure 5.4: Assembly of the Elliptical Hyperboloid Concentrator (EHC1)

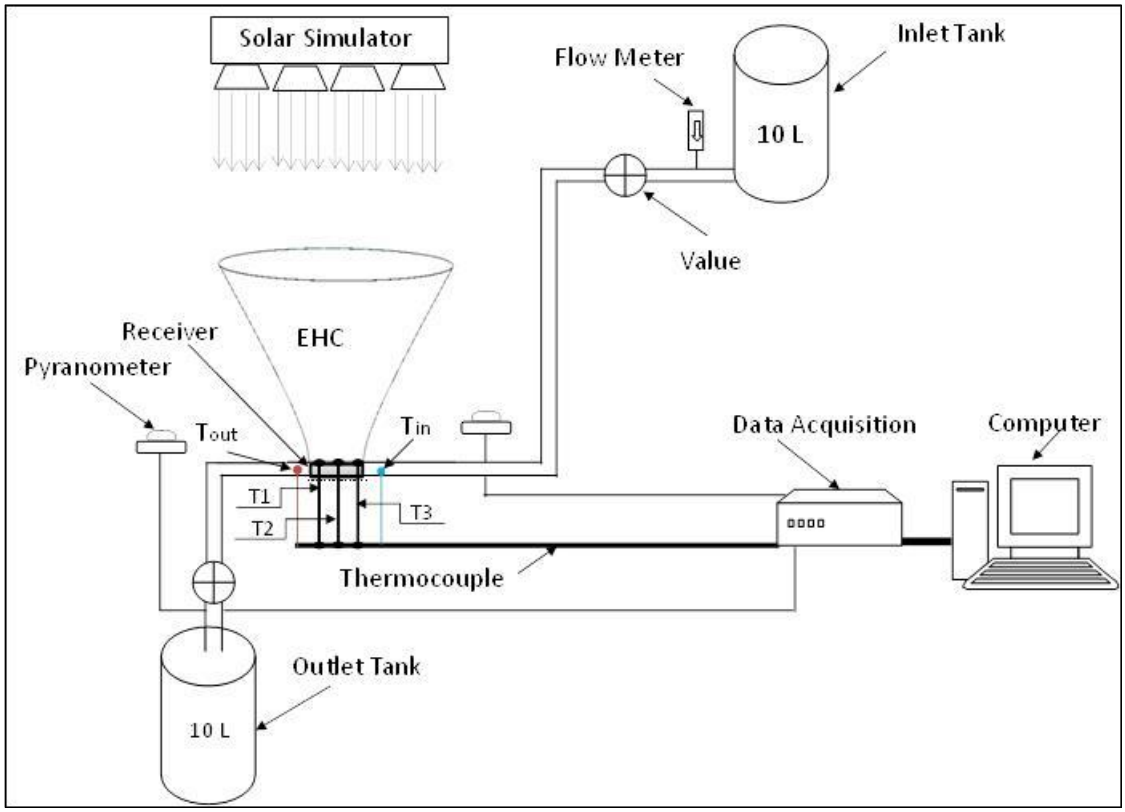

Figure 5.5: Schematic of the Indoor Open Cycle of the EHC1

5.1.3 Measurement of Concentration Ratio of EHC1

The experimental setup of EHC1 is fabricated. The concentration ratio of the fabricated EHC1 is obtained by measuring incoming and out coming radiation along the vertical axis. The radiations are measured by using two different Pyranometers. One is placed at the entry section of the concentrator and other at the base of the concentrator (receiver part). The concentration ratio of 16× is obtained for the elliptical hyperboloid. But, the geometrical concentration ratio of 18× is predicted for the present elliptical hyperboloid. The variation of the incoming and out coming radiation with time is plotted in figure 5.6.

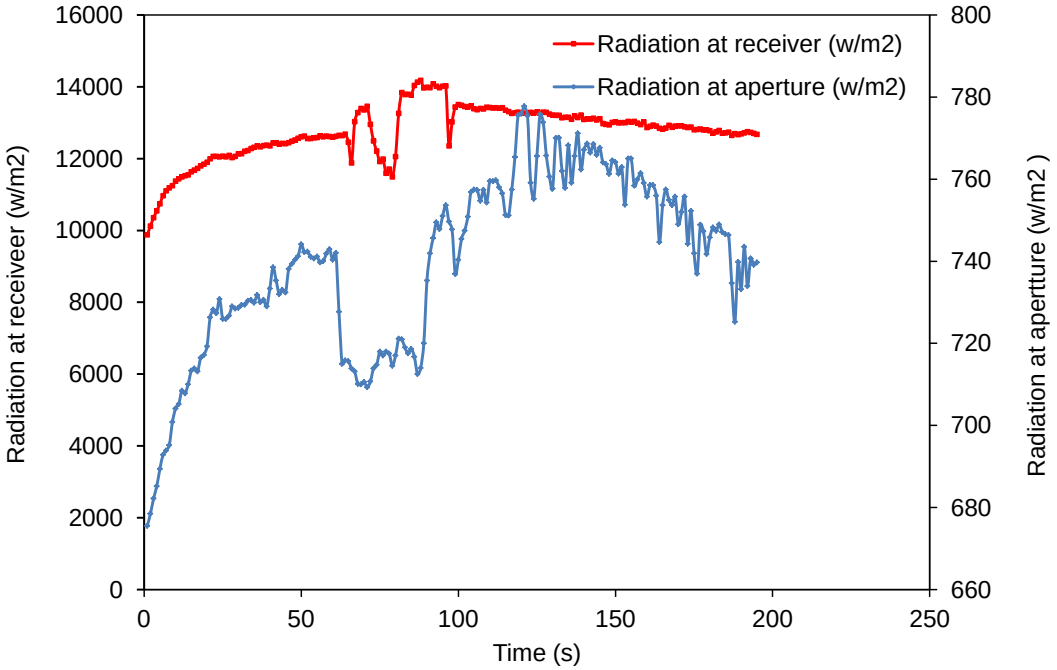

Figure 5.6: Variation of Solar Radiation Intensity at Receiver and Aperture with Time for EHC1

5.1.4 Inlet and Outlet Temperature of the Receiver

The concentration ratio of 16× is obtained for the fabricated EHC1. The fabricated EHC1 is used for process heat application. Hence, the measurement of stagnation temperature of the receiver of the EHC1 is important. The stagnation temperature corresponds to the maximum temperature of the receiver at no flow condition of the receiver. The water is admitted and no allowed to flow outside. The inlet and outlet temperatures of the receiver are measured. The maximum stagnation temperature and outlet temperature of 130 °C and 100 °C are observed in the receiver of the EHC1. The variation of the inlet and outlet temperatures of the receiver is shown in figure 5.7.

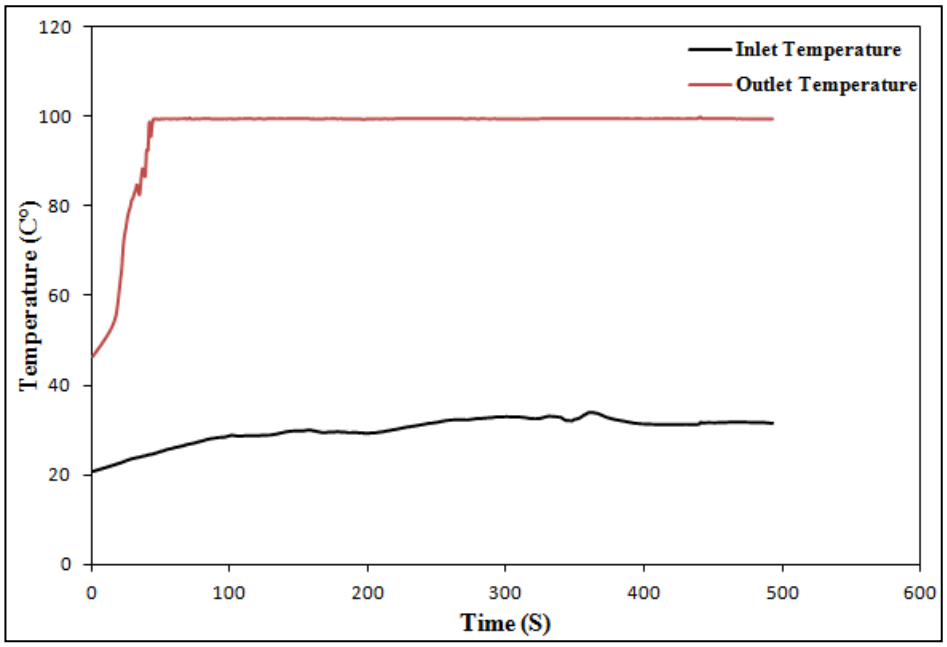

Figure 5.7: Variation of Inlet and Outlet Temperature of the Receiver for EHC1

5.1.5 Fabrication of Elliptical Hyperboloid Concentrator EHC2

Based on the optical analysis, circular and elliptical hyperboloid concentrators of concentration ratio of 20× and concentrator height of 0.4 m were fabricated from star prototype, China. The prototype of the circular and elliptical hyperboloid concentrator are shown in figure 5.8. The complete specifications of the circular and EHC2 fabricated from China are given in tables 5.2 and 5.3.

(a) Circular Hyperboloid Concentrator (CHC) (b) Elliptical Hyperboloid Concentrator (EHC2)

Figure 5.8: Prototype of Circular (CHC) and Elliptical Hyperboloid Concentrator (EHC2)

Table 5.2: Specifications of CHC

Specifications of the CHC	
Concentrator Material	Australian Broadcasting Corporation (ABC)
Receiver Material	Copper coil tube
Height of the concentrator	0.4 m
Reflectivity	Chrome coating, 0.92
Aperture dimension of the concentrator	0.447 m
Receiver dimension of the concentrator	0.1 m
Acceptance angle	$\pm 15^{o}$
Concentration ratio	20×

Table 5.3: Specifications of EHC2

Specifications of the EHC	
Concentrator Material	Australian Broadcasting Corporation (ABC)
Receiver Material	Aluminium grooved flat receiver
Height of the concentrator	0.4 m
Aperture major axis of the concentrator	0.447 m
Aperture minor axis of the concentrator	0.089 m
Receiver major axis	0.1 m
Receiver minor axis	0.02 m
Acceptance angle	$\pm 45^{o}$
Concentration ratio	20×
Reflectivity	Chrome coating, 0.92

5.2 Receivers

Two different types of receivers were fabricated for process heat applications. The first one was an Aluminium grooved flat receiver, and the second is a copper coil tube receiver. The Aluminium grooved flat receiver was fabricated from aluminium material and coated with high absorptive black colour paint. The diameter of the groove was 4.5 mm diameter. In order to minimise the losses, the receiver is covered with glass wool insulation with thermal conductivity 0.037 W/mK. In copper coil tube receiver, copper

coil tubes of 6 mm outer diameter and 4.5 mm inner diameter with and without black paint and covered insulating material. The two receivers of Aluminium grooved flat receiver and copper coil tube receiver are shown in figures 5.9 and 5.10.

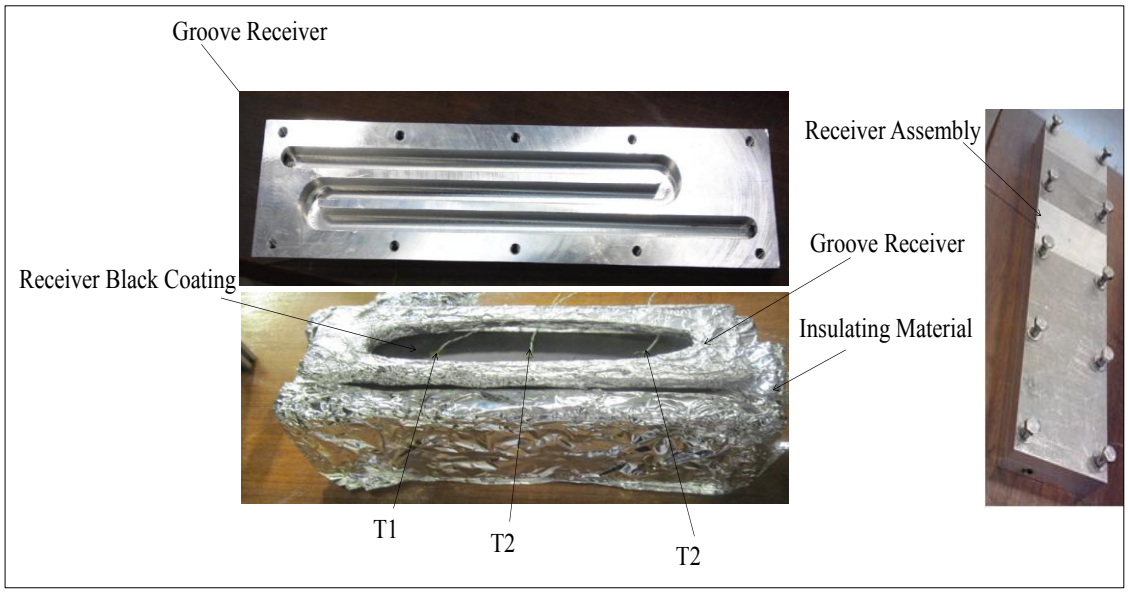

Figure 5.9: Aluminium Grooved Flat Receiver

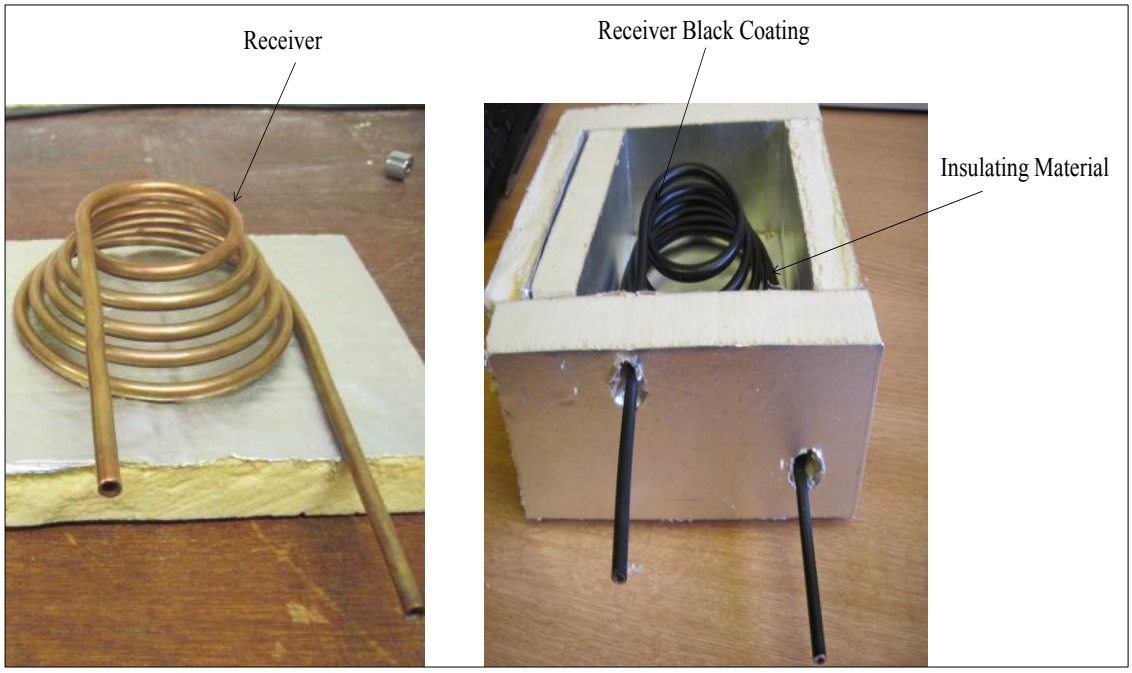

Figure 5.10: Copper Coil Tube Receiver

5.3 Solar Simulator for Indoor Characterisation

5.3.1 Design of a Solar Simulator for Characterisation of Solar Systems

A solar simulator has been developed for detailed characterisation of solar systems. In a solar simulator, large area solar thermal or PV system can be characterised for comparison. In the developed solar simulator, multiple light sources have been used in solar simulator to increase the illumination area. Hence, in few cases, the uniformity of intensity distribution and collimation of the light have to be compromised. The basic design of solar simulator includes:

- Light source has to be selected, such way that, spectral distribution of the solar simulator matching the solar spectrum.
- Solar simulator should have the provision of obtaining solar intensity from a minimum value to a maximum value above the solar terrestrial irradiation ($1200 W/m^2$).
- It should have capable of producing uniform distribution of the light intensity over the illuminated area.
- It should have capable of producing collimated rays.
- Selection of an appropriate spectral-correction filter

In reality, it is very difficult to generate light that is an exact match to the spectrum of solar radiation. All the lamps (Tungsten filament lamps, metal halide lamps, xenon-mercury arc lamps, and high pressure xenon lamps) that are used as light source in solar simulator have spectrum that nearly matches sun with addition of proper filters. A literature review and technical data shows that metal halide lamps are suitable for solar simulators with spectra very close to the solar spectrum for continuous radiation and have long life-times. Hence, metal halide lamps of 1200 Watt from OSRAM were chosen as the source lamps for the present solar simulator. A comparison of the spectral distribution of metal halide lamps (HMI 1200) with solar spectra is shown in figure 5.11. The structural dimensions of the lamp and the technical information of the lamp are given in table 5.4.

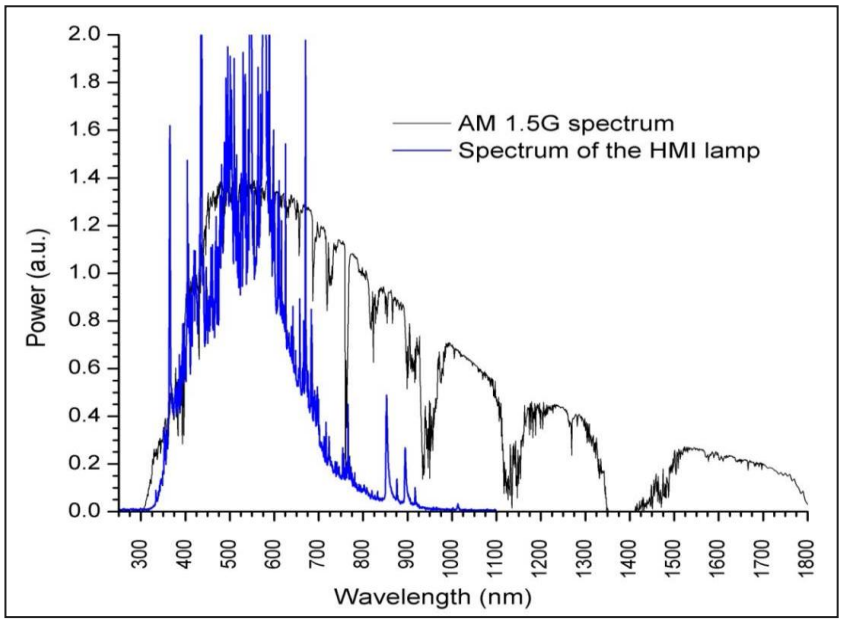

Figure 5.11: Comparison of the spectrum of HMI 1200 lamp and AM1.5G sun spectrum

Table 5.4: Properties of the OSRAM HMI 1200 W/SEL lamp [164]

Properties of the OSRAM HMI 1200 W/SEL lamp	
Rated Lamp Wattage (W)	1200
Ignition Voltage (kV)	5
Luminous flux (lm)	110,000
Colour Temperature (K)	6000
Light arc length (mm)	10
Average service life (h)	1000

5.3.2 Fabrication of Solar simulator

The base plate for fixing of the source lamps and reflectors was constructed from aluminum bars of 50 mm ×50 mm cross-sectional area and 2 mm thick aluminum sheet. Through optical simulation study, the proper positioning of lamps was made to achieve a homogeneous distribution of intensity. The positioning of the lamp bases is shown in figure 5.12.

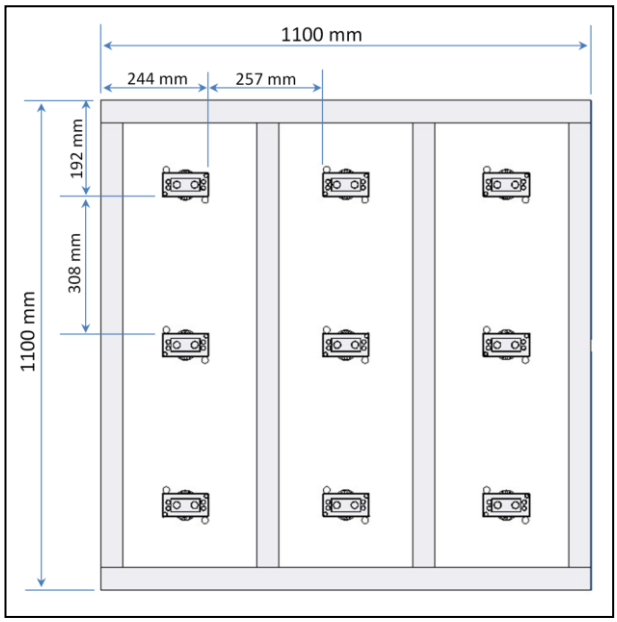

Figure 5.12: Dimensions of the Base Plate and Positioning of the Lamps.

5.3.3 Manufacturing of the reflectors

High accuracy of parabolic reflectors profile and good surface finish were manufactured by metal spinning process of aluminum by an external manufacturer. A low cost, light weight and longer life-time without corrosion, Aluminum grade 1100 was used. An aluminum coating of 85% reflectivity was applied on the inner surface of the reflector. The cross-sectional dimension of a reflector is shown in figure 5.13.

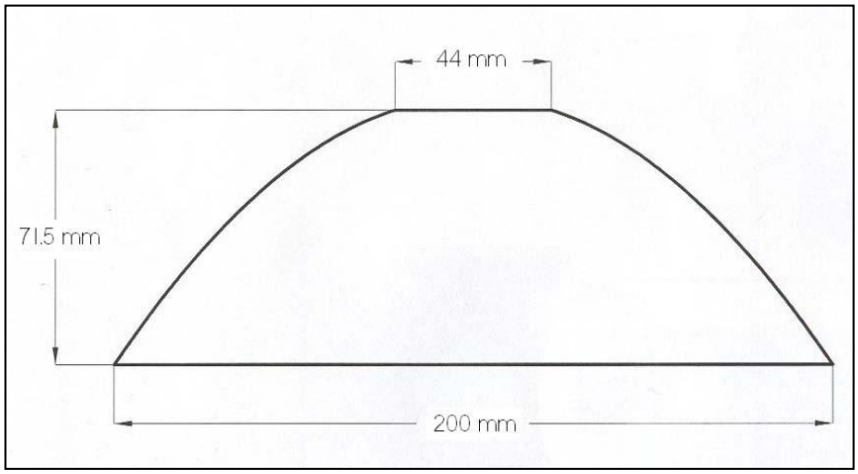

Figure 5.13: Cross Sectional View of Parabolic Reflector for Each Source Lamp

The base plate was mounted on a movable shaft and attached to the sliders with a bearing, to provide the necessary inclination and a braking system was provided to keep the plate at one position. The entire system was mounted on a floor at a height of 2.5 meters. The entire electrical components including ballast and igniter for the HMI lamps

were placed in a restricted area near the base plate for safety. The photograph of the solar simulator is shown in figure 5.14.

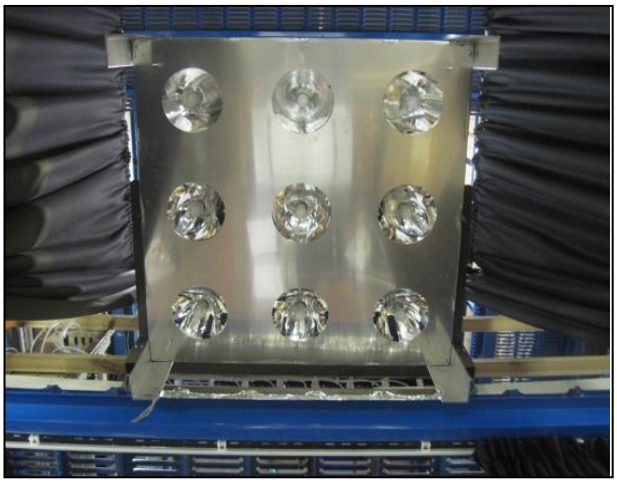

Figure 5.14: Photograph of the In-House Built Solar Simulator at Heriot-Watt University

5.4 Indoor Experimental Testing of Hyperboloid Concentrator

Indoor experimental temperature distribution of receiver was carried out for two different types of receiver. Temperature measurement was carried out based on 'flow' and 'no flow' conditions. The circular and elliptical hyperboloid concentrators (CHC) and (EHC2) (optical efficiency of 28% and concentration ratio of 20×) were tested.

Malotherm SH Oil was used as heat transferred fluid and made to pass through the receiver. A receiver was placed under the solar simulator, where average solar radiation of 1200 W/m^2 was obtained. The temperature of the receiver surface was increased and the oil was heated. The heated oil was made to flow through the system by using a peristaltic pump (Pump – Watson Marlow 323), which was placed after the receiver, and passed through a seawater tank. During the experimental measurement, inlet and outlet temperature of the receiver and the temperature of the tube were measured. The temperature measurements were carried out by means of two T-type thermocouples (for inlet and outlet temperature of the oil). In addition to that, solar radiation from the simulator was measured. For measuring the solar radiation, the pyranometer model of Kipp & Zonen CM21 / CM22 was used. For collecting all these data (temperature and solar radiation) a Keithley 2700 Multimeter / Data Acquisition System was used and the data was collected and processed in Microsoft Excel.

The experimental cycle consists of the elliptical solar concentrator with aluminium grooved flat receiver / copper coil receiver; one end of the receiver is connected to inlet tank and other end to the outlet of the tank. The entire experimental setup for EHC2 open cycle is shown figure 5.17. The schematic view of the solar collector with desalination system for CHC and EHC2 is shown in figures 5.15 and 5.16. EHC2 with water distillation and CHC with water distillation are also given in figures 5.18 and 5.19. In order to estimate the temperature distribution along the receiver, thermal imaging camera and FLIR Tools software were used to obtain the temperature variation along the receiver at three different points. At 'no flow 'conditions, stagnation temperatures were measured at three different points (T1, T2 and T3) on the receiver. The maximum stagnation temperatures of 93°C were observed for solar radiation of 1200 W/m^2 and the average stagnation temperature of 82 °C was observed. The variation of stagnation temperatures with time is shown in the figure 5.20. The measured stagnation temperatures were also compared with the results of thermal imaging camera. The temperatures from the thermal imaging camera were in close agreement with the estimated stagnation temperature. The photographs of thermal imaging temperature are also shown in figure 5.21. (a,b,c,d,e,f). At 'flow conditions' the inlet and outlet temperatures of water were measured. The flow rate of 0.12 kg/min was allowed to flow through the receiver.

The variation of inlet and outlet temperatures with time is shown in figure 5.22. It is observed that the maximum outlet temperature of 60°C was observed for the solar radiation of 1200 W/m^2. As a part of developing the desalination system, the solar concentrator with receiver was constructed and experimental measurements were taken for 'flow' and 'no flow' conditions. In the flow conditions, oil was allowed to flow through the receiver and heated depends on the solar concentration level. A solar concentrator was placed on the top of the receiver and radiation from the solar simulator reached the receiver through multiple reflections in the concentrator and finally absorbed by the receiver. The outlet temperature of the solar collector system was examined whether the outlet temperatures would be useful for a seawater desalination process or not.

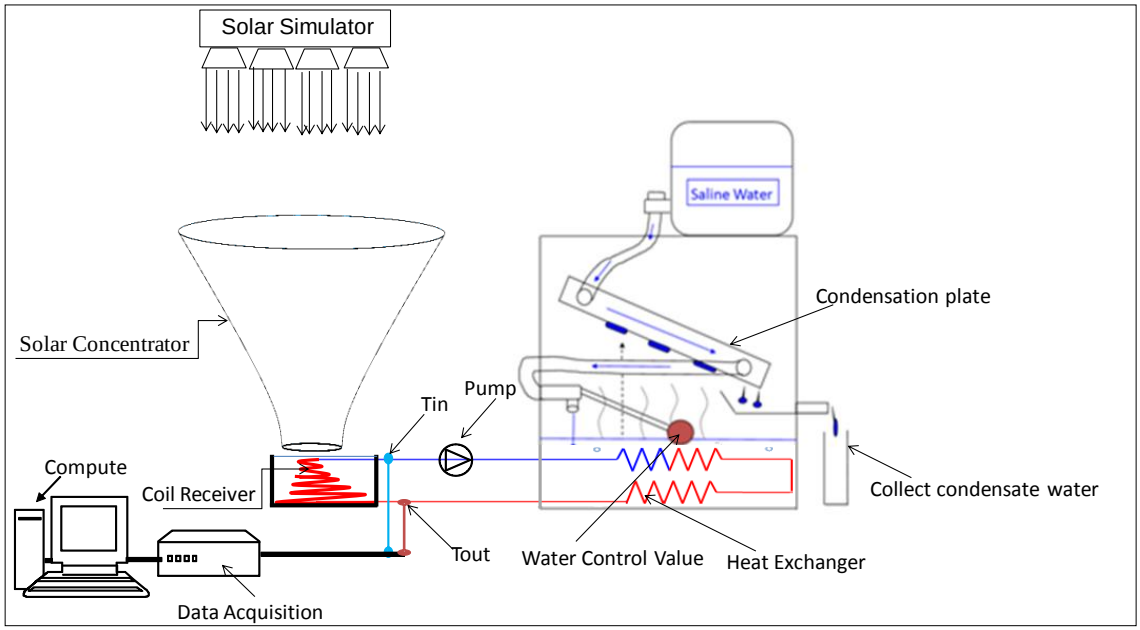

Figure 5.15: Schematic of the Solar Collector CHC with Desalination System

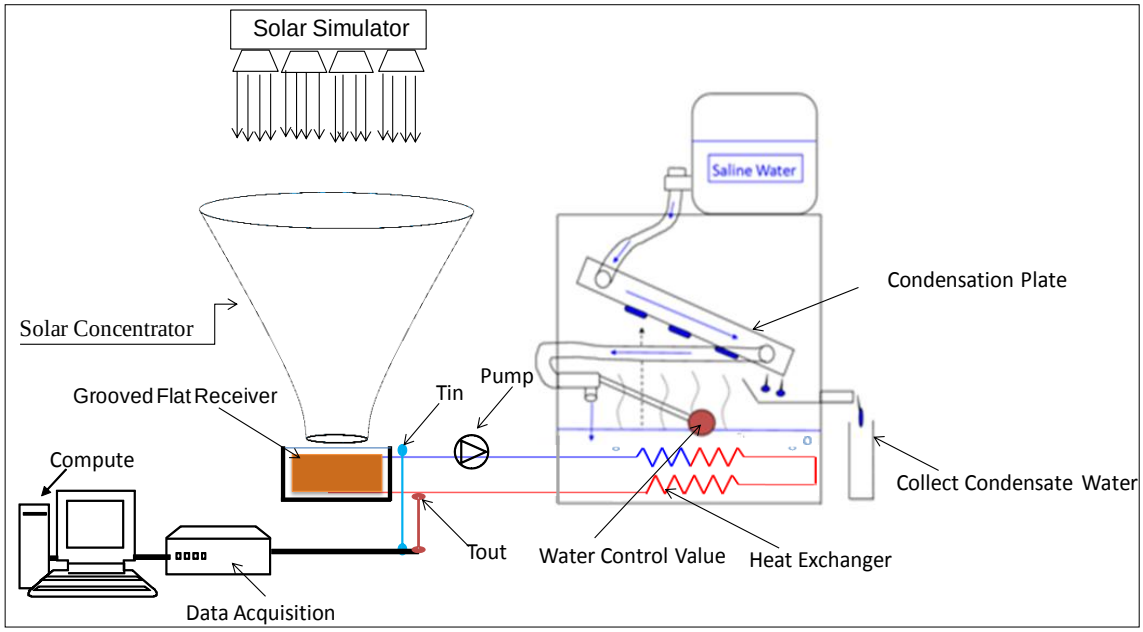

Figure 5.16: Schematic of the Solar Collector EHC with Desalination System

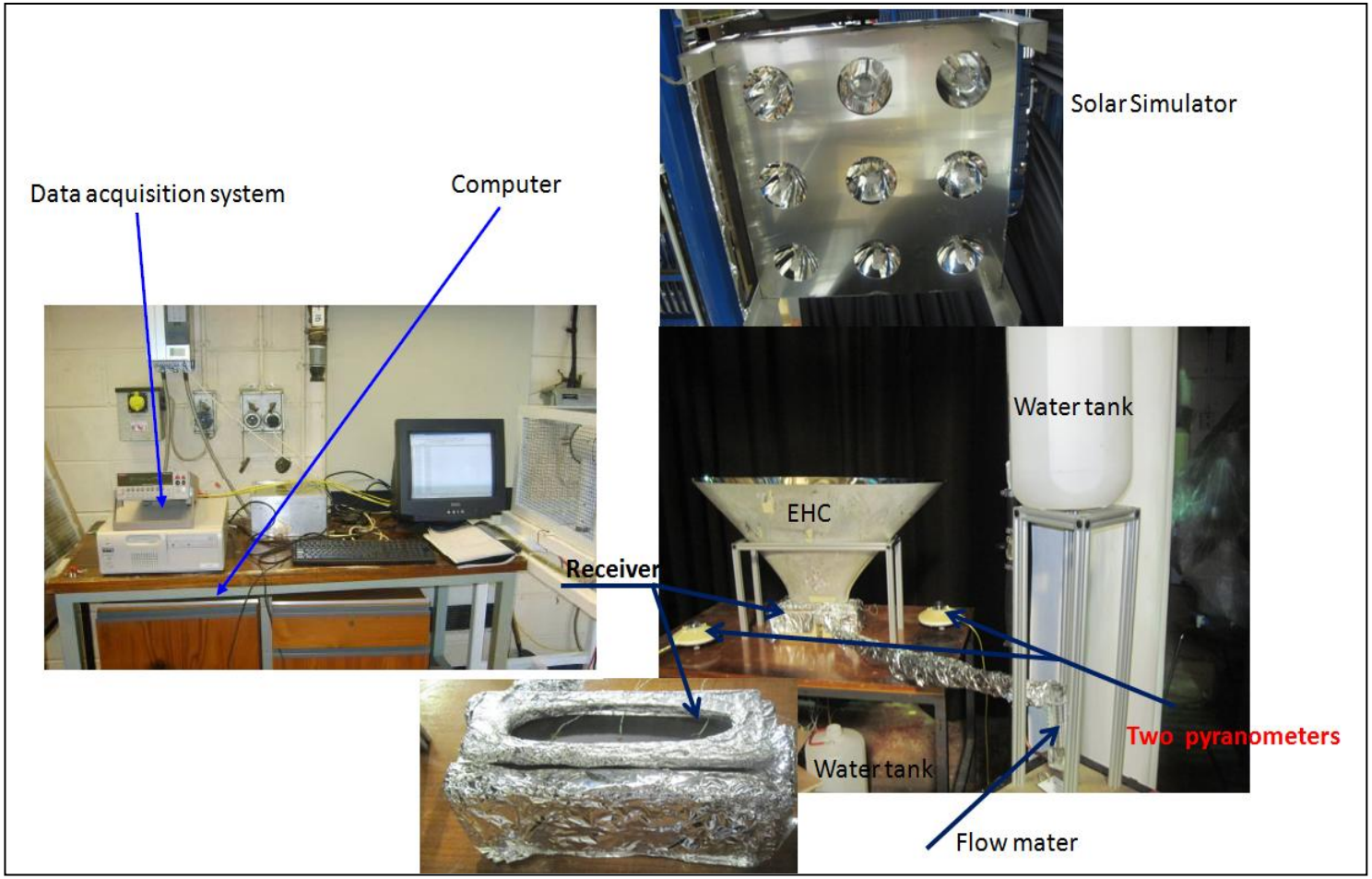

Figure 5.17 : Experimental Setup for EHC2 for Open Cycle

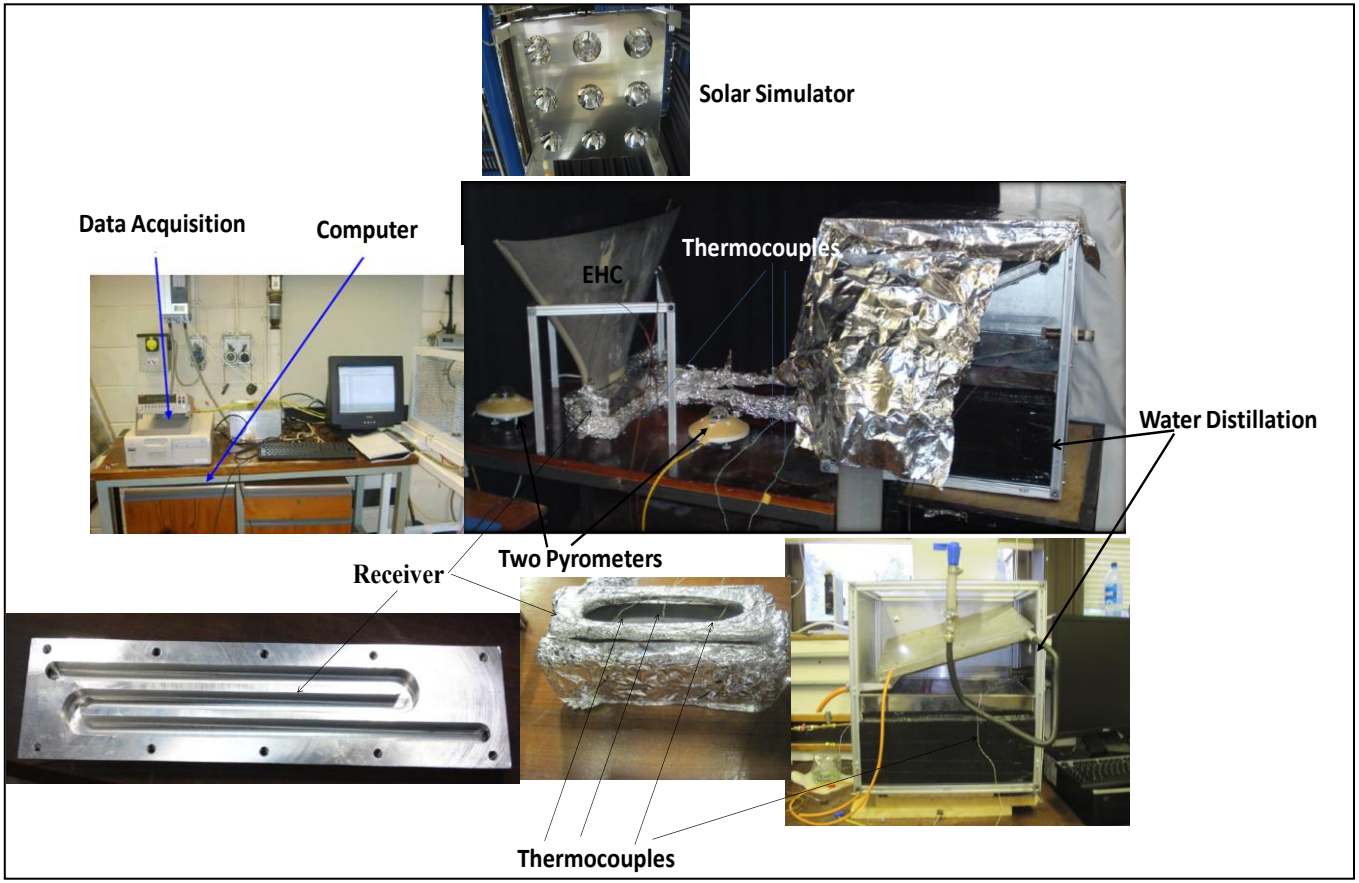

Figure 5.18: Experimental Setup for EHC2 for Water Distillation

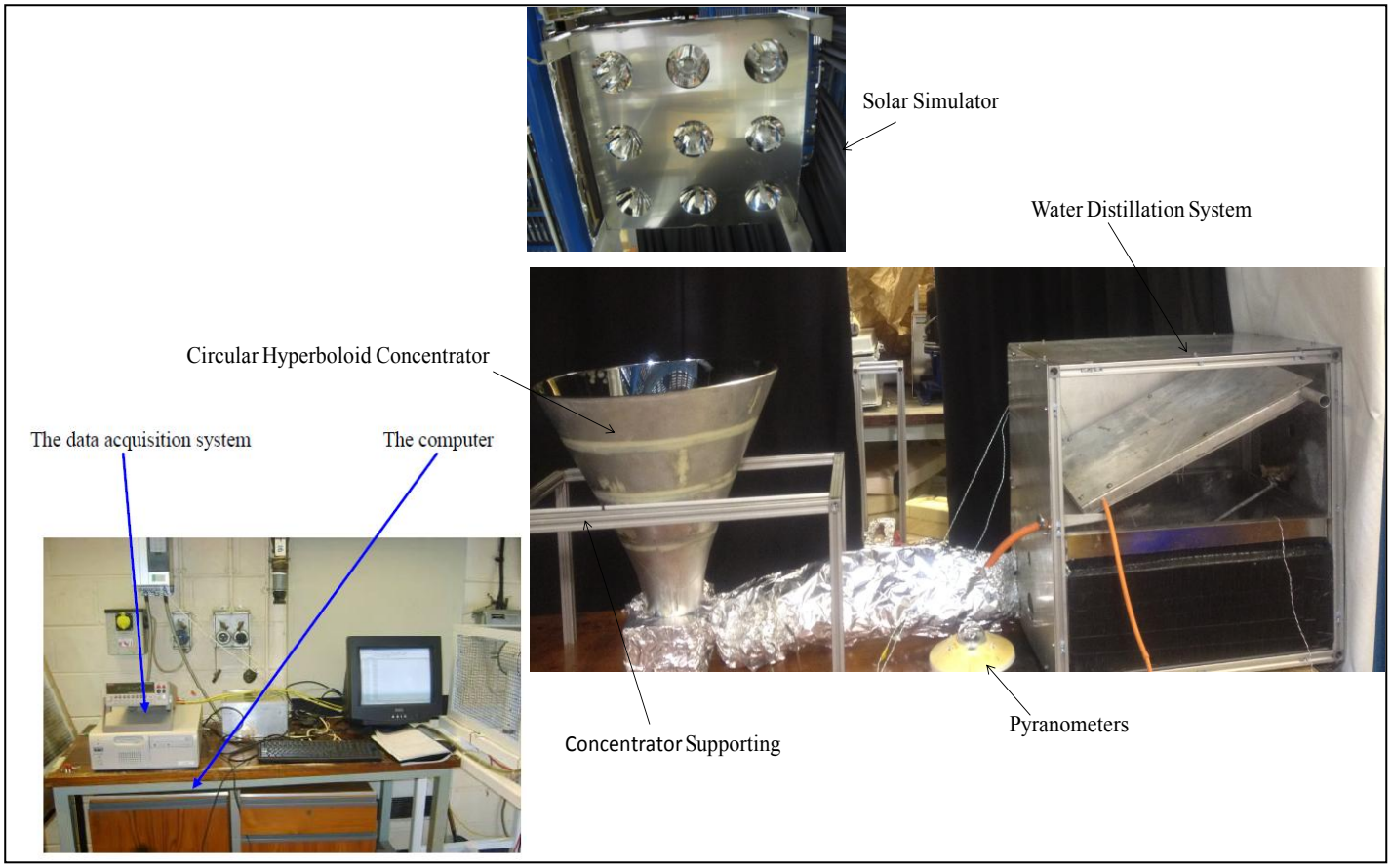

Figure 5.19: Experimental Setup for CHC for Water Distillation

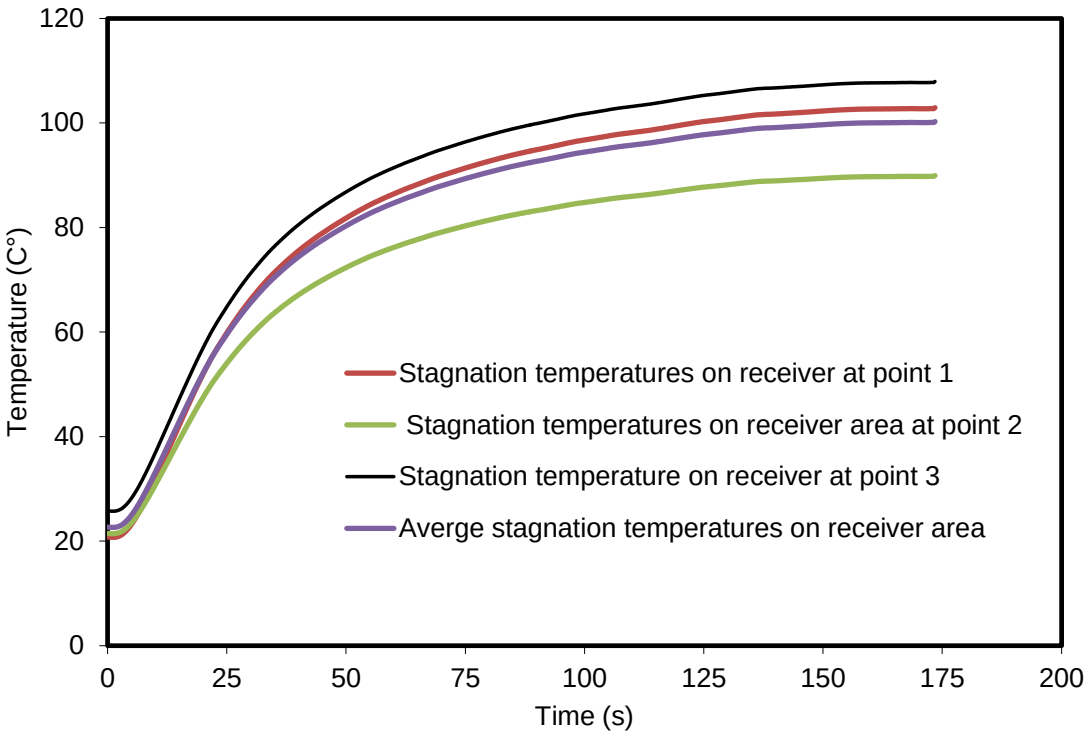

Figure 5.20: Variation of Stagnation Temperature with Time for EHC2

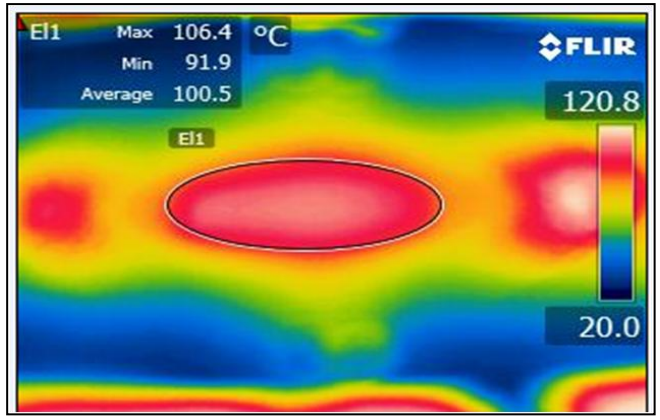
El1 Max 106.4 °C
Min 91.9
Average 100.5
El1
FLIR
120.8
20.0

(a)

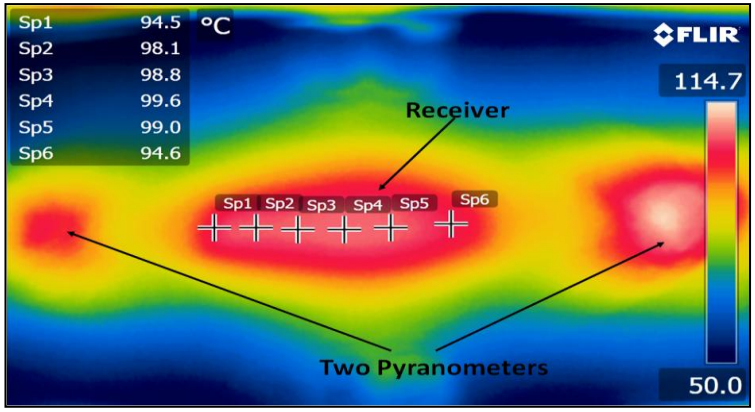
Sp1 94.5 °C
Sp2 98.1
Sp3 98.8
Sp4 99.6
Sp5 99.0
Sp6 94.6
FLIR
114.7
Receiver
Sp1 Sp2 Sp3 Sp4 Sp5 Sp6
Two Pyranometers
50.0

(b)

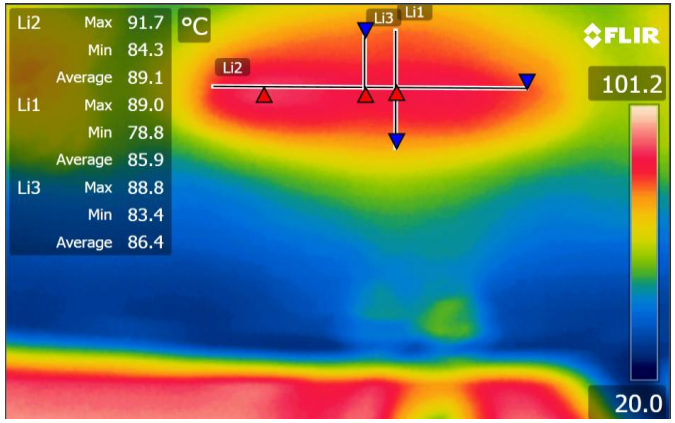
Li2 Max 91.7 °C
Min 84.3
Average 89.1
Li1 Max 89.0
Min 78.8
Average 85.9
Li3 Max 88.8
Min 83.4
Average 86.4
Li3
Li1
Li2
FLIR
101.2
20.0

(c)

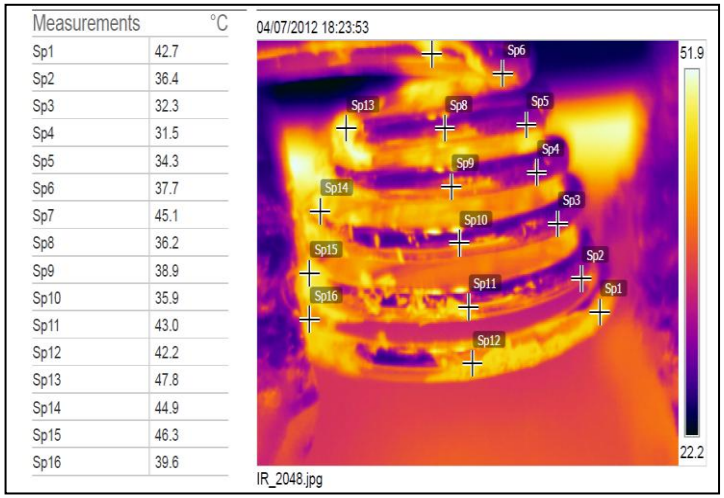

(d)

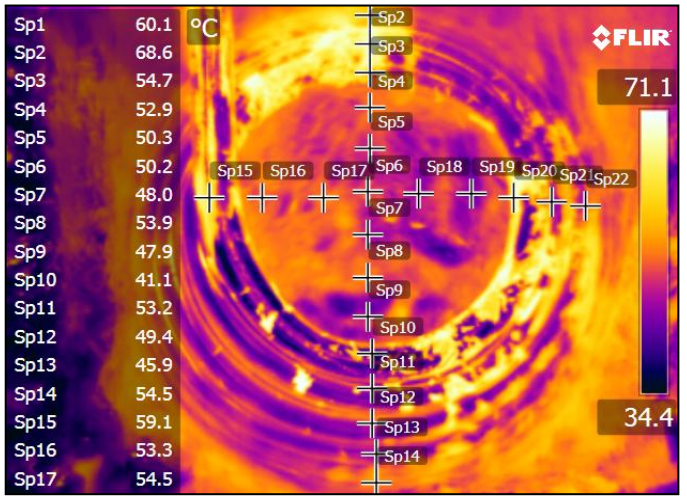

(e)

Figure 5.21: Photographs of Thermal Imaging Temperature of Flat Grooved Aluminium and Copper Coil Receiver Where (a) Avage Temperature on Groove Receiver Area for EHC2, (b) Temperature Different Along Major Axis (C) Temperature Different Along Major Axis and Minor Axis (d) Temperature Different Along Vertical on Coil Receiver for CHC (e) Temperature Different Along Major Axis and Minor Axis on Coil Receiver for CHC

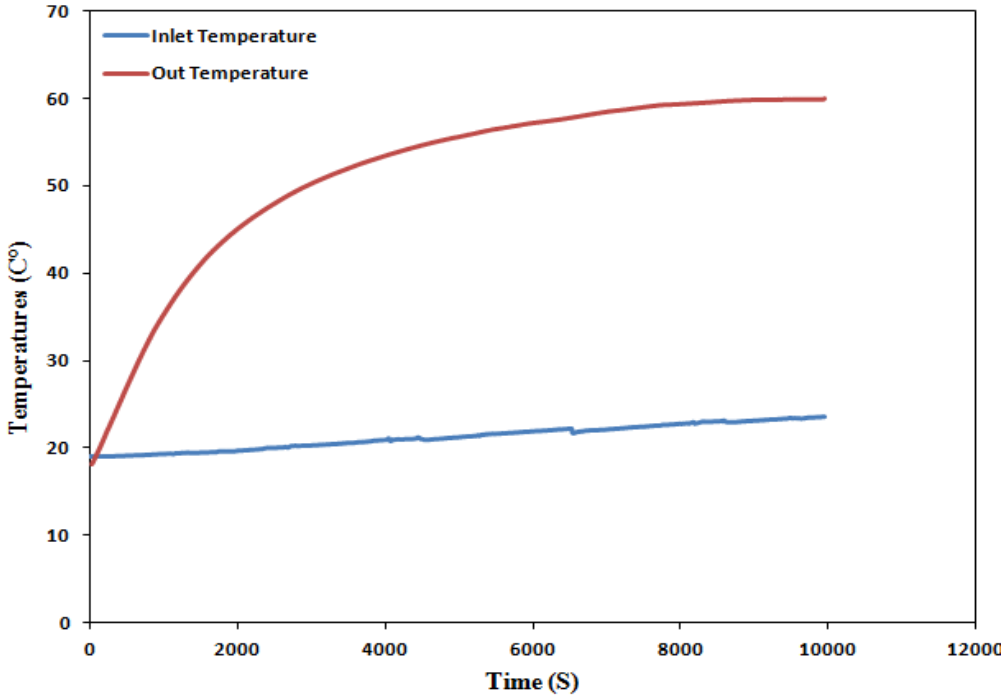

Figure 5.22: Variation of Inlet and Outlet Temperatures with Time for CHC

5.5 Closure

In this chapter, optical analysis of circular and elliptical hyperboloid concentrator were discussed. For indoor characterisation, an in-house built solar simulator has been constructed at Heriot-Watt University. The design, fabrication details and indoor characterisation of circular and elliptical hyperboloid concentrators with flat grooved aluminium and copper coil receiver have also been discussed. The temperature distributions of the flat grooved aluminium and copper coil receiver were also obtained. The next chapter deals with the outdoor characterisation of circular and elliptical hyperboloid concentrators.

CHAPTER 6: Outdoor Experimental Investigation of 3-D EHC

This chapter presents the design and experimental analysis of a static 3-D solar elliptical hyperboloid concentrator (EHC) for process heat applications. The 3-D static elliptical hyperboloid concentrator is designed to accept a wide range of incidence angles (±45°) and has a concentration ratio of 20× for medium temperature applications (100° C to 150° C). Ray tracing analysis has been used to obtain, the solar flux distribution on the receiver aperture plane for the EHC configuration. The optical efficiency has been obtained theoretically using Optis™, a ray tracing program and optimisation has been carried out, before the design of the EHC was finalised and experimentally tested.

The experiments were carried out for different conditions to study the performance of EHC. The experimental studies are to investigate the possibility of the proposed concept and to evaluate the theoretical results with the experimental ones. Experimental unit was designed in ITT Chennai, built and tested. This research concerns an experimental study of solar radiation energy convert into thermal energy by using a follower 3-D static elliptical-hyperboloid solar concentrator. The experiment was carried out on a 3-D hyperboloid concentrator of 1.64 m concentrator height , aperture major and minor axis were 1.7 m, 0.350 m where the exit area major and minor axis were 0.39 m, 0.062 m receptively. The system efficiency depends on the heat input; temperatures of the water at the inlet and outlet of the receiver and the mass flow rate have been carried out. The experimental study has also been carried out to obtain the inlet and outlet temperature of fluids supplied to a coil heat exchanger solar receiver.

6.1 Introduction

The design of the receiver is mainly depends on the ray tracing and flux distribution. Before making the experimental set-up, the optical study needs to be carried out. In the optical study, the information about ray tracing, flux distribution on the receiver of the EHC determines the size of the receiver. The following section discusses the optical study of EHC.

6.2 Optical study of EHC

6.2.1 Ray tracing of EHC at different incidence angles

The source rays have been modelled to follow a similar path to that of the sun for a typical daily cycle. Using the ray tracing method described in chapter 2, the following results were obtained for the 3-D EHC. Figure 6.1 shows the ray tracing diagram for the different incident angles of 0°, 15°, 30° and 60°. Based on these preliminary models, it can also be observed that the maximum number of rays reaching the receiver occurs when the radiation source is directly above the concentrator (θ is 0º). The number of rays reaching the receiver decreases as the angle of the incidence increased; no rays are absorbed by the receiver when the incident angle is ± 60º.

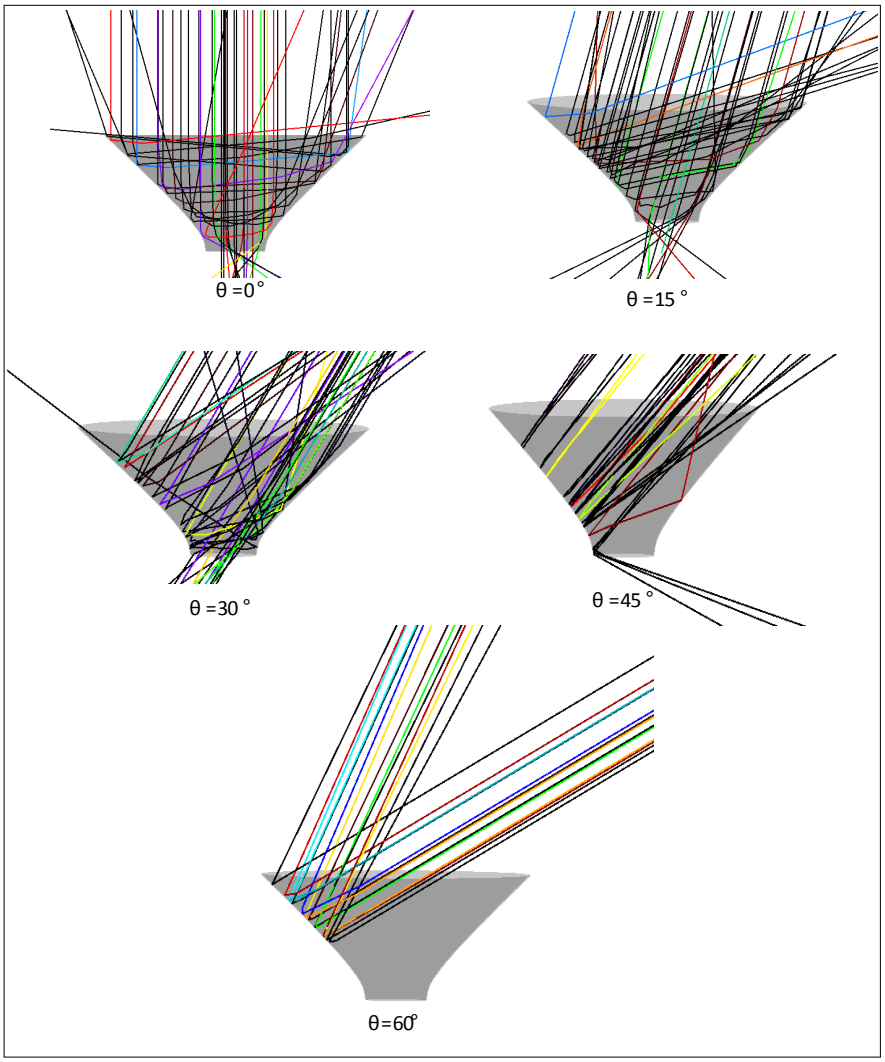

Figure 6.1: Ray Tracing of EHC for Different Incidence Angles (0°, 15°, 30°, 45° and 60°)

6.2.2 Effect of the variation of the solar azimuth angle

Using the ray tracing model, the effect of the variation of the solar azimuth angle (Ψ) on the optical efficiency of the EHC was investigated. The solar azimuth angle is the angular deviation of the sun from true south [6]. By moving the solar source along the *xy* plane of the major axis aperture through angular variation from 0° to 90° with an increment of 5°, for teach angle of interval the solar incidence angle is varied from 0° to 60°. The geometry considered for this simulation with variation of major axis aperture is shown in figure 6.2.

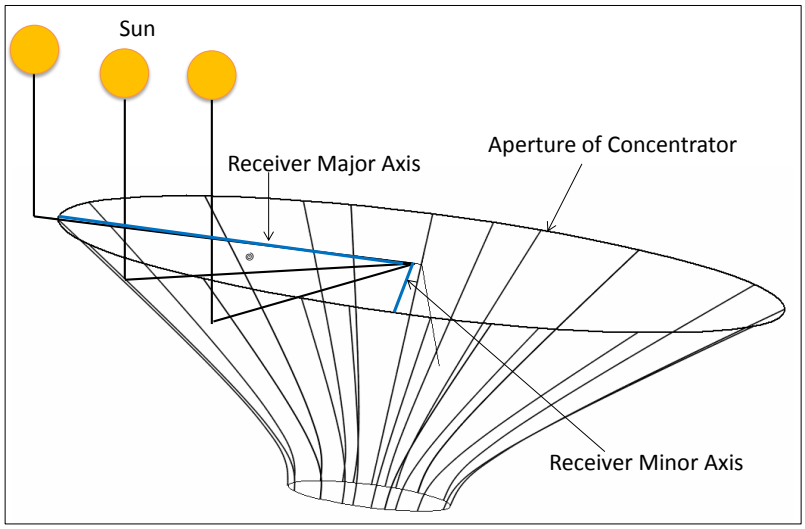

Figure 6.2: EHC with Variation of Major Axis Aperture

Next, the effect of variation of the solar azimuth angle on the optical efficiency was investigated. The variation of the optical efficiency with azimuth angle variation and incidence angle is shown in figure 6.3. It was observed that as the solar azimuth angle was increased from 0°-90°, that is the solar source was moved from the south to the north, the acceptance angle decreases from approximately 30° in the south to less than 5° as the solar source approaches the north. For each azimuth angle variation, one maximum optical efficiency is observed in those variations. The maximum optical efficiency observed for each angle decreases, as the solar source is moved from 0°-90°.

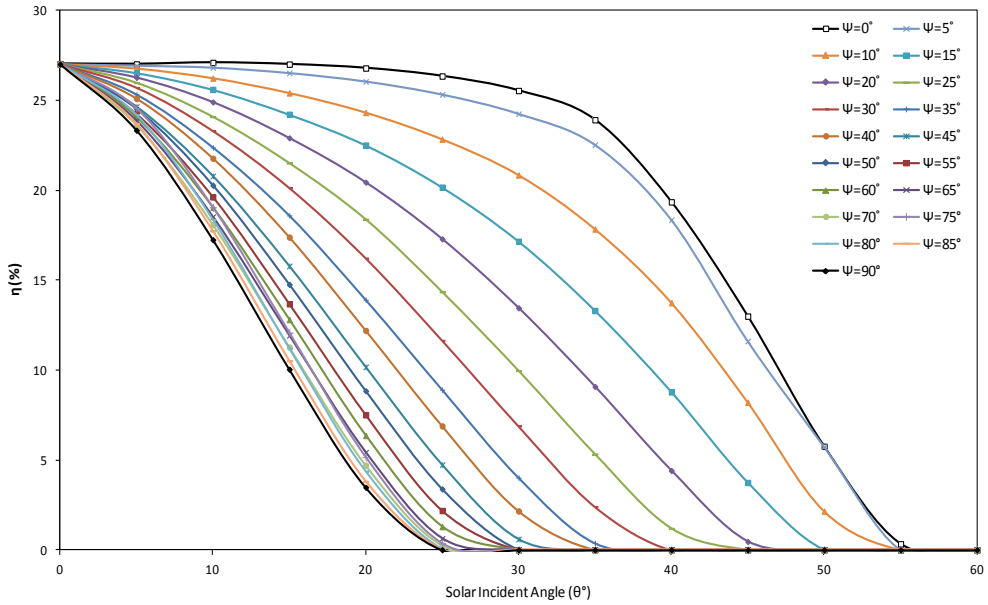

Figure 6.3: Variation Of Optical Efficiency with Azimuth and Incident Angles

6.2.3 Flux distribution on the receiver area for different azimuth angle

Using the 3-D tracing simulation, the effect of variation of the solar azimuth angle on the flux distribution on the receiver area of the EHC was examined by moving the solar source along the x-y plane of the aperture major axis from 0° to 90° with an increment of 15° intervals. The results obtained are shown in figures 6.4 to 6.6 respectively. It was observed from figures 6.4 and 6.5, at solar azimuth angle of 0° and 15°; the flux is uniformly distributed and spread over the receiver for the solar incidence angle of 0° to 30°. In the same figures, at 45° incidence angle, the flux is not uniformly distributed. The distribution is scattered non-uniformly over the receiver. And at one end of the receiver, it is concentrated, the flux value is higher. Similarly, from figures 6.6 and 6.7, at solar azimuth angle of 30° and 45° the distribution of the flux on the receiver area were uniformly spread when solar source incidence angle was 0 and 15, but when the solar source incidence angle of 30, the total flux measured on the receiver was concentrated at one side of the receiver, while at angles above 30° no radiation flux was observed at the receiver. Similarly variation is observed for solar azimuth angle of 75° and 90°, as shown in figures 6.8 and 6.9. Furthermore, the variation of the flux distribution along the receiver major axis and receiver minor axis; are also shown in figures 6.10 to 6.15.

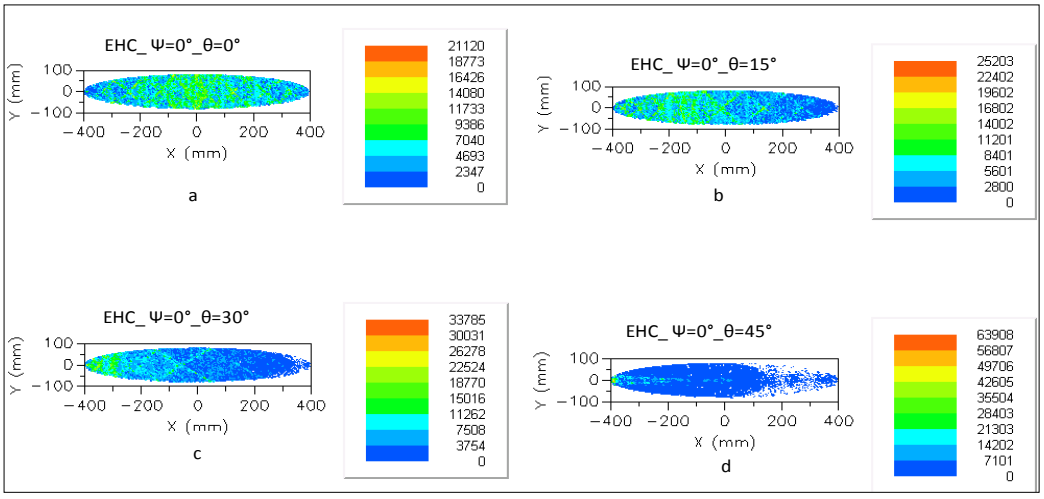

Figure 6.4: Flux Distributions on Plane Angle is 0° and Incidence Variation for 0°-45°

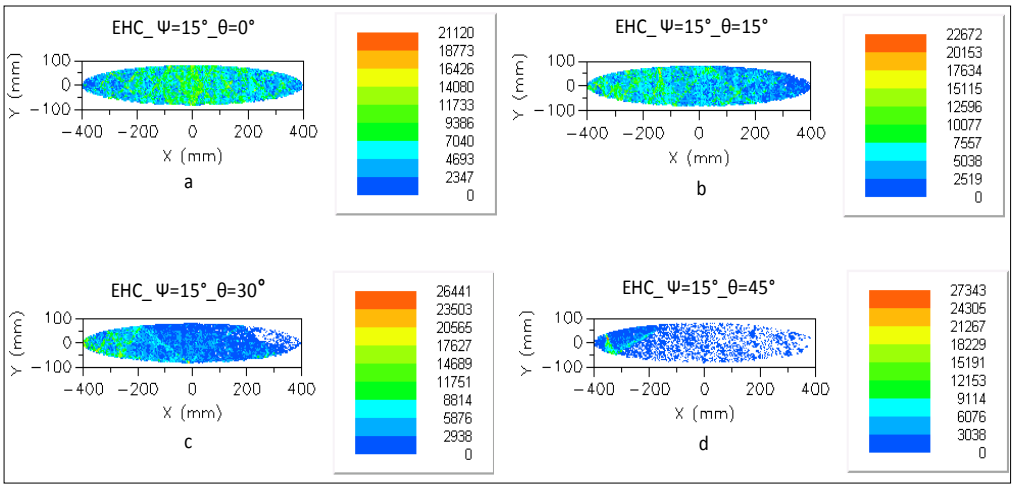

Figure 6.5: Flux Distributions on Plane Angle is 15° and Incidence Variation for 0°-45°

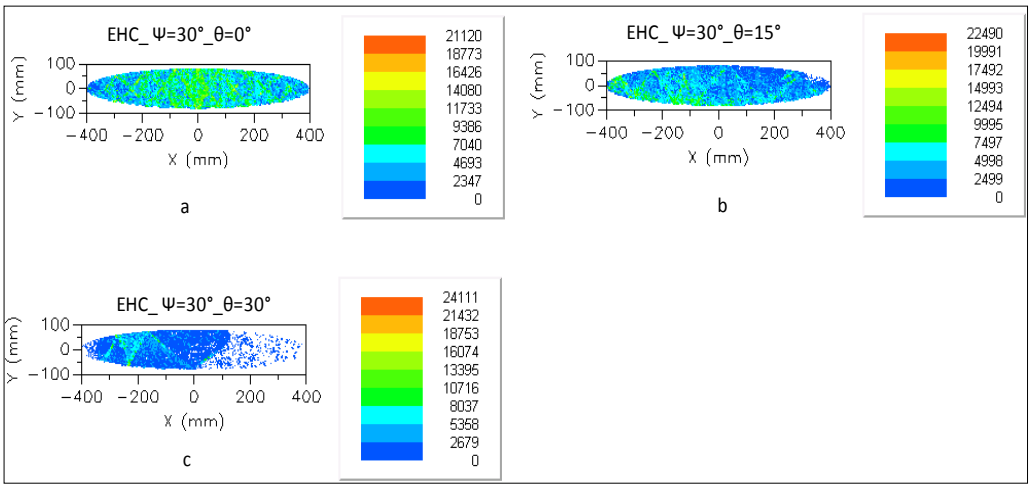

Figure 6.6: Flux Distributions on Plane Angle is 30° and Incidence Variation for 0°-30°

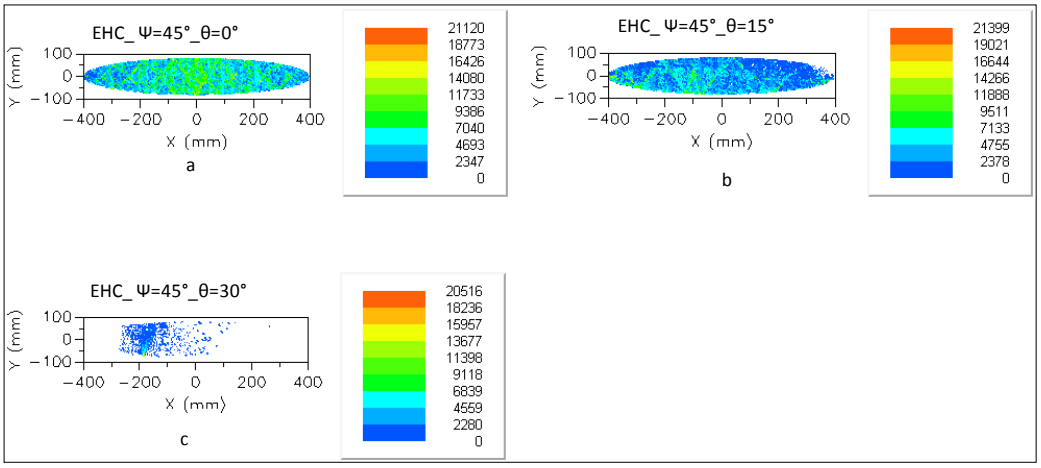

Figure 6.7: Flux Distributions on Plane Angle is 45° and Incidence Variation for 0°-30°

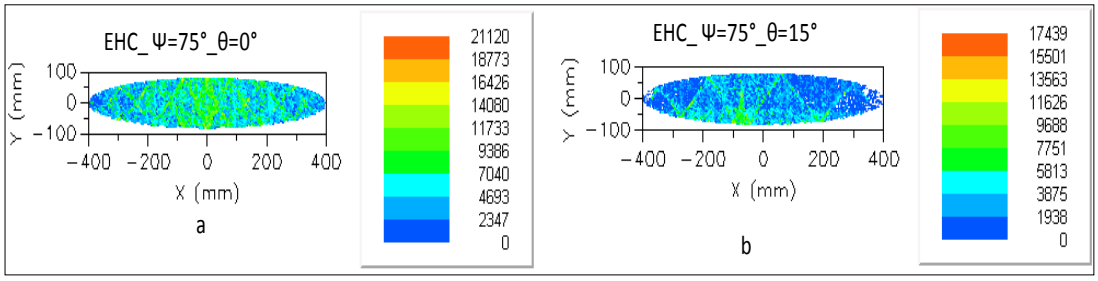

Figure 6.8: Flux Distributions on Plane Angle is 75° and Incidence Variation for 0° -15°

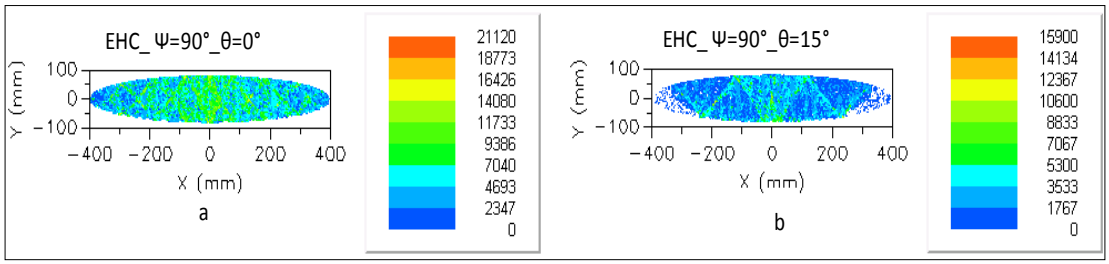

Figure 6.9: Flux Distributions on Plane Angle is 90° and Incidence Variation for 0° -15°

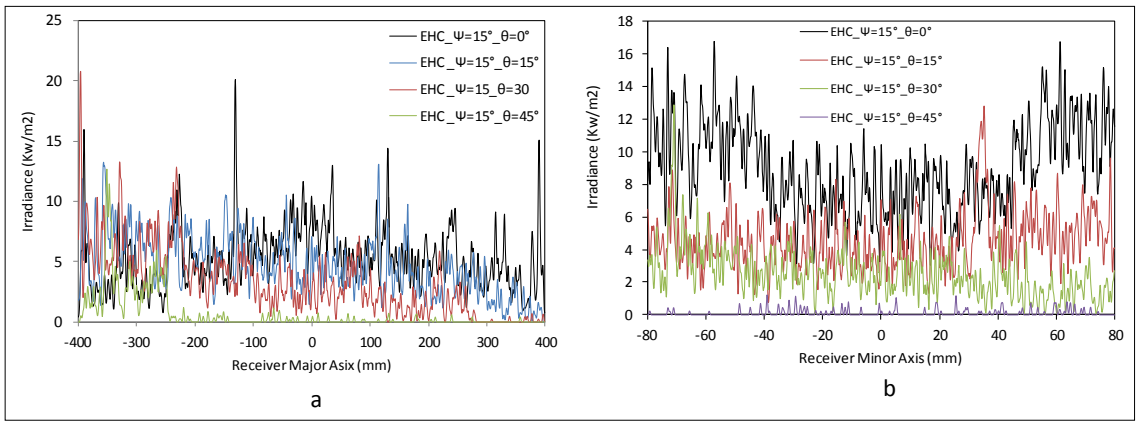

Figure 6.10: Flux Distributions on Centre Line of a) Major Axis and b) Minor Axis for Different Plan (ψ=15°) and Different Incident Angle

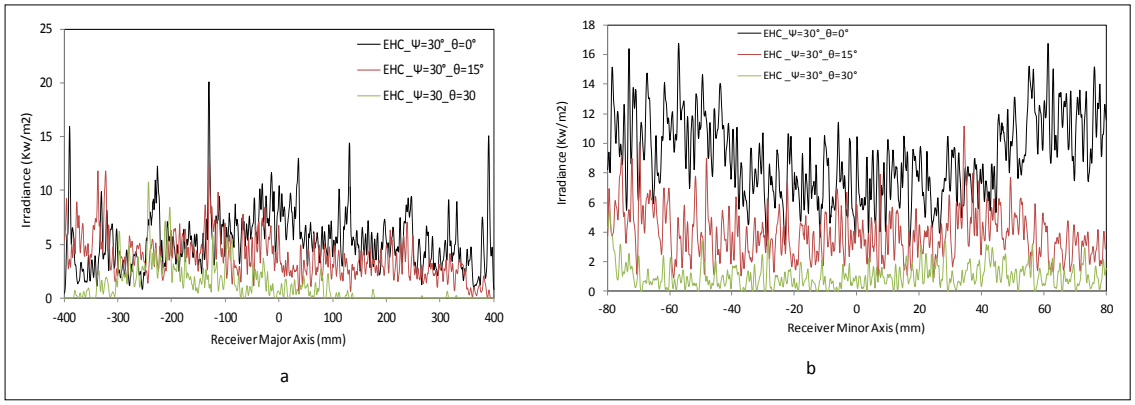

Figure 6.11: Flux Distributions on Centre Line of a) Major Axis and b) Minor Axis for Different Plan (ψ=30°) and Different Incident Angle

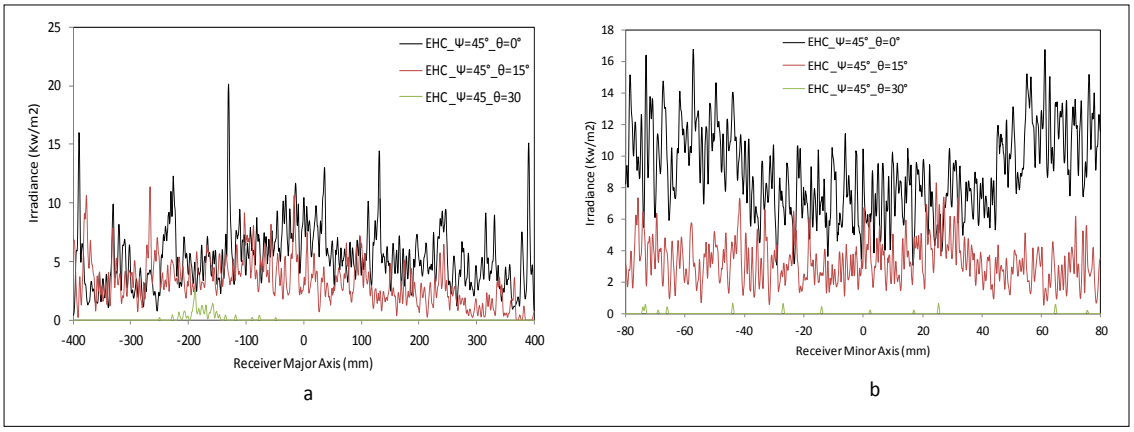

Figure 6.12: Flux Distributions on Centre Line of a) Major Axis and b) Minor Axis for Different Plan (ψ=45°) and Different Incident Angle

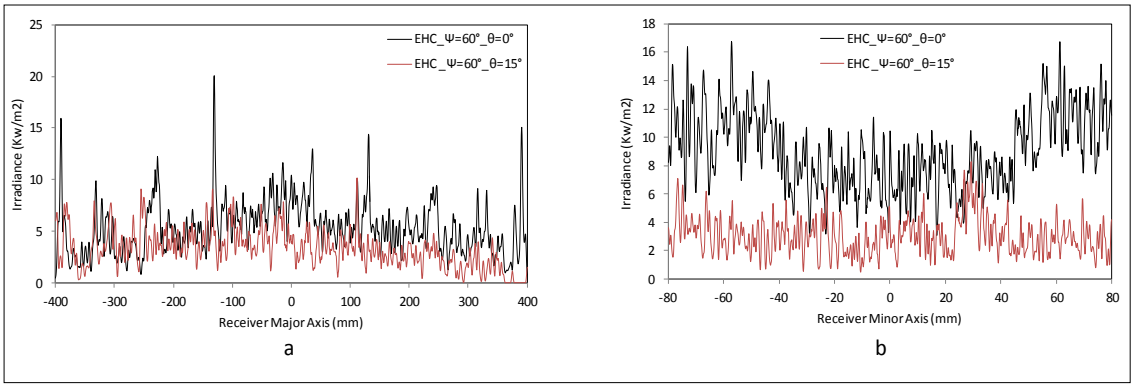

Figure 6.13: Flux Distributions on Centre Line of a) Major Axis and b) Minor Axis for Different Plan (ψ=45°) and Different Incident Angle

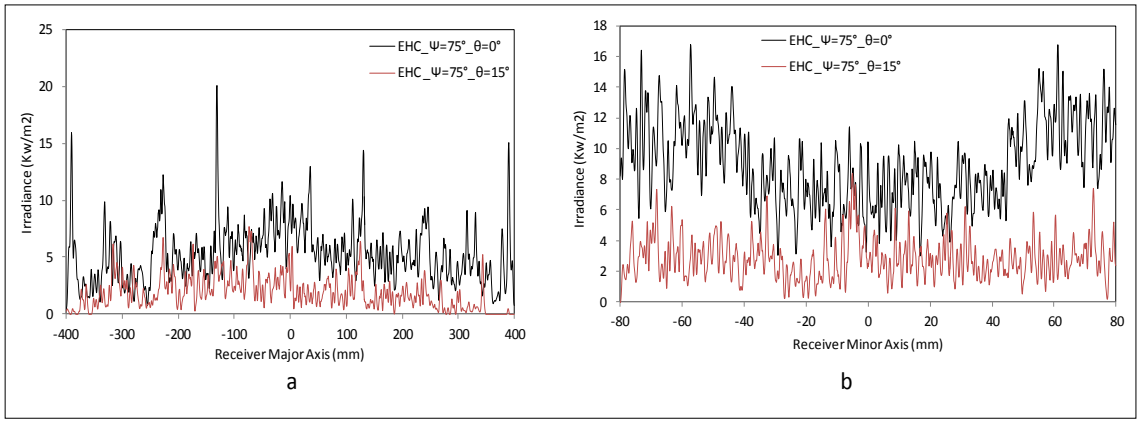

Figure 6.14: Flux Distributions on Centre Line of a) Major Axis and b) Minor Axis for Different Plan (ψ=75°) and Different Incident Angle

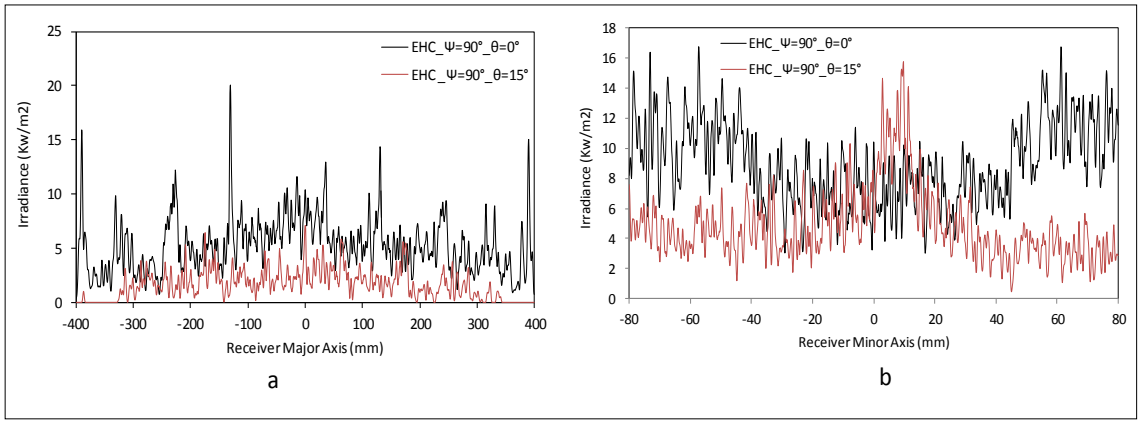

Figure 6.15: Flux Distributions on Centre Line of a) Major Axis and b) Minor Axis for Different Plan (ψ=90°) and Different Incident Angle

6.3 Outdoor Experimental Characterisation of EHC

This experimental characterisation of EHC is a systematic and comprehensive test for determining the thermal performance of 3-D elliptical-hyperboloid solar collectors for medium temperature applications. The shape of the receiver is trapezoidal and made by mild steel material. The receiver is fabricated by bending and welding process. The whole experimental analysis is carried out of determining the steady-state thermal performance of solar collectors, the instantaneous efficiency of solar collectors, and the thermal performance during the whole day operation. The optimum optical efficiency of the 2-D hyperboloid solar collector was determined by using the ray tracing technique using the MATLAB code for simulation. The optimum optical efficiency of the 3-D elliptical hyperboloid concentrator was also determined using the optics software. Theoretical and experimental research was conducted to validate the simulated results and develop a practical system based on the simulated concept. The experimental work is conducted, based on the findings of the theoretical study, which includes:

- Design, construction, instrumentation and calibration of the experimental set up.
- Data collection.
- Data reduction, analysis and comparison of theoretical and experimental results.

6.3.1 Materials and Equipment that will be used to perform the Experiment

6.3.2 Apparatus Required.

The following equipment was used to evaluate the thermal performance of the 3-D elliptical hyperboloid concentrator:

1. Pyranometer was used to measure the global solar radiation. It was mounted on the outer frame of the hyperboloid concentrator in such a manner that no shadow is cast on the exposed area of the collector, and it is in the normal direction to the plane of aperture.
2. Calibrated thermocouples for measurement of water temperature at inlet and the outlet of the heat receiver and also surface temperature of the receiver.
3. Data acquisition system.
4. Thermal imaging camera for taking temperature distribution images of the receiver area.

6.4 Assembling the Components and Conducting the Experiment

6.4.1 Components: Hyperboloid Concentrator

The 3-D elliptical hyperboloid concentrator was divided into two reflectors. It was supported firmly with a rigid frame which was also divided in two. The fabrication details of the elliptical hyperboloid is shown in figure 6.16 (a,b,c,d and e). The template of the simulated profile was made. By means of template of the profile, different aluminium frames were made and a 3-D elliptical hyperboloid structure was formed. The thickness of the aluminium frame was 3 mm. Aluminium sheeting of 1 mm thickness is covered over the inner surface of the hyperboloid. Above the aluminum surface, highly reflecting film material (ρ = 0.95) is placed. The dimension of the major and minor axis aperture of concentrator was found to be 1.8 m and 0.358 m.

Figure 6.16: Fabrication of the 3-D Elliptical Hyperboloid

6.5 Receiver Elliptical Shape

The receiver consists of copper tubing (6mm outer diameter and 4.5mm inner diameter) and formed a helical and flat portion to capture the maximum incident solar radiation. High absorptive and low reflective black paint was used to coat the receiver surface as shown in the figure 6.17. The entire receiver assembly is placed within a chamber and

covered with glass wool insulation with thermal conductivity 0.037W/mK to minimise losses, and fixed with thermocouple to measure the surface temperature, these are shown on figure 6.17 as T1, T2, T3 and T4. The receiver assembly with and without black coating is shown in figure 6.17 the measured reflective coefficient for the receiver with and without black paint is shown in figure 6.18. It can be observed from figure 6.18 that the reflectivity of the black coated receiver is very low in the range of about 6% with maximum of 10%, while the reflectivity of the uncoated receiver increases sharply from about 15% at the wavelength of 250 nm to a maximum of 86% at the wavelength of 850 nm and remain constant. A sufficient pressure head is created to circulate the water through the copper tubes.

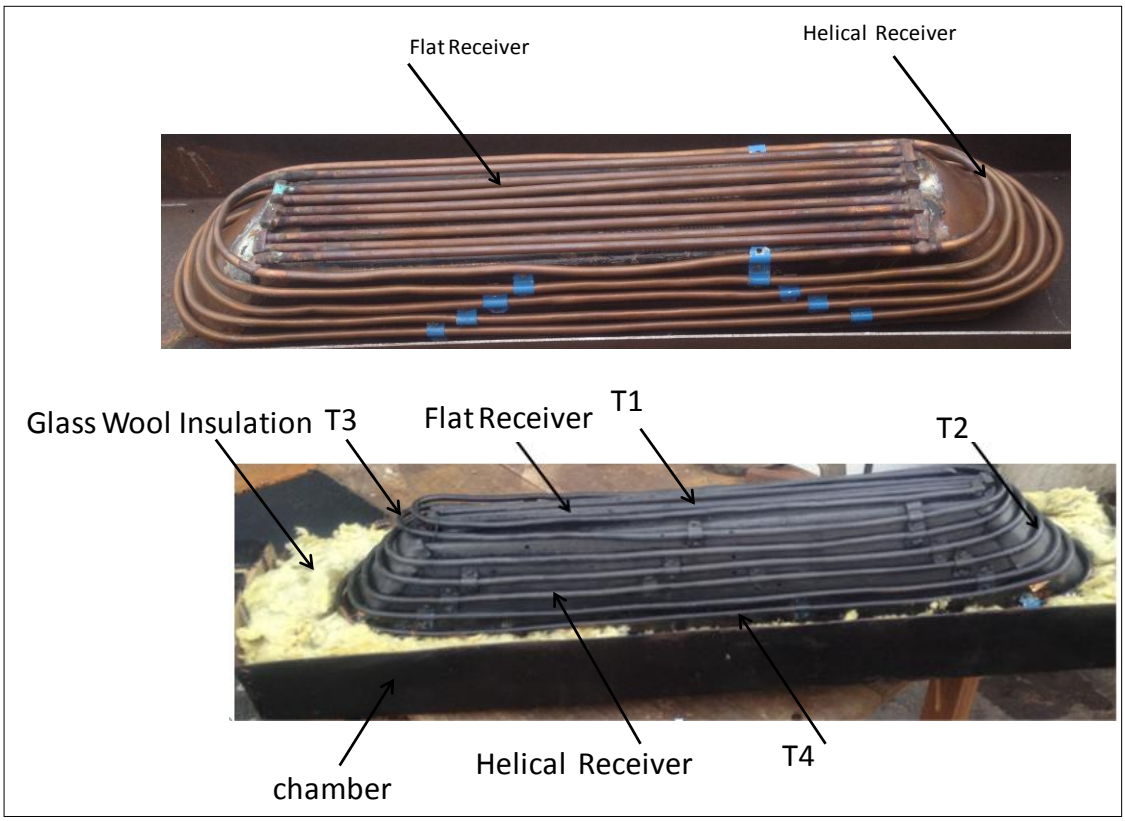

Figure 6.17: Receivers with High Absorptive Without and with Coating

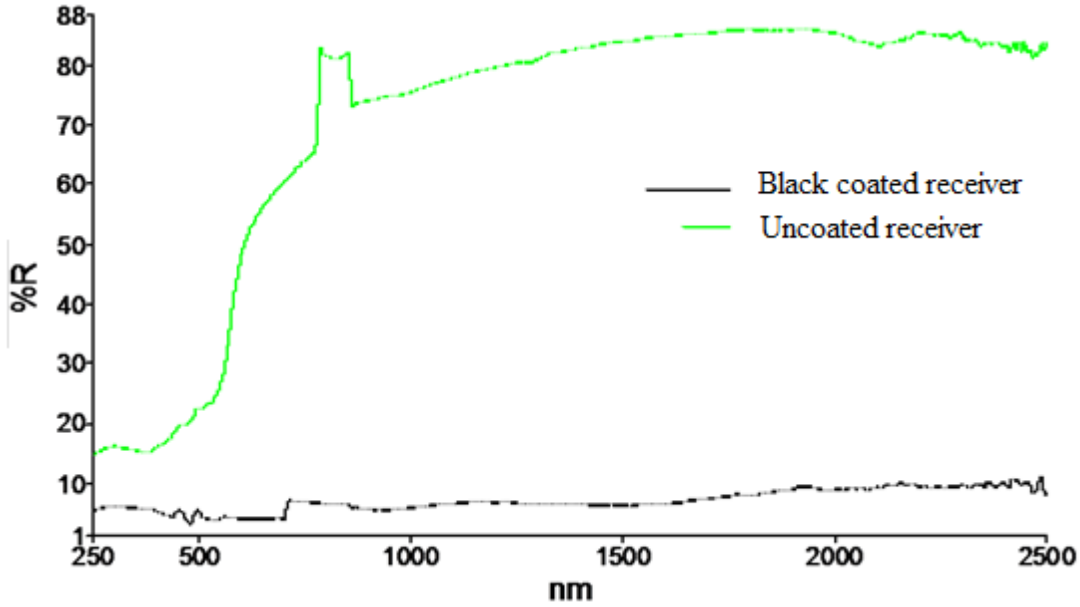

Figure 6.18: Measured Reflective Coefficient for Coated and Uncoated Receiver

Table 6.1: 2-D Dimension of the Receiver Dimension

Sl. No	Parameters	Dimensions of Receiver 1 (m)	Dimensions of Receiver 2 (m)
1	Length	0.81	0.75
2	Breadth	0.19	0.29
3	Thickness	0.003	0.003

6.6 Parameters Measurement

The temperature was measured, at different points of receiver system using thermocouples, and was recorded at each hour during a whole day. The thermocouple was inserted in the inlet of receiver and outlet of receiver, and the inlet storage tank of hot water and outlet cool water tank. A type-K thermocouple was used to measure the temperature in the solar collector system; on the outside surface of the copper piping was measured using a thermocouple and distribution temperatures were recorded using thermal camera. Ambient temperature was measured with a PT-100 (temperatures in the range -150 to +650°C). The global solar radiation flux on the hyperboloid collected was measured with a precision pyranometer. Manual valves and controls were included in the test system, operational parameters such as initial inlet water temperature, outlet water temperature, and flow rate was also measured. These parameters allowed for the evaluation of the effect of raising or lowering the water temperature, average thermal efficiency during the operation period and the performance analysis of this system was

reported. And also installation conditions of solar collectors are shown in tables 6.2 and table 6.3 shows specifications of hyperboloid collector design.

Table 6.2: Installation Conditions of Solar Collectors.

Location	India (IITM)
Longitude	80°2
Latitude	13°
Height from the ground	0.5 m

Table 6.3: Specifications of Hyperboloid Collector Design.

Parameters	Dimensions
Aperture Major Axis	1.7 m
Aperture Minor Axis	0.390 m
Aperture area= $\pi*A*B$	1.9 m^2
Height	1.640 m
Receiver Major Axis	0.390 m
Receiver Minor Axis	0.062.5 m
Receiver area= $\pi*a*b$	0.077 m^2
Concentration Ratio	24.5
Tube O.D (Out Diameter)	0.0045 m
Insulation conductivity	0.037 W/Mk
Collector frame	Aluminium
Flow tubes	Copper
Absorber	Copper w/ Black Coating
Insulation	Glass Wool Insulation
Reflector	ReflecTech® mirror film (94%)

6.7 Storage system for EHC

The cold water storage tank used in the experimental analysis is shown in figure 6.19. The dimensions of the cold water storage tank are given in table 6.4. The water passes through the 0.5 hp pump and circulates in the receiver. A photograph of the motor with pump is shown in figure 6.20. The water is heated in the receiver and the hot water

passes into the outlet hot water storage tank, which is shown in figure 6.21. The tank is well insulated; the outside ambient condition should not affect temperature of the water storage. The dimensions of the outlet hot storage tank are given in table 6.5. The stand is used to support the pipes for the circulating the water from inlet to outlet. A photograph of the stand is shown in figure 6.22. The stand consists of three parts: a square plate, hollow pipe and 'L' channel. The L channel has a hole to clamp the pipes in place.

Figure 6.19: Photograph of the Inlet Storage Tank (Cold Water Storage) for the System

Table 6.4: Dimensions of the Cold Water Storage Tank.

S No	Parameters	Dimensions (m)
1	Diameter	0.65
2	Length	1.2

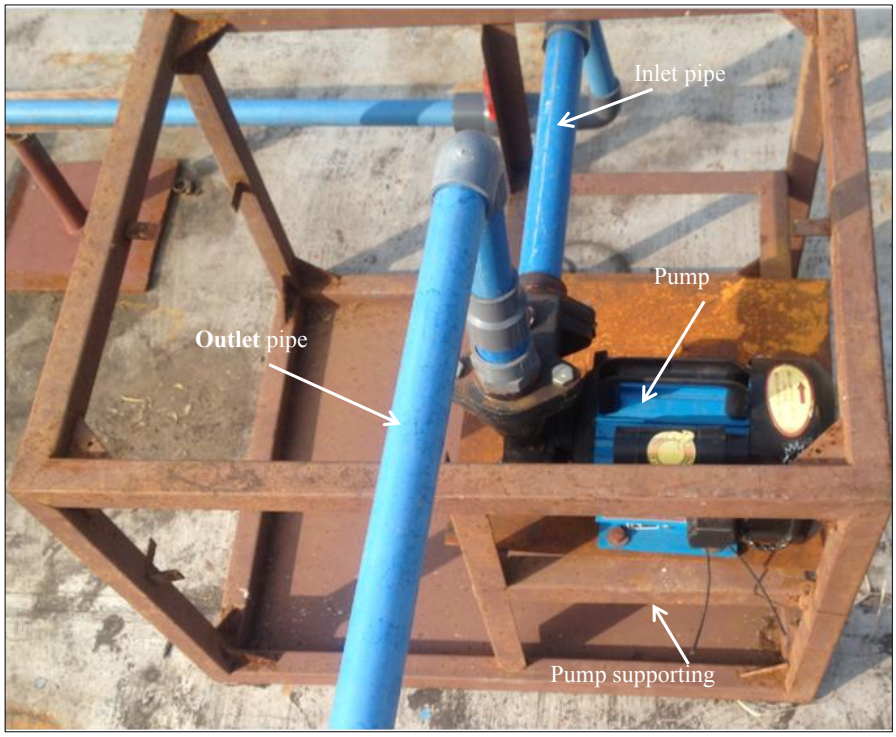

Figure 6.20: Photograph of the Motor and Pump Used in the Experimental Setup

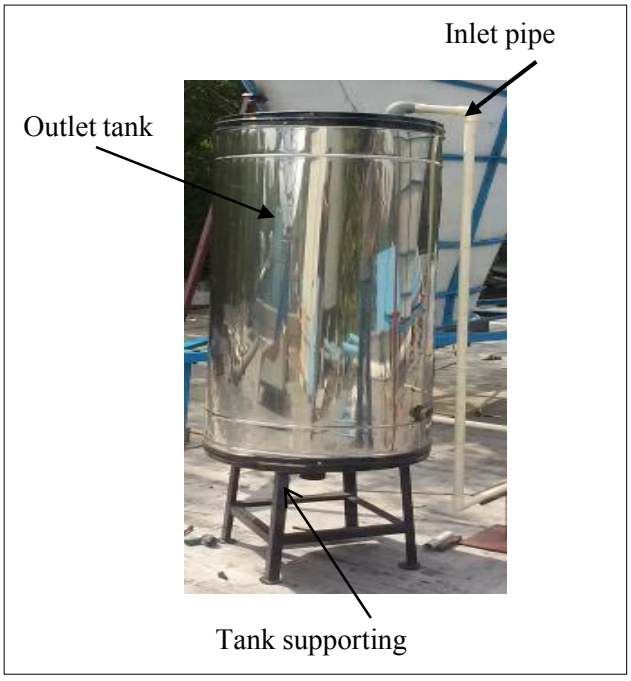

Figure 6.21: Photograph of the Storage Tank for Hot Water (Outlet Tank)

Table 6.5: Dimensions of the Outlet Storage Tank (Hot Water Tank)

S No	Parameters	Dimensions (m)
1	Diameter	0.495
2	Length	0.971

Figure 6.22: Stand for the Circulating Pipe

6.8 Piping line for circulating the water using CPVC Pipe

The Chlorinated Poly Vinyl Chloride (CPVC) is a thermoplastic pipe, which is used in the experimental set-up. Industrial CPVC pipe is manufactured by extrusion in sizes from ¼" to 12" diameter. The advantages of using this pipe are:

- Environmentally friendly.
- Provide long service life.
- Easy to install and handle.
- Corrosion resistant.
- Cost effective.
- Widely accepted by codes

The CPVC piping is used for hot and cold water distribution, it has a 400 psi pressure rating at room temperature, and a 100 psi pressure rating at 180 F. CPVC materials are resistant to many everyday household chemicals. The parameter definitions for the CPVC are shown in figure 6.23.

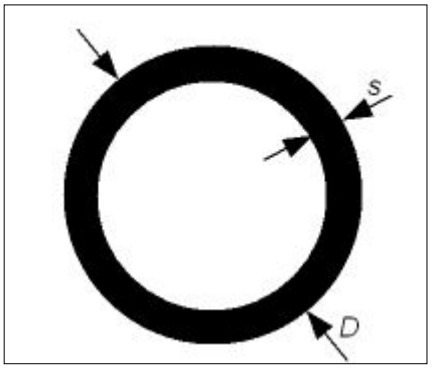

Figure 6.23: Dimension Definitions of the CPVC Pipe

Many pipe manufacturers use the "Standard Dimension Ratio" (SDR) method of rating pressure piping. The SDR is the ratio of pipe diameter to wall thickness and the SDR is expressed as: SDR = *D*/*S*; Where *D* is the pipe outside diameter (mm) and S is the pipe wall thickness (mm). A high SDR ratio means, the pipe wall is thin compared to the pipe diameter. A low value of SDR ratio means, the pipe wall is thick compared to the pipe diameter. A high SDR pipe is recommended for a low-pressure rating and low SDR pipe is recommended for high-pressure rating. The dimensions of the CPVC pipe are given in table 6.6.

Table 6.6: Dimension of the CPVC Pipe

S No	Parameters	Dimensions in (m)
1	Diameter	0.091
2	Length	7.54

6.9 Experimental testing of a 3-D EHC

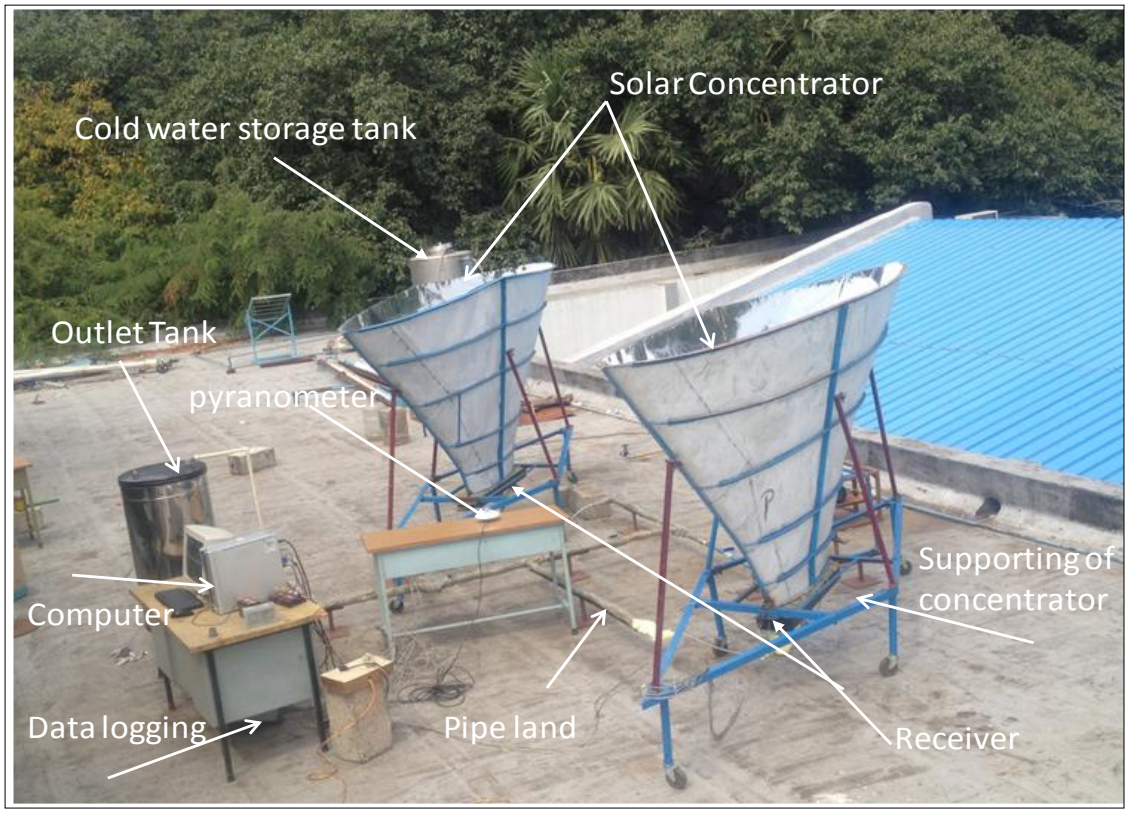

Figure 6.24: Photograph of the Experimental EHC Apparatus located at IITM Chennai

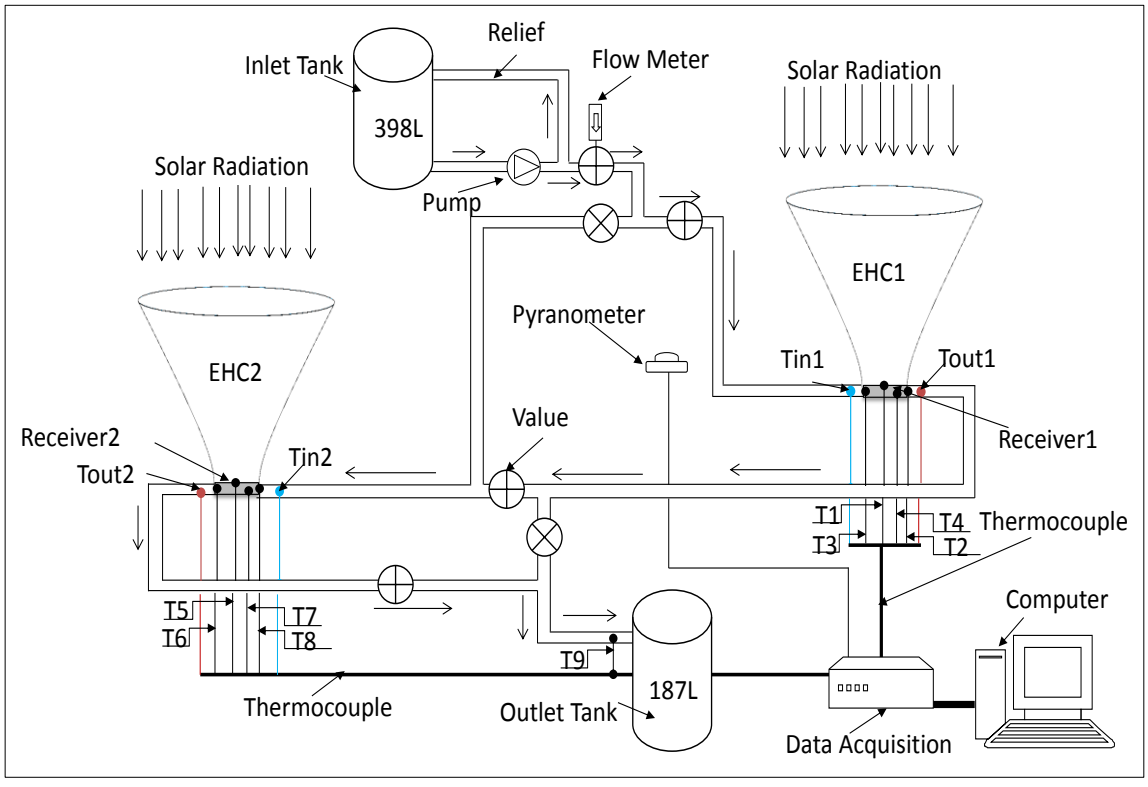

Figure 6.25: Schematic of the Experimental EHC at IITM Chennai

The 3-D solar EHC was designed and constructed for experimental testing as shown in figure 6.24 and schematic of the EHC at IITM Chennai is shown in figure 6.25 .The experiments were carried out with two EHC at IITM Chennai. The experimental setup included an elliptical helical receiver for each of the EHCs. The working fluid flows from the inlet tank of capacity (398 litters) to the helical receivers and the hot water is collected in the collection tank which has a capacity (187 litters). The two EHC are connected in series to study the heat transfer to the fluid and temperature rise of the system. All measurements, including inlet temperature, outlet temperatures, and surface temperatures of the receivers, inlet and collection tank temperatures, and solar radiation data have been recorded using a data acquisition system. The intensity of solar radiation was measured using the pyranometer. As shown in figure 6.24 the pyranometer was placed on a small table between the two EHCs instead of being placed high above the two EHCs; this is because after moving the pyranometer to different positions, the maximum radiation reading of about 900W/m^2 was obtained at this position. Also at higher positions above the ground there is interference from shadows of the trees as seen in the figure 6.24 which affects the radiation reading. There is also the danger of the pyranometer been taking away and broken by wild animals, for examples monkeys. This position of the pyranometer is not ideal but because of these extenuating circumstances it is ideal in this case. The various temperatures such as surface temperature of the receivers, inlet and outlet temperature of the receivers, and inlet collection tank temperatures were measured using K-type thermocouple.

6.10 Results and Discussion

6.10.1 Solar Radiation on the Receiver

Figure 6.26 (a), (b) and (c) shows the flux distribution on the receiver area for different incident angle using Optis^{TM} rays tracing analysis on the left hand side. In this study the incident angles were 0°, 15° and 30°. The flux was relatively uniformly distributed at the incidence angle of 0° as seen in figure 6.26 (a). The magnitude of the peak and area averaged flux decreases as the incident angle increases. For the incidence angle of 15°, the flux distribution was biased towards the left as seen in figure 6.26 (b). The overall magnitude of the flux was significantly reduced for the incidence angle of 30° and as seen in figure 6.26(c).

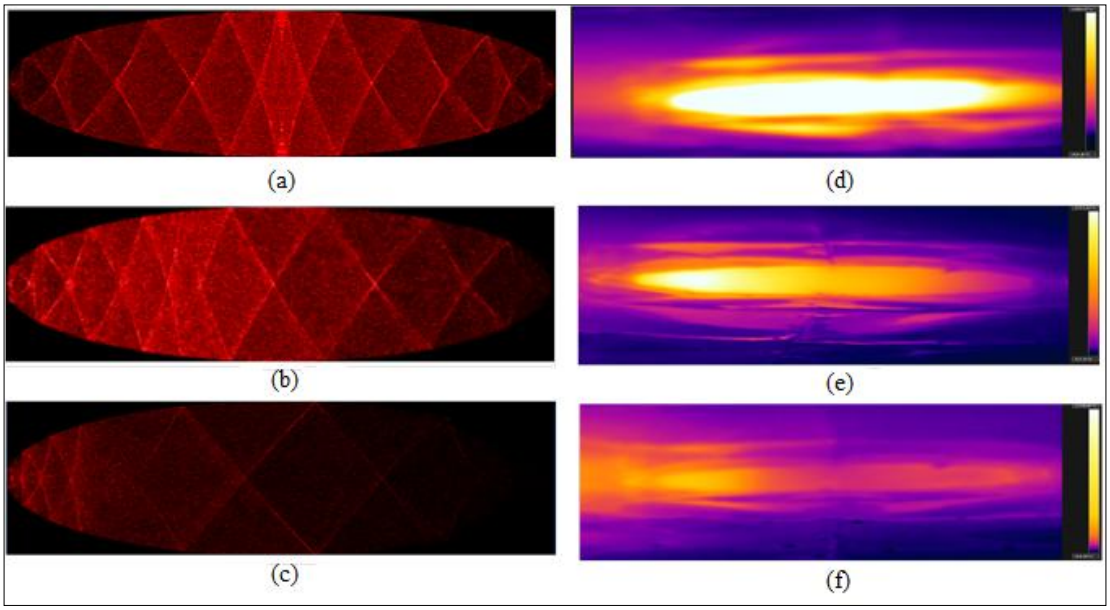

Figure 6.26: Comparison of Experimental and Numerical Receiver Performance Optical Ray Tracing ((a)-(c)) Thermal Imaging ((d)-(f)) of Receiver Aperture for Different Incident Angles (a, d) 0°(b, e) 15° (c, f) 30°

The flux distribution analysis using ray tracing software was compared with that of thermal images of the receiver in figure 6.26 (d), (e) and (f). Figure 6.26 (d), (e) and (f) for the same incidence angles of 0°, 15° and 30°. These IR images of the receiver are used to analyses the receiver image and to determine average temperature on receiver area. The experimentally measured temperatures agree overall with the numerical model of the flux distribution. When the incident angle is 0°, the temperature distribution is more uniformly distributed throughout the receiver area; whereas for the incident angle of 15°, the temperature distribution is biased towards the left of the aperture. Evenly distributed across on the top of the receiver surface area as shown in figure 6.26 (e). When the incident angle is 30°, the temperatures distribution is less than incident angle is 15°, and is shown in figure 6.26 (f) Both optical simulation and thermal imaging results show good qualitative agreement.

6.10.2 Stagnation Testing

The stagnation temperature of the receiver corresponds to the measurement of the surface temperature of the receiver at a zero flow rate. The stagnation temperature is measured with the aid of the thermocouple fixed at the surface of the receiver which is shown in figure 6.17 as T1, T2, T3 and T4. The stagnation test was carried out on the 1st February 2013, from 08:30 to 17:30 hrs. Under these conditions, the system can reach "stagnation" temperatures exceeding 125°C. These systems are particularly susceptible

to high stagnation temperatures because of the coincidence of high solar radiation levels (typically 900 W/m^2) on the solar concentrator and an average high ambient air temperature of 30°C. Figure 6.27 shows the surface temperature of a receiver and the variation of solar radiation throughout the day. Similarly, the stagnation temperature was also measured using the thermal camera and the maximum stagnation temperature observed was 150°C, this image of the maximum temperature on the receiver is shown in figure 6.28.

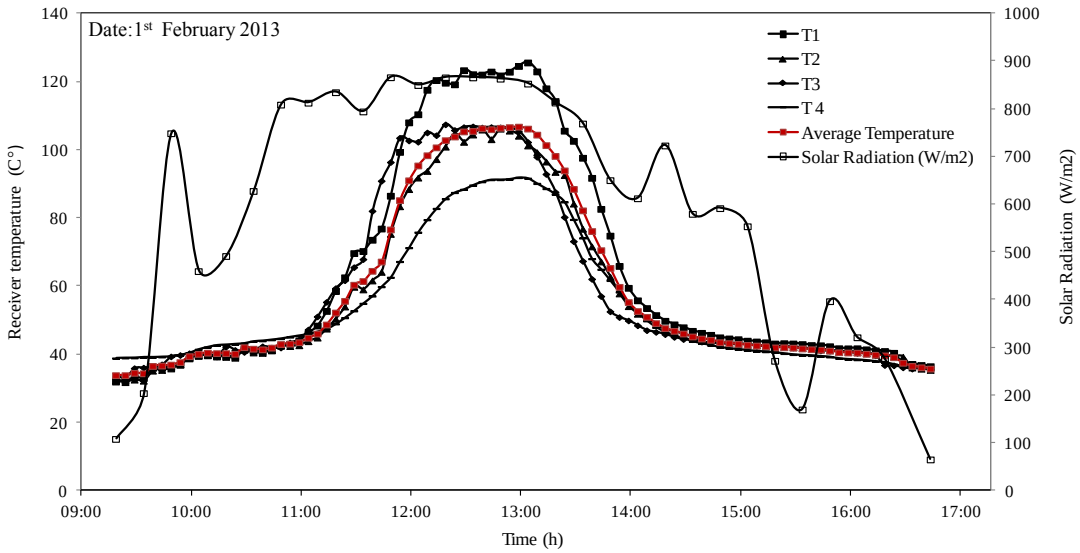

Figure 6.27: Stagnation Temperature of Receiver

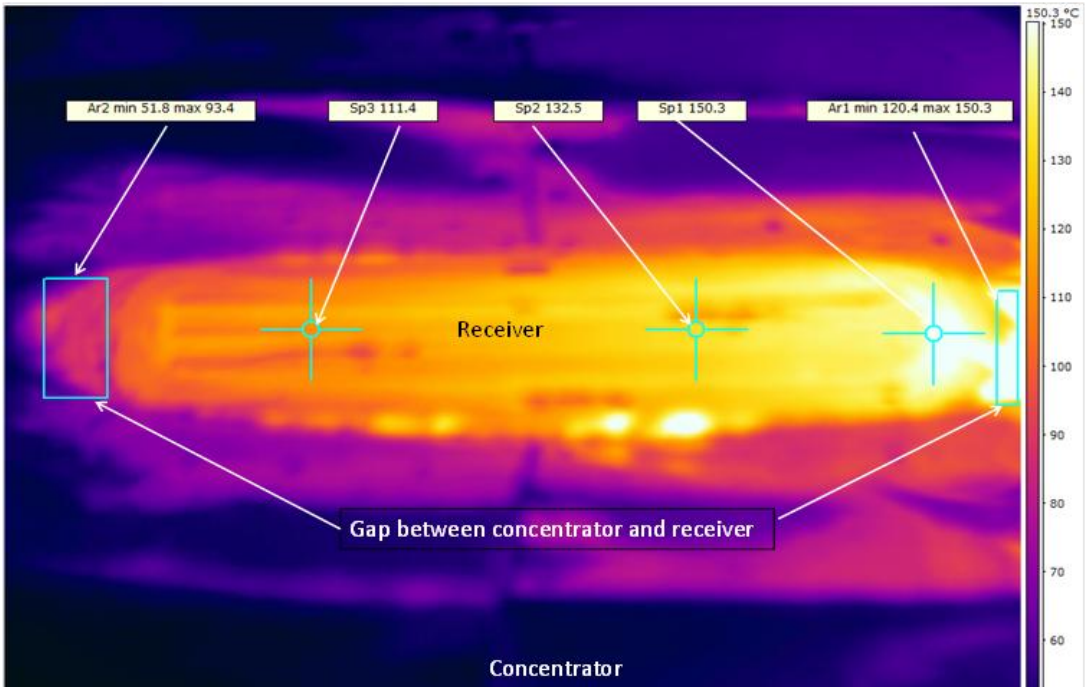

Figure 6.28: Image Thermal Shown the Stagnation Average Temperature and Solar Radiation of the Receiver for 1st Feb. 2013.

6.10.3 Thermal Performance Testing

Experimental thermal performance analysis was carried out for two different flow rates of 0.5 kg/min and 1 kg/min. The working fluid enters from inlet tank to the first collector and passes to the second collector which is connected in series and goes to outlet tank. Figure 6.29 shows the outlet temperatures of the system on 2nd of February 2013 for the flow rate is 0.5 kg/min. The temperatures increased when the hour angle increases up to 1pm and then start to decrease. The maximum temperature recorded was approximately 90 °C and occurred between 12:00 to 13:30 hrs. when the average solar radiation was 850 W/m^2. Figure 6.30 shows the outlet temperature when the flow rate was 1 kg/min, the experiment was carried out from 8:30 to 17:30 hrs. on 3rd February 2013. Again the temperatures increased when the hour angle increased up to 14:00 hrs. and decreased thereafter. The maximum temperature recorded was 68°C; this was recorded between 11:00 to 14:00 hrs. when the average solar radiation was 850 W/m^2. It was observed that temperature recorded was less than the expected temperature; this is due to the losses of the EHC collector listed below:

- Manufacturing defects: the area of the fabricated model of the EHC is 20% less than the optimum dimension.
- Reflectivity: loss of reflectivity of the thin film due to air traps in the internal surface of the concentrator.
- Heat loss from the surrounding: unwanted heat loss may have affected to the performance of the system, primarily due to variable wind speed during the testing.
- External shading: External shading during the experiment may have reduced its performance.

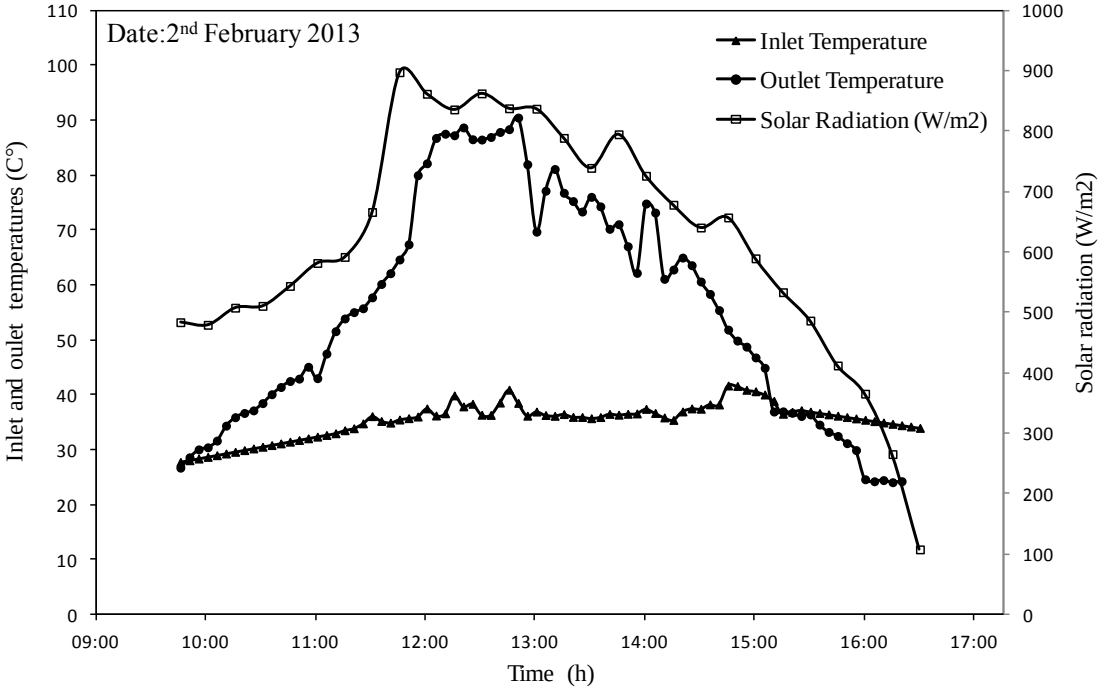

Figure 6.29: Inlet and Outlet Temperature of Fluid for Flow Rate of 0.5 kg/min on 2nd February 2013

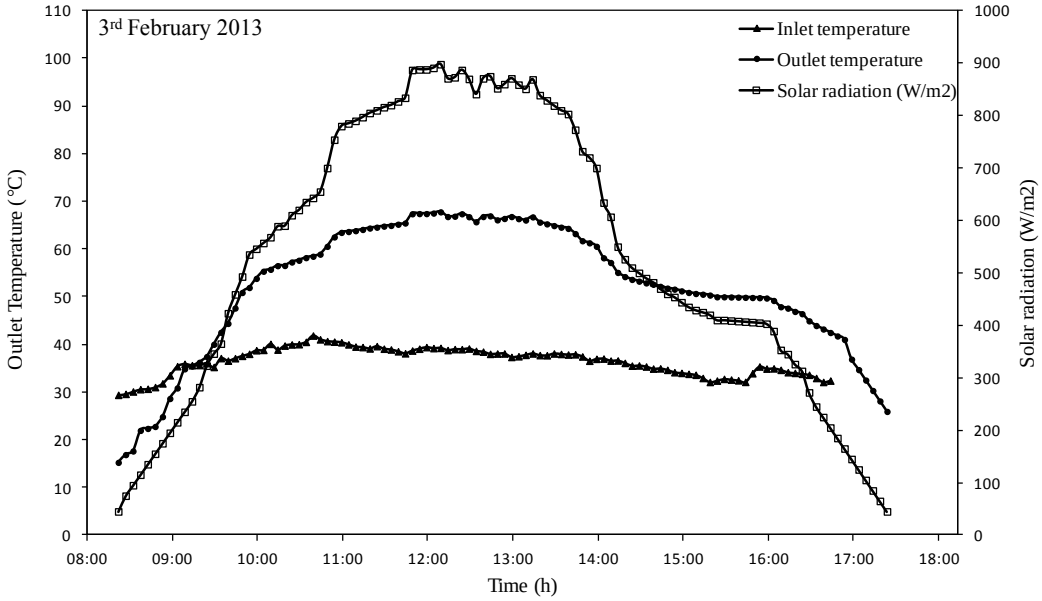

Figure 6.30: Inlet and Outlet Temperature of Fluid for Flow Rate of 1kg/min on 3rd February 2013

6.10.4 Thermal images on the receiver area

During the experimental thermal are used to analyse the receiver image and to determine average temperature on receiver area as shown in figure 6.31. The temperature distribution on the receiver area as shown in figure 6.32 (a-e). Figure 6.32 shows the temperature distribution on the receiver area.

Figure 6.31: Photograph of the Usage of Thermal Imaging Camera

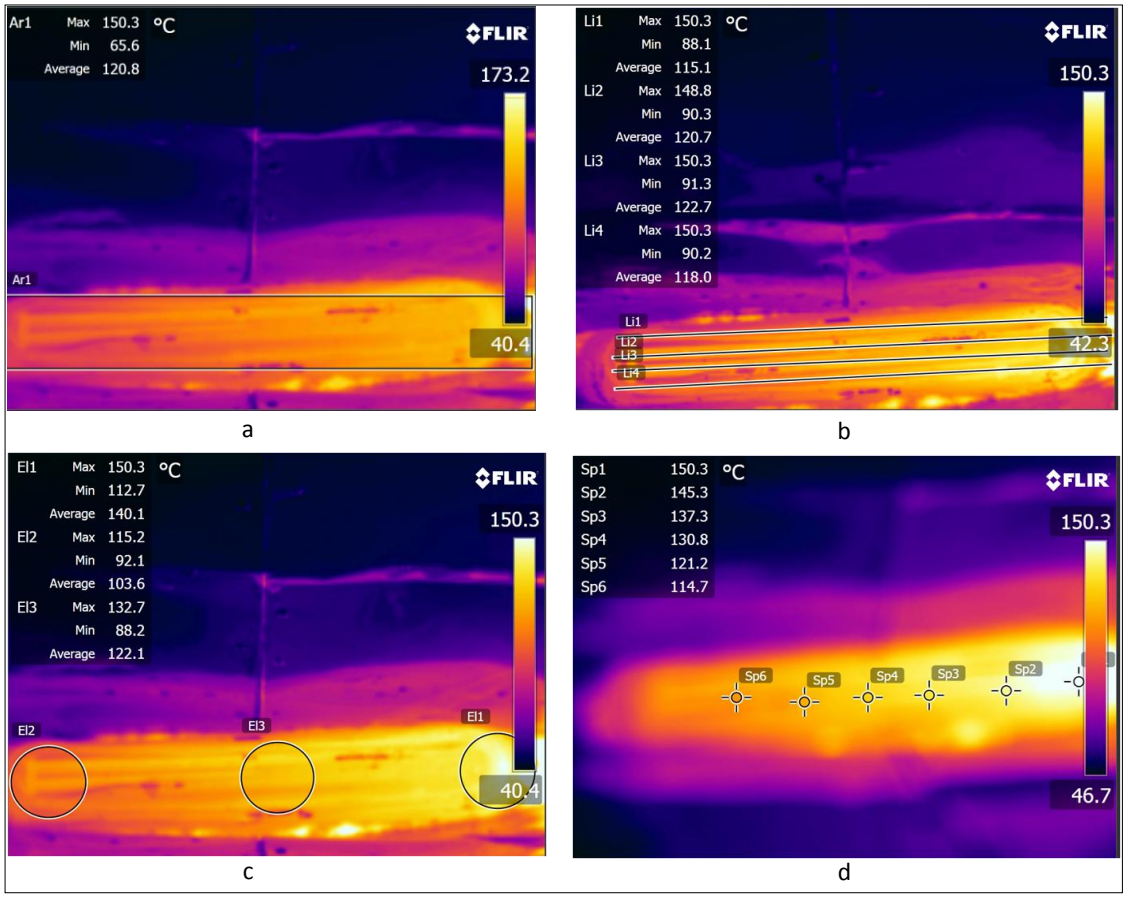

Figure 6.32: Experimental Thermal Imaging of Receiver Surface Area ((a)–(e))

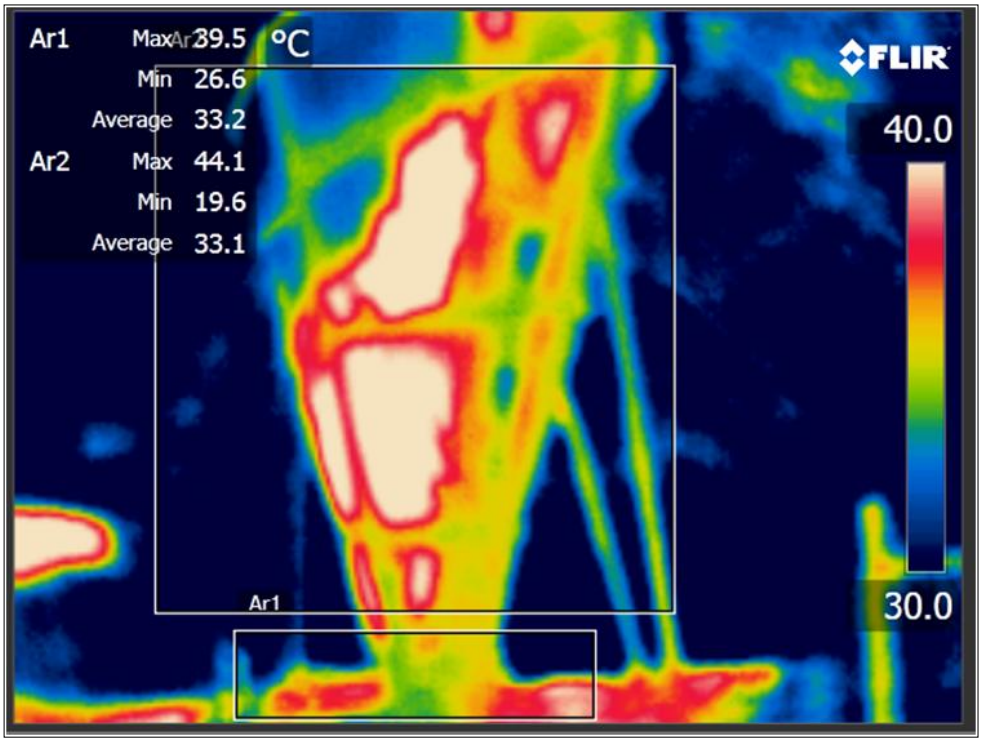

Figure 6.33: Experimental Thermal Imaging of Concentrator Surface

6.11 Closure

A new EHC with a helical flat shaped receiver has been developed for medium-temperature applications. Optical analysis has been carried out to predict the optimum concentration ratio and efficiency of the proposed EHC. An optimal concentration ratio of 20× with an optical efficiency of 28% was predicted. The experiments have also been carried to validate the optical parameters. During this study, an experimental investigation was carried out to verify its operation under outdoor test conditions for a 3-D EHC. The maximum stagnation temperature recorded was 125°C and outlet temperature from the system was 90°C when the flow was 0.5 kg/min. By increasing the flow rate to 1kg/min a maximum outlet temperature of 68°C was recorded. Further experimental work will be carried out to use the system for water desalination.

CHAPTER 7: Overall Conclusions and Future work

7.1 Overall Conclusion

This thesis, describes the design of a novel 3-D static non-imaging concentrator – an elliptical hyperboloid concentrator (EHC). The new 3-D static EHC was designed using the ray tracing concept. The 3-D static EHC is composed of two elliptical apertures (entrance and exit) and a hyperboloid concentrator (the profile connecting the two apertures). The shape of the elliptical apertures is configured to collect the solar beam radiation from any direction without using a tracking device. Thus, the new design enables the features of wider acceptance angle and also captures large part of the diffuse solar radiation component in addition to the direct radiation component. An elliptical absorber is placed at the bottom of the concentrator. The novel non-imaging profile increases the solar concentration and to produce medium temperature with high optical efficiency and less heat losses in the absorber. This thesis presents an insight into the design (optical design), fabrication and testing (indoor and outdoor testing) of a high optical efficiency 3-D solar thermal hyperboloid concentrator with wide acceptance angle for medium temperature applications.

In the optical study, an optimum configuration of 2-D elliptical hyperboloid concentrators (EHC) with high optical efficiency was determined using the ray tracing technique by simulation code written in MATLAB. The optimum configuration is achieved by studying the effects of incidence angle; the height of concentrator and the receiver dimension on the optical efficiency of a 2-D EHC. In the 2-D optical study, an optimum optical efficiency of 19 % was achieved. Further improvement in the optical efficiency was observed in the 3-D analysis. In order to improve the optical efficiency of the proposed novel 3-D static concentrator, a computational domain was developed to aid the design of a three-dimensional elliptical-hyperboloid concentrator with concentration ratio of 20×. This was carried out in the Optis^{TM} software by means of ray tracing simulation. In the 3-D analysis, the impacts of concentration ratio (5× to 40× with step of 5), aspect ratio (a/b = 1 to 10), height to major diameter ratio, and concentration height on optical efficiency were extensively investigated for different concentration ratios and concentrator heights. In general, the increase in the concentrator height increases the optical efficiency. And in contrast, the optical efficiency decreases for increasing concentration ratios. It was also observed that the lower receiver diameters lead to higher optical efficiency. Low acceptance angles and

higher receiver diameters lead to low optical efficiency and higher acceptance angles. Based on the 3-D ray tracing simulation, it was observed that the optical efficiency of 28% for an acceptance angle of ± 45˚ is achieved for the optimum receiver aspect ratio of 5, and a height to major diameter ratio of 4. The effect of truncation were also carried out to improve the performance and to reduce the material consumption.

In addition, geometrical optical performance comparisons of four different concentrator configurations (Elliptical Hyperboloid Concentrator (EHC); Circular Hyperboloid Concentrator (CHC); Elliptical Compound Parabolic Concentrator (ECPC), Circular Compound Parabolic Concentrator (CCPC)) were studied to compare the behaviour of EHC among similar type of configurations. The ray tracing study was carried out for all the four configurations to evaluate the optical efficiency of these configurations for a fixed concentration ratio of 20×, receiver area of 1 m^2 and an ellipse aspect ratio of 5. It was found that the EHC produced higher optical efficiency of 28% for an acceptance angle ±30˚. But the CHC produced lower optical efficiency of 21% for an narrower acceptance angle of ±15˚. It is very clear that the parabolic and hyperboloid concentrator has some advantages over other geometries. The parabolic concentrators have higher optical efficiencies at lower acceptance angle; such parabolic system can be used along with a tracking device. The hyperboloid concentrators have lower optical efficiency at wider acceptance angles; such device can be used for non-tracking system.It was observed that the EHC with wider acceptance angle shows better optical efficiency than others.

Through the information obtained in the optical study, four different types of prototypes were fabricated and tested. First prototype (EHC1) were fabricated and tested in HWU. The concentration ratio of 16× was obtained for the elliptical hyperboloid by measuring incoming and outcoming radiation along the vertical axis. At no-flow conditions, the maximum temperature of 100°C was measured. The same prototype was modeled in the Optis software to predict the optical efficiency and acceptance angle. It was predicted that the model based on the first prototype gives the optical efficiency of 87% and acceptance angle of ±15˚ was observed. Even though optical efficiency is very high, this prototype can be used along with tracking system, due to much decreased acceptance angle.

The second prototype (EHC2) was fabricated in china by Prototype Company. The optical efficiency of 28% and concentration ratio of 20× was achieved. The indoor testing under solar Solar Simulator in HWU laboratory was carried out. The maximum stagnation temperature of 93°C was observed for solar radiation of 1200 W/m^2. At 0.12 kg/min, the maximum fluid outlet temperature of 60°C was observed for the solar radiation of 1200 W/m^2 . In order to estimate the temperature distribution along the receiver, thermal imaging camera was used to obtain the temperature variation along the receiver at three different points.

The third prototype (CHC) was fabricated in china by Prototype Company. The optical efficiency of 23% and concentration ratio of 20× was achieved. The indoor testing was also carried out under Solar Simulator in HWU laboratory. In order to estimate the temperature distribution along the receiver, thermal imaging camera was used to obtain the temperature variation along the receiver at three different points. At 'no flow' conditions, stagnation temperatures were measured at different points the maximum receiver suface temperature was 61°C.

The fourth prototype (EHC) was fabricated in India, at Indian Institute of Technology, Chennai. This prototype was used for the outdoor testing in India. Based on this, the thermal performance of the medium temperature elliptical-hyperboloid solar collectors were presented. The stagnation test was carried out on the 1st February 2013, from morning 08:30 to 17:30 hrs. Under this stagnation condition, maximum temperature of 150°C was reached. The outlet temperatures of the system on 2nd of February 2013 for the flow rate is 0.5 kg/min. The temperatures increased when the hour angle increases up to 13:00 hrs and then start to decrease. The maximum temperature recorded was approximately 90°C and occurred between 12:00 to 13:30 hrs, when the average solar radiation was 850 W/m^2. As the flow rate increases, 0.5 kg/min to 1 kg/min, the maximum temperature of 68°C was recorded; this was recorded between 11:00 to 14:00 hrs when the average solar radiation was 850 W/m$^{2.}$ From the overall study, it is concluded that the present 3-D elliptical hyperboloid concentrator can very well be used for medium heat application.

7.2 Suggestion for Future Work

7.2.1 Suggestion 1:

While doing the outdoor experiments of EHC at IITM, Chennai India, it was observed that recorded temperature was less than the expected temperature; this is due to the losses of the EHC collector listed below:

- Manufacturing defects: the area of the fabricated model of the EHC is 20% less than the optimum dimension.
- Reflectivity: loss of reflectivity of the thin film due to air traps in the internal surface of the concentrator**.**
- Variable wind movements: Due to wind movements, unwanted heat loss may affect the performance of the system during the testing.
- External shading: External shading during the experiment may have reduced its performance.

In order to avoid the deviations between expected temperature and observed temperature, a separate fluid modelling can be performed in the ANSYS package to predict the fluid outlet temperature for different flow conditions.

7.2.2 Suggestion 2:

It was very well noted, that the optical efficiency of a solar concentrator depends largely on the geometry of the concentrator profile. In the present thesis, elliptical hyperboloid concentrator (EHC) was analysed. In EHC, both the entrance and exit of the concentrator are elliptic profile is considered. Instead of elliptic profile, square shape profile can be adopted in the hyperboloid concentrator for performance improvement. The new geometric design can be named as square hyperboloid concentrator (SHSC). The geometry of the square hyperboloid concentrator is shown in figure 7.1. Preliminary analysis was carried out for 20× SHSC to check and predict the optical efficiency and acceptance angle. It was noted that the optical efficiency of 39% and maximum absorbed energy of 18,455 W/m^2 were observed. The variation of the optical efficiency and absorbed energy with solar incidence angle are shown in figures 7.2 and 7.3. The flux distribution of the SHSC is also given in figure 7.4.

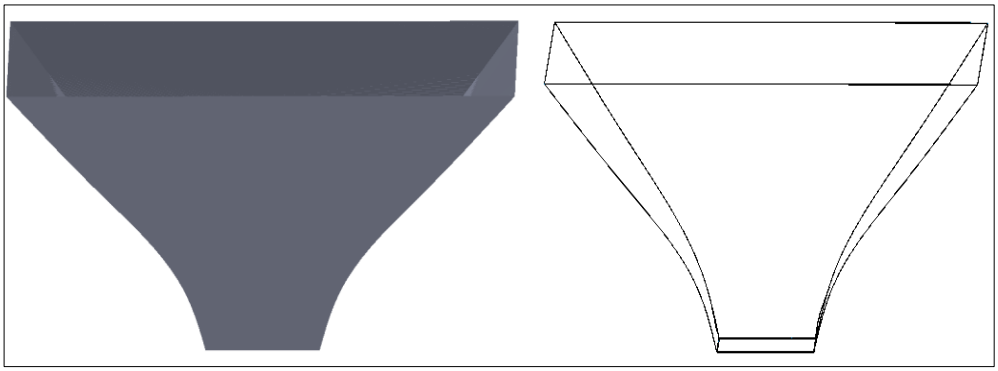

Figure 7.1: Geoemtry of Square Hyperboloid Concentrator

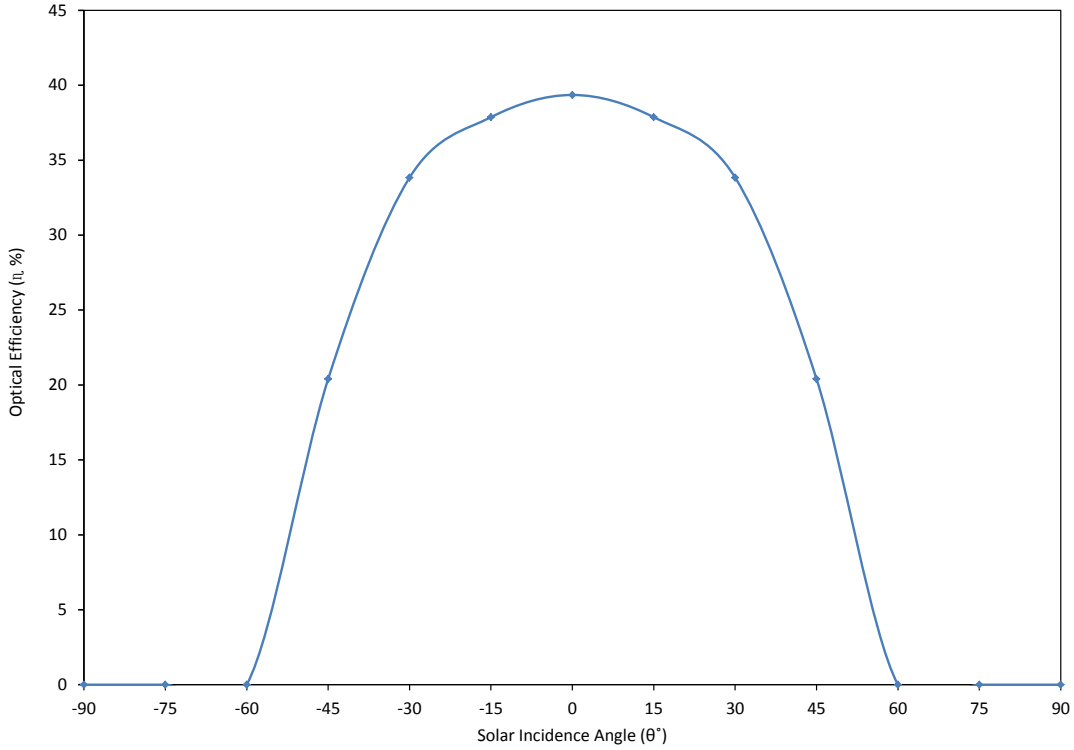

Figure 7.2: Variation of Optical Efficieny with Solar Incidence Angle

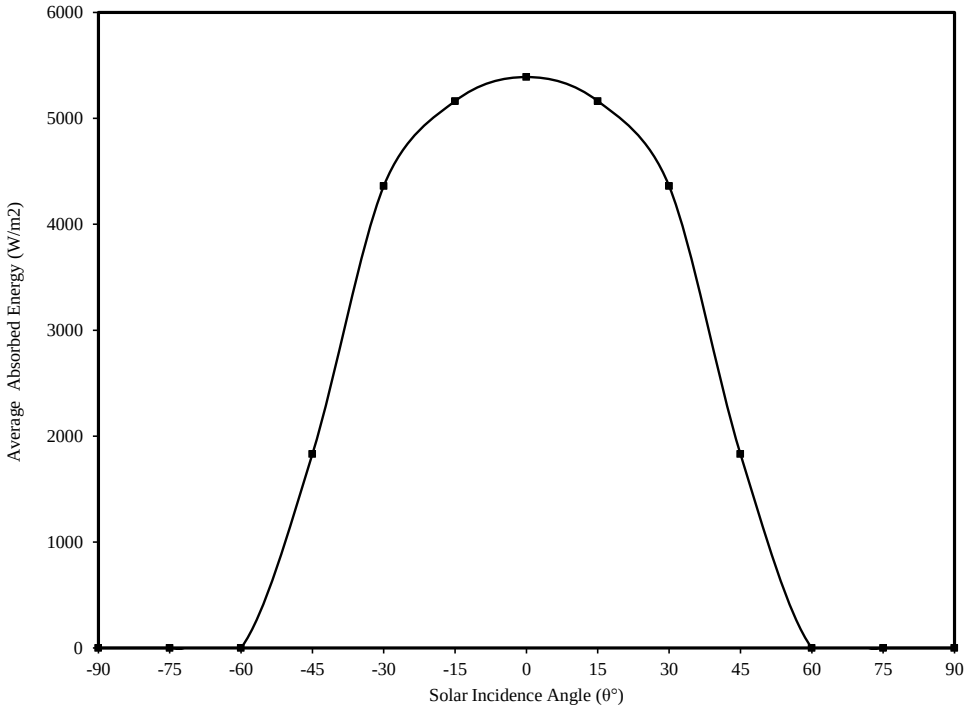

Figure 7.3: Varaiation of Absorbed Energy with Solar Incidence Angle

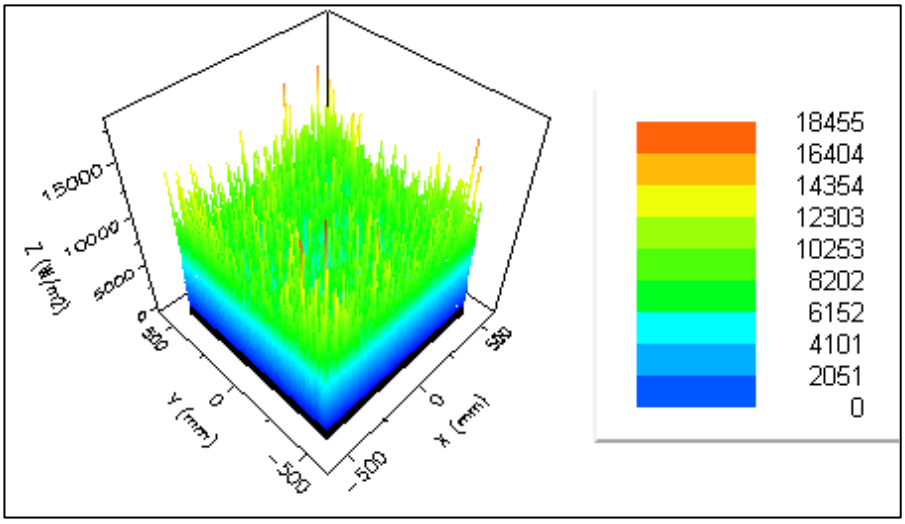

Figure 7.4: Flux Distribution of the Square Hyperboloid Concentrator

7.2.3 Suggestion 3:

- A high reflective film can be used as a reflector in the EHC to improve the stagnation and fluid outlet temperature.
- In the reciever coil, selecting coating can be used to transfer the heat effectively to the working fluid.

REFERENCES

[1] W.A.B. John A. Duffie Solar Engineering of Thermal Processes, America, 2006.

[2] Grass C, Benz N, Hacker Z, T. A, Tube collector with integrated tracking parabolic concentrator, in: Proceedings of the Eurosun, Copenhagen, Denmark, 2000.

[3] Kalogirou, S. A.Lloyd, S.Ward, J. Eleftheriou, Design and performance characteristics of a parabolic-trough solar-collector system, Applied Energy, 47 (1994) 341-354.

[4] Seitel, S. C., Collector performance enhancement with flat reflectors, Solar Energy, 17 (1975) 291-295.

[5] B. Perers, B. Karlsson, M. Bergkvist, Intensity distribution in the collector plane from structured booster reflectors with rolling grooves and corrugations, Solar Energy, 53 (1994) 215-226.

[6] J.A. Duffi, W.A. Beckman, Solar engineering of thermal processes, America, 2006.

[7] D.R. Mills, J.E. Giutronich, Asymmetrical non-imaging cylindrical solar concentrators, Solar Energy, 20 (1978) 45-55.

[8] D.P. Grimmer, K.G. Zinn, K.C. Herr, B.E. Wood, Augmented solar energy collection using different types of planar reflective surfaces; theoretical calculations and experimental results, Solar Energy, 21 (1978) 497-501.

[9] W.R. McIntire, New reflector design which avoids losses through gaps between tubular absorbers and reflectors, Solar Energy, 25 (1980) 215-220.

[10] J.J. O'Gallagher, K. Snail, R. Winston, C. Peek, J.D. Garrison, A new evacuated CPC collector tube, Solar Energy, 29 (1982) 575-577.

[11] M. Rönnelid, B. Perers, B. Karlsson, Construction and testing of a large-area CPC-collector and comparison with a flat plate collector, Solar Energy, 57 (1996) 177-184.

[12] T.B. Frank Buttinger, Markus Proll, Wolfgang Scholkopf, Development of a new flat stationary evacuated CPC-collector for process heat applications, Solar Energy 84 (2010) 1166–1174.

[13] C.K. Hsieh, Thermal analysis of CPC collectors Solar Energy, 27 (1981) 19–29.

[14] A.S. Jadhav, A.S. Gudekar, R.G. Patil, D.M. Kale, S.V. Panse, J.B. Joshi, Performance analysis of a novel and cost effective CPC system, Energy Conversion and Management, 66 (2013) 56-65.

[15] Gudekar, Ajitkumar S. Jadhav, Atul S. Panse, Sudhir V. Joshi, Jyeshtharaj B. Pandit, A. B., Cost effective design of compound parabolic collector for steam generation, Solar Energy, 90 (2013) 43-50.

[16] J. O'Gallagher, R. Winston, Test of a "trumpet" secondary concentrator with a paraboloidal dish primary, Solar Energy, 36 (1986) 37-44.

[17] E. Zarza, Medium Temperature Solar Concentrators (Parabolic-Troughs Collectors), Solar Energy Conversion and Photoenergy Systems, 1 (2005).

[18] A. Rabl, Active Solar Collectors and Their Applications, Oxford University Press, USA, 1985.

[19] Naib, Ten Questions For SCHOTT About Solar Thermal Electricity Part 3 Of 3(2013, October 29). Retrieved from:http://www.blog.thesietch.org/2007/01/09/10-questions-for-schott-about-solar-thermal-parabolic-trough-electricity-generation-3/.

[20] Lüpfert E, Geyer M, Z.E. Schiel W, Gonzalez-Anguilar RO, N. P., Euro-trough: a new parabolic trough collector with advanced light weight structure, in: Proceedings of Solar Thermal 2000 International Conference, Sydney, Australia, 2000.

[21] Geyer M, O.R. Lupfert E, S.W. Esteban A, Schweitzer A, N.P. Zarza E, Langenkamp J, M. E, Euro-trough: parabolic trough collector developed for cost efficient solar power generation, in: 11th Solar PACES International Symposium on Concentrated Solar Power and Chemical Energy Technologies, Zurich, Switzerland, 2000.

[22] Lovegrove, Keith Dennis, Mike, Solar thermal energy systems in Australia, International journal of environmental studies, 63 (2006) 791-802.

[23] D.R. Mills, G.L. Morrison, Compact Linear Fresnel Reflector solar thermal powerplants, Solar Energy, 68 (2000) 263-283.

[24] P.L. Singh, R.M. Sarviya, J.L. Bhagoria, Thermal performance of linear Fresnel reflecting solar concentrator with trapezoidal cavity absorbers, Applied Energy, 87 (2010) 541-550.

[25] Jiang, Zai Qiang Chen, Yan Zhou, Xin Jin, J. Xun, Investigation of solar thermal power technology, in: Applied Superconductivity and Electromagnetic Devices (ASEMD), 2011 International Conference on, IEEE, 2011, pp. 275-281.

[26] W. Meinecke, M. Bohn, M. Becker, B.P. Gupta, D.F.f.L.-u. Raumfahrt, Solar Energy Concentrating Systems: Applications and Technologies, Müller, 1995.

[27] T. Kodama, High-temperature solar chemistry for converting solar heat to chemical fuels, Progress in Energy and Combustion Science, 29 (2003) 567-597.

[28] A. Segal, M. Epstein, Comparative Performances of `Tower-Top' And `Tower-Reflector' Central Solar Receivers, Solar Energy, 65 (1999) 207-226.

[29] A. Yogev, A. Kribus, M. Epstein, A. Kogan, Solar "tower reflector" systems: A new approach for high-temperature solar plants, International Journal of Hydrogen Energy, 23 (1998) 239-245.

[30] G. Tyner, M. Kolb, G. Praire, A. Weinrebe, Valverde, M. Sanchez, Solar power tower development: recent experiences Solar thermal concentrating technologies, in: Eighth International Symposium, Köln, Germany Germany 1996, pp. 193–216.

[31] Dish Stirling Systems of SBP in Spain.jpg, in, 2013.

[32] K.J.F.a.F. Kreith, principles of solar engieering, in: principles of solar engieering, McGraw-Hill United States of America, 1978.

[33] Y. Chu, Review and Comparison of Different Solar Energy Technologies, (2011).

[34] S.A. Kalogirou, Solar thermal collectors and applications, Progress in Energy and Combustion Science, 30 (2004) 231-295.

[35] J. Li, Scaling up concentrating solar thermal technology in China, Renewable and Sustainable Energy Reviews, 13 (2009) 2051-2060.

[36] A. Rabl, Tower reflector for solar power plant, Solar Energy, 18 (1976) 269-271.

[37] C.J. Winter, R.L. Sizmann, L.L. Vant-Hull, Solar power plants: fundamentals, technology, systems, economics, Springer-Verlag, 1991.

[38] T. Kodama, N. Gokon, Thermochemical cycles for high-temperature solar hydrogen production, Chemical Reviews, 107 (2007) 4048-4077.

[39] A. Segal, M. Epstein, The optics of the solar tower reflector, Solar Energy, 69, Supplement 6 (2001) 229-241.

[40] P. Schwarzbözl, R. Pitz-Paal, W. Meinecke, R. Buck, Costoptimized solar gas turbine cycles using volumetric air receiver technology, Proceedings of the Renewable Energy for the New Millennium, Sydney, Australia, (2000) 171-177.

[41] Y.W. Wong, K. Sumathy, Solar thermal water pumping systems: a review, Renewable and Sustainable Energy Reviews, 3 (1999) 185-217.

[42] H.M. Qiblawey, F. Banat, Solar thermal desalination technologies, Desalination, 220 (2008) 633-644.

[43] Balaras, Constantinos A.Grossman, Gershon Henning, Hans-Martin Infante Ferreira, Carlos A. Podesser, Erich Wang, E. Lei Wiemken, Solar air conditioning in Europe-an overview, Renewable and Sustainable Energy Reviews, 11 (2007) 299-314.

[44] A. Sharma, C.R. Chen, V.V.S. Murty, A. Shukla, Solar cooker with latent heat storage systems: A review, Renewable and Sustainable Energy Reviews, 13 (2009) 1599-1605.

[45] K. Schwarzer, M.E.V. da Silva, Characterisation and design methods of solar cookers, Solar Energy, 82 (2008) 157-163.

[46] A. Sharma, C.R. Chen, N. Vu Lan, Solar-energy drying systems: A review, Renewable and Sustainable Energy Reviews, 13 (2009) 1185-1210.

[47] B. Schmitt, C. Lauterbach, K. Vajen, Investigation of selected solar process heat applications regarding their tech‐nical requirements for system integra‐tion, in: Proc. ISES Solar World Congress, Kassel.

[48] Lauterbach, Christoph Rad, Shahrdad Javid Schmitt, Bastian Vajen, Klaus, Feasibi‐lity assessment of solar process heat applications, in: Proceedings Solar World Congress, Kassel, 2011.

[49] M. Adsten, A. Helgesson, B. Karlsson, Evaluation of CPC-collector designs for stand-alone, roof- or wall installation, Solar Energy, 79 (2005) 638-647.

[50] M.E. Blanco, E. Gomez-Leal, J.M. Gordon, Asymmetric CPC solar collectors with tubular receiver: Geometric characteristics and optimal configurations, Solar Energy, 37 (1986) 49-54.

[51] S.M. Lu, Y.C.M. Li, J.C. Tang, Optimum design of natural-circulation solar-water-heater by the Taguchi method, Energy, 28 (2003) 741-750.

[52] A. Abbas, Solchrome solar selective coatings-an effective way for solar water heaters globally, Renewable Energy, 19 (2000) 145-154.

[53] M. Smyth, P.C. Eames, B. Norton, Integrated collector storage solar water heaters, Renewable and Sustainable Energy Reviews, 10 (2006) 503-538.

[54] Integrated Pressurized Coil Solar Water Heater Character, (2013, June 28) Retrieved from: http://www.diytrade.com/china/pd/4130206/Integrated_Pressurized_Coil_Solar_Water_Heater_Character.html.

[55] S.A. Kalogirou, Seawater desalination using renewable energy sources, Progress in Energy and Combustion Science, 31 (2005) 242-281.

[56] D. Probert, M. Newborough, Designs, thermal performances and other factors concerning cooking equipment and associated facilities, Applied Energy, 21 (1985) 81-222.

[57] O.V.N. Ekechukwu, B., Review of solar-energy drying systems II: an overview of solar drying technology, Energy Conversion and Management, 40 (1999) 615-655.

[58] G.L. Visavale, Design and Characteristics of Industrial Drying Systems, in: Institute of Chemical Technology, Institute of Chemical Technology, Mumbai, India, 2009.

[59] B. Norton, Solar process heat: distillation, drying, agricultural and industrial uses, Solar Energy, the State of the Art. James & James, Londres (ISBN 1-902916-23-9), (2001) 477-496.

[60] F. Spate, B. Hafner, K. Schwarzer, A system for solar process heat for decentralised applications in developing countries, in: Proceedings of ISES Solar World Congress on CD-ROM, Jerusalem, Israel, 1999.

[61] Benz N, Gut M, R. W., Solar process heat in breweries and dairies, in: EuroSun 98, Portoroz, Slovenia,, 1998.

[62] Benz, N Gut, M. Beikircher, Solar process heat with non-concentrating collectors for food industry, in: Proceedings of ISES Solar World Congress on CD ROM, Jerusalem, Israel, 1999.

[63] T. Müller, W. Weiß, H. Schnitzer, C. Brunner, U. Begander, O. Themel, PROMISE-Produzieren mit Sonnenenergie: Potenzialstudie zur thermischen Solarenergienutzung in österreichischen Gewerbe-und Industriebetrieben. Studie im Auftrag des Bundesministerium für Verkehr, Innovation und Technologie. Arbeitsgemeinschaft Erneuerbare Energien–Institut für Nachhaltige Technologien, Wien, Innovation und Technologie, Wien, Austria, (2004).

[64] H. Schweiger, J. Mendes, C. Schwenk, K. Hennecke, C. Barquero, A. Sarvisé, M. Carvalho, Poship–the potential of solar heat for industrial processes, Final Report, EU-Project No NNE-1999, 308 (2001).

[65] A. Rabl, Comparison of Solar Concentrators, Solar Energy 18 (1975) 93-111.

[66] W.S. C. Grass , L. Staudacher, Z. Hacker, Comparison of the optics of non-tracking and novel types of tracking solar thermal collectors for process heat applications up to 300◦C, Solar Energy 76 (2004) 207–215.

[67] T.C. Naveen Kumar, H.N. Mistry, A truncated pyramid non-tracking type multipurpose domestic solar cooker/hot water system, Applied Energy, 87 (2010) 471–477.

[68] Jaffe, L. D., Test results on parabolic dish concentrators for solar thermal power systems, Solar Energy, 42 (1989) 173-187.

[69] T.R. Mancini, Analysis and design of two stretched-membrane parabolic dish concentrators, Journal of Solar Energy Engineering;(United States), 113 (1991).

[70] K. Lovegrove, A. Luzzi, Solar Thermal Power Systems, in: A.M. Editor-in-Chief: Robert (Ed.) Encyclopedia of Physical Science and Technology (Third Edition), Academic Press, New York, 2003, pp. 223-235.

[71] Lovegrove, K Burgess, J. G Pye, A New 500 m2 Paraboloidal Dish Solar Concentrator, Solar Energy, 85 (2011) 620-626.

[72] L. Li, S. Dubowsky, A new design approach for solar concentrating parabolic dish based on optimized flexible petals, Mechanism and Machine Theory, 46 (2011) 1536-1548.

[73] L.D. Jaffe, Dish concentrators for solar thermal energy, Journal of Energy, 7 (1981) 9.

[74] L.D. Jaffe, Optimization of dish solar collectors, Journal Name: J. Energy; (United States); Journal Volume: 7:6, (1983) Medium: X; Size: Pages: 684-694.

[75] J.A. Harris, T.G. Lenz, Thermal performance of solar concentrator/cavity receiver systems, Solar Energy, 34 (1985) 135-142.

[76] N.D. Kaushika, Viability aspects of paraboloidal dish solar collector systems, Renewable Energy, 3 (1993) 787-793.

[77] W.B. Stine, R.B. Diver, A compendium of solar dish/Stirling technology, in, DTIC Document, 1994.

[78] M. Becker, B., W. Gupta, Meinecke, M.Bohn, Solar energy concentrating systems: Applications and Technologies, in, C.F.Muller Verlag Heidelberg, Germany, 1995. , 1995.

[79] F. Trieb, O. Langniβ, H. Klaiβ, Solar electricity generation-A comparative view of technologies, costs and environmental impact, Solar Energy, 59 (1997) 89-99.

[80] N.D. Kaushika, K.S. Reddy, Performance of a low cost solar paraboloidal dish steam generating system, Energy Conversion and Management, 41 (2000) 713-726.

[81] K. Lovegrove, A. Luzzi, I. Soldiani, H. Kreetz, Developing ammonia based thermochemical energy storage for dish power plants, Solar Energy, 76 (2004) 331-337.

[82] D. Mills, Advances in solar thermal electricity technology, Solar Energy, 76 (2004) 19-31.

[83] C.E. Kennedy, K.Terwilliger, Optical durability of candidate solar reflectors. , ASME Journal of Solar Energy Engineering, 127 (2005) 8.

[84] I. Palavras, G.C. Bakos, Development of a low-cost dish solar concentrator and its application in zeolite desorption, Renewable Energy, 31 (2006) 2422-2431.

[85] Klaib, Helmut Kohne, Rainer Nitsch, U. Joachim Sprengel, Solar thermal power plants for solar countries -Technology, economics and market potential, Applied Energy, 52 (1995) 165-183.

[86] Hassib, A. M., Compound conical concentrators with elliptical receivers, Solar Energy, 36 (1986) 89-92.

[87] M.F. El-Refaie, Theoretical analysis of the performance of a conical solar concentrator, Applied Energy, 12 (1982) 37-51.

[88] T.R. Mancini, Analysis and design of two stretched-membrane parabolic dish concentrators, Journal Name: Journal of Solar Energy Engineering; (United States); Journal Volume: 113:3, (1991) Medium: X; Size: Pages: 180-187.

[89] Garcia-Botella, Angel Fernandez-Balbuena, Antonio Alvarez Vazquez, Daniel Bernabeu, Eusebio Gonzalez Cano, Agustin, Hyperparabolic concentrators, Applied Optics, 48 (2009) 712-715.

[90] J. Bortz, N. Shatz, Relationships between the generalized functional method and other methods of nonimaging optical design, Appl. Opt., 50 (2011) 1488-1500.

[91] Garcia-Botella, Angel Fernandez-Balbuena, Antonio Alvarez Bernabeu, Eusebio, Elliptical concentrators, Applied Optics, 45 (2006) 7622-7627.

[92] Garcia-Botella, Angel Fernandez-Balbuena, Antonio Alvarez Vázquez, Daniel Bernabeu, Eusebio, Ideal 3D asymmetric concentrator, Solar Energy, 83 (2009) 113-117.

[93] J.C. Minano, J.C. González, New method of design of nonimaging concentrators, Appl. Opt., 31 (1992) 3051-3060.

[94] Senthilkumar, N. S Yasodha, Design and Development of a Three Dimensional Compound Parabolic Concentrator and Study of Optical and Thermal Performance, International Journal of Energy Science, 2 (2012).

[95] M. Gutiérrez, Lorentz Geometry Technique in Nonimaging Optics, in: Proc. of Dynamical systems and differential equations Congress, Wilmington, NC, 2002, pp. 386-392.

[96] Gutierrez, Manuel Minano, Juan C Vega, P. Carlos Benitez, Application of Lorentz geometry to nonimaging optics: new 3D ideal concentrators, in: SPIE's 1995 International Symposium on Optical Science, Engineering, and Instrumentation, International Society for Optics and Photonics, 1995, pp. 85-92.

[97] A. Kribus, P.R. Doron, J.R. R. Karni, R. Duchan, E. S. Taragan, A Multistage Solar Receiver:: The Route To High Temperature, Solar Energy, 67 (1999) 3-11.

[98] T.I. S.D. Sharma, Hiroaki Kitano, Kazunobu Sagara, Thermal performance of a solar cooker based on an evacuated tube solar collector with a PCM storage unit, Solar Energy, 78 (2005) 416–426.

[99] Garcia-Botella, Angel Alvarez Fernandez-Balbuena, Antonio Vazquez, Daniel Bernabeu, Eusebio, Ideal 3D asymmetric concentrator, Solar Energy, 83 (2009) 113-117.

[100] A.F.-B.A. Garcia-Botella A., and Bernabeu E., Vázquez. D, Elliptical concentrators, applied optics, 45 (2006) 7622- 7627.

[101] N. Sellami, T.K. Mallick, D.A. McNeil, Optical characterisation of 3-D static solar concentrator, Energy Conversion and Management, 64 (2012) 579-586.

[102] I.M.O.D. Saleh Ali, Tadhg S.Reddy, K. S. Mallick, Tapas K., An optical analysis of a static 3-D solar concentrator, Solar Energy, 88 (2013) 57-70.

[103] K.V. T. Arunkumar, Amimul Ahsan, R. Jayaprakash and Sanjay Kumar, , Experimental Study on a Compound Parabolic Concentrator Tubular Solar Still Tied with Pyramid Solar Still, (2012).

[104] I. Luminosu, I. Zaharie, R. Negrea, D. Ignea, The study of a static paraboloidal concentrator through the Ray-tracing method, incorporated in the Southern wall of a building, in: National Forum of Energy-FOREN 2008, Neptun, June 15, 2008.

[105] I. Luminosu, I. Zaharie, D. Ignea, The study of a paraboloidal optical concentrator by ray-tracing method: foundations, Moldavian Journal of Physics Sciences, 7 (2007) 2.

[106] I. Luminosu, I. Zaharie, M. Costache, I. Damian, Ray Tracing-an analysis method of optical concentrators, in: National Conference “Installation for Building and the Ambiental Comfort”, Timisoara, March, 2007.

[107] R. Winston, W.T. Welford, Geometrical Vector Flux and Some New Non-imaging Concentrators, Journal of the Optical Society of America, 69 (1979) 532-536.

[108] E. Kritchman, Optimized second stage concentrator, Appl. Opt., 20 (1981) 2929-2933.

[109] Flores, Vicente Almanza, Rafael, Direct steam generation in parabolic trough concentrators with bimetallic receivers, Energy, 29 (2004) 645-651.

[110] H. Yapıcı, B. Albayrak, Numerical solutions of conjugate heat transfer and thermal stresses in a circular pipe externally heated with non-uniform heat flux, Energy Conversion and Management, 45 (2004) 927-937.

[111] H. Yapıcı, G. Baştürk, Numerical solutions of transient conjugate heat transfer and thermally induced stress distribution in a heated and rotating hollow disk, Energy Conversion and Management, 46 (2005) 61-84.

[112] J. Ericsson, The sun motor and the sun's temperature, Nature, 29 (1884) 217-219.

[113] W.W. Shaner, W.S. Duff, Solar thermal electric power systems: Comparison of line-focus collectors, Solar Energy, 22 (1979) 49-61.

[114] J.A. Clark, An analysis of the technical and economic performance of a parabolic trough concentrator for solar industrial process heat application, International Journal of Heat and Mass Transfer, 25 (1982) 1427-1438.

[115] H. Yapici, G. Özişik, M. Serdar Genç, Non-uniform temperature gradients and thermal stresses produced by a moving heat flux applied on a hollow sphere, Sadhana, 35 (2010) 195-213.

[116] S.D. Odeh, G.L. Morrison, M. Behnia, Modelling of parabolic trough direct steam generation solar collectors, Solar Energy, 62 (1998) 395-406.

[117] Huang, S. Bj Hsieh, An automation of collector testing and modification of ANSI/ASHRAE 93-1986 standard, Journal of solar energy engineering, 112 (1990) 257-267.

[118] S. Kalogirou, Parabolic trough collector system for low temperature steam generation: Design and performance characteristics, Applied Energy, 55 (1996) 1-19.

[119] Q.C. Zhang, K. Zhao, B.C. Zhang, L.F. Wang, Z.L. Shen, Z.J. Zhou, D.Q. Lu, D.L. Xie, B.F. Li, New cermet solar coatings for solar thermal electricity applications, Solar Energy, 64 (1998) 109-114.

[120] M. Brooks, I. Mills, T. Harms, Performance of a parabolic trough solar collector, Journal of Energy in Southern Africa, 17 (2006) 71.

[121] A. Valan Arasu, T. Sornakumar, Design, manufacture and testing of fiberglass reinforced parabola trough for parabolic trough solar collectors, Solar Energy, 81 (2007) 1273-1279.

[122] E. Lüpfert, K.-J. Riffelmann, Henry , F. Burkholder, T. Moss, Experimental Analysis of Overall Thermal Properties of Parabolic Trough Receivers, Journal of solar energy engineering, 130 (2008).

[123] Liu, QiBin Wang, YaLong Gao, ZhiChao Sui, Jun Jin, HongGuang Li, HePing, Experimental investigation on a parabolic trough solar collector for thermal power generation, Science in China Series E: Technological Sciences, 53 (2010) 52-56.

[124] Qiu Zhong-Zhua, Li Qiminga, Li Pengb , Zhang Yia, He Jiaa, G. Wenwena, Studies on thermal perfotmance of closed type parabolic trough collector, Advanced Materials Research, 347 - 353 (2012) 10.

[125] F.A. Hamad, M.K. Khan, Natural convection heat transfer in horizontal and inclined annuli of different diameter ratios, Energy Conversion and Management, 39 (1998) 797-807.

[126] Dominic Groulx, B. Sponagle, Ray-Tracing Analysis of a Two-Stage Solar Concentrator Transactions of the Canadian Society for Mechanical Engineering, 34 (2010) 13.

[127] Antonio, Parretta Francesco, Aldegheri Andrea, Antonini Mariangela, Z. Butturi Paolo, Optical simulation of Rondine ® PV solar concentrators by two inverse characterization methods, Journal of Optics, 14 (2012) 125704.

[128] M. Shortis, G.Johnston, Photogrammetry: An available surface characterization tool for solar concentrators, Part II: Assessment of surfaces, ASME Journal of Solar Energy Engineering, 119 (1997) 6.

[129] P. Benítez, Elliptic ray bundles in three-dimensional geometry for nonimaging optics: a new approach, J. Opt. Soc. Am. A, 16 (1999) 2245-2252.

[130] D. Jenkins, R. Winston, Integral design method for nonimaging concentrators, J. Opt. Soc. Am. A, 13 (1996) 2106-2116.

[131] N.E. Wijeysundera, Effect of angular mis-orientation on the performance of conical, spherical and parabolic solar concentrators, Solar Energy, 19 (1977) 6.

[132] A. Rabl, N.B. Goodman, R. Winston, Practical design considerations for CPC solar collectors, Solar Energy, 22 (1979) 373-381.

[133] L. Sandia National, E. United States. Department of, D.L. Siebers, J.S. Kraabel, Estimating convective energy losses from solar central receivers, prepared by Sandia National Laboratories for the U.S. Dept. of Energy, Albuquerque, N.M., 1984.

[134] C.G. McDonald, Heat loss from an open cavity, in: Other Information: PBD: Dec 1995, 1995, pp. Medium: ED; Size: 207 p.

[135] J.M. Khubeiz, E. Radziemska, W.M. Lewandowski, Natural convective heat-transfers from an isothermal horizontal hemispherical cavity, Applied Energy, 73 (2002) 261-275.

[136] E.M.S. Kritchman, K. A. O'Gallagher, J. Winston, R., Stationary nonimaging concentrator as a second stage element in tracking systems, Solar Energy, 30 (1983) 601-602.

[137] R. Winston, Principles of solar concentrators of a novel design, Solar Energy, 16 (1974) 89-95.

[138] H. Tabor, Stationary mirror systems for solar collectors, Solar Energy, 2 (1958) 27-33.

[139] A. Rabl, Comparison of solar concentrators, Solar Energy, 18 (1976) 93-111.

[140] H. Ries, A. Rabl, Edge-ray principle of nonimaging optics, JOSA A, 11 (1994) 2627-2632.

[141] A. Rabl, Edge-ray method for analysis of radiation transfer among specular reflectors, Applied optics, 33 (1994) 1248-1259.

[142] R. Winston, J.C. Miñano, P. Benítez, Nonimaging optics, Academic Press, 2005.

[143] R. Winston, H. Hinterberger, Principles of cylindrical concentrators for solar energy, Solar Energy, 17 (1975) 255-258.

[144] A. Rabl, Solar concentrators with maximal concentration for cylindrical absorbers, Applied optics, 15 (1976) 1871-1873.

[145] T. Mallick, P. Eames, T. Hyde, B. Norton, The design and experimental characterisation of an asymmetric compound parabolic photovoltaic concentrator for building façade integration in the UK, Solar Energy, 77 (2004) 319-327.

[146] R. Winston, H. Ries, Nonimaging reflectors as functionals of the desired irradiance, JOSA A, 10 (1993) 1902-1908.

[147] H.R. Ries, R. Winston, Tailored edge-ray reflectors for illumination, JOSA A, 11 (1994) 1260-1264.

[148] J. Gordon, H. Ries, Tailored edge-ray concentrators as ideal second stages for Fresnel reflectors, Applied optics, 32 (1993) 2243-2251.

[149] J. Gordon, Simple string construction method for tailored edge-ray concentrators in maximum-flux solar energy collectors, Solar Energy, 56 (1996) 279-284.

[150] R. Winston, W. Welford, Ideal flux concentrators as shapes that do not disturb the geometrical vector flux field: a new derivation of the compound parabolic concentrator, JOSA, 69 (1979) 536-539.

[151] G. Spencer, M. Murty, General ray-tracing procedure, JOSA, 52 (1962) 672-676.

[152] U. Ortabasi, W.M. Buehl, An Internal Cusp Reflector for an Evacuated Tubular Heat Pipe Solar Thermal Collector, Solar Energy, 25 (1980) 67-78.

[153] A.Y. El-Assay Cairo, J.A. Clark, A thermal-optical analysis of a compound parabolic concentrator for single and multiphase flows, including superheat, Wärme - und Stoffübertragung, 21 (1987) 189-198.

[154] Y. Tripanagnostopoulos, P. Yianoulis, CPC solar collectors with multichannel absorber, Solar Energy, 58 (1996) 49-61.

[155] I. M. S. Ali, T.K. Malick, P.A Kew, T.S.O'Dononvan, K.S. Reddy, Optical performance evaluation of a 2-D and 3-D novel hyperboloid solar concentrator, in: World Renewable Energy Congress, Abu Dhabi 2010, pp. 1738 -1743.

[156] X. Wei, Z. Lu, W. Yu, W. Xu, Ray tracing and simulation for the beam-down solar concentrator, Renewable Energy, 50 (2013) 161-167.

[157] C.W. Chen, G.W. Hopkins, Ray tracing through funnel concentrator optics, Applied optics, 17 (1978) 1466-1467.

[158] M. Hammad, Y. Zurigat, Performance of a second generation solar cooling unit, Solar Energy, 62 (1998) 79-84.

[159] Anon, Solar simulation, in: Newport (Ed.) Oriel xenon arc lamp solar simulator,, in, Stratford, 2012.

[160] A.E.F. Taylor, Basic Radiometric and Photometric Measurement, in: R.P. Institute (Ed.) Illumination Fundamentals, California, 2000.

[161] Optis Workx software,(2011, November 28) (Ed.). Retrieved from in: http://www.optis-world.com/products/software.htmal,

[162] J. Wang, Solar Compound Parabolic Concentrator (CPC) modelling using OptisWorks in, OPTIS North America, 2009.

[163] R.P. Nadal, V.M. Moll, Optical Analysis of the Fixed Mirror Solar Concentrator by Forward Ray-Tracing Procedure, Journal of Solar Energy Engineering-Transactions of the Asme, 134 (2012).

[164] Anon, Technical information: Metal Halide Lamp: HMI 1200 W/SEL, OSRAM (Ed.), in, Munchen, Germany, (2008).

Appendix A

- ***MATLAB Code for 2-D Ray Tracing Simulation of 2-D Hyperboloid Concentrator***

```
 clc; clear all;
% Define Surface %
a=100;
b=80;
c=((a^2)-(b^2))^0.5;
lmda=(a^2)+1;
mu=(a^2+c^2)/2;
%g=100;
x1=-500:500;
Surf_y=((1-((x1.^2)/lmda)).*(mu-a^2)).^0.5;

I=(Surf_y<0.01);
Surf_y(I)=0;
figure;
plot(x1,abs(Surf_y),'k-','linewidth',[2]);
hold on;
I=(Surf_y==0);
plot(x1(I), abs(Surf_y(I)),'k-','linewidth',[1]); hold on;
plot( x1,abs(Surf_y),'k-');
set(gca, 'xlim', [-150 150], 'ylim', [0 880]);
grid on; axis equal;
hold on;
Total_incoming_ray=0;
Total_absorbing_R=0;
% Define Ray(s) %
alpha=(90*(3.1452/180)) ;      % Angle of Ray
%alpha=89.9999;
Ray_x=x1;    % X-Coordinate of Ray
    n = 0;
    counter =0;
for C=-54430:1500:55086;
    disp(' this how track value in C ');
```

```
    disp(C);
   % pause
     n=n+1;
M=tan(alpha);

%for n=21:1:2355        %nunmber of rays
    Ray_y=M*Ray_x+C;
    XR(1)=Ray_x(1);
    YR(1)=Ray_y(1);

    % Find Intersection between Surface & Ray %
    [a Int_Loc]=(min((Ray_y-Surf_y).^2.^.5));

 if (Ray_y(Int_Loc)>Surf_y(Int_Loc)) &&
(Ray_y(Int_Loc+1)<Surf_y(Int_Loc+1))||(Ray_y(Int_Loc)<Surf_y(Int
_Loc))&& Ray_y(Int_Loc+1)>Surf_y(Int_Loc+1)
mS=((Surf_y(Int_Loc+1)-(Surf_y(Int_Loc)))/((x1(Int_Loc+1))-
(x1(Int_Loc))));  %slope of surface

      cS=(Surf_y(Int_Loc))-(mS*x1(Int_Loc));

 mR=((Ray_y(Int_Loc+1)-(Ray_y(Int_Loc)))/((Ray_x(Int_Loc+1))-
Ray_x(Int_Loc)));  %slope of Ray

       cR=(Ray_y(Int_Loc))-(mR*Ray_x(Int_Loc));
    else
 mS=((Surf_y(Int_Loc-1)-(Surf_y(Int_Loc)))/((x1(Int_Loc-1))-
x1(Int_Loc)));  %slope of surface

        cS=(Surf_y(Int_Loc))-(mS*x1(Int_Loc));
mR=((Ray_y(Int_Loc-1)-(Ray_y(Int_Loc)))/((Ray_x(Int_Loc-1))-
Ray_x(Int_Loc)));  %slope of Ray

       cR=(Ray_y(Int_Loc))-(mR*Ray_x(Int_Loc));
   end
        x_int=(cR-cS)/(mS-mR);
        y_int=(mR*(x_int))+cR;

    XR(2)=x_int;
```

```
    YR(2)=y_int;
    if(abs(YR(2))<=0.1)
       counter=counter+1;
    plot((XR), YR, 'k-', 'markersize', 10, 'linewidth', 2)
    clear XR YR
    continue
    end

    SRayr_x=-500:500;

    beta=atan(mS)-alpha;
    Gamma=2*beta+alpha-pi;
    MR=tan(Gamma);
    SRayr_y =MR*((SRayr_x-x_int))+y_int;
    SRayr_x=-500:500;
    SRayr_y(Int_Loc)=10000;
 [b Int_Loc]=min(((SRayr_y-Surf_y).^2).^0.5);
    if (SRayr_y(Int_Loc)>Surf_y(Int_Loc)) &&
(SRayr_y(Int_Loc+1)<Surf_y(Int_Loc+1))||(SRayr_y(Int_Loc)<Surf_y
(Int_Loc))&& SRayr_y(Int_Loc+1)>Surf_y(Int_Loc+1)
        mR1=((SRayr_y(Int_Loc+1)-
(SRayr_y(Int_Loc)))/((SRayr_x(Int_Loc+1))-SRayr_x(Int_Loc)));
%slope of Ray
        cR1=(SRayr_y(Int_Loc)-(mR1*SRayr_x(Int_Loc)));
        mS1=((Surf_y(Int_Loc+1)-
(Surf_y(Int_Loc)))/((SRayr_x(Int_Loc+1))-SRayr_x (Int_Loc)));
%slope of surface
        cS1=(Surf_y(Int_Loc)-(mS1*SRayr_x(Int_Loc)));
    else
        mR1=((SRayr_y(Int_Loc-1)-
(SRayr_y(Int_Loc)))/((SRayr_x(Int_Loc-1))-SRayr_x(Int_Loc)));
%slope of Ray
        cR1=(SRayr_y(Int_Loc)-(mR1*SRayr_x(Int_Loc)));
        mS1=((Surf_y(Int_Loc-1)-
(Surf_y(Int_Loc)))/((SRayr_x(Int_Loc-1))-SRayr_x(Int_Loc)));
%slope of surface
        cS1=(Surf_y(Int_Loc)-(mS1*x1(Int_Loc)));
    end
        x_int1=(cR1-cS1)/(mS1-mR1);
```

```
        y_int1=(mR1*(x_int1)+cR1);

    XR(3)=x_int1;
    YR(3)=y_int1;
     if(abs(YR(3))<=0.01)
           counter=counter+1;
        plot((XR), YR, 'y-', 'markersize', 10, 'linewidth', 2)
        clear XR YR
    continue
     end
  MR2=tan(-pi+2*(atan(mS1))-atan(mR1));
    SRayr_y(Int_Loc)=1000;
    SRayr_x1=-500:500;
    SRayr_y1 =MR2*((SRayr_x1-x_int1))+y_int1;
    SRayr_y1(Int_Loc)=1000;
  %  [f Int_Loc]=min(((SRayr_y1-Surf_y).^2).^0.5);
    if (SRayr_y1(Int_Loc)>Surf_y(Int_Loc)) &&
(SRayr_y1(Int_Loc+1)<Surf_y(Int_Loc+1))||(SRayr_y1(Int_Loc)<SRay
r_y1(Int_Loc))&& (SRayr_y1(Int_Loc+1)>Surf_y(Int_Loc+1))

        mS2=((Surf_y(Int_Loc+1)-
(Surf_y(Int_Loc)))/((SRayr_x1(Int_Loc+1))-SRayr_x1 (Int_Loc)));
%slope of surface
        cS2=(Surf_y(Int_Loc))-(mS2*SRayr_x1(Int_Loc));
        mR2=((SRayr_y1(Int_Loc+1)-
(SRayr_y1(Int_Loc)))/((SRayr_x1(Int_Loc+1))-SRayr_x1(Int_Loc)));
%slope of Ray
        cR2=(SRayr_y1(Int_Loc))-(mR2*SRayr_x1(Int_Loc));
    else
        mS2=((Surf_y(Int_Loc-1)-
(Surf_y(Int_Loc)))/((SRayr_x1(Int_Loc-1))-SRayr_x1(Int_Loc)));
%slope of surface
        cS2=(Surf_y(Int_Loc))-(mS2*SRayr_x1(Int_Loc));

        mR2=((SRayr_y1(Int_Loc-1)-
(SRayr_y1(Int_Loc)))/((SRayr_x1(Int_Loc-1))-SRayr_x1(Int_Loc)));
%slope of Ray
        cR2=(SRayr_y1(Int_Loc))-(mR2*SRayr_x1(Int_Loc));
    end
```

```
        x_int3=(cR2-cS2)/(mS2-mR2);
        y_int3=(mR2*(x_int3))+cR2;

        XR(4)=x_int3;
        YR(4)=y_int3;
        if(abs(YR(4))<=0.01)
             counter=counter+1;
        plot((XR), YR, 'k-', 'markersize', 10, 'linewidth', 2)
        clear XR YR
    continue
        end

     SRayr_x=-500:500;
      Surf_y=Surf_y;
    MR5=tan(-pi+2*(atan(mS2))-atan(mR2));

    SRay_y5 =MR5*((SRayr_x-x_int3))+y_int3;
    SRayr_x=-500:500;
    SRay_y5(Int_Loc)=1000;
   % [k Int_Loc]=min(((SRay_y5-Surf_y).^2).^0.5);
      if (SRay_y5(Int_Loc)>Surf_y(Int_Loc)) &&
(SRay_y5(Int_Loc+1)<Surf_y(Int_Loc+1))||(SRay_y5(Int_Loc)<SRay_y
5(Int_Loc))&& (SRayr_y5(Int_Loc+1)>Surf_y(Int_Loc+1))

        mR5=((SRay_y5(Int_Loc+1)-
(SRay_y5(Int_Loc)))/((SRayr_x(Int_Loc+1))-SRayr_x(Int_Loc)));
%slope of Ray
        cR5=(SRay_y5(Int_Loc)-(mR5*SRayr_x(Int_Loc)));
        mS5=((Surf_y(Int_Loc+1)-
(Surf_y(Int_Loc)))/((SRayr_x(Int_Loc+1))-SRayr_x (Int_Loc)));
%slope of surface
        cS5=(Surf_y(Int_Loc)-(mS5*SRayr_x(Int_Loc)));
    else
        mR5=((SRay_y5(Int_Loc-1)-
(SRay_y5(Int_Loc)))/((SRayr_x(Int_Loc-1))-SRayr_x(Int_Loc)));
%slope of Ray
        cR5=(SRay_y5(Int_Loc)-(mR5*SRayr_x(Int_Loc)));
```

```
        mS5=((Surf_y(Int_Loc-1)-
(Surf_y(Int_Loc)))/((SRayr_x(Int_Loc-1))-SRayr_x(Int_Loc)));
%slope of surface
        cS5=(Surf_y(Int_Loc)-(mS5*SRayr_x(Int_Loc)));
    end
        x_int5=(cR5-cS5)/(mS5-mR5);
        y_int5=(mR5*(x_int5)+cR5);

        XR(5)=x_int5;
        YR(5)=y_int5;
       % plot( XR, YR, 'g-x', 'markersize', 10, 'linewidth', 2);
       %clear XR YR
      if(abs(YR(5))<=0.01)
 plot( XR, YR, 'g-', 'markersize', 10, 'linewidth', 2);
   counter=counter+1;
    clear XR YR
    continue
      end


      SRayr_x=-500:500;
      Surf_y=Surf_y;
    MR6=tan(-pi+2*(atan(mS5))-atan(mR5));
    SRay_y6 =MR6*((SRayr_x-x_int5))+y_int5;
    SRayr_x=-500:500;
    SRay_y6(Int_Loc)=1000;
    [z Int_Loc]=min(((SRay_y6-Surf_y).^2).^0.5);
      if (SRay_y6(Int_Loc)>Surf_y(Int_Loc)) &&
(SRay_y6(Int_Loc+1)<Surf_y(Int_Loc+1))||(SRay_y6(Int_Loc)<SRay_y
6(Int_Loc))&& (SRayr_y6(Int_Loc+1)>Surf_y(Int_Loc+1))

        mR6=((SRay_y6(Int_Loc+1)-
(SRay_y6(Int_Loc)))/((SRayr_x(Int_Loc+1))-SRayr_x(Int_Loc)));
%slope of Ray
        cR6=(SRay_y6(Int_Loc)-(mR6*SRayr_x(Int_Loc)));
        mS6=((Surf_y(Int_Loc+1)-
(Surf_y(Int_Loc)))/((SRayr_x(Int_Loc+1))-SRayr_x (Int_Loc)));
%slope of surface
        cS6=(Surf_y(Int_Loc)-(mS6*SRayr_x(Int_Loc)));
```

```
    else
        mR6=((SRay_y6(Int_Loc-1)-
(SRay_y6(Int_Loc)))/((SRayr_x(Int_Loc-1))-SRayr_x(Int_Loc)));
%slope of Ray
        cR6=(SRay_y6(Int_Loc)-(mR6*SRayr_x(Int_Loc)));
        mS6=((Surf_y(Int_Loc-1)-
(Surf_y(Int_Loc)))/((SRayr_x(Int_Loc-1))-SRayr_x(Int_Loc)));
%slope of surface
        cS6=(Surf_y(Int_Loc)-(mS6*SRayr_x(Int_Loc)));
    end
        x_int6=(cR6-cS6)/(mS6-mR6);
        y_int6=(mR6*(x_int6)+cR6);

        XR(6)=x_int6;
        YR(6)=y_int6;
% plot( XR, YR, 'g-x', 'markersize', 10, 'linewidth', 2);
       %clear XR YR
      if(abs(YR(6))<=0.01)
 plot( XR, YR, 'g-', 'markersize', 10, 'linewidth', 2);
    clear XR YR
    counter=counter+1;

    continue
    end

    plot(XR, YR, 'r-', 'markersize', 10, 'linewidth', 2)
   clear XR YR
      SRayr_x=-1000:1000;
      Surf_y=Surf_y;
    MR7=tan(-pi+2*(atan(mS6))-atan(mR6));
%
    SRay_y7 =-MR7*((SRayr_x-x_int6))+y_int6;
    SRayr_x=-500:500;
    SRay_y7(Int_Loc)=100;
 [l Int_Loc]=min(((SRay_y7-Surf_y).^2).^0.5);
 if (SRay_y7(Int_Loc)>Surf_y(Int_Loc)) &&
(SRay_y7(Int_Loc+1)<Surf_y(Int_Loc+1))||(SRay_y7(Int_Loc)<SRay_y
7(Int_Loc))&& (SRayr_y7(Int_Loc+1)>Surf_y(Int_Loc+1))
```

```
  mR7=((SRay_y7(Int_Loc+1)-
(SRay_y7(Int_Loc)))/((SRayr_x(Int_Loc+1))-SRayr_x(Int_Loc)));
%slope of Ray
        cR7=(SRay_y7(Int_Loc)-(mR7*SRayr_x(Int_Loc)));
        mS7=((Surf_y(Int_Loc+1)-
(Surf_y(Int_Loc)))/((SRayr_x(Int_Loc+1))-SRayr_x (Int_Loc)));
%slope of surface
 cS7=(Surf_y(Int_Loc)-(mS7*SRayr_x(Int_Loc)));
    else
        mR7=((SRay_y7(Int_Loc-1)-
(SRay_y7(Int_Loc)))/((SRayr_x(Int_Loc-1))-SRayr_x(Int_Loc)));
%slope of Ray
        cR7=(SRay_y7(Int_Loc)-(mR7*SRayr_x(Int_Loc)));
        mS7=((Surf_y(Int_Loc-1)-
(Surf_y(Int_Loc)))/((SRayr_x(Int_Loc-1))-SRayr_x(Int_Loc)));
%slope of surface
        cS7=(Surf_y(Int_Loc)-(mS7*SRayr_x(Int_Loc)));
    end
        x_int7=(cR7-cS7)/(mS7-mR7);
        y_int7=(mR7*(x_int7)+cR7);

        XR(7)=x_int7;
        YR(7)=y_int7;
      % plot( XR, YR, 'g-x', 'markersize', 10, 'linewidth', 2);
       clear XR YR
     % if(abs(YR(7))<=0.01)
 %plot( XR, YR, 'r-', 'markersize', 10, 'linewidth', 1);
    clear XR YR

    continue

end

         Total_incoming_ray=Total_incoming_ray+n
        Total_absorbing_R=Total_absorbing_R+ counter
        optical_eff=Total_absorbing_R/Total_incoming_ray
        concentration_ratio=((x1(end)-(x1(1)))^2/(2*a)^2);
     disp(['Concentration
Ratio=',num2str(concentration_ratio)]);
```

- ***MATLAB code for 3-D Ellptical Hyperboliod Concentrator***

```
close all; clear all; clc;

a=200;
b=120;
c=((a^2)-(b^2))^0.5;
lmda=(a^2)+1;
mu=(a^2+c^2)/2;

X=[-1000:1000];
Y=[-500:500];

indx=0;
for x=X
    indx=indx+1;
    indy=0;
    for y=Y
        indy=indy+1;
        num=((1-((x^2)/lmda)-((y^2)/(mu-c^2)))*(mu-a^2))^0.5;
        if isreal(num)==1

        Z(indx, indy)=num;

        else
            Z(indx, indy)=0;

     end
        end
end
    I=find(Z>min(Z(1,:)));
   Z(I)=nan;

surf(Y,X,Z); shading interp; axis equal
```

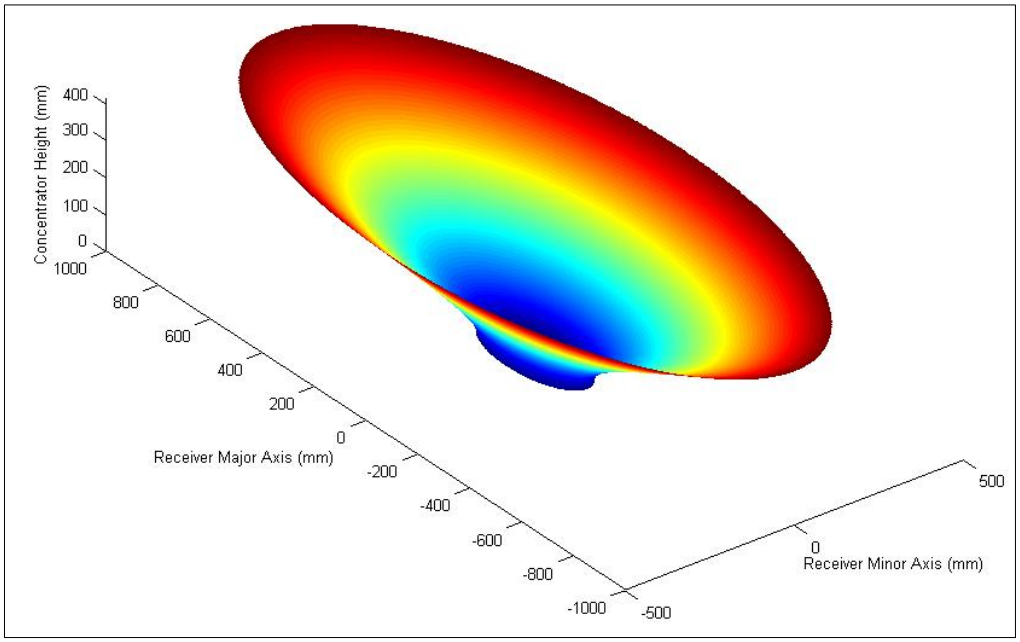

Star Prototype China Limited
Add: 10a Seapower Industrial Center, 177 Hoi Bun Road, Kwun Tong, Hong Kong SAR
Web: www.star-prototype-china.com
Email: sales@star-prototype-china.com Tel: +86 760 22 22 25 56 Fax: +86 760 22 22 25 58

STARPROTOTYPE
The "Best of the West" in China

Invoice

To:
Attn of: Imhamed M. Saleh Ali
Email: isa6@hw.ac.uk Tel: :+44 (0) 131 451 8083
Add: PhD Student, Department of Mechanical Engineering
School of Engineering and Physical Sciences
Heriot-Watt University
Edinburgh, EH14 4AS, UK

Invoice No.:	112110
Date:	December 14, 2011
Currency:	GBP
Invoice Value:	3,182.00
Payment Due:	pay in advance

Please accept our invoice for Quotation 1107307 as per your f#

No.	Part Name	Material	Process	Finish	Unit Price	Quantity	Amount
1	protoype1	ABS	CNC	Chroming	1834.00	1	1834.00
2	Prototype circular	ABS	CNC	Chroming	1148.00	1	1148.00
3							
4							
5							
6							
7							
8							
9							
10							
						Shipment Cost	200.00
						Total Amount	3182.00

Notes:
1) A 4% fee will be applied to orders that are paid via PayPal
2) You may be required to pay VAT and Import Duties in your own Country
3) Inco-Terms: DDU

Bank Information:
Bank: HSBC (The Hong Kong and Shanghai Banking Corporation Limited)
Address: 1 Queen's Road, Central, Hong Kong
Account Name: Star Prototype China Limited
Account Number: 116-838418-838
Swift Code: HSBCHKHHHKH

Sales: Max Zhan
Email: Max.Zhan@star-prototype-china.com
Accountant: Tracy Hu
Email: accounts@star-prototype-china.com

Managing Director